WELDING Journal

Aluminum Welding

Alternate Fuel

Filler Metals for LNG Tank Welding

FEBRUARY 2021

PUBLISHED BY THE AMERICAN WELDING SOCIETY TO ADVANCE THE SCIENCE, TECHNOLOGY, AND APPLICATION OF WELDING AND ALLIED JOINING AND CUTTING PROCESSES WORLDWIDE, INCLUDING BRAZING, SOLDERING, AND THERMAL SPRAYING

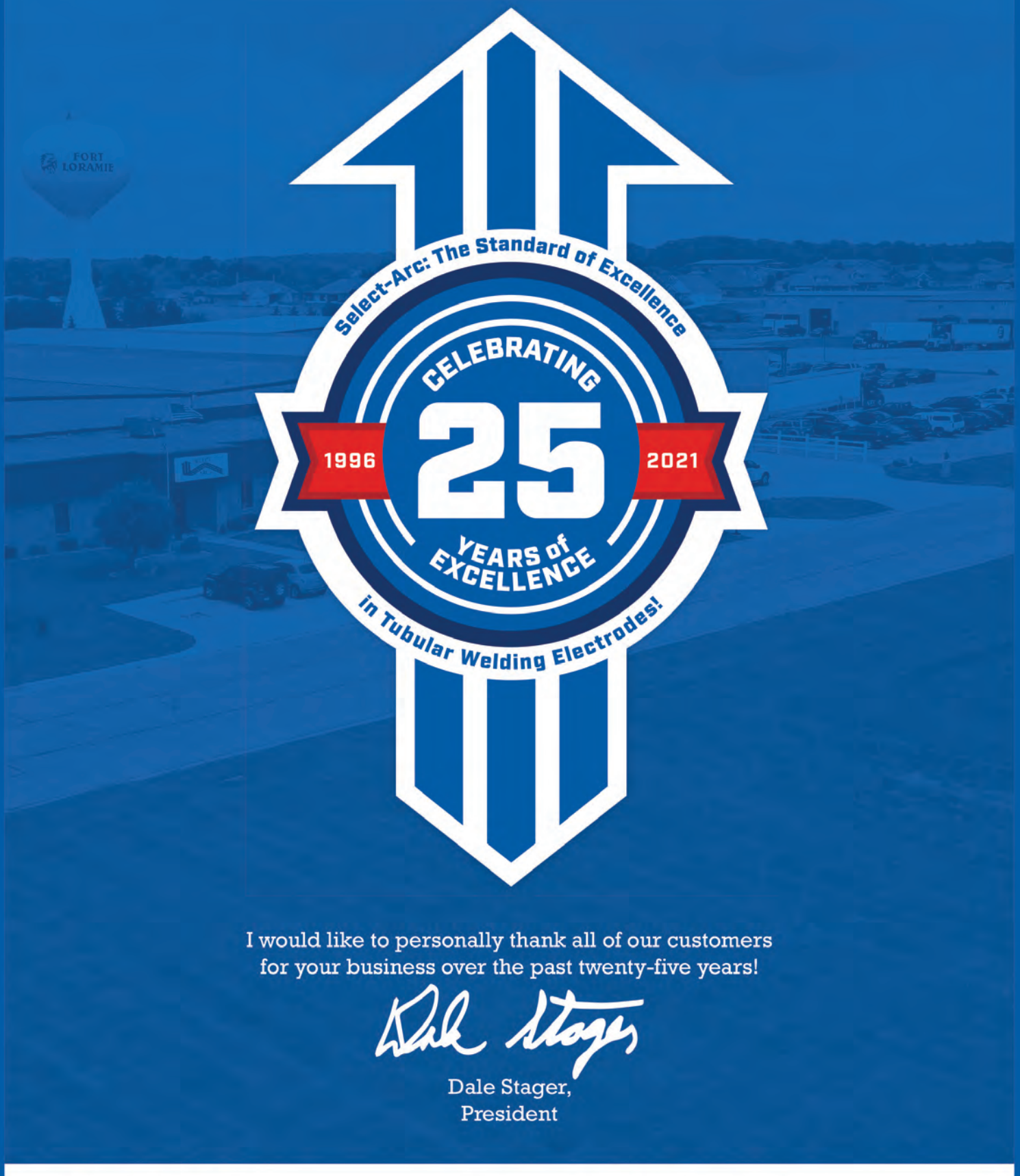

I would like to personally thank all of our customers
for your business over the past twenty-five years!

Dale Stager,
President

SELECT ARC INC.®

Experience the full line of Select-Arc products today!

800-341-5215 | www.select-arc.com

American Welding Society®

CALL FOR PAPERS

2021 AWS PROFESSIONAL PROGRAM

September 13-16 | McCormick Place | Chicago, IL

The American Welding Society is accepting abstract submissions to be considered for presentation during the AWS Professional Program held at FABTECH 2021 in Chicago, IL.

AWS welcomes abstract submissions on novel developments and research related to materials joining technology and processes, including additive manufacturing. Although full papers are not required for consideration, authors are encouraged to submit them to the *Welding Journal* at ***editorialmanager.com/wj/default.aspx*** for possible publication.

- **Additive Manufacturing**
- **Battery and Energy Systems Welding**
- **Industrial Applications and Technologies**
- **Modeling and Numerical Analysis**
- **Sensors, Controls and Robotics**
- **Surfacing and Overlay**
- **Weldability and Properties of Welded Components**
- **Weld Repair and Performance of Welded Joints including Corrosion, Creep and Fatigue**
- **Welding Processes/Methods**
  - **High Energy Density (Laser and Electron Beam) and Laser Hybrid Welding**
  - **Solid State Welding**
  - **Arc Welding Processes and Methods**

Authors with accepted abstracts are required to give oral presentations and will receive complimentary registration for the 2021 AWS Professional Program, along with free access to FABTECH 2021. Authors/Presenters are also encouraged to attend the following events held during the Professional Program:

- **Opening Ceremony:** Join us as the new AWS President and officers are introduced and new AWS Fellows and Counselors are inducted
- **The Comfort A. Adams Lecture:** Follows the Opening Ceremony
- **Plenary Presentation:** by Prof. Patricio Mendez, *University of Alberta*
- **Plenary Presentation:** by Prof. Sindo Kou, *University of Wisconsin*
- **Poster Competition:** The link for the Poster Competition will be released soon

Submit your abstract for review and consideration today.

Abstract submission deadlines will be released soon. For the latest updates, including how to submit your abstract for review and consideration, please visit us at ***programmaster.org/2021awsprofessional***

CERTIFIED WELDING INSPECTOR
Lifetime Achievement Award

IMPORTANT
Announcement!

American Welding Society®

Friends and Colleagues:

In 2018, The American Welding Society established the honor of the **Certified Welding Inspector Lifetime Achievement Award (CWI-LAA)**. The award is intended to recognize individual members for a career of distinguished service, outstanding accomplishments, exceptional leadership, and innovative contributions in the area of welding inspection and welding inspection technology. Individuals receiving the award may be currently working as a CWI, or have worked as one in the past. The selection committee is seeking nomination packages for qualified individuals who have demonstrated specific accomplishments in one or more of the following areas:

- Advancements in the field of welding inspection.
- Mentorship of individuals entering the field of welding inspection.
- Effective application of existing and new inspection technology.

This could be evidenced by one or more of the following:

1. Development of novel concepts or tools related to welding inspection.
2. Participation in activities directly related to the recruitment, training, education and/or mentorship of individuals entering the field of welding inspection.
3. Leadership in AWS or private industry, particularly as it impacts advancement of the welding inspection profession.
4. Consultancy in technical matters or welding industry business matters, including expert witness activities related to welding inspection.
5. Publication of books, papers, articles or other significant works related to welding inspection.
6. Meaningful participation in AWS committees, Sections or other AWS voluntary contributions related to welding inspection.

For more specifics on the nomination requirements, please contact Malisa Mercado at mmercado@aws.org at AWS headquarters in Miami, or simply follow the instructions on the AWS CWI Lifetime Achievement Award nomination form located at: *aws.org/cwilaa.*

Please remember, we all benefit in the honoring of those who have made major contributions to our chosen profession and livelihood. The deadline for submission is July 1, 2021. The CWI Lifetime Achievement Award Committee looks forward to receiving numerous nominations for 2022 consideration.

Sincerely,

Kerry Shatell
Chair, CWI Lifetime Achievement Award Committee

Nominate

Your Colleague for the American Welding Society

CWI Lifetime Achievement — Award —

July 1, 2021
Submission Deadline

February 2021 • Volume 100 • Number 2

CONTENTS

FEATURES

WELDING RESEARCH SUPPLEMENT

DEPARTMENTS

On the cover: Large diameter welding of aluminum plate. (Courtesy of AlcoTec Wire Corp., Traverse City, Mich.)

aws.org
8669 NW 36 St., # 130, Miami, FL 33166-6672
(305) 443-9353 or (800) 443-9353

AWS Promotes Diversity

AWS values diversity, advocates equitable and inclusive practices, and engages its members and stakeholders in establishing a culture in the welding community that welcomes, learns from, and celebrates differences among people. AWS recognizes that a commitment to diversity, equity, and inclusion is essential to achieving excellence for the Association, its members, and employees.

Welding Journal (ISSN 0043-2296 Print) (ISSN 2689-0445 Online) is published monthly by the American Welding Society for $120.00 per year in the United States and possessions, $160 per year in foreign countries: $7.50 per single issue for domestic AWS members and $10.00 per single issue for non-members and $14.00 per single issue for international. Not available for resale in either print or electronic form. American Welding Society is located at 8669 NW 36 St., # 130, Miami, FL 33166-6672; telephone (305) 443-9353. Periodicals postage paid in Miami, Fla. and additional mailing offices. **POSTMASTER:** Send address changes to *Welding Journal*, 8669 NW 36 St., # 130, Miami, FL 33166-6672. **Canada Post:** Publications Mail Agreement #40612608 Canada Returns to be sent to Bleuchip International, P.O. Box 25542, London, ON N6C 6B2, Canada.

AWS Claims Policy: All hardcopy editions are shipped FOB Origin. Publisher reserves the right to investigate and make a determination on all claims submitted for missing editions not received by a subscribing member or institution. Any claim request determined to be valid will be fulfilled with a digital copy of the edition. Publisher will NOT send any hardcopy replacement issues for any reason.

Aluminum Continues to Grow within the Welding Fabrication Industry

The process of converting aluminum ore into the aluminum that we know and use every day was discovered relatively recently. Industrial production of aluminum only began in the late 19th century, making this material very much a latecomer among the common metals.

The first commercial applications of aluminum were novelty items such as mirror frames and serving trays. Cooking utensils were also a major early marketed product.

Today, aluminum's unique characteristics of light weight, high strength, high toughness, extreme temperature capability, versatility of extruding, excellent corrosion resistance, and recycling capabilities make it the obvious choice of material by engineers and designers for a wide variety of welding fabrication applications. When we consider the advancement of aluminum within the welding fabrication industry, it becomes clear that there is a definite need for a better understanding of how to successfully weld this material.

The earliest welding techniques suitable for aluminum included oxyfuel gas welding and resistance welding. The arc welding of aluminum was restricted to shielded metal arc welding. Most of the welding processes had limitations and inherent problems, making it very challenging to produce sound welds. The breakthrough for aluminum as a structural material occurred with the introduction in the 1940s of the inert gas welding processes. First came the gas tungsten arc welding (GTAW) process, which was sometimes referred to as Heliarc and also known as the tungsten inert gas (TIG) process. This was followed shortly after by the gas metal arc welding (GMAW) process, also known as the metal inert gas (MIG) process. With the introduction of welding processes that used inert gas to protect the molten aluminum during welding, it became possible to make high-quality, high-strength welds at high speeds and in all positions without corrosive fluxes. Today, aluminum and its many alloys are readily weldable using a variety of techniques and welding processes, including newer processes such as laser beam welding and friction stir welding; however, the GTAW/TIG and GMAW/MIG processes remain the most popular.

The automotive industry continues to increase its use of aluminum. Environmental issues such as increased fuel efficiency are promoting more aluminum components to be used within the average automobile.

The shipbuilding industry has developed high-speed aluminum ferries (fast ferries) as a means of fast, efficient, low-maintenance transport. The advantages of aluminum are also being used for small pleasure craft, fishing boats, work boats such as coast guard vessels, and large high-speed military ships, some of which are almost exclusively manufactured from aluminum.

The recreation and sporting equipment industry produces high-tech products through the increased use of high-strength, heat-treatable aluminum alloys such as the 7xxx series. Bicycle frames, baseball bats, golf clubs, sleds, and snowmobiles are some of the many products within this industry dependent on aluminum alloys.

The transportation and containers industry primarily uses the 5xxx series aluminum/magnesium alloys and the 6xxx series aluminum/magnesium-silicide alloys. Large dump trucks, flatbed trailers, livestock trailers, liquid natural gas tankers, and many other types of containers are fabricated from aluminum and its alloys.

The defense and aerospace industries make use of high-strength 5xxx series non-heat-treatable alloys for some applications but also make use of some of the more specialized heat-treatable aluminum alloys with superior mechanical properties. Aluminum armor plating is used for its impact strength and strength-to-weight ratio. Perhaps the most exotic aluminum alloys, with exceptional strength over a wide range of operating temperatures, are used in the aerospace industry. These alloys are typically used in specialized high-performance applications and have their own welding characteristics and sometimes associated problems.

With the continued growth of aluminum within our industry, the American Welding Society (AWS) continues to support the industry with codes and standards such as AWS D1.2, *Structural Welding Code — Aluminum*, and AWS A5.10, *Specification for Bare Aluminum and Aluminum-Alloy Welding Electrodes and Rods*, along with numerous training conferences and seminars devoted to the welding of aluminum. WJ

Tony Anderson
AWS Director-at-Large

"Aluminum's unique characteristics of light weight, high strength, high toughness, extreme temperature capability, versatility of extruding, excellent corrosion resistance, and recycling capabilities make it the obvious choice of material by engineers and designers for a wide variety of welding fabrication applications."

AWS Foundation Presents Scholarship Opportunities

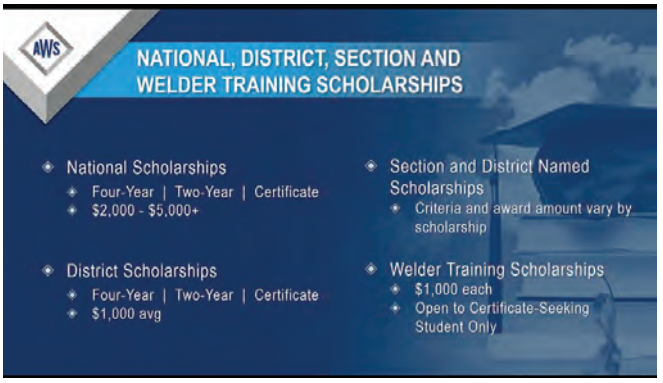

A slide from the "Understanding the AWS Foundation Scholarship Application Process" webinar listing different scholarships.

In a recent webinar and podcast, the American Welding Society (AWS) Foundation took center stage.

• The webinar "Understanding the AWS Foundation Scholarship Application Process" was held on December 17.

The webinar's objective was to teach welding students how they can take advantage of AWS Foundation scholarship opportunities and navigate the scholarship portal. Its guest speakers were Whitney Minor and Nazdhia Prado, both AWS Foundation program administrators. Trish Claussen, AWS content manager, served as the moderator.

The AWS Foundation will be awarding more than $1.5 million in scholarships in 2021. Minor and Prado walked viewers through the steps of applying, which include completing an academic profile, reviewing eligible scholarships, and providing documentation. Different aspects of the AWS Foundation were also covered, such as scholarships and grants available to educational institutions, research fellowships, workforce development, and social media.

The webinar ended with a Q&A session. To watch the 20-min presentation, visit *aws.org/webinars*.

• Applications for 2021–2022 National, District, and Section Scholarships are now open. Apply online at *scholarship.aws.org.* The deadline is March 1.

• Additional information on the AWS Foundation scholarships and grants was also shared in the Arc Junkies podcast. Host Jason Becker spoke with John Douglass, associate director of the AWS Foundation, and Shane Goslin, a past recipient of an AWS National and District Scholarship. Go to *aws.org/podcasts* to listen to the episode. — *Alexandra Quiñones, associate editor*

Participate in the 2021 AWS Professional Program

Attention Authors/Presenters: The American Welding Society (AWS) is accepting abstract submissions to be considered for presentation during the AWS Professional Program held at FABTECH 2021 (*fabtechexpo.com*) in Chicago, Ill. The trade show will take place September 13–16 at McCormick Place.

Abstract submissions on novel developments and research related to materials joining technology and processes — including additive manufacturing, battery and energy systems welding, industrial applications and technologies, modeling and numerical analysis, sensors, controls, and robotics, surfacing and overlay, weldability and properties of welded components, weld repair and performance of welded joints, and welding processes/methods — are sought.

Deadlines will be released soon. For the latest updates, including how to submit your abstract for review and consideration, visit *programmaster.org/2021awsprofessional*.

Full papers are not required for consideration, but authors are encouraged to submit them to the *Welding Journal* at *editorialmanager.com/wj/default.aspx* for possible publication.

In addition, authors with accepted abstracts are required to give oral presentations and will receive complimentary registration for the 2021 AWS Professional Program, as well as free access to FABTECH 2021. Authors/presenters are further encouraged to attend these events held during the Professional Program: Opening Ceremony; Comfort A. Adams Lecture; Plenary Presentations by Prof. Patricio Mendez, University of Alberta, and Prof. Sindo Kou, University of Wisconsin; and the Poster Competition.

Tech and Philanthropic Leaders Launch Million Girls Moonshot to Close Gender Gap in STEM

The Intel Foundation and the Gordon and Betty Moore Foundation have joined STEM Next Opportunity Fund and the Charles Stewart Mott Foundation to launch the Million Girls Moonshot, which is designed to engage one million school-age girls in the United States in science, technology, engineering, and math (STEM) learning opportunities over the next five years. The organizations will provide grant funding and in-kind resources to Mott-funded afterschool networks in all 50 states to increase access to hands-on, immersive STEM learning experiences.

"When my father, Robert Noyce, and Gordon Moore founded Intel, they built upon the experiences of their youth, where they had opportunities to build, invent, engineer, and experiment. These hands-on experiences gave them a sense of initiative, perseverance, and a belief that they could create revolutionary new technologies," said Penny Noyce, founding board chair, STEM Next Opportunity Fund. "The Million Girls Moonshot will help girls from diverse backgrounds develop this same engineering mindset, and I'm thrilled at the way it continues the legacy of Intel's founders and their passion for advancing STEM."

Million Girls Moonshot aims to create a national movement to change the trajectory of women and girls in STEM. To support programs as they pivot to meet students' needs, the Million Girls Moonshot will provide afterschool networks with technical assistance, educational resources, access to Intel's She Will Connect partners, and mentorship from STEM experts, including Intel employee volunteers.

To learn more, visit *milliongirlsmoonshot.org*. WJ

U.S. Environmental Protection Agency Finalizes Ozone NAAQS

Following its statutorily required five-year review, the U.S. Environmental Protection Agency (EPA) has decided to retain, without changes, the current ozone National Ambient Air Quality Standards (NAAQS), which was originally established in 2015. The Clean Air Act requires EPA to set NAAQS for criteria pollutants. Currently, ozone and five other major pollutants are listed as criteria pollutants. The law requires the EPA to periodically review the relevant scientific information and revise standards, if appropriate, to ensure they provide the requisite protection for public health and welfare. In the prior review of the ozone standards in 2015, the EPA increased the stringency of the levels of the ozone standards to 70 parts per billion (ppb), from the 2008 standard of 75 ppb.

Senate Unveils House-Approved Rural STEM Bill

Introduced in the Senate in December, the Rural STEM Education Act (S. 4972) would direct the National Science Foundation to support rural science, technology, engineering, and manufacturing (STEM) education and workforce development through grants for research on teaching STEM in rural schools, barriers rural students face in accessing STEM education, and solutions to improve the participation of rural pre-K to twelfth-grade students in STEM. This bill would also direct the National Institute of Standards and Technology to establish a prize competition to stimulate innovations in technologies, deploy broadband connectivity to unserved rural communities, and establish a working group to set key research priorities for improving broadband access in rural communities. A similar bill (HR 4979) was approved by the House in October.

Antitrust Whistleblower Protection Becomes Law

The Criminal Antitrust Anti-Retaliation Act, which prohibits employers from retaliating against certain individuals who report criminal antitrust violations, has been approved by Congress and signed by the president. Under this new federal law, employers cannot "discharge, demote, suspend, threaten, harass, or in any other manner discriminate against" an employee for the following: 1) providing or helping to provide information to the federal government, to a "supervisory authority figure," or to an individual working for the employer with investigative powers pertaining to violations (or suspected violations) of antitrust laws; and 2) assisting in a federal investigation or proceeding related to antitrust violations. Common antitrust violations include price fixing, wage fixing, bid rigging, customer or market allocations, conspiracies to restrain supply, boycotts, and so-called naked no-poach agreements.

U.S. Equal Employment Opportunity Commission Issues COVID-19 Guidance

The U.S. Equal Employment Opportunity Commission (EEOC) has released a guide for U.S. employers regarding employees and the COVID-19 vaccines. The EEOC generally allows employers to mandate that their workers be vaccinated. While there are other legal considerations for employers in imposing such a requirement, acquiescence by the EEOC is significant. The remainder of the guidance focuses largely on the need to make reasonable accommodations for employees or applicants for employment who cannot, or refuse to, be vaccinated for medical, religious, or other reasons. The EEOC guidance is available at *eeoc.gov/wysk/what-you-should-know-about-covid-19-and-ada-rehabilitation-act-and-other-eeo-laws*.

U.S. Department of Labor Provides the Latest Work Injury Data

There were 5333 fatal work injuries recorded in the United States in 2019, a 2% increase from 5250 in 2018, according to the U.S. Department of Labor Bureau of Labor Statistics. This is the most recent data available. However, the fatal work injury rate of 3.5 fatalities per 100,000 full-time equivalent workers was roughly the same rate that was reported in 2018. Other key findings from the 2019 Census of Fatal Occupational Injuries include the following:

- The 5333 fatal occupational injuries represents the largest annual number since 2007.
- Fatalities among workers aged 55 and over accounted for 38% of all workplace fatalities and increased by 8% from 1863 in 2018 to 2005 in 2019.
- Fatalities in the private construction industry increased 5% to 1061.
- Transportation incidents continued to account for the largest share of fatalities.
- Falls, slips, and trips increased 11% in 2019 to 880.
- Construction and extraction occupation fatalities increased by 6% in 2019 to 1066.

OSHA Announces Most Frequently Cited Standards Related to COVID-19 Inspections

The U.S. Occupational Safety and Health Administration (OSHA) has disclosed which standards are most frequently cited during coronavirus-related inspections. The following are the most cited standards: failure to perform an appropriate fit test for workers using tight-fitting respirators; failure to train workers to safely use respirators and/or other personal protective equipment (PPE) in the workplace; failure to retrain workers about changes in the workplace that might make previous training obsolete; and failure to properly store respirators and other PPE to protect them from damage, contamination, and, where applicable, deformation of the facepiece and exhalation valve. WJ

HUGH K. WEBSTER, AWS WASHINGTON GOVERNMENT AFFAIRS OFFICE — Contact the AWS Washington Government Affairs Office at 1747 Pennsylvania Ave. NW, Washington, DC 20006; email *hwebster@wc-b.com*; fax (202) 835-0243.

AWS Foundation Awards up to $25,000 to Nine Welding Programs

The American Welding Society (AWS) Foundation has been dedicated to building the welding workforce through its Welding Workforce Grant. The grant awards up to $25,000 to high schools, trade/technical schools, and community colleges seeking to enhance and improve their welding education programs, including making facility improvements or investing in welding or metalworking equipment.

The following lists the nine 2020 fall grant recipients and details how the schools hope to enhance their welding programs with the funds received.

Grant Offers Growth

Aiken Technical College (ATC), Aiken, S.C., is currently upgrading its welding facilities, which will include a renovated fume extraction system and expanded welding space. With the $25,000 in grant funding, the college will purchase 6 × 6 ft welding booths and Miller® Dynasty® 280 multiprocess welding machines with wire feeders and carts. These advancements will help provide the technical education welding students need to be highly trained, skilled, and employable.

"The increased enrollment of the welding program has opened up the need for additional welding booths and machines," said Keith Cusey, ATC welding instructor. "When setting up lab schedules, we currently have to closely monitor the class sizes during the registration process to avoid any overlaps of more students than welding booths."

ATC Foundation Director Beth LaClair added, "This grant opportunity came at just the right time. This is a wonderful opportunity for the AWS to provide funding support to the already ongoing enhancements to the ATC welding facilities."

ATC will use its grant funds to support the ongoing enhancements to the college's welding facilities. (Photo courtesy of Aiken Technical College.)

Crowder College Advanced Training and Technology Center (ATTC), Joplin, Mo., will utilize its $25,000 in grant funds to procure a computer numerical control (CNC) plasma cutting machine to fabricate precision parts. With the equipment, the school will be able to train welding, drafting, and advanced manufacturing students in the fabrication process. Crowder anticipates the equipment will be installed and ready for students to use by the spring 2021 semester.

Crowder College ATTC was awarded a $25,000 grant to add a CNC plasma cutting machine to its welding technology lab (pictured here) to train students in the fabrication process. (Photo courtesy of Kent Pruitt, Crowder College ATTC.)

"By receiving the AWS Foundation grant, the Crowder College ATTC welding technology program will provide training to the welding technology students [as well as] the computer-aided drafting and advanced maintenance technology students. This equipment will give Crowder's ATTC students greater employment opportunities than surrounding training facilities," explained Kent Pruitt, Crowder College ATTC welding instructor.

Kankakee Area Career Center (KACC), Bourbonnais, Ill., received $25,000 to purchase four Miller XMT® 350

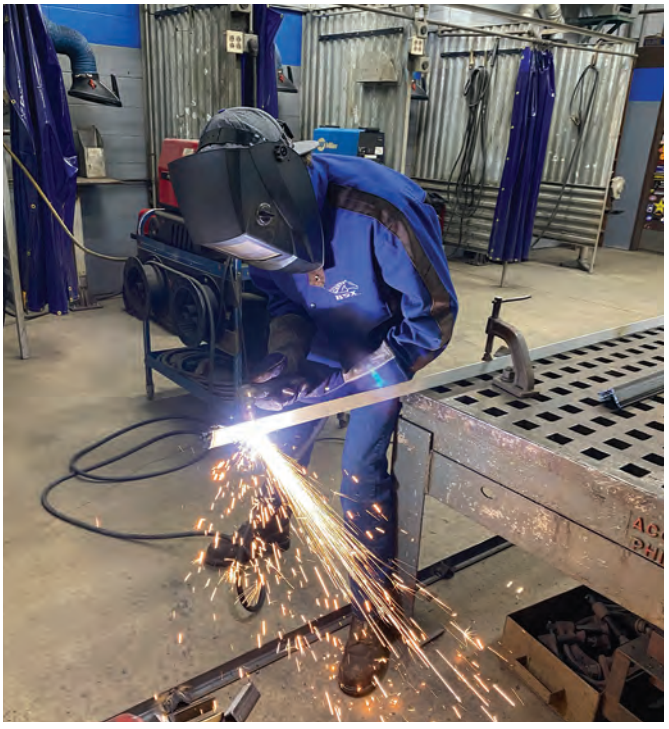

KACC has plans to upgrade its welding lab equipment using the awarded funds. Pictured is a welding student practicing plasma cutting on a 3⁄16-in. angle iron. (Photo courtesy of Mike Gall, KACC.)

Series gas metal arc welding machines with support equipment. This will allow the school to upgrade its welding lab equipment from its current state, which, according to the college, is broken down and outdated.

"KACC's class enrollment has exploded in the past few years. We have gone from one to 17 students per session, three sessions per day, to a whopping 30 students per session, adding an additional fourth session," said Mike Gall, KACC welding instructor. "The incredible amount of interest is holding steady, creating more urgency in our need for newer, more reliable equipment. Suffice it to say, our welding program has grown exponentially more than our budget, pushing us to look outward for financial assistance."

Kansas City Kansas Community College (KCKCC), Kansas City, Kans., will use the awarded $25,000 to expand its welding technology program as well as educate and train incarcerated students at Lansing Correctional Facility through the Second Chance Pell program. Funds provided by this grant will be used to buy six welding booths, six welding tables, and one partial ironworker, thus fulfilling the program's need for welding lab equipment. The program will provide up to 48 students per year with welding education, certification prep, and job placement assistance to fill the existing employment gap.

Mifflin County Academy of Science and Technology, Lewistown, Pa., will apply its $25,000 to acquire weld testing equipment for its new adult welding training and testing program. This addition to the shop will allow the college to provide feedback and assessment of weld quality for current and future students. In addition, the school's most recent expansion project was an adult Certified Welding program. By offering on-site testing at the school, the program will be able to make AWS testing more accessible for local individuals and provide more opportunities to become AWS Certified Welders.

"We initially applied for the grant to help get some of the critical testing equipment needed to become an Accredited Test Facility through AWS," said Mike McMonigal, supervisor of adult and postsecondary education. "We hope that utilizing the grant will get our students and the program the edge it needs to be a leading welding facility within central Pennsylvania."

Mifflin County Academy of Science and Technology applied its funds to purchase weld testing equipment for its new adult welding training and testing program. (Photo courtesy of Mifflin County Academy of Science and Technology.)

The $25,000 grant will provide much-needed equipment, electrical upgrades, and the necessary safety materials for the agricultural engineering and applied technologies program at **Mount Pleasant High School**, Columbia, Tenn. Specifically, the grant will enable the purchase of safety curtains for welding and grinding, an improved ventilation system, and multiprocess machines. It will also allow the school to elevate the available electrical output to appropriately handle the equipment as well as upgrade flexible welding and project stations.

Texarkana College (TC), Texarkana, Tex., will use its $25,000 grant to purchase four Miller XMT 350 welding machines to replace four of the older Miller Dimension™ 452 machines.

Texarkana College has plans to upgrade its outdated training machines with four Miller welding machines. Pictured is a welding student working with older equipment. (Photo courtesy of Texarkana College).

"The grant allows Texarkana College to upgrade existing training machines with equipment that provides students with access to the most current industrial technology found in today's workforce," said Texarkana College Welding Instructor Kevin Burns. "Students will benefit by learning welding skills on state-of-the-art training machines that will give them a competitive edge for employment and will provide them with greater career opportunities and higher earning potential. Despite the COVID-19 pandemic, TC's enrollment numbers are up in the program and welders are in high demand at many of our local manufacturing facilities."

The Adult & Continuing Education Center at York County School of Technology, York, Pa., is in the process of converting a classroom into a hands-on welding education workspace, which will improve the region's manufacturing workforce by increasing training capacity, with its $24,610 in grant funding. The creation of an adult education welding technology classroom will allow the school to run a day program with the potential to train up to 100 additional welders per year.

The welding technology program at **Waubonsee Community College**, Sugar Grove, Ill., will utilize its $22,500 to purchase a hydraulic wrap-around bender, a back-strap removal and preparation tool, along with associated accessories. In addition, the school plans to become an AWS Accredited Test Facility (ATF). Having the capability to offer welder performance qualification tests per code will allow the program faculty along with local and regional businesses to identify the proficiency level of welding students and cur-

rent technicians seeking professional development and/or advancement. It will also allow for certifications to be issued, and position the program to earn the AWS ATF accreditation that will result in a projected increase in the number of welding graduates and placements in welding or welding-related jobs throughout the district, region, and greater Chicago area.

Time to Apply

The AWS Foundation is committed to securing the future of the welding industry by positively impacting welding education, and the Welding Workforce Grant is the latest effort to ensure a skilled workforce is ready when industry calls.

The application cycle is currently open and schools may apply for the spring grant before the deadline. To learn more, visit *aws.org/workforcegrant* or contact John Douglass, associate director of the AWS Foundation, at *jdouglass@aws.org*. — *Roline Pascal, education editor*

General Dynamics Electric Boat Awarded $9.5 Billion by U.S. Navy for Columbia-Class Submarines

Electric Boat is the prime contractor on the design and production of a new class of submarines.

General Dynamics Electric Boat, Groton, Conn., announced the U.S. Navy has awarded it a $9.474 billion contract modification option for construction and testing of the lead and second ships of the Columbia class, as well as associated design and engineering support.

Electric Boat is the prime contractor on the Columbia-class program, which will replace the aging Ohio class of ballistic missile submarines. It will perform about 78% of the construction of the Columbia class. Not that long ago, the company shifted the program to full-scale construction at its manufacturing complex in Quonset Point, R.I. Construction of four of the six "supermodules" will take place at Electric Boat's Quonset Point facility. They will then be transported by barge to the company's Final Test and Assembly yard in Groton, Conn., where the components will be assembled into a complete submarine in a 200,000-sq-ft facility.

"Electric Boat has been making preparations for construction of the Columbia class for nearly a decade, including advancing the design of this critical Navy asset, hiring

—*continued on page 67*

The Metal Maiden Takes Its Final Form

Viewers from around the world got their first glimpse of the completed AWS welder Statue of Liberty

After months of hard work, sweat, and sparks, the American Welding Society's (AWS's) metal Statue of Liberty was revealed in its final form.

Barbie the Welder and Stephanie Hoffman co-hosted an Instagram Live from each of their shops to unveil the sculpture, which was named Metal Maiden — Fig. 1. The statue's moniker was selected in an Instagram contest posted by AWS.

During the live video, viewers tuned in from all over the world, with the post reaching more than 13,000 views at press time. The two artists talked about the project and answered questions from viewers. Metal Maiden had been

The completed Metal Maiden sits atop a forklift before being transported to Stephanie Hoffman's shop. (Photo courtesy of Hoffman.)

Fig. 1 — Stephanie Hoffman (top) and Barbie the Welder discuss the Metal Maiden project over an Instagram Live.

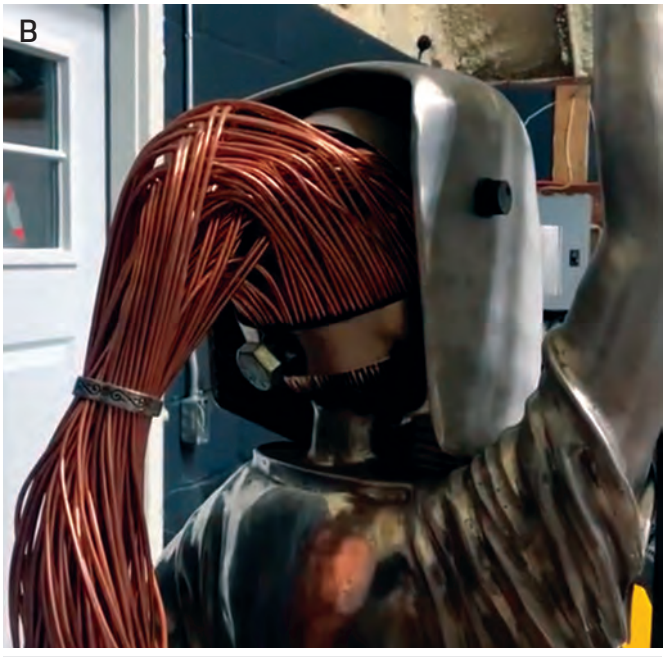

Fig. 2 — Hoffman gives viewers a look at the statue during the live video. A — The upper half of Metal Maiden; B — a close-up view of the hair.

transported to Hoffman's shop, and she panned the camera over the statue, showing off details like the engraved copper panels and riveting on the base, the foiled leaf American flag, aluminum helmet, AWS code book, and the statue's hair — Fig. 2. The live video can be seen on the AWS Instagram page *@americanweldingsociety*.

Challenges Overcome

With the fruit of their labor realized, the artists reflected on the hardest parts of the project. For Barbie, it was the body.

"Just when I thought I'd gotten done with the dress, I needed to cut her back apart," said Barbie. "So it took a very long time just to get that body where I wanted it to. But weirdly, the arms and the hands and the sleeves came together quite quickly after that."

Fig. 3 — Hoffman lays out the stars and stripes for the gold leafing. (Photo courtesy of Hoffman.)

The most challenging aspect for Hoffman was the flag draped on the body, which both artists worked on together and completed in a week filled with 12-h work days.

"Honestly, the hardest part about this was the stress I felt when we were laying out the stars and stripes . . . It was hard because [the flag] was so narrow at the top and then it flowed down. Trying to get it to make sense, that was a little bit weird. Then I had to just kind of step back for a minute and think, alright this isn't just like drawing it on a picture. It needs to have dimension; you need to remember these curves and all that," said Hoffman.

It's All in the Details

The flag has gold and silver stripes, and the canton is copper with silver stars. Hoffman used foiled gold and silver leaf to make the stripes and copper foil for the canton — Fig. 3. For the stars, she opted for vinyl over foiled leafing.

"I think the definitions of the lines would have been lost [with foil leafing], so I had some metallic silver vinyl cut for the stars. I really wanted to make sure they popped when they were all done. I didn't want it to look mushy. With all those curves, it was definitely hard to get that leafing on there," Hoffman explained.

Hoffman brought the camera down to the copper panels on the base of the sculpture, which are adorned with riveting and engravings that represent the different industries in

welding. Close-up views of the panels revealed scenes such as a chemical plant, flying airplane, oil field, skyline of New York City, a nuclear plant, robotics, and a bridge and train. The back panels feature the artists' signatures. All of the artwork was engraved by hand with multiple passes. Hoffman guessed that she spent 16 to 20 h engraving, drilling holes, and polishing the panels.

With so much metal in the sculpture, moving it was no easy feat and required a forklift — Fig. 4. Hoffman estimated the Metal Maiden weighed upward of 250 lb, standing at about 5 ft 4 in. The statue's body and the base bolt together with brackets under the dress and in the foundation. For transport, Hoffman took the pieces apart because the fully assembled statue was too heavy.

A Teaching Moment with Metal Maiden

There will be one more episode of this series in the Arc 2 Art project. Then the statue is tentatively set to reside in the AWS Careers in Welding Trailer, which Hoffman tours with across the United States to teach people about welding. The trailer's travel plans were halted in 2020 due to the COVID-19 pandemic, but Hoffman and Barbie used the live video as an opportunity to educate viewers. One person asked for advice as a woman welder who wants to take welding further than a hobby.

Hoffman suggested the viewer get lots of practice, learn as much as possible, and apply to different companies.

Barbie offered her perspective as an artist. "It is almost zero days off, and when I work in the shop or in my business, we're talking about 12- and 14-h days for like the first four and a half years," she said. "It takes an insane amount of work, so I would highly suggest if you do want to go full-time as an artist, be deeply in love with what you're doing . . . If you put in the work, it's the most glorious experience ever."

Both artists have embodied their advice, investing many hours of work and learning new skills, all culminating in the satisfaction of a job well done. WJ

Fig. 4 — At an estimated 250-plus lb, the Metal Maiden needs a forklift to be moved. (Photo courtesy of Hoffman.)

ALEXANDRA QUIÑONES (aquinones@aws.org) *is associate editor of the* Welding Journal.

AWS COUNSELOR NOMINATION

American Welding Society®

Friends and Colleagues:

The American Welding Society established the honor of Counselor of the Society to recognize members for a career of distinguished leadership contributions in the advancement of welding science and technology. Election as a Counselor is based upon an individual's career of outstanding achievements and accomplishments. The selection committee is seeking qualified individuals who can demonstrate their leadership in the welding industry as evidenced by:

- Sustained service and performance in the advancement of welding science and technology
- Publication of papers, articles and books which enhance knowledge of welding
- Innovative development of welding technology
- Society, National and Section contributions
- Professional recognition
- Leadership in AWS or other corporate levels, particularly as it impacts the advancement of welding technology
- Facilitating others to participate as a volunteer in the advancement of welding technology

For specifics on the nomination requirements, please contact Chelsea Steel at csteel@aws.org at AWS headquarters in Miami, or simply follow the instructions on the Counselor nomination form located at *www.aws.org/counselor*. Please remember, we all benefit in the honoring of those who have made major contributions to our chosen profession and livelihood. The deadline for submission is June 1, 2021. The Counselor Committee looks forward to receiving numerous Counselor nominations for 2022 consideration.

Sincerely,

David J. Nangle
Chair, Counselor Committee

IMPORTANT
Announcement

Now is your opportunity to recommend someone with a career of outstanding achievements and accomplishments in the welding industry.

Nominations For Counselor of the Society are Open.

June 1, 2021
Submission Deadline

BY TONY ANDERSON

Q: I was informed some time ago that the American Welding Society (AWS) A5C Subcommittee on Aluminum Alloy Filler Metals was working toward adding the minimum strength of aluminum filler metals as a requirement for aluminum filler metal classification in A5.10. Is this true, and if so, could you please provide some details?

A: You are correct, the AWS A5C Subcommittee, which is responsible for the A5.10 document, has been working for some time on revising this specification to include minimum tensile strength as a requirement for classification.

What is the AWS A5.10 Aluminum Filler Metal Specification?

This specification provides the manufacturing and testing requirements with which the aluminum welding wire manufacturers must comply to provide certification for their aluminum filler metal. This is also the specification referenced in many manufacturing codes and standards as a requirement for filler metal conformance for use in fabrication.

Some Recent History on the AWS A5.10 Aluminum Filler Metal Specification

The 2012 Edition of AWS A5.10

This was the first edition that incorporated a modified adoption of the ISO 18273 Standard, along with the addition of several aluminum alloy classifications from ISO 18273. One other change was the addition of filler metal classification ER4943, which was submitted as a new classification from the United States. This filler metal is a modification of Alloy 4043, which was designed to provide improved as-welded strength.

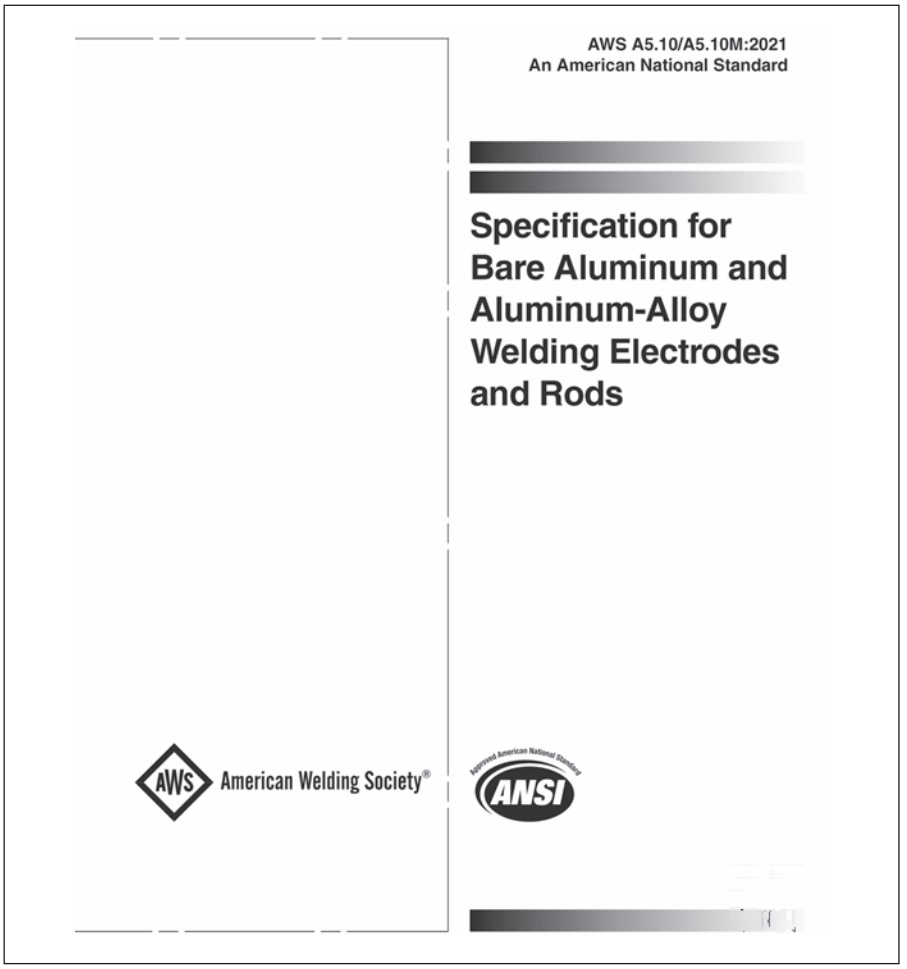

Fig. 1 — The forthcoming edition of AWS A5.10 — AWS A5.10/A5.10M:2021 (ISO18273:2015 MOD), Specification for Bare Aluminum and Aluminum-Alloy Welding Electrodes and Rods*, will be available for purchase at* pubs.aws.org.

The 2017 Edition of AWS A5.10

This was the first edition to address the strength of filler metals through the introduction of Section A10, "Mechanical Properties of Weld Metal," to Annex A. The mechanical properties of weld metal are not a mandatory requirement for classification in this edition. Typical weld metal tensile strengths were added to the annex of this specification for informational purposes only.

The 2021 Edition of AWS A5.10

The AWS A5.10/A5.10M:2021 (ISO18273:2015 MOD), *Specification for Bare Aluminum and Aluminum-Alloy Welding Electrodes and Rods*, (Fig. 1) is the most recent edition of this specification. The most significant change to this edition is the addition of a minimum tensile strength requirement for classification of filler metals. Table 2 — Required Tests has been revised to show the requirement for weld metal tensile tests for all ER classifications. The radiographic soundness test for all ER classifications and the bead-on-plate test for all R classifications remains the same.

A new table, Table 5 — Mechanical Testing Requirements (see Fig. 2), has been added to show the minimum tensile strength requirements for each filler metal classification listed in the table. The notes in Table 5 state not all the classifications listed in Table 2 are provided with minimum tensile strengths. There are currently 11 clas-

Table 5
Mechanical Testing Requirements[a]

AWS Classification	Tensile Strength, minimum (ksi) [MPa][c]	Yield Strength (ksi) [MPa][b]	Percent Elongation[b]
ER1100	11 [75]	Not specified	Not specified
R1100	11 [75]	Not specified	Not specified
ER2319	35 [240]	Not specified	Not specified
R2319	35 [240]	Not specified	Not specified
ER4043	24 [165]	Not specified	Not specified
R4043	24 [165]	Not specified	Not specified
ER4047	25 [170]	Not specified	Not specified
R4047	25 [170]	Not specified	Not specified
ER4145	40 [275]	Not specified	Not specified
R4145	40 [275]	Not specified	Not specified
ER4943	30 [205]	Not specified	Not specified
R4943	30 [205]	Not specified	Not specified
ER5183	40 [275]	Not specified	Not specified
R5183	40 [275]	Not specified	Not specified
ER5356	35 [240]	Not specified	Not specified
R5356	35 [240]	Not specified	Not specified
ER5554	31 [215]	Not specified	Not specified
R5554	31 [215]	Not specified	Not specified
ER5556	42 [290]	Not specified	Not specified
R5556	42 [290]	Not specified	Not specified
ER5654	30 [205]	Not specified	Not specified
R5654	30 [205]	Not specified	Not specified

[a] Listed classification must meet the minimum tensile strength shown. For all other classifications, tensile testing is required to be reported, but minimum requirements have not yet been established for those classifications. As additional data is made available, alloys will be added to this table. Inclusion in this table may be necessary for use in some design codes.
[b] The Yield Strength and Percent Elongation shall be tested and reported on the test certificate.
[c] The minimum tensile strength of R classifications is addressed by the testing requirements of the same ER classification as prescribed in Table 2.

Fig. 2 — Table 5 from AWS A5.10/A5.10M:2021.

sifications listed with minimum tensile strength requirements in Table 5. These include all the commonly used classifications and some less commonly used. Any classification listed in Table 2 that does not have a minimum tensile strength listed in Table 5 is still required to be tested and reported for it to be eligible for AWS A5.10 classification. As additional data is made available to the AWS A5C Subcommittee, additional filler metal classifications will be added to Table 5.

Conclusion

For some years, the AWS A5 Committees have discussed adding the minimum strength of aluminum filler metal as a requirement for classification to the A5.10 Standard. The minimum strength requirement of many other filler metal materials has been addressed in the relevant A5 Standards for many years. It was seen by the A5 Committee, which approved the latest edition of the A5.10 document, to be the time for aluminum filler metals to also have an appropriate strength value designation attached to their specific classifications.

I believe providing the selection of a filler metal that is certified by its AWS classification to provide a minimum required strength, as well as the other minimum quality requirements addressed by the standard, to be a good thing for our industry. WJ

TONY ANDERSON is director of aluminum technology, ITW Welding North America. He is a Fellow of the British Welding Institute (TWI), a Registered Chartered Engineer with the British Engineering Council, and holds numerous positions on AWS technical committees. He is chairman of the Aluminum Association Technical Advisory Committee for Welding and author of the book Welding Aluminum — Questions and Answers *currently available from AWS. Questions may be sent to Tony Anderson c/o* Welding Journal, *8669 NW 36 St., #130, Miami, FL 33166-6672, or via email at* tony.anderson@millerwelds.com.

BY ALEXANDER E. SHAPIRO

Q: Our company is manufacturing instruments working in deep cryogenic environments at temperatures close to liquid helium. We are looking for appropriate filler metals that possess superconductivity but found no standard filler metal for this application. Maybe you can recommend superconductive brazing alloys suitable for industrial application? Stable production quality is a plus.

A: Several standard solders and brazing filler metals are utilized to join oxygen-free copper, stainless steels, niobium, titanium, and alumina ceramic in the manufacture of superconducting cavities used in particle accelerators for electrons and ions, helium isotope dilution refrigerators, coils in engineering devices, the cryogenic plumbing system in the cryomodule, electrical connectors of Nb_3Sn/Cu superconducting strands, etc. Solders Sn-4Ag, Sn-40Pb, and Sn-58Bi as well as silver brazing filler metals BAg-1, BAg-1a, BAg-2, BAg-3, BAg-7, BAg-8, Cusil®ABA, and Palcusil® (Refs. 1–3) are among them.

Advantages of these solders and filler metals are easy availability, predicted strength and microstructure, and the stable quality that you requested. Also, these alloys are compatible with a broad spectra of base materials and are not brittle at liquid helium temperatures. The most important drawbacks are a very low temperature T_C < 0.1 K of superconductivity or no superconductivity at all. This means that electrical resistivity along electrical conducting lines is drastically changed in brazed or soldered joints, which may also affect local changes of temperature and magnetic field. For example, values of electrical resistivity of copper and solders in cryogenic environments are presented in Table 1 (Ref. 2).

An important characteristic of this joint is the electrical resistance, which determines the heat generation during the passage of an electric current through it. This influences the transfer of liquid helium to the gas and the conditions of cooling the superconducting coils. Critical temperatures of superconducting alloys are presented in Table 2. Electrical resistance is zero below these temperatures. Soldered copper lap joints immersed in liquid helium (at the temperature ~ 4 K) exhibit electrical resistance at 1000 A, shown in Table 3. The solder was a standard lead-free Sn-4Ag alloy (Ref. 2).

We can see that standard solders are not superconductors, as the electrical resistance of soldered joints is > 0 at temperatures lower than critical for base metals to be joined. Besides, electrical resistance-to-overlap ratios are not linear: Increasing overlap five times results in the decrease of electrical resistance around eight times. This means that the edge effect is valuable due to a large local change of physical properties of the solder and base alloys. Also, there is a problem in soldering technology: We still do not have soldering fluxes compatible with niobium alloys, which are contained in all industrial superconductors.

Silver-based filler metals also have a critical temperature significantly below T_C of superconducting base materials. For example, the critical temperature of BAg-3 (Ag-Cu-Zn-Cd) is ~ 0.096 K, which cannot be obtained in liquid helium. Furthermore, silver-copper alloys partially display the Meissner effect (exclude magnetic fields in the superconducting state), which limits their use in many applications (Ref. 1).

Table 1 — Electrical Resistivity of Oxygen-Free Copper and Solders at Cryogenic Temperatures

Alloy or Solder	Electrical Resistivity, nΩ·m	Temperature, K
Oxygen-free copper	0.2	4–20
Oxygen-free copper	1.0	50
Oxygen-free copper	10.0	200
Sn-40Pb	1.5	10
Sn-40Pb	3.0	20
Sn-4Ag	0.4	4–10
Sn-4Ag	1.5	20
Sn-4Ag	100	300
Indium	0.03	5

Table 2 — Electrical Resistance of Superconducting Alloys below the Critical Temperature T_c

Superconductors	Electrical Resistance, nΩ	T_c, K
Nb	0	9
Nb_3Sn	0	18
Nb_3Ge	0	23
NbZr	0	11
NbTi	0	10
Nb_3Al	0	18

Table 3 — Electrical Resistance of Copper Soldered Joints in Liquid Helium at the Current 1000 A

Electrical Resistance, nΩ	Length of Overlap, cm
42	1.0
20	2.0
9	3.0
5	5.0

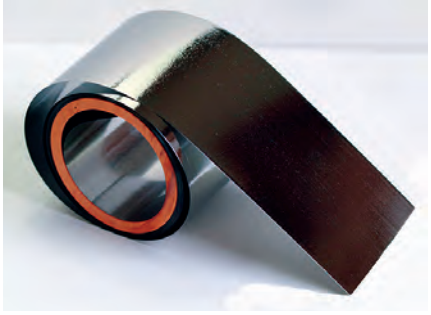

Fig. 1 — Amorphous foil TiBraze620 to form NbTi and NbZr superconducting phases after brazing.

To provide physical properties of filler metals compatible to the base materials at liquid helium temperatures, our industry continues to design and try to manufacture superconducting brazing filler metals, such as Nb-(44-49)Sn wt-% or Nb-(30-38)Sn wt-%, that can be made as powders sintered further in strips 0.4–0.5 mm thick. Vacuum brazing with these alloys can be done at 930°–960°C.

The alloy TiBraze620 containing Ti, Zr, and Nb is already in use as amorphous foil 65–75 microns thick — Fig. 1. Superconducting phases NbTi and NbZr can be obtained after diffusion heat treatment of brazed joints.

Copper-based powdered brazing alloys containing Nb, Sn, and Ti are manufactured from the existing TiBraze900V (Cu-20Sn-18Ti wt-%) filler metal having brazing temperatures in the range 900°–950°C (Ref. 4). These brazing alloys use the so-called "bronze method," where tin and niobium form a superconductive Nb_3Sn phase, while copper does not react with niobium according to the binary Cu-Nb phase diagram. Additionally, the superconductive NbTi (Table 2) phase can be obtained in brazed joints during a post-braze diffusion heat treatment. WJ

References

1. Thompson, J. R., and Thomson, J. O. 1978. Superconducting silver brazing alloy. *Rev. Sci. Instrum.* 49(10): 1485, 1486.

2. Schoerling, D., Heck, S., et al. 2012. Electrical resistance of Nb3Sn/Cu splices produced by electromagnetic pulse technology and soft soldering. *Supercond. Sci. Technol.* 25: 025006.

3. Calliari, I., Ramous, A. E., et al. 2004. Characterization of vacuum brazed joints for superconducting cavities. *Microchim. Acta* 147: 141–146.

4. Shapiro, A. E. 2020. Future applications and new brazing materials. Lecture, Columbus, Ohio.

ALEXANDER E. SHAPIRO (ashapiro@titanium-brazing.com) *is CEO of Titanium Brazing Inc., Columbus, Ohio. This column is written sequentially by TIM P. HIRTHE, ALEXANDER E. SHAPIRO, and DAN KAY. Hirthe and Shapiro are members of and Kay is an advisor to the C3 Committee on Brazing and Soldering. All three have contributed to the 5th edition of the AWS* Brazing Handbook. *Readers are requested to email their questions for use in this column to the authors,* aquinones@aws.org, *or send to their attention at* Welding Journal, *8669 NW 36 St., #130, Miami, FL 33166.*

BY JOSH PAWLEY

Cobot Welding Produces Aluminum Rim Products

Specialty Rim Supply (SRS), a provider of precision spun-forged aluminum rims founded in a former brewery building in Terre Haute, Ind., has reinvented the aluminum wheel with its proprietary radial forging process. This process produces a seamless 6061-T6 aluminum rim with an extremely fine radial grain structure that provides the highest strength-to-weight ratio.

A key success factor of SRS from the outset has been leveraging innovative and entrepreneurial manufacturing methods to supply high-quality custom aluminum rims made in the United States.

SRS Co-owner Rich Cuvelier, who has been with the company since it was founded in 1995, had an idea early on to provide rims with a welded flange assembly to address a specific market need. He knew that the welding of the flange assembly would need to be automated. Both robotic and fixed-automation options were evaluated at the time, ". . . but the problem 20-plus years ago was that the upstream manufacturing processes weren't consistent enough to enable automation in the weld shop," Cuvelier said.

The importance of consistent upstream processes in facilitating successful weld automation hasn't changed over the last 25 years, but luckily, the capabilities of upstream equipment have. So, in 2020, now armed and experienced with upstream processes that provide exceptional consistency, Cuvelier revisited the welded modular assembly rim.

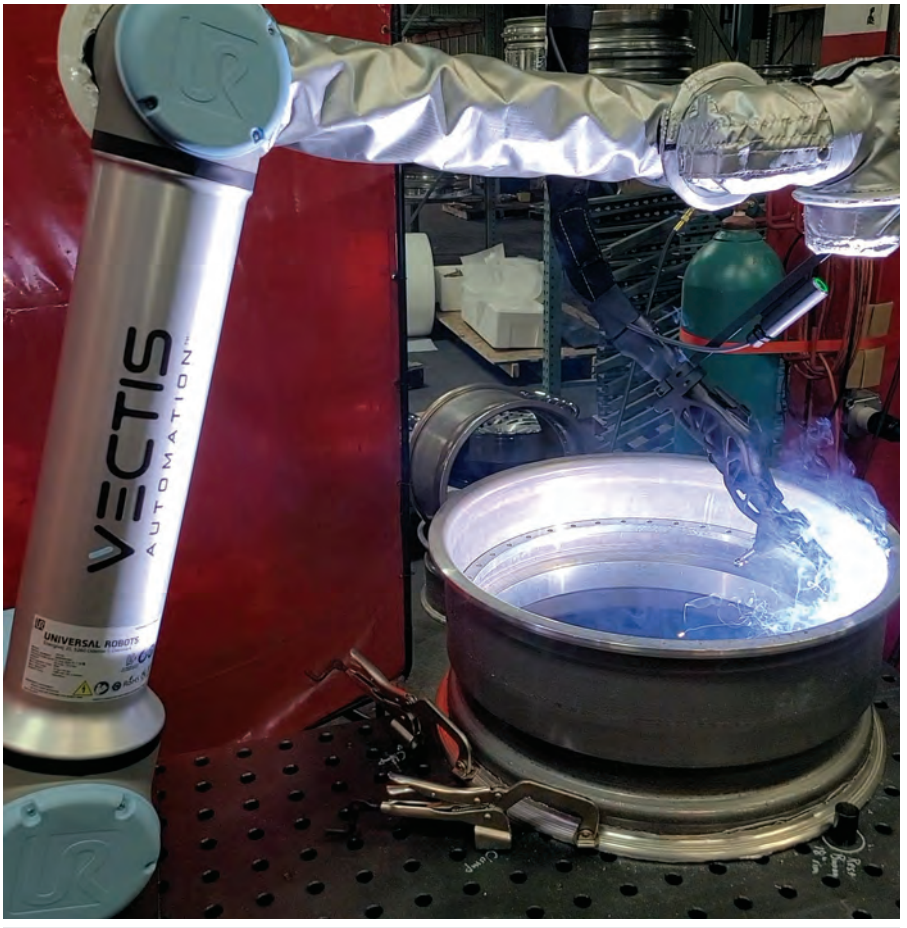

The Cobot Welding Tool is shown here in production at Specialty Rim Supply's facility on a program they created in-house.

Baby Steps: Leveraging Automation Experts for the Proof-of-Concept

Cuvelier knew that automation in the weld shop was the right path for the new rim design to achieve quality and production standards that are typical of SRS products. He turned to welding automation industry experts, including Vectis Automation, to help evaluate the project's feasibility.

Vectis Automation is a Colorado-based integrator that empowers manufacturers to automate their welding with an easy-to-use, flexible, and affordable collaborative robot (cobot) welding system. The company's Cobot Welding Tool is a 3 × 6 ft mobile welding tool that incorporates a Universal Robots cobot. The cobot tool has built-in safety sensors that allow it to operate without costly peripheral safety equipment or external perimeter caging.

"The small and mobile footprint of the cobot-based system was really valuable to us — especially when paired with the Vectis platform's easy programming," Cuvelier said.

After an initial application discussion with the Vectis team, Cuvelier sent rim samples to Vectis and a few other integrators for initial weld trials to determine which integrator would serve as the best long-term partner.

"It was important for me to not only see the weld results upfront before pulling the trigger but also to see how each integrator operates," Cuvelier said.

Vectis's Director of Business Development and Founding Partner Josh Pawley agreed with Cuvelier's sentiment.

"We are the only integrator in the market that offers a 30-day return pol-

Fig. 1 — The Vectis applications engineering team used a tight, crisp arc paired with a heavy push angle to achieve both deep penetration and an ideal bead profile.

Fig. 2 — The touch probe leverages a 3D printed design and Vectis's unique force-based Touch Sensing feature to accommodate the wide variety of SRS custom rims.

icy on our systems. Many think that's crazy, but we've never had a system returned. The pre-sale application evaluation process led by our team of technical experts is a key reason why," Pawley said.

Using the aluminum configuration of their Cobot Welding Tool that employs Miller® synergic pulse welding equipment and a push-pull gun for reliable feeding of soft aluminum, the Vectis and SRS team collaborated remotely, due to COVID-19, to hone in the weld process to SRS's needs. A key design consideration of the welding process was to achieve sound penetration with a 3/64-in. 4043 wire while also minimizing the size of the bead face, so the weld didn't obstruct the bolt and nut that would later be added to the assembly flange. To achieve this, the Vectis team tightened the arc cone by lowering the trim and increasing the SharpArc setting. They then paired that with a 30-deg push angle and a travel speed of 27.5 in./min to promote proper wet-in at the toes.

"The welds were gorgeous, and the penetration on the etched cross section was exceptional. Exactly what we were looking for and at a very quick weld travel speed to boot," Cuvelier said. The etched trial is shown in Fig. 1.

From Proof to Production

With the weld parameters proven out, Cuvelier and the Vectis team continued to collaborate on the next challenge — how to economically program SRS's broad range of part configurations.

"Our batch size can often be as small as four rims. The flange's axial location will vary based on our customer's needs, so I needed an automation solution that could handle that product spread . . . it just wouldn't be economical for us to hand-program every batch," Cuvelier noted.

To solve this challenge, the Vectis team leveraged its unique force-based Touch Sensing software feature, which allows the cobot to search a surface with tactile feedback and then offset a weld path based on that search — Fig. 2. A custom touch probe was designed and fabricated that would allow the cobot to reach and reliably search the various conditions of the flange assembly location.

The final piece of the puzzle was ensuring that the SRS team had the tools and training they needed to be successful with the system.

"We didn't have to pay for Vectis to come onsite or have our guys go to their facility during COVID-19. They provided a shell program and instructional videos that our team used to get the system setup and producing very quickly," Cuvelier said.

Since receiving the system, the SRS team has added programs for different sizes of wheels and made slight adjustments to the weld parameters to get the exact weld profile they are looking for — Figs. 3, 4. In addition, the Vectis

Fig. 3 — A close-up of the live welding shown in the lead photo.

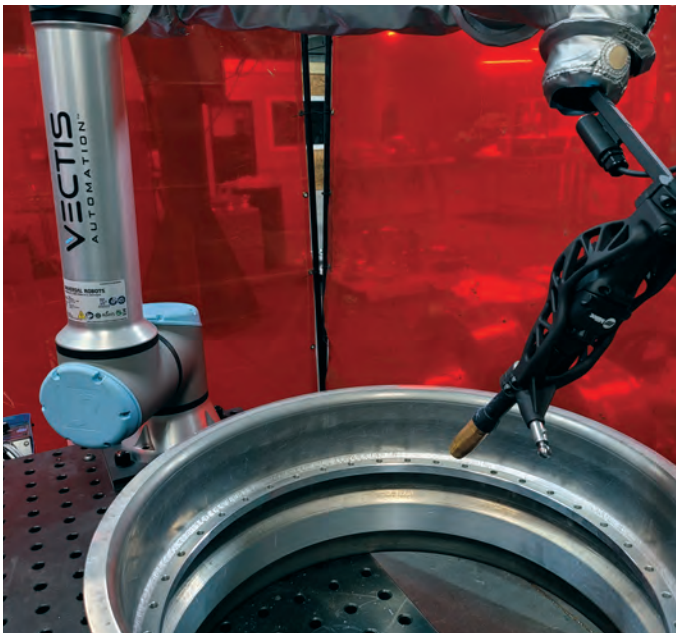

Fig. 4 — Final product of the fully welded wheel.

and SRS teams have continued to collaborate on how to further improve the process. One suggestion that came up during preproduction trials was to increase the bevel angle on the flange assembly, which would both increase penetration depth and decrease bead size to help keep weld material out of the bolt/nut areas.

Automation Advice

For those looking at automating, Cuvelier offers the following advice: "First, go with an automation partner that knows the technical side of the application you are looking at. That was critical to us in deciding who to go with and has since been key to success in our project throughout. Second, you've got to have the part and fixture consistency. We didn't have it 25 years ago but we've got it now, and it's another key to our success. Lastly, we've got the right people on our team [who] are programming and running the system . . . they've really taken ownership of the project."

"[Cuvelier] hit on two of the three key points we always talk about with customers: repeatable parts and fixturing and an eager cobot champion [who] takes ownership of the project success. Only thing I'd add is, when possible, start with the low-hanging fruit (brackets, subassemblies, piece parts, etc.) to build quick wins, confidence, and start the ROI [return on investment] . . . then graduate to the more complex weldments," Pawley affirmed. WJ

JOSH PAWLEY (josh.pawley@vectisautomation.com) *is a founding partner and director of business development, Vectis Automation, Loveland, Colo.*

The Value of a Trade School Education

The article "Battling the Trades Stigma" in the April 2020 *Welding Journal* (p. 52–55) drew my immediate attention and brought back many fond memories of my high school days at St. James Trade School in Riverton, Ill. My name is Robert (Bob) Doan. I was born three years before Bugs Bunny (1937) and became a cross-country pipeline welder at the age of 19. In 1973, I started the R. L. Doan Welding Co. and employed 27 pipe and structural welders. In 1980, I designed my first pipe fitting tool and called it a Flange Wizard. This tool was the first of 60-some fit-up tools my company offers today. I formed my present company, Flange Wizard Inc., 40 years ago in 1981. It is a successful manufacturing company of precision welding tools sold all over the world.

My point is this: A lot of high school students are not interested in being in the medical field or studying law or entering the teaching profession. I was one of those students. I attended a trade school from 1951 until 1955. I graduated with two diplomas — a high school diploma and a four-year apprenticeship in machine shop and welding trades. I have never been without a job. Our country needs many more of these trade schools to educate our children who have the imagination and motor skills to keep our highways, refineries, and bridges from deteriorating.

William Rice, chair of the AWS Foundation, said it well in the *Welding Journal's* October 2020 Editorial. "Welding professionals and businesses will be essential to the reindustrialization of America. It is critical that we put a focus on training and educating the next generation of leaders for our industry."

I am a Life Member of the American Welding Society and was honored to be a recipient of the Excellence in Welding Award in 2016. I have stayed with my trade all my life.

Robert L. Doan, "The Wizard"
Placentia, Calif.

American Welding Society

Dear Readers

The *Welding Journal* encourages an exchange of ideas through letters to the editor. Please send your letters to Cindy Weihl, *cweihl@aws.org*.

Consumables System Adds Pin Offering for GMAW Guns

The expanded AccuLock™ S consumables system includes Lincoln® and Tweco® #4 and #5 power pins. All of the power pins are configurable options for the company's BTB semiautomatic air-cooled gas metal arc welding (GMAW) guns using the online configurator. The consumables system addresses errors in liner trimming by locking and concentrically aligning the liner between the contact tip and the power pin without the need for fasteners. Installation and replacement of the liner is an error-proof process that requires no measuring; users simply load the liner and trim it flush with the power pin. The consumables system also provides a wire feeding path that minimizes the downtime associated with issues like burnback and birdnesting. With optimized wire feeding, the contact tips in the system last two to three times longer.

Bernard®
bernardwelds.com
(855) 644-9353

Abrasive Disc Uses a Paired Flap to Enable Aluminum Grinding

The Tiger® Aluminum flap disc features a paired flap for easy grinding of aluminum. The design has a top flap with a coating that prevents loading, provides a high cut rate, and eliminates the need to apply wax or lubricant prior to grinding. Additionally, its

alternating flaps of self-sharpening zirconia aluminum grains offer aggressive material removal. The 4½-in. flap disc comes in Type 27 or 29 with either ⅞ or ⅝–11 arbor holes. They are also offered with two grit options: 36 or 60. The 36-grit disc works for chamfering, weld removal, and stock removal. The 60-grit disc performs weld blending, finishing, and cosmetic detail work. The flap discs are suited for applications found in general metal fabrication, shipbuilding, rail, and automotive industries.

Weiler Abrasives
weilerabrasives.com
(800) 835-9999

Consumables Showcase a Pointed Geometry

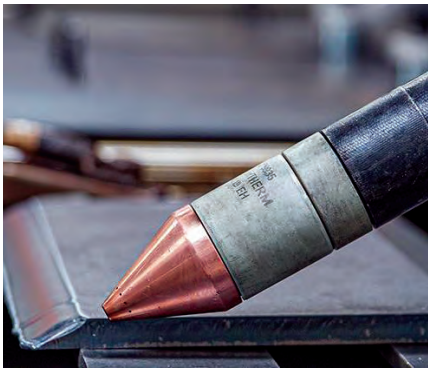

The extreme bevel consumables offer an aggressive pointed geometry so the plasma torch can tilt to an angle of up to 66.5 deg. The consumables are designed for mechanized, robotic, and handheld cutting. This makes them suitable for a range of jobs, including steep mechanized beveling, tube and pipe cutting, structural steel work, and pressure vessel construction. The con-

sumables also allow operators to see what they are cutting and gives them better access to beam flanges and areas with limited clearance to achieve better cuts and fewer secondary operations. Designed for the MAXPRO200® LongLife® plasma cutting system, the consumables are available for both air and oxygen cutting at 130 and 200 A. They can be purchased separately or as part of a starter kit that includes consumables for all the extreme bevel cutting processes offered for the plasma cutting system.

Hypertherm
hypertherm.com
(800) 737-2978

Report Predicts Growth for the 2021–2026 Aluminum Welding Wire Sales Market

Global Aluminum Welding Wires Sales Market Report 2020 estimates this industry will reach $510.2 million from 2021 to 2026, an increase from $391.8 million in 2020, at a compound annual growth rate of 4.5%. The 141-page report is segmented by company; region (United States, Europe, China, Japan, Southeast Asia, India, etc.); type of aluminum (pure, aluminum-magnesium, and aluminum-silicon); and application (automotive, shipbuilding, appliance, etc.). It also offers a dashboard overview of leading companies, including their marketing strategies, market contribution, and developments from 2015 to 2020. It identifies North American and Europe as having the highest concentration of major manufacturers of aluminum welding wires. Additionally, it distinguishes ESAB as a world leader with 23% of the market's share in 2017.

360 Research Reports
360researchreports.com
(424) 253-0807

Pin Location Jaws Provide a Firm Grip on Fragile Workpieces

The pin location jaws for air chucks offer accurate gripping on fragile components — such as deformation-sensitive parts and thin-walled workpieces — without damaging surfaces. They are computer numerical control milled and manufactured for Northfield®, Microcentric®, and more to provide workpiece location accuracy. Made for chuck sizes ranging between 4 and 10 in. diameters, the full-grip (pie) jaws come in 1018 steel and 6061 aluminum with jaw heights between 1 ft and 4 in. They can also be customized per customer request.

Dillon Mfg. Inc.
dillonmfg.com
(888) 908-8762

Calculator Determines Viable Dissimilar Materials Joining

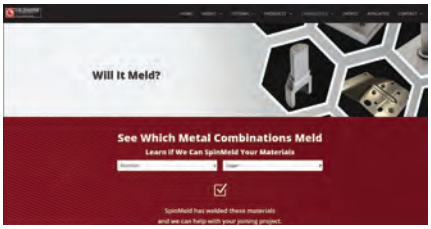

The Will It Meld calculator enables companies to determine if dissimilar materials can be joined by SpinMeld™ rotary friction welding systems. To use the calculator, users can visit *coldwatermachine.com/will-it-meld* and select the two materials they would like to weld from a drop-down list of more than 35 substances, including aluminum, magnesium, and composites. Depending upon the selected materials, the result will either say that the materials can be joined, the materials have not yet been proven to be joined, or to contact the company for more information on the application.

Coldwater™ Machine Co.
coldwatermachine.com
(419) 678-4877

Free Learning Management Software Facilitates Welding Education

OpenBook™, a free learning management software, provides welding instructors with an easy tool to teach welding concepts and techniques that are aligned with American Welding Society SENSE standards. The updated online learning tool features curated courses, e-learning modules, and quizzes to keep students engaged and help instructors spend less time compiling resources. It also delivers real-time student feedback to easily monitor and assess student performance. Other features include hyperlinks and formatting tools that allow instructors to connect lessons, materials, and videos from outside sources right into the quiz builder platform; custom certificates of achievement that are automatically generated; and a help page that supplies the latest information so instructors can find answers to their questions. The learning management software can be accessed at *openbook.millerwelds.com*.

Miller Electric Mfg. LLC
millerwelds.com
(920) 734-9821

Risk Management App Boosts Safety on Construction Sites

The Construction Solutions mobile app helps construction workers manage their risks while improving safety and quality on the job. It allows workers to digitally complete reports and assign observations related to dangerous conditions or subquality work on construction sites. This information is then available to risk managers and supervisors in near real-time, allowing them to quickly react to individual issues and see trends across the larger data set. The app also tracks and confirms that safety, program, and quality controls are being addressed. Additionally, it can also be used to send messages, such as product recall alerts, risk alert notices, reminders about webinars, and information about emergency preparedness for storms and other important topics. If a user has not downloaded the app, it offers the ability to link a specific form to a QR code so any employee, contractor, subcontractor, or vendor involved with a specific job site can complete a required form.

Zurich North America
zurichna.com
(800) 382-2150

Multiprocess Welding System Unveils Enhanced Capabilities

The Gold Track® VII orbital welding power supply with controller delivers the functionality of its predecessor but with improved speed and efficiency.

Delivering 600 A at 100% duty cycle, the multiprocess system performs gas tungsten, gas metal, and plasma arc welding processes. To facilitate welding, it comes with automatic weld-head recognition and calibration management. The welding system is also easy to use due to its large, 12-in. touch screen and multilanguage interface as well as its built-in data logger with graphical user interface. Some of its other standard features include a programming and setup tablet; four servos with digital current limiting; encoder, tach, and back electromotive force feedback support; telemetry monitoring with fault detection and event trigger; and MODBUS connectivity for system integration. Optional features are also available, including eight servos, a stepper drive, smart motor support, CANBUS connectivity for factory automation, and additional gas controls (up to three).

Liburdi Dimetrics Corp.
liburdi.com
(800) 991-2100

THE SWITCHOVER SYSTEM WITH SMART TECH

HARRIS® SPECIALTY GAS Equipment

STRENGTHEN YOUR BUSINESS STRATEGY WITH DATA.

DataSMART™ uses the most advanced reporting features in the market today to collect and report usage data for easy analysis. Choose the smart solution to help your customers fully maximize their gas usage.

PERFECT FOR

- Laser Cutting Operations
- Metal Fabricators
- Welding Job Shops
- Analytical Laboratories

EASY-TO-USE TOUCH SCREEN SETUP

DATA AT YOUR FINGERTIPS

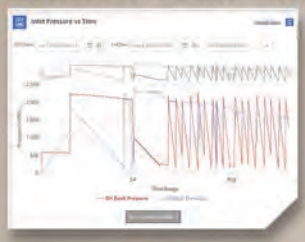

Turn to the Pros

HARRIS
A LINCOLN ELECTRIC COMPANY

CONTACT A HARRIS® SPEC GAS EXPERT
1.800.733.4043 *ext. 2*

harrisproductsgroup.com
harrisspecgas@lincolnelectric.com
www.HarrisSpecGas.com

IF IT USES GAS, IT NEEDS HARRIS.®

Using Alternate Fuel for Heating Applications

To achieve optimal performance, efficiency, and safety in heating, it is key to have the correct fuel gas and equipment

BY TIMOTHY READING

Oxyfuel has been used in a variety of applications for cutting, brazing, welding, and heating for more than 100 years. In fact, John Harris invented the flame cutting torch in 1899, which led to the founding of Harris Calorific (Ref. 1).

While much has been written about oxyfuel as it relates to cutting, brazing, and welding, its significant role in preheating applications has not been as widely addressed, nor has the increasing role played by alternate fuels in this process.

The Preheating Process

Preheating or heating involves heating the base metal, either in its entirety or just the region surrounding the joint, to a specific desired temperature, called the preheat temperature, before welding. Heating may be continued during welding, but frequently the heat from welding is sufficient to maintain the desired temperature without a continuation of the external heat source.

Reasons for Implementation

Typically, preheating is essential when there are larger, thicker pieces of material, such as in large-scale manufacturing, shipbuilding, or construction.

There are four primary reasons to utilize preheat, as detailed below.

1) It lowers the cooling rate in the weld metal and base metal, producing a more ductile metallurgical structure with greater resistance to cracking;

2) The slower cooling rate provides an opportunity for any hydrogen that may be present to diffuse out harmlessly without causing cracking;

3) It reduces the shrinkage stresses in the weld and adjacent base metal, which is especially important in highly restrained joints; and

4) It raises some steels above the temperature at which brittle fracture would occur in fabrication.

Additionally, preheat can be used to help ensure specific mechanical properties, such as notch toughness.

For optimal performance, efficiency, and safety in heating, it is important to have both the proper fuel gas along with equipment.

Alternate Fuel Highlights

Using an alternate fuel, such as propane, propylene, natural gas, and proprietary gas blends, in heating can provide cost and performance benefits.

Acetylene can be used for heating applications, but there are many restrictions and safety concerns. With acetylene, there is a limit to the amount of gas that can be withdrawn from a cylinder; only one-seventh of the volume of the cylinder can be withdrawn at any one time. Even the largest acetylene cylinders will not provide enough gas for the flow rates required by larger heating tips. Therefore, to properly and safely heat with acetylene, you have to use small heating tips and typically pigtail multiple cylinders together to allow

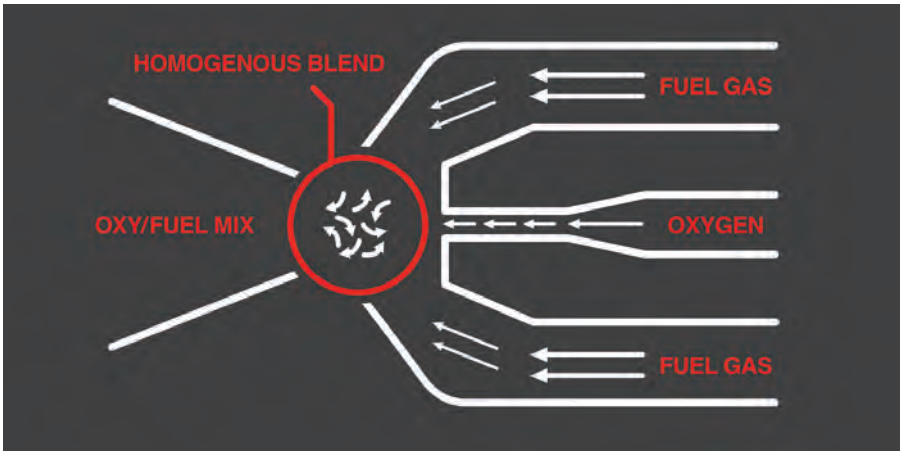

Fig. 1 — Alternate fuel torches incorporate injector mixers designed to reduce preheat times and deliver more BTUs, which results in a greater combustion efficiency.

for the needed withdrawal rates. In addition, acetylene cannot be used at pressures higher than 15 lb/in.^{2}, where the gas becomes unstable and can decompose explosively.

With alternate fuels, you are not limited to the one-seventh withdrawal rule or pressure restrictions, so larger tips can be used. In addition, fewer cylinders of gas are needed, so there are lower handling costs and rental charges, adding to the cost savings of alternate fuels.

Alternate fuels produce more BTU/ft^3 without extreme high pressures, allowing for better heating efficiency. By using alternate fuels in the oxyfuel heating process, you will reach the targeted heating temperature faster than with acetylene.

The Importance of Pressure Settings, Avoiding Restrictions

Two main issues need to be addressed in heating applications when compared to cutting applications. Both issues relate to the volume of gas used in heating processes. One issue concerns having proper pressure settings at the regulators, and the other issue concerns avoiding restrictions in the torch, the tip, the hose, or even within the safety devices (flashback arrestors).

For proper and safe heating, the gas must come out of the tip at the same rate or velocity as the flame burning back, so an equilibrium is created. That equilibrium should happen at the end of the tip. With too much gas (pressure settings too high), the flame is not able to burn or propagate at a fast enough rate, and the flame can be blown off the tip. If there is not enough gas (pressure settings too low or restrictions in line) to equal the burning velocity of the flame, the flame will burn back into the equipment. These burn backs not only cause damage to the equipment (the tips can melt, closing some of the orifices and compounding the restrictions), they also put the operator at even greater risk of injury.

Ideal Equipment

Different heating tips should be used depending on the heating application, as opposed to just decreasing or increasing the pressures for one tip size. But more must be done than merely changing tip sizes.

Fig. 2 — The K-43 heating torch assembly by Harris contains the Model 43-2 high-capacity torch handle to provide adequate gas flow for use with the largest heating tips.

Use the Proper Size Flashback Arrestor

A common heating problem seen with our customers concerns backfires or flames coming back into the torch. We often find they were using acetylene and had improper equipment, and this has resulted in injuries. They may try putting on additional flashback arrestors without realizing these devices can be making the problem worse.

Flashback arrestors inherently cause about a 25% restriction of the flow of gas. This being said, flashback arrestors may be used between the regulators and the torch, but you must be sure to use the proper size. For example, a standard size flashback arrestor can be used for The Harris Products Group acetylene tips up to #4 and the company's alternate fuel tips up to #2. For tips larger than those, high-flow flashback arrestors must be installed. Also, it is not recommended to use multiple sets of flashback arrestors (i.e., on both the regulators and the torch) in a single setup. A single set of flashback arrestors sized properly for either the torch or the regulators should be used.

Handles and Mixers

For safe and proper heating, the operator should have a heavy-duty, high-flow capacity handle. These handles have larger tubes and valves to accommodate the increased volume of the gas flow needed. Along with the proper handle and tips, hose size is important. Just like with flashback arrestors, a ¼-in. oxyfuel hose can be used for Harris alternate fuel tip sizes #1 and #2. But for tip sizes #3 and above, a ⅜-in. hose is required to allow enough gas flow.

Manufacturers have developed special torches and tips to meet the exacting demands of heating. For example, Harris has designed heavy-duty handles and mixers that help reduce heating times and provide optimal BTU efficiency — Fig. 1. In particular, the K-43 heating torch assembly features the Model 43-2 high-capacity torch handle to provide adequate gas flow for use with the largest heating tips — Fig. 2. In addition, the K-43 assembly includes the Model E3-43 mixer, which can be used with any size heating tip, and a 2393 stainless steel tip tube.

Recently, one of our structural manufacturing customers asked for help with their submerged arc welding application. They were trying to heat using multiple cylinders of acetylene and were not able to achieve the temperatures needed for the application. They also melted multiple heating tips in the process. Following the advice of changing to alternate fuel and using the K-43 assembly, they were able to achieve the preheating that was essential for the project with one cylinder of fuel gas.

Parting Thoughts

With alternate fuel and the proper equipment, a user can generate up to a million BTUs and handle any heavy-duty heating application. More information about the uses and benefits of alternate fuels can be found at *harrisproductsgroup.com/alternatefuel*. WJ

Reference

1. The Harris Products Group, History. Retrieved December 23, 2020, from *harrisproductsgroup.com/en/company/History.aspx*.

TIMOTHY READING (timothy_reading@lincolnelectric.com) *is district sales manager with Harris Products Group, Mason, Ohio.*

Advances in Filler Metals for LNG Tank Welding

Experts share challenges and solutions

BY NEIL FARROW

From extraction, to processing, to transportation to points of use, natural gas and liquefied natural gas (LNG) seem inexorably linked to welding. This trend is set to continue as the global demand for cleaner energy drives the preference for natural gas. Composed of 85 to 95% methane — the cleanest burning fossil fuel — natural gas feeds the energy needs of more than 1900 U.S. power plants, about 195,000 industrial facilities, and more than 60 million U.S. homes.

Worldwide, LNG is now replacing heavy fuel oil in marine propulsion systems because the International Maritime Organization (IMO) decreased the permissible sulphur content in marine fuels to curb greenhouse gas emission. LNG does not emit sulphur oxides or particulate matter, and it releases about 90% less nitrogen oxides and 30 to 50% less CO_2 compared to conventional fuels such as diesel. Even better, LNG offers a lower energy cost per ton because it contains 20% more energy for a given mass compared to fuel oil. Today, the U.S. has several LNG bunkering (storage and transfer) facilities to provide LNG fuel for ships.

In North America, there are 15 to 20 large projects that have been approved or recently completed, including several peak shaving operations. One of the most common uses for LNG, peak shaving, is when power plants store LNG so that they can draw on it to meet spikes in electricity demand during periods of extreme heat or cold.

Converting natural gas to LNG requires removing almost all other elements so that the gas is almost pure methane. Then, by applying extreme refrigeration technology (cryogenics), the gas is cooled to approximately –162°C (–270°F), at which point it becomes a liquid that weighs about half as much as the same volume of water. Most importantly, liquifying natural gas reduces its volume 600 times compared to its volume at ambient temperature, making it convenient to store and transport.

For cryogenic applications, most engineers around the world choose

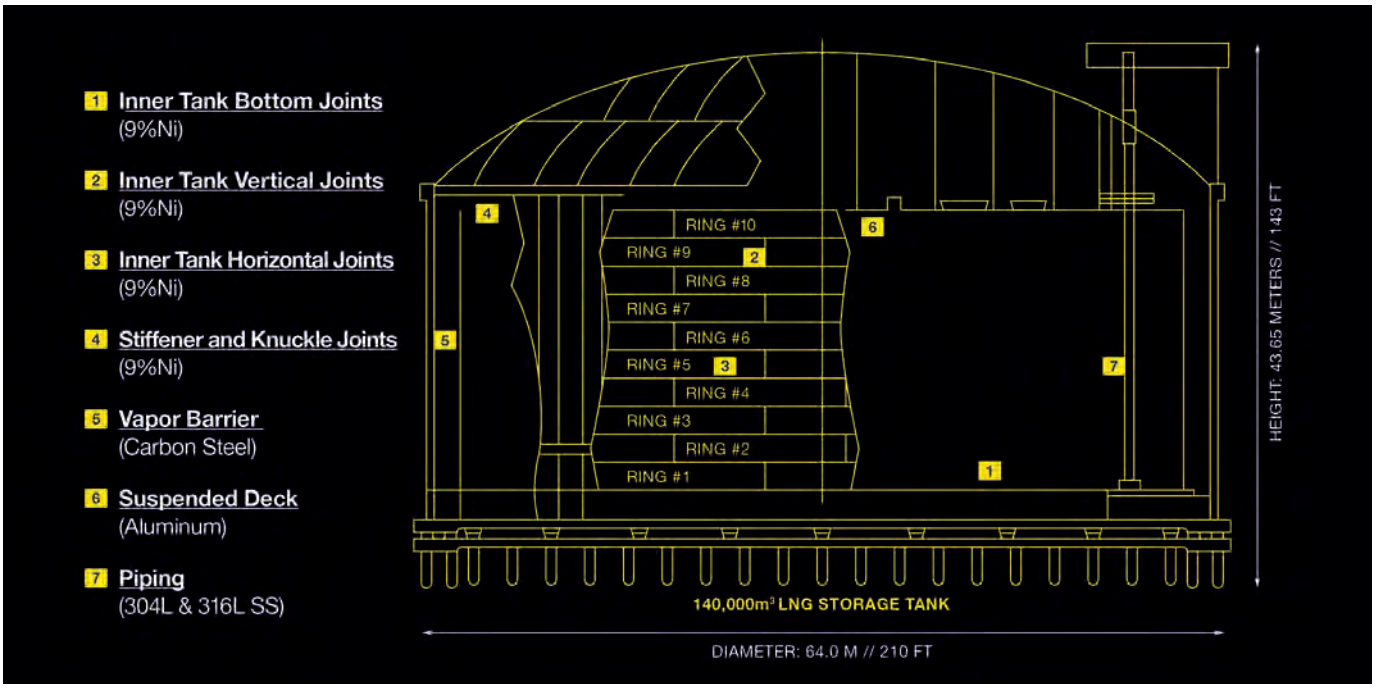

Fig. 1 — Tank fabricators use a combination of the SAW, FCAW, and SMAW processes.

All-Weld Deposit	C	Mn	Si	P	S	Cr	Ni	Mo	Nb	Fe	Ti
NiCrMo3-T1 (Typical)	0.02	0.20	0.35	0.005	0.003	21.0	Bal.	8.5	3.3	0.3	0.1
ESAB AWS A5.34 ENiCrMo3T1-4	0.10 max	0.50 max	0.50 max	0.02 max	0.015 max	20.0 23.0	58.0 min	8.0 10.0	3.15 4.15	5.0 max	0.40 max

Fig. 2 — Enhanced metallurgy for this ENiCrMo3T1-4 electrode improves performance in LNG tank applications.

9% nickel (Ni9) steel (ASTM A553/A553M-17e1, *Standard Specification for Pressure Vessel Plates*) for LNG tank construction because of its mechanical properties. Ni9 steel has a relatively higher strength and allowable stress than austenitic stainless steels and exhibits excellent fracture toughness at low temperatures. It also has a high melting point and retention of strength at elevated temperatures, which provide fire-safe integrity. It has relatively low thermal expansion, low thermal conductivity, and good corrosion resistance as well. It is, however, very susceptible to magnetization, which can create additional challenges during welding.

Processes used for welding LNG tanks can include mechanized submerged arc welding (SAW) tractors for the tank bottoms; automatic girth welding systems with single- or double-sided SAW for the horizontal joints; and flux-cored arc welding (FCAW) or shielded metal arc welding (SMAW) for the vertical seams and stiffener and knuckle joints — Fig. 1. In this article, experts from ESAB's LNG segment division, who work with customers around the globe, share some of the solutions developed to solve LNG tank welding challenges.

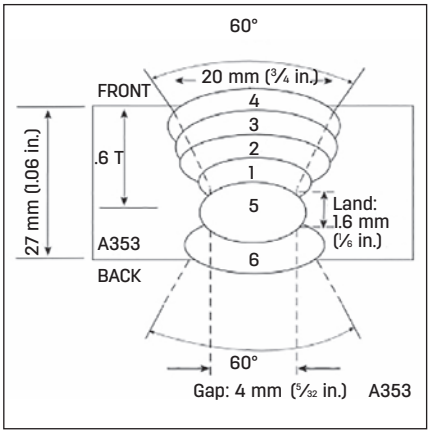

Fig. 3 — Typical welding procedure specification for automatic FCAW in the 3G position.

New FCAW Formulation

Some of the FCAW on LNG tanks remains semiautomatic, where operators backgouge the weld before completing it. However, in the U.S., much of the industry has moved to automatic uphill (3G) FCAW using a ceramic backing bar and no backgouging. With this move, the industry has shifted from a 3- to a 4-mm root opening (⅛ vs. 5⁄32 in.) between tank plates. One millimeter might not seem like much, but the difference increases the challenge for welding vertical seams on Ni9 steel.

Frank Lake, a senior product development engineer with ESAB since 1972, said, "A wider gap [opening] provides better joint access for automated welding and makes it easier to create a flatter bead profile with reduced risk of stress concentration and slag inclusions. However, because tank joints are highly restrained, the welds are particularly prone to hot cracking."

A traditional LNG FCAW filler metal choice is either AWS A5.34/A5.34M ENiCrMo3T1-1/4 or ENiCrMo3T1, both commonly called a "625-type" electrode because INCONEL® 625 is classified as ENiCrMo-3. Some formulations of this FCAW electrode make welds that can sag in the middle, and the weld pool can be very sluggish.

"If the melting point of the slag

Fig. 4 — Bead profile of an enhanced ENiCrMo-4T1-1/-4 in the 3G position with automated welding.

Fig. 5 — Setting up the final ring of a LNG tank for DSAW.

Fig. 6 — DSAW carriage and flux support system.

isn't high enough, the slag will fall away from the weld pool and will not support the weld metal, which then sags," Lake explained. "On the other extreme, if the slag melting point is too high, the slag will freeze too quickly, causing problems for the welder. Because these are weave welds, if the arc travels back over the solidified slag, which is nonconductive, it results in arc instability [and] poor control and can lead to slag entrapment."

To better meet the needs of both semiautomatic and automatic wide-weave applications, Lake and other filler metal experts at ESAB's Bowling Green, Ky., facility have developed an enhanced ENiCrMo3T1-4 electrode through critical control of the composition — Fig. 2. This electrode has been qualified for use on four recent LNG projects. The tank fabricators have confirmed that the electrode significantly reduced hot cracking susceptibility with wider root opening pass welding on thick plate (see Fig. 3), while delivering mechanical properties above customer requirements. The tensile strength is > 100 ksi (690 MPa) and Charpy impact toughness at –196°C (–320°F) is > 52 ft lb (70 J).

"Through improved wire chemistry and slag systems, the next generation of all-position nickel alloy electrodes can have a weldability that is close to that of a mild steel electrode; they provide an extremely flat bead profile," Lake said — Fig. 4. "Radiography shows no indications, while weld parameter monitoring showed no voltage or amperage fluctuations beyond nominal."

The 1.2-mm (0.045-in.) electrode deposited 2.38 kg/h (5.25 lb/h) during testing in the 3G position.

Double-Sided SAW Success

Double-sided submerged arc welding (DSAW) offers the highest level of productivity for on-site LNG tank welding. The plates are prepared with a double-V bevel so that a self-propelled carriage can make a horizontal (2G) weld on both sides of the tank at the same time.

The carriage, which has matching cabins on either side of the tank, travels on the top edge of the plate. As another option, the carriage can travel on a separate rail and the operator can walk along with it on a catwalk — Fig. 5. The cabin adjusts up and down on a telescoping frame to accommodate different plate heights; a cage provides operator safety, and curtains provide weather protection.

The system consists of SAW power source with a suitable output (a 1000 A alternating current [AC]/direct current system is common), a process controller that allows the operator to set welding variables and control travel speed, a welding carriage with manually adjustable torch mount, a flux hopper, and an endless rubber belt to support the flux in the welding position (Fig. 6) and allow it to be recovered and recirculated.

Travel speed must be synchronized between the two welding carriages so that the leading electrode and trailing electrode maintain a distance of about 70 mm (2.75 in.) between each other. Torch angle, travel speed, welding parameters, and wire diameter selection (typically 2.4 mm/3⁄32 in. diameter) all play critical roles.

DSAW is complex and requires highly skilled and experienced welding personnel to execute the process in a highly productive manner. One such company is Paresa S.p.A. of Cesena, Italy. Founded in 1978, this multidiscipline, single-source contractor is a leading fabricator and installer of storage facilities used by refineries, terminals, depots, and power plants throughout Europe, Africa, and South America. In 2018, the company invited ESAB to help improve DSAW results for tanks made from Ni9 nickel steel.

Paresa wanted to have a greater margin of safety for meeting mechanical properties while reducing concerns related to hot cracking and moisture absorption in filler metals.

To start, ESAB SAW technical experts Paolo Torchiana, global product line manager for stainless steel and nickel alloy SAW and ESW; and Gabriele Gallazzi, product manager, worked with Paresa to develop new welding procedure qualification records (WPQR) that have been certified by Bureau Veritas. For the 26-mm wall thickness at the bottom ring, the WPQR for the outside of the joint requires seven welding passes and the

	ESAB Solution (As Welded)	Minimum Requirements
Tensile strength	720 MPa	680 MPa
Yield strength	480 MPa	430 MPa
Elongation	42%	35%
Charpy V-notch energy	100 J @ -196°C	56 J @ -196°C
Charpy V-notch lateral expansion	0.8 mm @ -196°C	0.38 mm @ -196°C (ductile fracture > 0.3 mm)

Fig. 7 — Properties of an enhanced AWS A5.9/A5.9M ERNiCrMo-4 electrode with neutral flux for AC current.

Ni9 LNG Tank	Conventional ENiCrMo-6 4.0 mm dia. × 350 mm length	Advanced ENiCrMo-6 4.0 mm dia. × 350 mm length
Customer electrodes consumed per year	39,000 kg	35,537 kg
Deposition efficiency	61%	67%
Deposition rate	1.73 kg/h	1.90 kg/h
Welding speed	285 mm/min	313 mm/min
Total weld joint length	19,621 m	19,621 m
Total working hours	64,031 h	57,067 h
Savings — hours		6964 h saved
Savings — filler metal		3463 kg less filler metal used

Fig. 8 — When more of an electrode can be consumed, the savings add up to thousands of hours.

inside requires eight.

The industry standard prior to the 1980s had been to use an ERNiCrMo-3 SAW electrode. While it produces strong welds, its niobium and lower molybdenum content make it more susceptible to hot cracking. ERNiCrMo-4 SAW electrodes became the industry standard, with niobium eliminated and with higher molybdenum. Further development by ESAB refining the ERNiCrMo-4 composition range has made it less crack susceptible. Further, because impurities exploit stresses that occur as the weld pool solidifies, the electrode's metallurgical composition and consistency is tightly controlled by working with the mill supplying the metal.

Of course, proper electrode selection is only half the story with DSAW. In conjunction with the new electrode, ESAB developed a new flux specifically to weld Ni9 alloys using AC current (AC current eliminates magnetic arc blow, an effect to which Ni9 is sensitive). The neutral flux has a high basicity that provides good mechanical properties with better impact toughness values (Fig. 7) while delivering a stable arc and good weldability in the 2G position. The flux is shipped in a 25-kg (55-lb) steel drum to prevent moisture absorption until use and provide easier handling and storage during field erection.

"While Paresa needed to learn to walk before running, the company now welds at a marathon pace, giving it production efficiencies and a competitive advantage," Torchiana said.

SMAW Advances

China will soon become the world's largest importer of LNG, and current LNG demand could almost double to 550 billion m^3 by 2030. Although LNG terminal and cargo tank contractors in China want to erect tanks at a rapid pace, they face several challenges.

Jack Gu, director of segment sales at ESAB Shanghai, recently worked with a pressure vessel fabricator to address these issues for fabricating four 6500 m^3 LNG cargo tanks. He recommended SMAW electrodes meeting the AWS ENiCrMo-6 classification. While several electrodes meet the need, differences between the coating formulation and electrode wire metallurgy between providers can produce different results — Fig. 8. By comparing electrodes, the tank fabricator reduced filler metal consumption by 3463 kg (7635 lb).

"Scrapping of expensive Ni-alloy electrodes is an easily identifiable point of waste that impacts welding costs for tank construction," Gu shared. "Electrodes with a higher current carrying capacity address this issue. Operators can weld with almost the entire length of such electrodes. Conversely, if a nickel alloy core wire electrode gets too hot toward the end of consumption, operators must discard a longer stub. This can waste up to 15% more of an expensive electrode. In addition, excess heat poses the risk of degrading metallurgical composition and mechanical properties."

Gu noted conventional Ni-alloy electrodes are separated by three types depending on welding position usage: one type optimized for 1, 2, and 3G positions, another type for the 4G position, and a third certified for use in all four positions.

"If contractors can use one electrode type instead of two, they can reduce the risk of mixing up the types on the jobsite, as well as lower stock keeping unit costs," Gu said.

Conclusion

LNG tanks require tens of thousands of kilos of filler metals that can cost more tha $50 per kg (nearly $23/lb). As has been shown in this article, even well-established companies can benefit by starting a dialogue with experts who combine filler metal, process, and LNG tank application expertise. The process of customers sharing their challenges is the genesis of innovation, whether that is something as simple as designing packaging for better moisture resistance or the years of R&D that lead to formulation advancements. WJ

NEIL FARROW (Neil.Farrow@esab.co.uk) *is global product manager, cored wires, ESAB, London, England.*

Feedability: The Quintessential Problem with the GMAW of Aluminum

Learn what factors will prevent interruption in feeding aluminum welding wire

BY THOMAS PFALLER

Whenever discussions regarding the gas metal arc welding (GMAW) of aluminum arise, it is a safe bet that the topic will be centered on one of a handful of topics. Among these are filler selection, porosity, distortion, and feedability. While one might expect the first three items in that list to also be applicable to the GMAW of steel and stainless steel, feedability is one that aluminum seems to have exclusive discussion rights. The properties of aluminum welding wire make it particularly sensitive to the creation of shavings, microfines, and tangles within feeding systems.

With the continued growth in the aluminum welding industry, more and more companies are dipping their toes into the ocean that is aluminum welding. Any production-minded manager or engineer should be sensitive to this topic because any interruption in the feeding of welding wire means a loss of productivity. The foundational knowledge relating to aluminum feedability can be segregated into the following points: wire quality, system considerations, and usage techniques. Each of these will be explored to ensure a comprehensive understanding of how to overcome the challenges of feeding aluminum welding wire.

Alloys and Characteristics

For anyone not intimately familiar with aluminum welding, a good baseline to start with is the differences in characteristics of aluminum filler wires. Within the aluminum welding world, the filler alloys are generally grouped into two families, each having relatively distinct features. The two families are hard wire and soft wire. The hard-wire alloys are the various 5xxx series alloys that are commercially available as filler alloys. Some common examples of these include 5356, 5183, 5554, and 5556. The two primary feedability characteristics of these alloys is that they are relatively stiff with good columnar strength. This makes the hard wires less prone to tangling but more susceptible to the formation of microfines.

On the other hand, the soft-wire alloys include representatives from a few other alloy families: 1xxx, 2xxx, and 4xxx. A few of the common welding alloys include: 1100, 2319, 4043, and 4047. The soft-wire alloys have notably reduced columnar strength and are more prone to tangles anytime there is even a slight interruption in the feeding system. These wires also have a higher propensity to form shavings due to incorrectly configured equipment. These distinctions between hard- and soft-wire alloys will serve as a baseline for the following investigation into feeding aluminum wires.

Types of Shavings

During the explanation regarding the different aluminum alloys, two other foundational elements were mentioned: microfines and shavings. These terms are sometimes used interchangeably even though they identify two distinct failures within welding systems. Shavings are characterized by large chips or strands of aluminum, which are mainly the result of mechanical damage done to the wire — Fig. 1. Microfines, on the other hand, are much smaller particles similar to very coarse grain sand — Fig. 2. These can come from mechanical damage from drive wheels but are commonly a function of the flaking surface of the hard-wire alloys. Once these fines start to build up in a feeding system, their propagation and accumulation

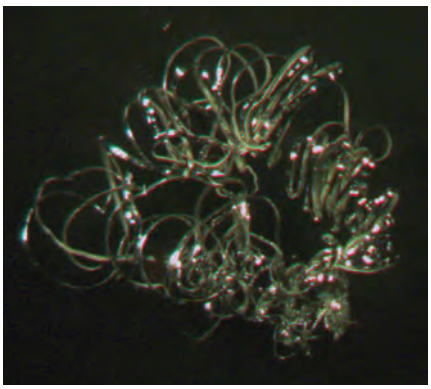

Fig. 1 — Shavings are characterized by relatively long strands indicative of mechanical damage.

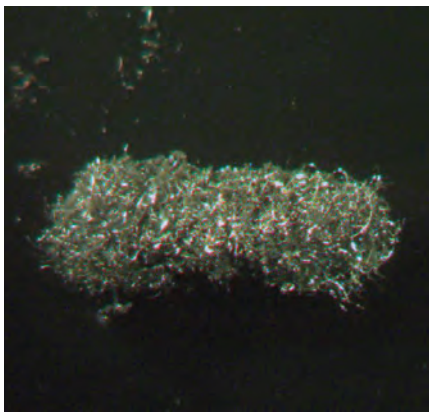

Fig. 2 — Microfine is characterized by very small course grains.

Fig. 3 — Even subtle bends in the wire can cause feeding issues as the wire passes through the contact tip.

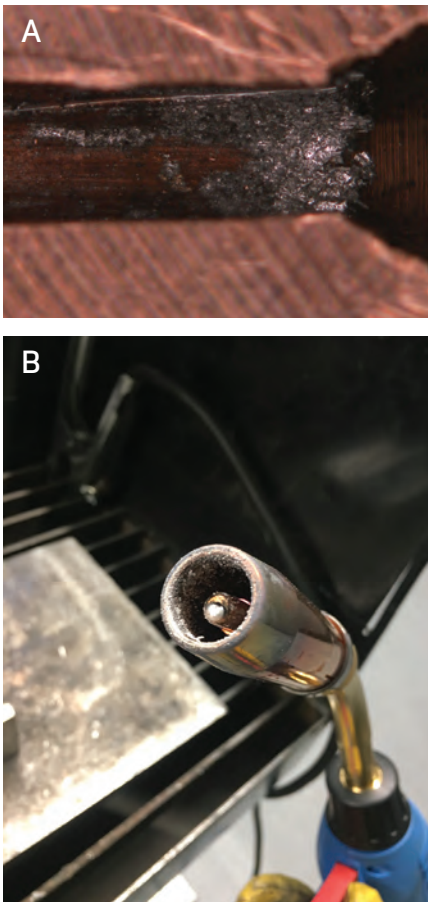

Fig. 4 — A — Buildup from arcing in the contact tip caused by lack of connectivity; B — the ever so familiar view that a welding operator has after suffering a burnback.

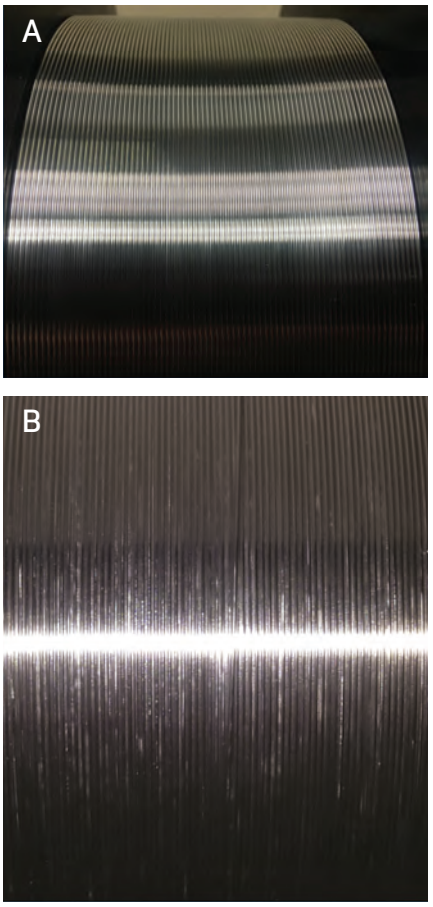

Fig. 5 — AlcoTec Wire's patented New Technology (NT) wire has improved surface smoothness that prevents build up of microfines. A — NT wire; B — legacy wire.

increase significantly. As one might expect, both the shavings and microfines will cause interruptions in feeding. Understanding the differences between the appearance and causes can greatly assist in troubleshooting feedability issues.

Manufacturing Quality

As with any process, if the starting material is of poor quality, a user can expect the end result to suffer. When looking at aluminum welding wire, there are a few attributes that help to ensure robust feedability. The first of these is level layer winding. This gives the user confidence that the wire has not become crossed on the spool. It also ensures that the wire is smooth and does not develop inconsistent bends that could interrupt feeding while passing through the contact tip — Fig. 3.

One attribute that goes hand in hand with precision level layer winding is diameter tolerance. This comes from the fact that the process of precision winding aluminum wire is very sensitive to changes in wire diameter. A common tolerance that one might see in precision-wound wire is measured in ten-thousands of an inch. This is important for a welder because changes in wire diameter can affect the electrical connectivity of the wire in the contact tip. Loss of conductivity will result in either a burnback or arcing within the contact tip — Fig. 4.

The final concern from a wire standpoint is the surface quality of the wire. Having aluminum wire with a smooth surface with good lubricity ensures that the wire will not hang up or snag in the feeding system. Unfortunately, even minute aluminum fines can build up and generate until feeding issues result. AlcoTec® Wire Corp. has developed a patented solution to this for the 5xxx products referred to as New Technology wire. This process ensures that the surface of the wire is slippery and free from the microfines that have traditionally wreaked havoc for aluminum welding machines across the globe — Fig. 5. It is through the utilization of quality inputs that a process can have the best chance of producing a quality product with a high level of efficiency.

Welding Systems

When looking at the big picture of an aluminum welding system, we have addressed material attributes and wire manufacturing and quality. The next piece of the puzzle is the welding system itself. With a few exceptions, most welding machines are configured for welding with steel or stainless steel wire. This means that certain components may need to be checked to verify that they are optimal for the utilization of aluminum welding wire. There

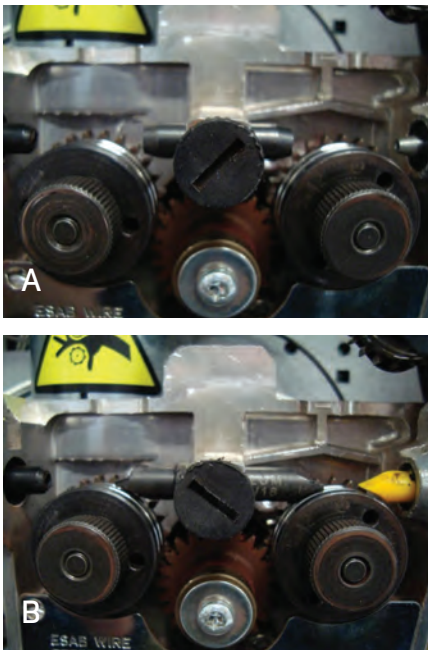

Fig. 6 — A — Pictured is how welding feeder equipment is commonly configured. Note the steel guides and space between the guides and the drive wheels; B — a welding feeder optimized for feeding softer aluminum wire. Note the nylon guides and the proximity to the drive wheels.

are a few key components to consider when moving aluminum wire from the spool to the welding torch.

The guides going in and out of the wire feeder should be made from a soft nonabrasive material. Common materials that work well are nylon/plastic guides. These keep the wire aligned while limiting abrasion on the soft surface of the aluminum wire. These guides should also be designed to limit the amount of open space available for the wire to be pushed into in the event of feeding issues — Fig. 6. Drive wheels should be polished smooth to keep from galling the wire or peeling flecks off the surface of the wire — Fig. 7. The most common geometry of drive wheels is polished U-groove. However, users may have success with other geometries given the wheels grip the wire without damaging the wire surface. The final element to be considered regarding drive wheels is that the pressure should be kept as low as possible. High drive roll pressure has a two-pronged damaging effect on the wire. The first is that excessive drive roll pressure can smash the softer alloys causing the wire geometry to be oval rather than round. When utilizing the harder 5xxx filler wires, excessive

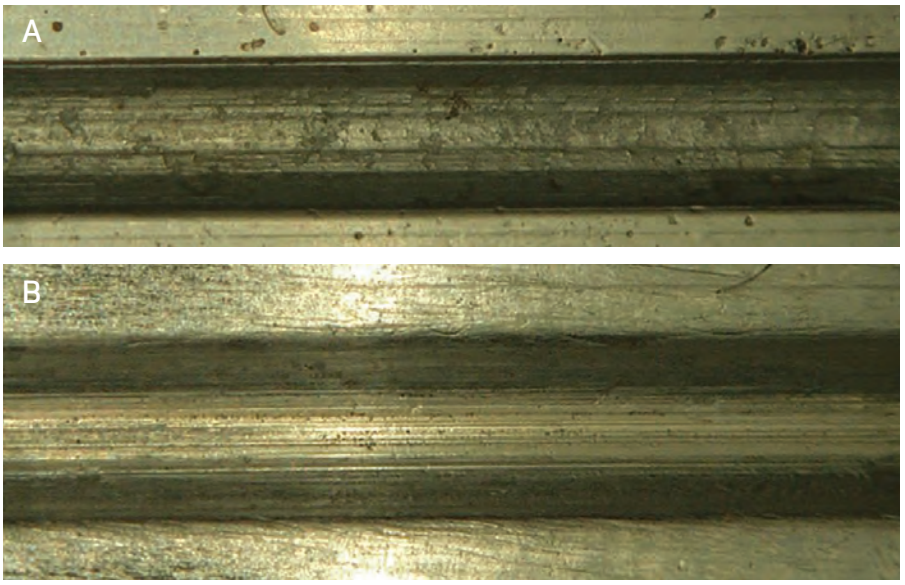

Fig. 7 — Drive wheel surfaces. A — Unpolished; B — polished. Note how much smoother the polished drive wheel is.

drive role pressure can result in the additional creation of microfines. Drive wheels should be cleaned periodically to remove any aluminum build up and to ensure that they "float" or self-align; thus, avoiding additional damage to the welding wire.

After the feeder, the wire travels through a liner to the welding torch. Like the guides, this liner should be a material that is soft to minimize abrasion on the wire. Common materials are nylon or nylon mixed with graphite. The length of the distance between the feeder and the torch is also important. When utilizing a push-only system, one can expect to have issues with a torch length greater than 12 ft (4 m). Quality push/pull type systems can successfully feed wire up to 30 ft (10 m).

The final component to consider for robust feedability is the contact tip. Contact tips have few attributes that often go overlooked in favor of buying based on sticker price, namely the quality of the copper alloy, size, geometry, and machining. The quality of the copper can ensure that the tip does not prematurely wear from the heat of welding and the thousands of feet of wire that pass through it. When considering size, the typical expectation is that the inside diameter of the contact tip should be approximately 10% oversized. Quality contact tip manufacturers will often figure this into their machining processes. Finally, if the manufacturers cut corners in their machining of the tips, burrs can be left behind. A common location to find machining burrs is at the inlet chamfer of the tip. This can affect the inside diameter of the tips and also shave the surface of the wire — Fig. 8.

Tricks of the Trade

While the welding system configuration has an effect on the robustness of the aluminum wire feedability, the usage techniques also cannot be ignored. While the list could quickly get very exhaustive, here are a handful of things that many welders struggle against without even knowing it. First is keeping the liner from the feeder to the welding torch as straight as possible. Every loop and bend in the liner results in additional friction and the opportunity for fines to be created. The next item to consider is the importance of preventative maintenance on

Fig. 8 — Shavings built up from severe rubbing on the inlet of a contact tip.

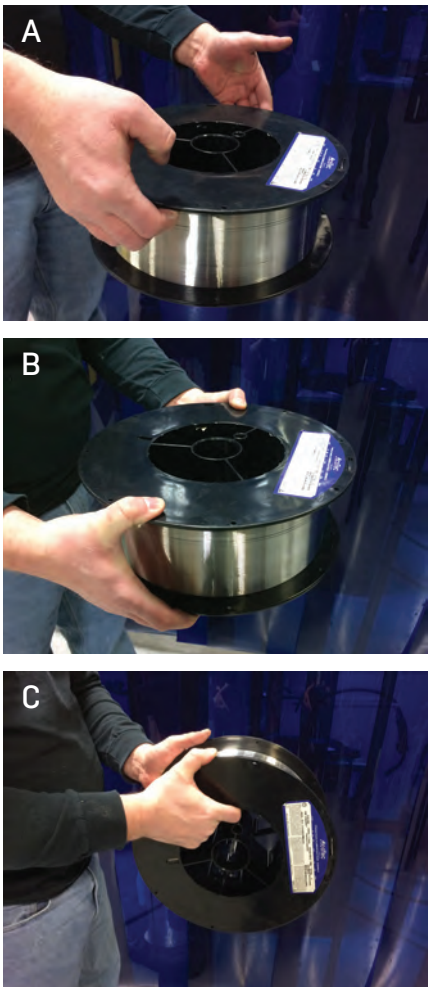

Fig. 9 — Although convenient, spools should not be lifted by the inside of the flanges. Lifting should be done to support the flanges and limit any possible flexing. A — Incorrect way to lift a spool; B, C — better alternatives for lifting a wire spool.

the equipment. Preventative maintenance (PM) can often be a challenge; however, it is important to make sure that the PM schedule makes sense and is effective. Depending on the welding shop, this could be as complex as a managed control plan or as simple as having the welder blow out the liner with compressed air at the beginning of a shift. Taking care of equipment will ensure that every time the welder initiates the welding arc feedability of the aluminum wire is not a concern. Finally, when handling full spools of aluminum welding wire, it is important to lift it from the center hub. If the spool is lifted by the flanges, the flanges may spread slightly, allowing the wire wraps in the corners to become pinched — Fig. 9. This undoubtedly will cause feeding issues as the wire is paying off the spool during welding.

Summary

Welding is a complex activity with many nuanced components and theories to consider. As one small piece of the puzzle of the aluminum GMAW process, feedability is no exception. However, through the diligent consideration of the quality of the wire, equipment configuration, and usage techniques, a welder can keep his or her hood down satisfied at having overcome the quintessential problem relating to the GMAW of aluminum. This will ultimately lead to fewer production headaches and more production throughput. WJ

THOMAS PFALLER (tpfaller@alcotec.com) *is a process engineer at AlcoTec Wire Corp., Traverse City, Mich. This article is based on a presentation from the American Welding Society Aluminum Virtual Conference — Back to Basics held October 20 and 21, 2020.*

Aluminum Metallurgy Basics:

Strengthening Methods and Welding Effects

With some fundamental knowledge on metallurgy along with proper technique, it is possible to establish practices that facilitate the welding of aluminum.

How aluminum alloys react to arc welding and the mechanisms used to make them stronger

BY CARSON WILLIAMS

Aluminum alloys are split into series that are based on the primary alloying elements added. They range from 1xxx to 8xxx series. These series can also be grouped into two classes that are based largely on the strengthening methods used: heat-treatable and nonheat-treatable alloys. Heat-treatable alloys can gain significant strength through heat treatment at specific temperatures and times, whereas nonheat-treatable alloys get their strength mainly through solid solution strengthening and coldworking. Each alloy series has its specific advantages and usages.

Nonheat-treatable aluminum includes four distinct alloy series that are usable for specific applications. Each has a main element that provides strength and other characteristics.

- **1xxx** is a pure aluminum that delivers excellent electrical conductivity and corrosion resistance for welding chemical tanks.
- **3xxx** has higher levels of manganese and offers good thermal conductivity for welding heat exchangers.
- **4xxx** encompasses higher levels of silicon (Si) and is known for its weldability in general applications. There are also some heat-treatable 4xxx series alloys.
- **5xxx** contains magnesium (Mg) as a main element and works well for general structures and truck fabrication due to its welded strength.

The heat-treatable aluminum alloys include four alloy series that feature specific characteristics for different applications:

- **2xxx** has higher amounts of copper, which increase tensile strength, making it a good choice for use in the aerospace industry.
- **4xxx** that is heat treatable is known for its castability and contains Si as its main element.
- **6xxx** works well for color matching in structural and architectural jobs and consists of higher levels of both Mg and Si for strengthening.
- **7xxx** contains zinc for strength and is often used for fabricating sports products.

The 8xxx series are novel alloys with unique alloying additions and are not commonly used.

This article will break down the strengthening methods used for these alloys and how the extreme heat from arc welding affects them.

Metallurgy and Metal Microstructure

To understand the physical phenomena involved in the strengthening and welding of aluminum alloys, it's important to start with a brief overview of metallurgy and metal microstructure. The vast majority of metals exhibit polycrystalline microstructures, meaning that the metal atoms arrange themselves in a repeating pattern called a crystal lattice to form crystals (also called grains). There are many of these crystals, which form the bulk of the material, at different orientations to each other (note that single-crystal and amorphous metals do exist through special processing techniques). In addition, each metal has its own characteristic crystal structure, ranging from very simple to quite complex. While many of these concepts apply to most metals, from here on this article will focus on aluminum.

Within the aluminum crystal structure, there are inevitable defects or variances. There are multiple types of defects possible, but of particular interest are defects called dislocations. Several types of dislocations can occur, but in general dislocations are either mobile or immobile; the mobile dislocations are the focus here. These dislocations can move throughout the aluminum crystals, which is largely what makes plastic deformation possible in aluminum vs., for example, brittle ceramics. Without dislocation motion, plastic deformation is not possible. This idea of dislocation movement is crucial for understanding strengthening methods.

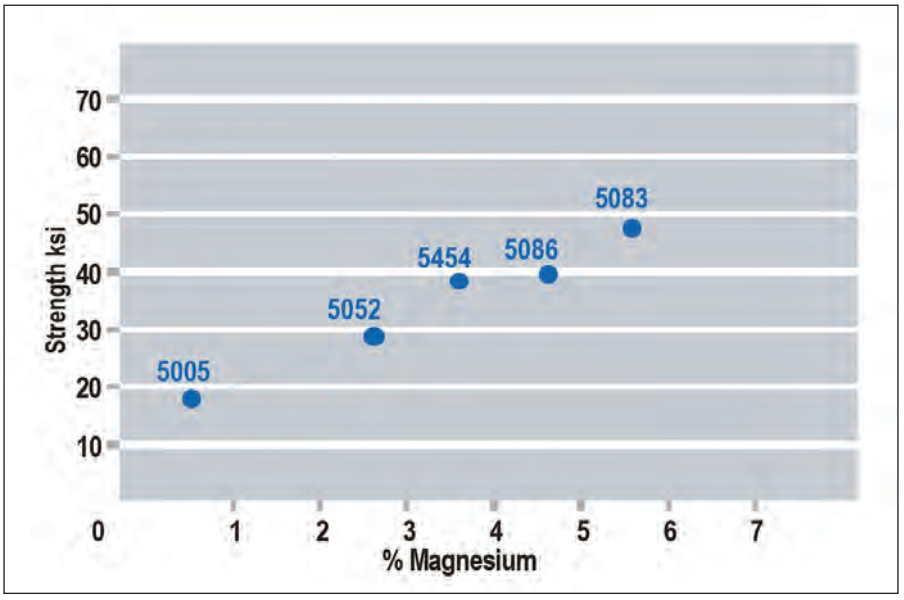

Fig. 1 — Strength increase shown as Mg solid solution content in selected 5xxx series aluminum alloys.

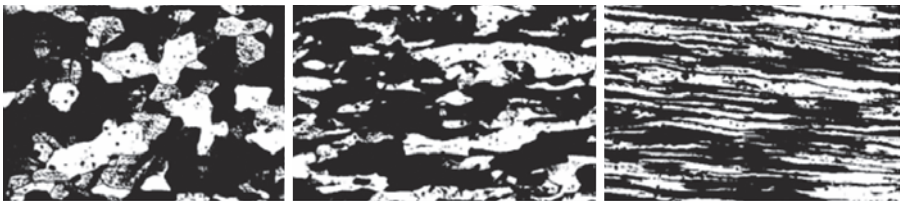

Fig. 2 — Changes in grain structure as a result of increased coldwork. (Credit: Reprinted with permission of ASM International, asminternational.org. *All rights reserved.)*

The basis of strengthening aluminum is to inhibit dislocation motion, so to make aluminum stronger, barriers must be created. There exists in-depth analyses of dislocations and their movements, breaking and forming of metallic bonds, interactions with barriers, and thermal activation, but the basic information in this article should be helpful in gaining a better understanding of aluminum alloys and welding.

Strengthening Methods

There are multiple strengthening methods found in the two groups of aluminum alloys, and they all relate back to the concept of dislocation motion. Nonheat-treatable alloys do not see appreciable strengthening from thermal treatment. Instead, they get strength from other elements in solution with the aluminum and through deformation processes. For example, consider the 5xxx series of aluminum, where Mg is the primary alloying element.

Certain elements, such as Mg, have considerable solubility in aluminum. These elements fit within the crystal structure of aluminum — either by substitutionally replacing aluminum alloys within the crystal structure or interstitially fitting between the aluminum atoms. In either case, there is a size mismatch between the aluminum atoms and the alloying elements that presents a strain on the crystal lattice. This held strain inhibits dislocation motion and adds strength to the metal. As more Mg is added to aluminum, strength is increased (note that there are limits to this).

This is the process known as solid solution strengthening; alloying elements in solution adds strength to the metal by inhibiting dislocation motion. It is worth noting that certain elements have more solid solution strengthening potential than others. Mg is one of the most potent solid solution elements, which is why the 5xxx series is so widely used. A chart showing the strength increase from Mg additions is shown in Fig. 1.

In wrought aluminum alloys, the metal can be coldworked (deformed at low temperature) to add strength, which relates to dislocation motion. Deforming the aluminum does two things to add strength: 1) Residual stress is stored in the metal; and 2) the metal grains or crystals are deformed, which results in an increased dislocation density and a grain boundary area. Both work against dislocation motion, adding strength to the aluminum. An illustration of grain structure changes is shown in Fig. 2.

The strengthening mechanism in heat-treatable alloys is different but still relates back to dislocation motion. In aluminum alloys, the bulk of the material carries the same crystal structure, all existing as a single phase called the primary phase. In heat-treatable aluminum, alloying elements are added that can then form secondary phases, often called precipitates. This happens when sufficient heat and time allow the alloying elements to diffuse through the material and form separate structures in a process referred to as heat treating or aging.

These secondary phases generally exhibit a crystal structure that is different from the primary phase, with varying degrees of dissimilarity. Secondary phases can be found in many alloys, including nonheat-treatable aluminum alloys, but not all secondary phases add strength to the metal. The heat-treatable aluminum alloys, such as the 6xxx series, form secondary phases that do add strength. The exact interaction between dislocation motion and precipitates can be complex, but in essence these precipitates add strength by resisting dislocation motion.

The Effect of Welding on Aluminum

In aluminum arc welding, the arc reaches many thousands of degrees in temperature. As a result, there is a large amount of heat that is transferred to the base material surrounding the weld. This area is known as the heat-affected zone and sees significant effects from the heat. The exact physical effects of this heat are different for heat-treatable and nonheat-treatable aluminum alloys, but in both, heat input from the process alters the base material and creates loss of strength. A smart weld design accounts for those strength losses to ensure the integrity of the completed weld.

In nonheat-treatable aluminum, strength gained from the solid solution, as explained before, is inherent to the chemistry and is generally not affected by the heat from arc welding. However, the fine, deformed grains and stored strain seen in coldworked aluminum are greatly affected. The heat provides energy for new grains to form and grow, resulting in a much coarser and softer microstructure. It also releases the stored energy from coldworking. This thermal process is known as annealing, and the formation of new grains is recrystallization.

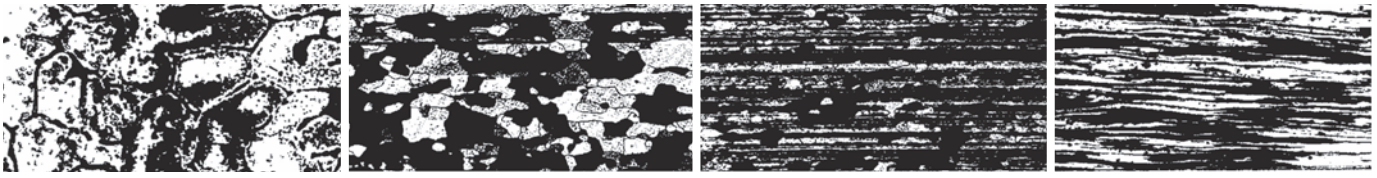

Fig. 3 — Microscopic images showing (from left) the fusion, annealed, partially annealed, and unaffected zones. (Credit: Reprinted with permission of ASM International, asminternational.org. *All rights reserved.)*

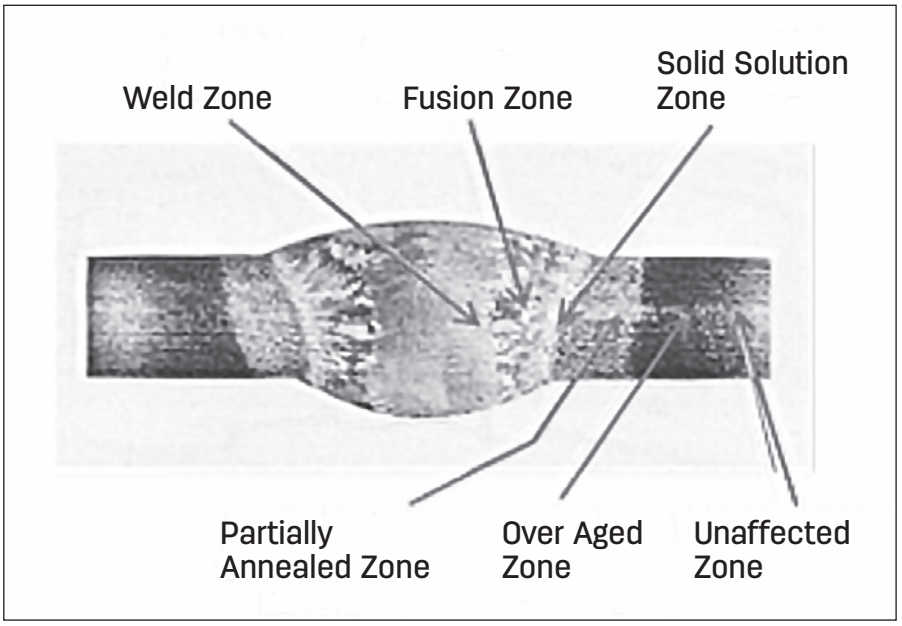

Fig. 4 — Macroetch of a weld showing the different zones of a welded heat-treatable base metal. (Credit: Reprinted with the permission of ASM International, asminternational.org. *All rights reserved.)*

The effect of heat lessens farther away from the weld, and there are different zones in the base material.

The zone farthest from the weld is the unaffected zone, where the grains remain the same as at the end of cold-working. Moving toward the weld is a partially annealed zone, where some new grains form and some of the stored stress is relieved. Next, there's the annealed zone where large grains form with random orientation, and all the stored stress is released. Lastly, there is the fusion zone, the point where the filler metal and base metal have completely melted, solidified, and cooled. An illustration of these zones is shown in Fig. 3.

The effects of the welding process and heat input on heat-treatable aluminum differ from nonheat-treatable aluminum. One constant, however, is the strength losses that occur along the way.

Heat input alters the grain and precipitate structure when welding heat-treatable aluminum. At the weld zone (the center point of the weld that has been liquified from the welding arc and resolidified), the weld itself is primarily made of filler metal.

Moving outward from the center weld zone, the fusion zone is a combination of filler metal and the aluminum base metal that has been liquified and solidified. It can be stronger than the weld zone. Beyond that is the solid solution zone, where the aluminum hasn't liquified but the temperature from the welding arc was high enough that precipitates have returned to solution.

The overaged zone in the aluminum weld is exposed to the high-enough heat inputs from the arc to overage all of the precipitates in that part of the weld, making them coarse and resulting in loss of strength. Finally, there is the unaffected zone where the aluminum is in its original state. An illustration of these zones is shown in Fig. 4.

Conclusion

Aluminum is considered by many to be difficult to weld, but it doesn't have to be. Learning the basic metallurgy of aluminum will help welders achieve a better understanding of how the material reacts to heat during the welding process. With this information and proper technique, it is possible to establish practices that facilitate the welding of aluminum. WJ

CARSON WILLIAMS (carson.williams@hobartbrothers.com) *is technical product manager — aluminum, Hobart Brothers LLC, Troy, Ohio.*

This article is based on a presentation from the American Welding Society Aluminum Virtual Conference — Back to Basics held October 20 and 21, 2020.

The Voyage of Repairing Aluminum Bronze in Marine Vessels

This study covers two tests that used continuous GTAW-ACHF, different percentages of tungsten, and more

BY CATHERINE GOSSER, FRANK GOSSER, AND ISAAC STEELE

In marine applications, when vital vessel components such as aluminum bronze propellers and piping cannot be repaired by a typical fabrication shop, they must be done during emergency dockside repairs.

The study presented in this article investigated whether a broken piece can be repaired in place and to the standard of American Society of Mechanical Engineers (ASME) *Boiler and Pressure Vessel Code* (BPVC), Section IX, Welding, Brazing, and Fusing Qualifications. The Cu-7Al-3Fe alloy was welded using gas tungsten arc welding-alternating current high frequency (GTAW-ACHF) parameters and ERCuAl-A2 filler wire. Guided bend tests and x-rays were also applied to determine mechanical properties.

Importance of Aluminum Bronze

Aluminum bronze is used frequently in the marine industry for propellers and pumps (Ref. 1) — Fig. 1.

Dockside repair of these elements has been limited in its use and study. For dissimilar steel types, offshore investigations have found promising results with bend and tensile tests (Ref. 2). Best practices for welding parameters have been investigated recently by authors in laboratories under ideal conditions for Cu-7Al-3Fe. As an example, in the Abbasi investigation (Ref. 3), bend tests or x-rays were not taken, and gas tungsten arc welding-direct current electrode negative (GTAW-DCEN) parameters were used. Guided bend tests or x-rays are required by BPVC, Section IX. However, the type of bend test is not well investigated, and the code gives options depending on the bending properties in QB-161.4.

A ship with a broken propeller loading into drydock in Wrangle, Alaska.

Fig. 1 — A bronze alloy propeller before (dirty/silver colored) and after (gold/copper colored) drydock restoration on a nearly 100-year-old wooden boat that's still used for fishing in Alaska.

The face-centered cubic (FCC) alpha alloys of this type, containing 3% iron, are single-phase compositions not exceeding 9% aluminum (Ref. 1). The concern with common filler metal having the higher end of the aluminum percentage, and the continuous heat of welding, is that it can create α-β duplex structures, and the β phase can decompose into a brittle eutectoid and is less resistant to corrosion (Ref. 4).

The corrosion resistance of aluminum bronze in marine environments is due to a film of self-healing aluminum oxide (Ref. 1). Unfortunately, this also makes the material more difficult to weld under any conditions due to the formation of constant contamination. Plate and wire must be thoroughly prepared by rigorous cleaning prior to welding.

The mechanical properties of aluminum bronze per the plate manufacturer's testing results are as follows: yield strength is 68.3 ksi and tensile strength is 93.8 ksi.

Experimental Methodology

The filler metal and plate were chosen for their 7–9% aluminum and 0.8–3% iron content. This encourages an FCC alpha alloy for enhanced corrosion resistance.

The chemical composition of the plate and wire alloys, detailed in Table 1, was provided by the manufacturers. In particular, MKM Mansfelder Kupfer und Messing GmbH, Germany, the supplier of copper and brass for the plate used, meets the Unified Numbering System for Metals and Alloys C61400. Additionally, the ER-CuAl-A2 wire by Hy-Weld Inc., Norcross, Ga., meets American Welding Society (AWS) A5.7/A5.7M, *Specification for Copper and Copper — Alloy Bare Welding Rods and Electrodes*, and is acceptable to BPVC, Section IX.

Welding Parameters and Experimental Setup

The GTAW-ACHF process was se-

Table 1 — Chemical Composition of Base Metal and Filler Metals (wt-%)

Plate/Filler Metal	Cu	Pb	Fe	Zn	Al	Mn	P	Si
C61400/2.7 mm	remainder	0.010%	3.32%	0.01%	7.10%	0.92%	0.010%	—
ERCuA1-A2/3.2 mm	remainder	0.002%	0.85%	0.005%	9.05%	—	—	0.046%

Table 2 — GTAW-ACHF Parameters

Polarity	ACHF
Welding current (min/max)	190 A/265 A
Voltage (min/max)	21 V/26 V
Welding speed	0.762 mm/s
Shielding gas/flow rate	Argon 100%/14.2 L/min
Interpass temperature (avg. min/avg. max)	106°C/165°C
Heat input	7.35 kJ/mm
Filler metal diameter	3.2 mm, 2.5 mm, 1.6 mm

lected because filler materials bias toward AC power. Table 2 shows the welding parameters. Designs were single-V-groove and double-V-groove welds — Fig. 2. Ambient temperature for the shop was 5°–10°C during testing.

First Test. The first test was run with a water-cooled Miller Electric Syncrowave® unit. The torch was equipped with a 25.4-mm glass lens and 2% thoriated tungsten with 12.7-mm stickout.

Two 12.7-mm plates were beveled to 30 deg on each side for a total angle of 60 deg, then bolted in a 1G position jig. There was no opening in between the beveled plates, and it contained a 1.6-mm landing.

Plates were preheated to 66°C; welded with a root, fill, and cover pass for each side; and received a total of six passes, as well as mechanical cleaning between passes. The finished plate was wrapped in a heat blanket overnight.

Second Test. The second test changed the grain direction of the plate by turning the plate 90 deg from the previous test.

Again, the water-cooled unit was used. The torch was equipped with a 31.75-mm glass lens and 100% pure tungsten with 12.7-mm stickout. Two 12.7-mm plates were beveled to 30 deg on one side. The total angle was 60 deg, with a backup bar of 3 mm tacked to the two plates.

The complete unit was bolted in a 1G position jig. There was a 4-mm opening in between the beveled plates, and it contained a knife edge with no landing. Plates were preheated to 121°C. The weld design contained ten passes on a single side. Each pass was mechanically cleaned. The finished plate was cut and bent following a short cool down period.

After cooling, 16-mm coupons were removed from either end of the weld, mechanically ground, and radiused. These samples were then cut into weld-side, face, and root bends in guided bend tests.

Results and Discussion

Given the high copper content of Cu-7Al-3Fe, the assumed welding polarity should be DCEN, as used in copper nickel. Through preliminary testing and machine calibration, it was found that the weld using DCEN on Cu-7Al-3Fe had poor penetration from insufficient heat transfer. The resulting DCEN was not bendable. The expected reaction to ACHF continuous mode would have been a "snap and pop" sounding aluminum weld. In contrast, ACHF continuous mode ran smooth with complete penetration into the base metal at lower travel speeds; higher travel speed caused incomplete base metal penetration, per x-ray results.

The interpass temperatures ranged drastically between 76° and 287°C. The plate built up heat rapidly with slow welding speeds and cooled down quickly with faster welding speeds.

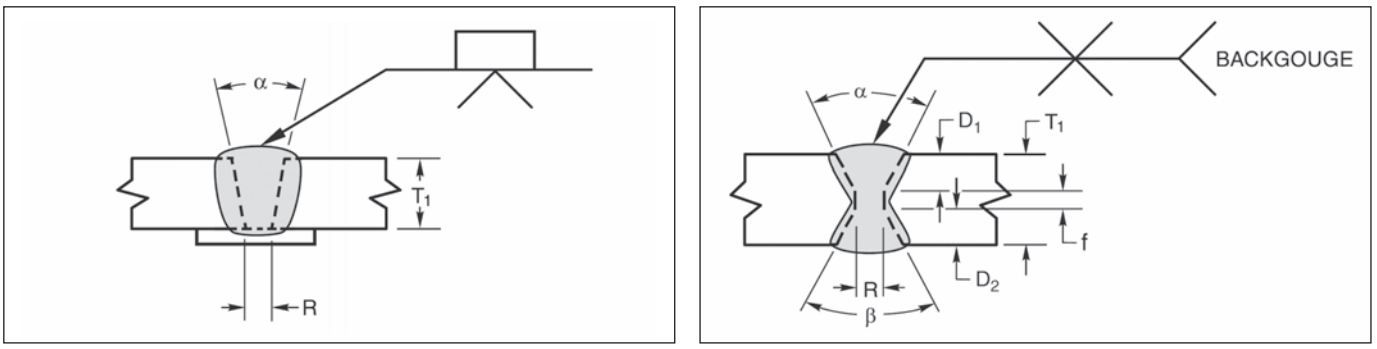

Fig. 2 — Single-V-groove weld (left) and double-V-groove weld (right). (Sourced from Fig. 5.1, pages 83 and 86, in AWS D1.1/D1.1M:2020, Structural Welding Code — Steel.*)*

Fig. 3 — Different angles of sample 1.

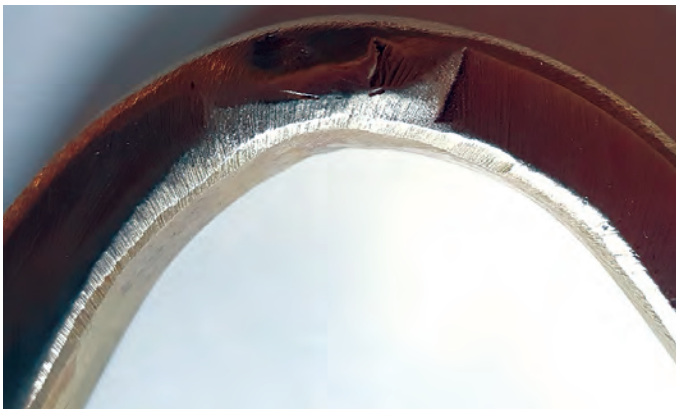

Fig. 4 — Different angles of sample 2.

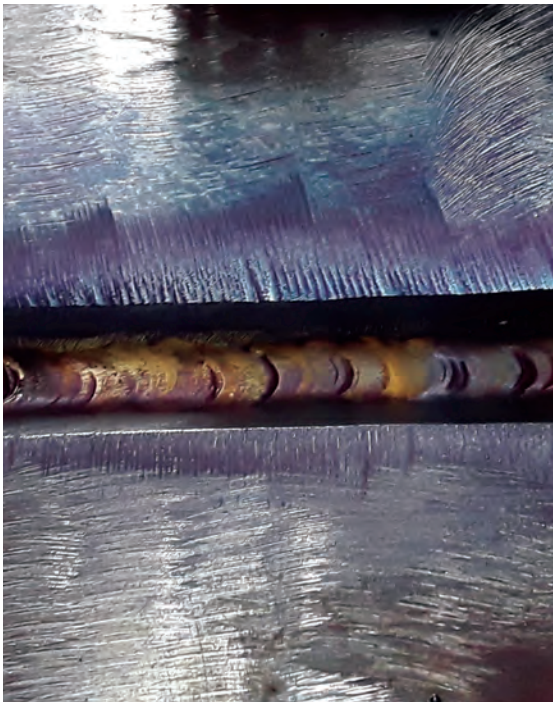

Fig. 5 — Root pass test 2 is pictured.

Fig. 6 — Welding in progress.

The reduced speed of 0.4 mm/s created the highest temperatures at 278°C. The increased speed of 1.1 mm/s reflected a temperature of 106°C. The faster speed with a lower temperature may not be sufficient heat to pass the x-ray for base metal penetration. Interpass temperatures were carefully monitored to avoid heating the base metal into the brittle beta phase.

Post cooling, several samples were taken and prepared for a U-shaped guided bend test that meets the requirements of BPVC, Section IX. Three of the side bend samples passed visual inspection by a qualified welding inspector.

Side bend coupon samples are pictured — Figs. 3, 4. Face and root bend tests cracked during bends and are not pictured — Fig. 5. In addition, the welding process is shown in Fig. 6.

Conclusion

The process of continuous GTAW-ACHF demonstrated a superior quality weld along with larger 31.75-mm diameters of glass cup sizes for increased cover gas protection for offshore or dockside repair.

The heat of the weld must be closely monitored for both high and low temperatures. The increased heat input can cause brittle beta phase formations, and the lower temperatures can cause insufficient penetration into the base metal.

The tungsten should be 100% pure, as the thoriated was too soft for the base metal and sloughed off during welding, causing an inclusion. With the 100% pure tungsten, care must be taken to avoid poking or splashing of the tungsten with the filler metal, as it causes inclusions easily.

Given the ability to bend test, x-ray, tensile, and Charpy impact (the two latter shown in previous studies), it is likely that welding and welder procedures for dockside repairs can be written and applied to Cu-7Al-3Fe as well as the corresponding wire ERCuAl-A2.

The grain direction of Cu-7Al-3Fe appears to be of importance. When bending samples of this material, cracks in the base metal appeared dur-

ing face and root bend tests. Preliminary tests on this material were 90 deg off of the first testing to ensure successful bend tests. This material appeared to be longitudinal-only bend tested; in both directions, only the side bend tests were successfully bent. WJ

References

1. Callcut, V. 2002. Aluminum bronzes. *copper.org/publications/newsletters/innovations/2002/08/aluminum_bronze.pdf*.

2. Mendoza, B. I., Maldonado, Z. C., Albiter, H. A., and Robles, P. E. 2010. Dissimilar welding of superduplex stainless steel/HSLA steel for offshore applications joined by GTAW. *Proceedings of the Estonian Academy of Sciences: Engineering* 2(07): 520.

3. Abbasi, M., and Derakhshandeh-Haghighi, R. 2018. The role of welding parameters on achieving a combination of high strength and ductility in gas tungsten arc welding of Cu–7Al–3Fe aluminum bronze. *Physics of Metals and Metallography* 119(5): 497–503.

4. Türker, M., Acar, S., Cömert, Z. Y., Kisasoz, A., and Guler, K. A. 2018. Characterization of mechanical properties and corrosion behaviours of Mn and Al bronze castings. *Practical Metallography* 55(1): 5–18.

Works Consulted

AWS D1.1/D1.1M:2020, *Structural Welding Code — Steel*. American Welding Society, Miami, Fla.

Hill, M. R., and Nelson, D. V. 1998. A simplified eigenstrain approach for determination of sub-surface triaxial residual stress in welds. *researchgate.net/publication/228548937_A_Simplified_Eigenstrain_Approach_for_Determination_of_Sub-surface_Triaxial_Residual_Stress_in_Welds*.

Kaplan, M., and Yildiz, A. K. 2003. The effects of production methods on the microstructures and mechanical properties of an aluminum bronze. *Materials Letters* 57(28): 4402–4411.

Li, J., Guo, H., and Zhou, P. 2015. Experimental study and analysis of the dynamic mechanical properties of aluminium bronze/eksperimentalna studija in analiza dinamicnih mehanskih lastnosti aluminijevega brona. *Strojniski Vestnik-Journal of Mechanical Engineering* 61(11): 680–88.

ASME Section IX: 2010, *Qualification Standard for Welding and Brazing Procedures, Welders, Brazers, and Welding and Brazing Operators*. The American Society of Mechanical Engineers, New York, N.Y.

Türker, M., Acar, S., Cömert, Z. Y., Kisasoz, A., and Guler, K. A. 2018. Characterization of mechanical properties and corrosion behaviours of Mn and Al bronze castings. *Practical Metallography* 55(1): 5–18.

CATHERINE GOSSER (gossermarine@gmail.com) *is an engineering student and ISAAC STEELE is an engineering instructor at Everett Community College, Everett, Wash. FRANK GOSSER is an American Welding Society Certified Welding Inspector and Washington Association of Building Official certified welder.*

Photo credits for the lead and Fig. 1: Frank Gosser. Figs. 3–6: Catherine Gosser.

CERTIFICATION SEMINARS, CODE CLINICS, AND EXAMINATIONS

Note: The 2021 schedule for all certifications are posted online at *awo.aws.org/instructor-led-seminars/seminar-exam-schedule.*

Certified Welding Inspector (CWI)

Seminar covers Parts A, B, and C of the CWI exam. Only Part B of the exam is taken following the conclusion of the seminar. Parts A and C are given at Prometric testing centers.

Location	Seminar Dates	Part B Exam Date
Miami, FL	March 7–12	March 13
Salt Lake City, UT	March 7–12	March 13
Houston, TX	March 7–12	March 13
Chicago, IL	March 14–20	March 21
Phoenix, AZ	March 14–20	March 21
Boston, MA	March 21–26	March 27
Portland, OR	March 21–26	March 27
Dallas, TX	April 11–16	April 17
Minneapolis, MN	April 11–16	April 17
Norfolk, VA	April 11–16	April 17
Las Vegas, NV	April 18–23	April 24
St. Louis, MO	April 18–23	April 24
Cleveland, OH	April 25–30	May 1
Bakersfield, CA	April 25–30	May 1
Baton Rouge, LA	May 2–7	May 8
Sacramento, CA	May 2–7	May 8
Detroit, MI	May 2–7	May 8
Denver, CO	May 16–21	May 22
Nashville, TN	May 16–21	May 22
Pittsburgh, PA	June 6–11	June 12
Birmingham, AL	June 6–11	June 12
Benicia, CA	June 13–18	June 19
Spokane, WA	June 13–18	June 19
Hartford, CT	June 13–18	June 19
Farmingdale, NJ	June 20–25	June 26
Beaumont, TX	June 20–25	June 26
Louisville, KY	July 11–16	July 17
Phoenix, AZ	July 11–16	July 17
Miami, FL	July 18–23	July 24
Cleveland, OH	July 18–23	July 24
Milwaukee, WI	July 25–30	July 31
Orlando, FL	July 25–30	July 31
Charlotte, NC	Aug. 1–6	Aug. 7
Los Angeles, CA	Aug. 1–6	Aug. 7
Denver, CO	Aug. 8–13	Aug. 14
Salt Lake City, UT	Aug. 8–13	Aug. 14

Certified Welding Inspector (CWI) Part B

Course covers only Part B of the CWI exam. The Part B exam follows the conclusion of the three-day course.

Location	Seminar Dates	Part B Exam Date
Sacramento, CA	March 10–12	March 13
Las Vegas, NV	May 19–21	May 22
Minneapolis, MN	July 28–30	July 31
Cleveland, OH	Sept. 29–Oct. 1	Oct. 2
Miami, FL	Dec. 15–17	Dec. 18

9-Year Recertification Seminar for CWI/SCWI

For current CWIs and SCWIs needing to meet education requirements without taking the exam.

Location	Seminar Dates
St. Louis, MO	March 7–12
Seattle, WA	March 21–26
Dallas, TX	April 18–23
Denver, CO	May 2–7
Miami, FL	May 2–7

Certified Welding Educator (CWE)

Seminar and exam are given at all sites listed under Certified Welding Inspector. Seminar attendees will not attend the Code Clinic portion of the seminar (usually the first two days).

Certified Welding Sales Representative (CWSR)

CWSR exams are given at Prometric testing centers. More information at *aws.org/certification/detail/certified-welding-sales-representative*.

Certified Resistance Welding Technician (CRWT)

A comprehensive two-day seminar to arm attendees with the knowledge needed to take the exam with confidence. More information at *aws.org/certification/page/certified-resistance-welding-technician*.

Certified Welding Supervisor (CWS)

CWS exams are given at Prometric testing centers. More information at *aws.org/certification/detail/certified-welding-supervisor.*

Certified Radiographic Interpreter (CRI)

The CRI certification can be a stand-alone credential or can exempt you from your next 9-Year Recertification. More information at *aws.org/certification/detail/certified-radiographic-interpreter*.

Location	Seminar Dates	Exam Date
Dallas, TX	April 26–30	May 1
Las Vegas, NV	June 7–11	June 12

Certified Robotic Arc Welding (CRAW)

OTC Daihen Inc., Tipp City, OH; (937) 667-0800, ext. 218
The Lincoln Electric Co., Cleveland, OH; (216) 383-4723
Wolf Robotics, Fort Collins, CO; (970) 225-7667
Milwaukee Area Technical College, Milwaukee, WI; (414) 456-5454
College of the Canyons, Santa Clarita, CA; (661) 259-7800, ext. 3062
Ogden-Weber Applied Technology College, Ogden, UT; (801) 627-8448
Genesis Systems IPG Photonics Co., Davenport, IA; (563) 445-5688

IMPORTANT: This schedule is subject to change without notice. Please verify your event dates with the Certification Dept. to confirm your course status before making travel plans. Applications are to be received at least six weeks prior to the seminar/exam or exam. Applications received after that time will be assessed a $395 Fast Track fee. Please verify application deadline dates by visiting our website at *aws.org/certification/docs/schedules.html.* For information on AWS seminars and certification programs, or to register online, visit *aws.org/certification* or call (800/305) 443-9353, ext. 273 for Certification; or ext. 455 for Seminars.

Safeguarding against Fumes and Gases

Adapted from American Welding Society (AWS) Safety and Health Fact Sheet No. 1, Fumes and Gases. All of the AWS Safety and Health Fact Sheets are available through the AWS website at aws.org. *Click on Standards on the home page and then on Safety & Health.*

Introduction

Many welding, cutting, and allied processes produce fumes and gases that may be harmful to your health. Fumes are solid particles that originate from welding consumables, the base metal, and any coatings present on the base metal. In addition to shielding gases that may be used, gases are produced during the welding process or may be produced by the effects of process radiation on the surrounding environment. The amount and composition of these fumes and gases depend upon the composition of the filler metal and base material, welding process, current level, arc length, and other factors.

Acquaint yourself with the effects of these fumes and gases by reading the Safety Data Sheets for all materials used (e.g., consumables, base metals, coatings, and cleaners). For help, consult a qualified person such as an industrial hygienist.

Possible Effects of Overexposure

Depending on the material involved, the effects of overexposure to fumes and gases can range from irritation of eyes, skin, and respiratory system to more severe complications. Effects can occur immediately or some later time.

Fig. 1 — In some cases, natural air movement provides enough ventilation and fresh air to protect against overexposure to gases and fumes. (Photo credit: AWS Welding Handbook, *Ninth Edition, Volume 2, Welding Processes, Part 1.)*

Welding fume is on the International Agency for Research on Cancer list as posing a lung cancer risk to humans. It can cause symptoms such as nausea, headaches, dizziness, and metal fume fever. The possibility of more serious health issues exists when highly toxic materials are involved. For example, manganese overexposure can affect the central nervous system, resulting in impaired speech and movement. Additionally, in confined spaces, gases can displace breathing air and cause asphyxiation (see AWS Safety and Health Fact Sheet No. 11, *Hot Work in Confined Spaces*).

How to Avoid Overexposure

The following are recommendations for preventing overexposure to fumes and gases:

- Keep your head out of the fumes.
- Do not breathe the fumes.
- Use enough ventilation or exhaust at the arc, or both, to keep fumes and gases from your breathing zone and general area.
- In some cases, natural air movement provides enough ventilation and fresh air — Fig. 1.
- Where ventilation is questionable, use air sampling to determine the need for corrective measures.
- Use mechanical ventilation to improve air quality.
- If engineering controls are not adequate to prevent overexposures, use proper respiratory protection (see AWS Safety and Health Fact Sheet No. 38, *Respiratory Protection Basics for Welding Operations*).
- Whenever the following materials are identified as other than trace constituents in welding, brazing, or cutting operations, and unless breathing zone sampling under the most adverse conditions has established that the level of hazardous constituents is below the allowable limits specified by the authority having jurisdiction, special ventilation precautions shall be taken: antimony, arsenic, barium, beryllium, cadmium, chromium, cobalt, copper, lead, manganese, mercury, nickel, ozone, selenium, silver, and vanadium. (See section 5.5, Special Ventilation Concerns, in ANSI Z49.1, *Safety in Welding, Cutting, and Allied Processes*.)
- Work in a confined space only if it is well ventilated or while wearing an air-supplied respirator. Fumes from welding or cutting and oxygen depletion can alter air quality, causing injury or death. Be sure the breathing air is safe.
- Follow Occupational Safety and Health Administration guidelines for permissible exposure limits for various fumes.
- Follow American Conference of Governmental Industrial Hygienists recommendations for fume and gas threshold limit values.
- Have a qualified person, such as an industrial hygienist, check the operation and air quality and make recommendations for the specific welding or cutting situation. WJ

Industry Leaders Recognized in 2020

Meet the Class of 2020 Fellows and Counselors

The 2020 class of American Welding Society (AWS) Fellows and Counselors were recognized at the 101st Annual Meeting held during the AWS Education 2020 Virtual Summit, which took place the week of November 16.

The Fellows are Susan Fiore, Michael Karagoulis, and Alexander Shapiro. The Counselor is Richard Corbit.

AWS Fellows are cited for "*serving the welding community and industry with great distinction as individuals whose careers have contributed significantly to the knowledge, science, and application of welding.*"

Susan Fiore is recognized as a spokesperson and industry-leading expert in the area of safety and health for more than 30 years. Throughout her career, she has emphasized the importance of understanding how to reduce welder exposure to fumes. Her career also includes more than 20 years in welding filler metal research, development, and application engineering.

Michael Karagoulis is recognized for sustained and innovative contributions to automotive resistance welding, including the creation of a practical standard approach to weld process control, the development of hermetic seam welding for the first ethanol-tolerant steel fuel tank, and the redesign of electrode tip dressers, electrodes, and cooling systems for broader process control.

Alexander Shapiro is recognized for his pioneering work in titanium and advanced materials, including refractory metals, ceramic, and composites; brazing processes; and alloy developments that have made a significant impact on technology advancement.

AWS Counselors are recognized for "*serving the welding community and industry with distinction and organizational leadership that has enhanced the image and impact of the welding industry*."

Richard Corbit is recognized for more than 40 years as a welding professional and his widely known contributions. A well-respected contributor to the AWS D1 Committee on Structural Welding, his depth and breadth of technical knowledge has been a trusted source to the Committee and industry at large.

Susan Fiore

Michael Karagoulis

Alexander Shapiro

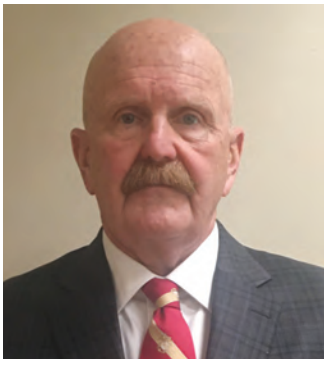

Richard Corbit

2020 Achievement Award Recipients

Adams Memorial Membership Award

This award recognizes educators for outstanding teaching activities in undergraduate and postgraduate engineering institutions.

Jeffrey B. Hardesty is a professor at Ferris State University, where he has worked since 2004 and taught numerous classes across the welding engineering technology curriculum. An AWS member for more than 30 years, he serves on the AWS Education Scholarship Committee, B5C Subcommittee on Qualification of Welding Engineers, and B5F Subcommittee on Qualification of Welding Technicians. He is also an AWS Certified Welding Inspector (CWI).

A. F. Davis Silver Medal Award

This award recognizes authors of papers published in the Welding Journal *during the previous calendar year that represent the best contributions to the progress of welding in the categories of machine design, maintenance and surfacing, and structure design.*

Machine Design

"Bubble Evolution in Ultrasonic Wave-Assisted Underwater Wet FCAW"

Jicai Feng is a tenured professor at the School of Materials Science and Engineering at Harbin Institute of Technology (HIT). He has worked at the State Key Laboratory of Advanced Welding and Joining at HIT since 1983. His research areas include brazing, diffusion bonding, friction stir welding, underwater welding, and space welding.

Jeffrey B. Hardesty

Jicai Feng

Qingjie Sun

Junbo Teng

Jianfeng Wang

Jonah Duch

John N. DuPont

Mathieu Brochu

Nejib Chekir

JJ Sixsmith

He has authored/co-authored more than 200 technical papers and has published four textbooks.

Qingjie Sun is a professor of welding technology and engineering at HIT. His research interests include automatic welding methods and equipment, magnetic field and acoustic field-assisted arc welding, and wire arc additive manufacturing of dissimilar metal. He has authored/co-authored more than 50 peer-reviewed journal papers and holds 18 authorized patents.

Junbo Teng is a postgraduate student at the College of Materials Science and Opto-Electronic Technology at the University of Chinese Academy of Sciences. He holds a bachelor's degree from the State Key Laboratory of Advanced Welding and Joining at HIT. He has published four papers that appeared in influential publications, one of which was named "key scientific article" by *Advances in Engineering*.

Jianfeng Wang is a postdoctoral Fellow at the School of Metallurgy at Northeastern University in China. His research centers on underwater wet welding processes with an emphasis on arc bubble control via ultrasonic waves, arc behavior issues, metal transfer, and microstructure modification of weld metal. He has published more than 30 papers.

Maintenance and Surfacing

"Effect of Multiple Weld Thermal Cycles on HSLA-100 Steel"

Jonah Duch is a research assistant in the Materials Science and Engineering Department at Lehigh University, where he works under the direction of John N. DuPont. His award-winning publication in the *Welding Journal* was also his master's thesis. His current PhD research focuses on the stain aging response of precipitate-strengthened alloys. He is slated to complete his studies this year.

John N. DuPont is the R. D. Stout distinguished professor in the Materials Science and Engineering Department as well as the associate director of the Energy Research Center at Lehigh University. He holds a joint appointment in the Mechanical Engineering Department and is the site director for the National Science Foundation Manufacturing and Materials Joining Innovation Center. He has also won numerous AWS awards and is an AWS Fellow.

Structure Design

"Laser Wire Deposition of a Large TI-6AL-4V Space Component"

Mathieu Brochu is an associate professor in the Department of Mining and Materials Engineering at McGill University, a Gerald Hatch engineering faculty Fellow on additive manufacturing, and the director of the Powder Processing and Additive Manufacturing of Advanced Materials Laboratory. He is also co-director of the Natural Sciences and Engineering Research Council of Canada Network for Holistic Innovation on Additive Manufacturing as well as co-director of the Canadian Additive Manufacturing Network.

Nejib Chekir is an additive manufacturing specialist at Liburdi Automation Inc., where he is involved in various aerospace welding projects. He graduated with a PhD in materials science in 2018 from McGill University. His graduate research focused on laser additive manufacturing of titanium alloys with a focus on the aerospace industry.

JJ Sixsmith is a general manager at Liburdi Automation Inc. and has more than 20 years of experience in welding and professional management. His responsibilities include managing a team of multidisciplined engineering groups as well as performing technical research and development for automated welding systems globally. He is a member of AWS and the Canadian Welding Association and has published in the AWS *Welding Journal*.

Robert Tollett is the director of marketing for Liburdi Turbine Services


Robert Tollett


James D. Corbin


Jonathan Parker


John A. Siefert


Rachel Thomson


Daniel Allford


Barbie Parsons


Rute Ferraz


Richard Freeman


YuMing Zhang

Inc. During the last 40 years, he has worked for a number of aerospace firms in various roles from quality control to general management and marketing. This includes working at the Pratt & Whitney Training Facility and the Teleflex Sermatech International Facility. He holds degrees from John Abbott College/McGill University and McMaster University.

Dalton E. Hamilton Memorial CWI of the Year Award

This award recognizes AWS members participating in the SCWI/CWI programs whose inspection, Society, and civic activities have enhanced public awareness of the Society and the CWI program or who have otherwise made an outstanding contribution to the science of welding inspection.

James D. Corbin is a project special inspector with Shrewsberry & Associates, where he is involved with expansion projects at Denver International Airport. He was an AWS Certified Welder for 26 years as well as a CWI and Certified Welding Educator for the last 22 years. For 25 years, he has served the AWS Colorado Section in multiple capacities, including secretary, education chair, and section chair. He currently serves on several AWS Subcommittees.

W. H. Hobart Memorial Award

This award is presented to the authors of the paper published in the Welding Journal *during the previous calendar year that describes the best contribution to pipe welding, the structural use of pipe or similar applications, excluding the manufacture of pipe.*

"Cross-Weld Creep Performance in Grade 91 Steel: Macro-Based Assessment"

Jonathan Parker is a senior technical executive at the Electric Power Research Institute (EPRI), where he provides technical support for projects associated with understanding the factors affecting damage in critical components in both traditional and advanced power plants. He is the editor of three books as well as the author/co-author of more than 50 major reports and 200 publications.

John A. Siefert is a program manager for the materials and repair program at EPRI. He holds a PhD from Loughborough University, where his areas of research included examination and behavior of creep-strength-enhanced ferritic materials, advanced stainless steels, nickel-based alloys, and dissimilar metal welds. He is also the author/co-author of more than 150 manuscripts.

Rachel Thomson is the pro-vice chancellor for teaching at Loughborough University. Her research combines materials modeling and advanced experimental characterization, which has enabled industrial partners to improve the efficiency, lifetime, and environmental performance of metallic components used in power generation. She is also the 2018 East Midlands Inspirational Female Leader of the Year and a Fellow of the Royal Academy of Engineering.

Honorary Membership Award

This award is presented to a person of acknowledged eminence in the welding profession or who is credited with exceptional accomplishments in the industry.

Daniel Allford, an AWS Life Member, has been president and owner of ARC Specialties for more than 33 years. He grew the company from a one-person operation into a 65-person team of engineers and craftspeople. He holds several patents in the field of welding automation as well as degrees from the University of Houston and the Texas State Technical Institute.

Barbie Parsons, known as "Barbie the Welder," is a metal sculptor who has created works for clients such as Harley Davidson, Carolina Shoe Co., Miller Electric, Weiler Abrasives, Chicago Pneumatic, and more. She teaches metal art creation through her


William F. Newell Jr.


Daryush Aidun


John Goldak


Marcias Martinez

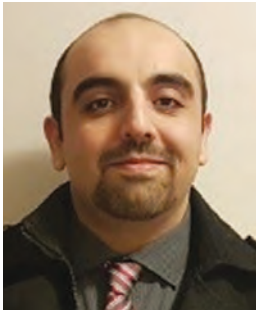
Hossein Nimrouzi


Marharyta Pliazhuk


Carlos Reyes


Nathan Switzner

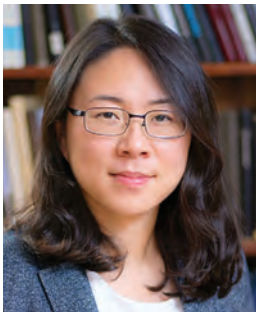
Zhenzhen Yu


Duane K. Miller

YouTube channel, which is viewed in 51 countries, and has a product line of metal art welding kits. She has also written five books.

International Meritorious Certificate Award

This certificate recognizes an individual who has made significant contributions to benefit the worldwide welding industry.

Rute Ferraz has more than 35 years of experience in quality management systems and training. She is chief executive of both the European Welding Federation and the International Institute of Welding's (IIW's) International Authorization Board. She was also the training department director at Instituto de Soldadura e Qualidade from 2001 to 2019.

Richard Freeman is the associate director and industrial membership group manager at TWI, where he has worked since 1996. He has also been involved in welding and additive manufacturing standards committees, including the AWS D17 Committee on Welding in the Aircraft and Aerospace Industry as well as its subcommittees.

YuMing Zhang is a professor of electrical engineering at the University of Kentucky. He has been involved with more than 200 peer-reviewed journal papers and holds ten U.S. patents in advanced sensing and control of innovative welding processes, intelligent robotic systems, and learning/modeling of human welder intelligences. He is also a Fellow of AWS, ASME, and SME.

William Irrgang Memorial Award

This award recognizes the individual who has done the most to enhance the Society's goal of advancing the science and technology of welding over the last five years.

William F. Newell Jr., an AWS Life Member and Counselor, has more than 40 years' experience in welding engineering applications and consulting, domestically and internationally. He is president of W. F. Newell & Associates Inc. and co-founder/vice president of engineering at Euroweld Ltd. He is also chair, second vice chair, and member of several AWS committees.

Charles H. Jennings Memorial Award

This award is presented for the most valuable paper written by a college student or faculty representative published in the Welding Journal *during the previous calendar year.*

"In-Situ Monitoring of Transient Strain Formation in Vertical Welds"

Daryush Aidun teaches welding metallurgy and additive manufacturing at Clarkson University. He has also been director of the university's Welding Research Lab since 1982. Additionally, he was the editor of chapter 3, "Heat Flow in Welding," for the AWS *Welding Handbook*, Vol. 1 (2019). His areas of research include weld process modeling, additive manufacturing of duplex stainless steels, and nickel-based superalloys.

John Goldak is founder and president of Goldak Technologies Inc., a developer of software for design-driven analysis and optimization of welds and welded structures. He is best known for his development of the double-ellipsoid weld pool model. He has also been the recipient of numerous accolades, including the Pioneers of Computational Weld Mechanics Award and the AWS Comfort A. Adams Award.

Marcias Martinez works in the Department of Mechanical and Aeronautical Engineering at Clarkson University, where he performs research on the integrity of aerospace structures. His role includes teaching and supervising students in finite elemental analysis, experimental mechanics, smart materials, and load monitoring. He is also an associate editor for the *Journal of*


Jeff Deckrow


Scott Witkowski


Esteban Guerrero


Alice Kilgo


Bonnie McKenzie


William J. Price


Paul T. Vianco


Shelley Williams


Rishi Kant


Manabu Tanaka

Intelligent Material Systems and Structures.

Hossein Nimrouzi is a welding simulation finite element method analyst at Goldak Technology Inc., where he has worked for six years. He has also worked with Atomic Energy of Canada Ltd. to design supercritical water reactors. He holds a bachelor's in mechanical engineering from Azad University and a master's in applied mechanical engineering from Carleton University.

Marharyta Pliazhuk is a lead engineer at Wabtec Corp. She graduated from Clarkson University in May 2020 with great distinction and was actively involved in student organizations and professional/honor societies. She presented her first published paper at a conference in 2018 and won first place in the engineering category for oral presentation.

Carlos Reyes is a mechanical designer at Royal Power Solutions, where he develops and designs new parts and tooling for the automotive industry. He holds a master's degree in mechanical design from the Center for Engineering and Industrial Development in Mexico and completed a research stay at Clarkson University.

McKay-Helm Award

This award is presented for the best contribution to the advancement of knowledge of low-alloy steel, stainless steel, or surfacing welding metals involving the use, development, or testing of these materials, as represented by articles published in the Welding Journal *during the previous calendar year.*

"Austenitic Stainless-Steel Cladding Interface Microstructures Evaluated for Petrochemical Applications"

Nathan Switzner is a metallurgical engineering consultant at RSI Pipeline Solutions. He earned a PhD from the Colorado School of Mines, where he conducted research on dissimilar welding and cladding for corrosion resistance. He previously held positions at Honeywell Federal Mfg. & Technologies as well as Exponent Failure Analysis Associates.

Zhenzhen Yu is an assistant professor in the Metallurgical and Materials Engineering Department at the Colorado School of Mines as well as the director of the Center for Welding, Joining and Coatings Research. She also serves on the AWS Education and Technical Papers Committees as well as the ASM International Joining Critical Technologies Sector.

Professor Koichi Masubuchi Award

This award is presented to an individual who has made significant contributions to the advancement of science and technology of materials joining through research and development.

John A. Siefert (See bio under W. H. Hobart Memorial Award.)

Samuel Wylie Miller Memorial Medal Award

This award is given for meritorious achievements that have contributed conspicuously to the advancement of the art and science of welding and cutting.

Duane K. Miller, an AWS Fellow, is manager of engineering services at The Lincoln Electric Co. as well as an adjunct professor at the University of Alberta. He is a member of the AWS D1 Committee on Structural Welding and formerly served as chair of several committees. He also served as member of the AWS Board of Directors. Additionally, he has appeared as a subject expert on the *History* and *Discovery* channels.

National Meritorious Award

This award recognizes good counsel, loyalty, and devotion to the affairs of the Society as well as the promotion of cordial relations with industry and other organizations.

Before his retirement, Jeff Deckrow was vice president, Americas, at Hypertherm. He is chair of the AWS

Careers in Welding Committee and serves on the AWS Foundation Board of Trustees. He also served as chair of the Welding Equipment Manufacturers Association (WEMCO) and on its Executive Committee for 19 years. He is the recipient of the WEMCO Excellence in Welding Award in the Exceptional category.

Scott Witkowski founded the largest independent welder/materials testing laboratory in the United States, has co-authored papers that advance the industry, and is regularly featured as a guest speaker at technical conferences and symposiums on the subject of welding performance and procedure qualifications. He is also one of the founding organizers of the annual AWS Welding Summit.

Robert L. Peaslee Memorial Brazing Award

This award recognizes the paper considered to be the best contribution to the science or technology of brazing published in the Welding Journal *during the previous calendar year.*

"The Mechanical Performance of Sn-Pb Solder Joints on LTCC Substrates"

Esteban Guerrero is a retired senior materials engineer from Honeywell Federal Mfg. & Technologies. During his career, he worked in research, process development, failure analysis and applications of solders, and gold-based alloys used for electronic packaging. He holds a master's in materials science from Polytechnic University.

Alice Kilgo was a technologist at Sandia National Laboratories for more than 33 years prior to her retirement. Her work focused on metallography, failure analysis, and image analysis.

Bonnie McKenzie spent 34 years working as a technologist at Sandia National Laboratories until her retirement in 2019. She worked in the Materials Characterization Department performing scanning electron microscopy and analyses on different materials — including solder alloys — and types of welds.

William J. Price, a retiree, works on bioresearch projects on his farm in Kansas. He previously worked as a technical specialist in the Physical Vapor Deposition Lab at Honeywell Federal Mfg. & Technologies. He has more than 40 years' experience in the material coating industry, including electroplating of printed circuits, heavy metal plating, and physical vapor deposition.

Shinichi Tashiro

Anh Van Nguyen

Dongsheng Wu

Paul T. Vianco, a Fellow of AWS and ASM International, is a technical staff member at Sandia National Laboratories, where he has worked since 1987. He is the author of the *Soldering Handbook*, third edition, and the *Guideline for Hand Soldering Practices*, first edition, both of which were published by AWS. He is also co-author of the TurboSiP v2.0 solder fatigue software and holds five U.S. patents.

Shelley Williams is a principal technologist with 13 years of experience at Sandia National Laboratories, where she oversees the laboratories and equipment that support the advancement of solder technology. Specializing in test design and execution for determining material properties, she evaluates the performance and reliability of solder joints and soldered components to assess the impact of aging and degradation over operational lifetimes.

Warren F. Savage Memorial Award

This award recognizes the paper published in the Welding Journal *Research Supplement the previous calendar year that best represents innovative research resulting in a better understanding of the metallurgical principles related to welding.*

"Stress Relief Cracking Susceptibility in High-Temperature Alloys"

John N. DuPont (See bio under A. F. Davis Silver Medal Award.)

Rishi Kant is a fifth-year materials science PhD student at Lehigh University. He is also a Rossin Doctoral Fellow and a recipient of the Richard Hay Barkalow Outstanding Graduate Student Award for academic excellence and service to the materials science department. His research centers on joining low-density, high-Mn-Al steels for automotive applications.

William Spraragen Memorial Award

This award recognizes the best paper published in the Welding Journal *Research Supplement during the previous calendar year.*

"Undercut Formation Mechanism in Keyhole Plasma Arc Welding"

Manabu Tanaka is a professor and director of the Joining and Welding Research Institute (JWRI) at Osaka University. He is also chair of the Council of Joint Usage/Research Centers in National Universities. His research areas involve the physics of welding, including plasma diagnostics, electrode phenomena, and numerical modeling.

Shinichi Tashiro is an assistant professor at the JWRI in Osaka University. His research focuses on the keyhole and weld pool formation mechanism of arc welding as well as hybrid plasma gas metal arc welding of thick plates. He has published more than 150 papers in peer-reviewed journals and is an editorial board member of the *Materials* journal.

Anh Van Nguyen is the leader of the welding technology study group at Murata Welding Laboratory. The group recently developed a novel welding technology for joining ultra-thin sheets. His research interests include the arc phenomena and thermodynamic of the weld pool in arc welding processes. He has a PhD in material science and engineering and has published more than 30 scientific papers.

Dongsheng Wu is a doctoral student at the JWRI in Osaka University. His research focuses on equipment development, process, online detection, and numerical simulation of advanced hybrid arc welding and hybrid gas metal arc welding. He has published more than 30 papers in international journals.

Douglas Kautz

Peng-Sheng Wei

Teresa Melfi

R. D. Thomas Memorial Award

This award recognizes a member of the American Council of IIW or an AWS member who has made a substantial contribution to IIW activities.

Douglas Kautz, an AWS Counselor, is a policy analyst for Leidos Inc., where he supports the National Nuclear Security Administration. He has served on numerous AWS committees, including the C7 Committee on High Energy Beam Welding and Cutting. He is currently chair of the AWS Welding Handbook Committee. He is also active in IIW Commissions I (additive manufacturing, thermal cutting, and surfacing), where he is chair, and IV (high-energy beam processes).

Elihu Thomson Resistance Welding Award

This award recognizes an outstanding contribution to the technology and application of resistance welding, including equipment innovations, unique applications in production, a published paper, or other activity of merit.

Peng-Sheng Wei, a Fellow of AWS and ASME, is a professor in the Department of Mechanical and Electro-Mechanical Engineering at National Sun Yat-Sen University (NSYSU). He is also a Xi-Wan chair professor at NSYSU and a senior technical consultant on resistance spot welding (RSW) for the R&D center at Hotway Technology Corp. He has published more than 70 papers and delivered 75 keynote speeches or invited lectures on RSW. He is also the recipient of multiple AWS awards.

George E. Willis Award

This award recognizes an individual for promoting the advancement of welding internationally by fostering cooperative participation in areas such as technology transfer, standards rationalization, and promotion of industrial goodwill.

Teresa Melfi has been in the welding industry for more than 30 years, with roles in the manufacture, design, and application of welding machines, consumables, and processes. She supports the global welding community through involvement in standards bodies, industry and academic projects, peer reviews, and technical seminars. She serves on multiple AWS committees and is chair of the A5 Committee on Filler Metals and Allied Materials. She also holds numerous United States and international patents.

AWS Raises Money to Support Feeding South Florida

The AWS Campaign to support Feeding South Florida exceeded its goal and raised enough funds to provide 7380 meals to local families.

TECH TOPICS

Welding Handbook Committee Seeks Volunteers

The AWS *Welding Handbook* will need volunteers (chapter chairs and chapter committee members) for Vol. 3 of the 10th Ed.

For more information, contact Kathy Sinnes, *ksinnes@aws.org*, ext. 255.

Opportunities to Contribute to AWS Technical Committees

The following committees welcome new members. Some committees are recruiting members with specific interests in regard to the committee's scope, as marked below: Producers (P), General Interest (G), Educators (E), Consultants (C), and Users (U). For more information, contact the staff member listed or visit *aws.org/library/doclib/Technical-Committee-Application.pdf*.

S. Borrero, *sborrero@aws.org*, ext. 334. **Definitions and symbols**, A2 Committee (E). **Titanium and zirconium filler metals**, A5K Subcommittee. **Piping and tubing**, D10 Committee (C, E, U). **Welding practices and procedures for austenitic steels**, D10C Subcommittee. **Aluminum piping**, D10H Subcommittee. **Chromium molybdenum steel piping**, D10I Subcommittee. **Welding of titanium piping**, D10K Subcommittee. **Purging and root pass welding**, D10S Subcommittee. **Low-carbon steel pipe**, D10T Subcommittee. **Orbital pipe welding**, D10U Subcommittee. **Duplex pipe welding**, D10Y Subcommittee. **Joining metals and alloys**, G2 Committee (E, G, U). **Reactive alloys**, G2D Subcommittee (G).

R. Gupta, *gupta@aws.org*, ext. 301. **Filler metals and allied materials**, A5 Committee (E). **Magnesium alloy filler metals**, A5L Subcommittee.

P. Portela, *pportela@aws.org*, ext. 311. **Additive manufacturing**, D20 Committee (C, E, G). **Titanium structural welding**, D1N Subcommittee (C, E, G, P, U).

J. Molin, *jmolin@aws.org*, ext. 304. **Structural welding**, D1 Committee (E). **Sheet metal welding**, D9 Committee (C, G, P).

K. Bulger, *kbulger@aws.org*, ext.

306. **Methods of weld inspection**, B1 Committee (C, E). **Brazing and soldering**, C3 Committee (C, E, G). **Welding in marine construction**, D3 Committee (C, E, G, U). **High energy beam welding and cutting**, C7 Committee (C, E, G). **Hybrid welding**, C7D Subcommittee (G). **Welding of machinery and equipment**, D14 Committee (C, E, G, U).

M. Diaz, *mdiaz@aws.org*, ext. 310. **Resistance welding**, C1 Committee (C, E, G, U). **Friction welding**, C6 Committee (C, E). **Automotive welding**, D8 Committee (C, E, G, U).**Resistance welding equipment**, J1 Committee (C, E, G, U). **Welding in the aircraft and aerospace industry**, D17 Subcommittee (C, E, G).

S. Hedrick, *steveh@aws.org*, ext. 305. **Metric practice**, A1 Committee (C, E). **Mechanical testing of welds**, B4 Committee (E, G, P). **Joining of plastics and composites**, G1 Committee (C, E, G). **Safety and health**, SHC Committee (E, G). **Welding in sanitary applications**, D18 Committee.

J. Rosario, *jrosario@aws.org*, ext. 308. **Procedure and performance qualification**, B2 Committee (E, G). **Thermal spraying**, C2 Committee (C, E, G, U). **Oxyfuel gas welding and cutting**, C4 Committee (C, E, G). **Welding iron castings**, D11 Committee (C, E, G, P, U). **Railroad welding**, D15 Committee (C, E, G, U). **Robotic and automatic welding**, D16 Committee (C, E).

Standards for Public Review

AWS was approved as an accredited standards-preparing organization by the American National Standards Institute (ANSI) in 1979. AWS rules, as approved by ANSI, require that all standards be open to public review for comment during the approval process. This column also advises of ANSI approval of documents.

C3.6M/C3.6:2016-AMD2, *Specification for Furnace Brazing*. Addenda Standard. $36.00. ANSI public review expires 2/1/2021. Contact: K. Bulger, *kbulger@aws.org*, ext. 306.

D1.6/D1.6M:2017-AMD1, *Structural Welding Code — Stainless Steel*. Addenda Standard. $146.00. ANSI public review expires 2/8/2021. Contact: S. Borrero, *sborrero@aws.org*, ext. 334.

D10.10/D10.10M:20XX, *Recommended Practices for Local Heating of Welds in Piping and Tubing*. Revised Standard. $32.00. ANSI public review expires 2/1/2021. Contact: S. Borrero, *sborrero@aws.org*, ext. 334.

D15.2/D15.2M:20XX, *Specification for Joining Railroad Rail and Related Rail Components*. Revised Standard. $40.00. ANSI public review expired 1/25/2021. Contact: J. Rosario, *jrosario@aws.org*, ext. 308.

AWS D1.1/D1.1M:2020 Errata

Errata have been identified and will be incorporated into the next reprinting of AWS D1.1/D1.1M:2020, *Structural Welding Code — Steel*. To view the errata, visit *aws.org/standards/page/errata*.

Technical Committee Meetings

All AWS technical committee meetings are open to the public. Contact the staff members listed or call (800/305) 443-9353 for information.

Feb. 2, 3. D15 Committee and Subcommittees on Railroad Welding. Miami, Fla. Contact: J. Rosario, ext. 308, *jrosario@aws.org*.

March 19, 20. C3 Committee and Subcommittees on Brazing and Soldering. Miami, Fla. Contact: K. Bulger, *kbulger@aws.org*, ext. 306.

MEMBERSHIP ACTIVITIES

2020 Membership Challenge

Listed here are the members who participated in the 2020 Membership Challenge — point standings as of December 17. The campaign ran from Jan. 1 to Dec. 31, 2020. Members received 5 points for each Individual Member and 1 point for every Student Member they recruited.

J. W. Fregia, Houston — 95
J. W. Morris, Mobile — 75
A. P. Duris, NW Ohio — 51
A. D. Dillon, Detroit — 38
S. A. Milner, San Francisco — 36
B. J. Cain, Los Angeles/Inland Empire — 34
J. P. Theberge, Boston — 31
A. D. Stute, Madison-Beloit — 30
J. C. Durbin, Tri-River — 30
V. O. Harthun, Northern Plains — 30
D. L. Galiher, Detroit — 29
T. A. Uff, Lehigh Valley — 29
D. P. Thompson, SW Virginia — 29
R. Young, Iowa — 24
T. Edwards, Tulsa — 20
H. J. Merrill II, Louisville — 20
D. S. Beecher, San Diego — 20
R. K. McClure, Los Angeles/Inland Empire — 18
J. Napier, Cleveland — 17
W. H. Wilson, New Orleans — 17
B. A. Cheatham, Columbia — 17
O. Ortiz, Los Angeles/Inland Empire — 16
G. J. Smith, Lehigh Valley — 15
C. W. Gilbertson, Northern Plains — 14
C. Consentino, Pittsburgh — 13
R. Riggs, Tulsa — 13
T. A. Harris, Johnstown-Altoona — 13
S. Silverstein, Milwaukee — 12
M. D. Stein, Detroit — 11

New AWS Supporters

Welding Distributor Member

Global Shop Solutions
975 Evergreen Circle
The Woodlands, TX 77380

Educational Institution Members

Alfredo's Iron Works Inc.
280 W. Lincoln Hwy.
Cortland, IL 60112

Elizabethtown Community and Technical College
620 College St. Rd.
Elizabethtown, KY 42701

RK Mechanical
3800 Xanthia St.
Denver, CO 80238

Seymour High School — Seymour Community School
1638 S. Walnut St.
Seymour, IN 47274

Welding & Joining Management Group
3756 Monarch St.
Frederick, CO 80516

Affiliate Corporate Members

Advanced Manufactured Products
12550 Wiles Rd.
Coral Springs, FL 33076

Aeroforge
609 N. Levee Rd.
Puyallup, WA 98371

Capone Iron Corp.
20 Turcotte Memorial Dr.
Rowley, MA 01969

Diamond
243 W. 8 St.
Wyoming, PA 18644

G&G Enterprises Construction Corp.
3260 E. Texas Fwy.
Beaumont, TX 77703

Garco Construction
4114 E. Broadway Ave.
Spokane, WA 99202

Geib Industries Inc.
901 E. Jefferson St.
Bensenville, IL 60106

Idaho Transportation Department
3311 W. State St.
Boise, ID 83703

Miller Gases & Equipment Corp.
181 S. Wineville Ave.
Unit Q
Ontario, CA 91761

W. M. Keck Observatory
65-1120 Mamalahoa Hwy.
Kamuela, HI 96743

Walters Buildings
6600 Midland Ct.
Allenton, WI 53002

Sustaining Members

Air Products and Chemicals Inc.
Port Manatee Manufacturing
2525 Inland Transport St.
Palmetto, FL 34221

CO2Meter
131 Business Center Dr.
Ormond Beach, FL 32174

Fincantieri Bay Shipbuilding
605 N. 3 Ave.
Sturgeon Bay, WI 54235

Garco Construction
4114 E. Broadway Ave.
Spokane, WA 99202

George's Welding Services Inc.
11400 NW 134 St.
Miami, FL 33178

Industrial Inspection Co.
399 Detroit Ave.
Monroe, MI 48162

Supporting Company Member

LAL Acquisition Inc.; Lift-A-Loft Corp.
9501 S. Center Rd.
Muncie, IN 47302

AWS Member Counts January 1, 2021

Sustaining	*570*
Supporting	*342*
Educational	*830*
Affiliate	*648*
Welding Distributor	*61*
Total Corporate	***2451***
Individual	*55,487*
Student + Transitional	*9,746*
Total Members	***65,233***

Candidates Sought to Receive the MIT Masubuchi Award

The Prof. Koichi Masubuchi award, with a $5000 honorarium, is presented to one person, 40 years old or younger, who has made significant contributions to the advancement of materials joining through research and development.

Send a list of your candidate's experience, publications, honors, awards, and at least three letters of recommendation from fellow researchers to Prof. Todd Palmer, *tap103@psu.edu*. This award is sponsored annually by the Massachusetts Institute of Technology, Dept. of Ocean Engineering.

Distinguished Welder Award Nominations

The Distinguished Welder Award recognizes an individual whose welding skills and experience would earn him or her the recognition of being an AWS Distinguished Welder.

A complete nomination packet should include information addressing the candidate's definition and application criteria as outlined in the AWS Distinguished Welder Award Nomination Form found at *aws.org/about/page/outstanding-achievement-awards*. The focus of the nomination packet should include specifics of the individual's skills.

Send nominations by the May 1 deadline to Malisa Mercado at *mmercado@aws.org*.

AWS Member Profile

Kaitlynn Lurie

"To any young person who wants to learn welding, I say, 'Do it. You will NOT regret it.'"

For most of her young life, Kaitlynn Lurie felt like a fish out of water. All of that changed when she discovered welding during an eighth-grade tour of Old Colony Regional Vocational Technical High School (RVTHS), Rochester, Mass. As a 13 year old, Lurie felt an inexplicable pull toward the welding shops even though she had never welded before.

"I knew before I had even stepped foot in the welding shop that I wanted to visit it," she recalled. "The second I entered the shop, I knew I belonged there. It felt like I had finally found somewhere I fit in."

Lurie wasn't able to weld that day because she wore a mitten cast due to a sports injury, but that didn't diminish her excitement. With the help of an older student, she was able to use the shop's jig to bend a metal bar. The experience set her on a course for a career in welding.

"I watched the students of the older classes do such cool things from oxyfuel to TIG [gas tungsten arc] welding and knew that was the path for me," she recollected. "I left the building that day certain in my future in welding and worked hard to achieve that goal the following year."

Soon after, Lurie enrolled in the metal fabrication and joining technology program at Old Colony RVTHS.

"It was scary being a young teen learning a dangerous skill, but it opened up a world of possibilities for me," she explained. "To any young person who wants to learn welding, I say, 'Do it. You will NOT regret it.'"

As a student, she took part in SkillsUSA competitions, where she did well.

"The experience of meeting hundreds of people who are also very passionate about their trade is unforgettable," she said. "If given the chance, I would do it all over again."

In her junior year in high school, Lurie became a member of the American Welding Society (AWS). She took on an executive committee role in the Central Massachusetts/Rhode Island Section soon after. She is said to be the first young woman and the youngest person to serve on the Section's executive committee.

Lurie has also held multiple welding and manufacturing jobs since 2017. Her first job was a co-op position making artistic tables and wall decorations out of different types of metal.

"I learned basic machining skills and how to patina — a special type of finish using acid to basically dye metal a different color," she said.

Today, Lurie is 21 years old and working as a welding technician in a warehouse, where she has been for more than two years. She takes pride in knowing she is the only welding technician in the building. Lurie is also the second vice chair and student member liaison for the AWS Central Massachusetts/Rhode Island Section.

"I act as a team leader for the membership, attendance, hospitality, entertainment, and publicity committees, essentially dealing with membership promotion," she explained. "As a student member liaison, I act as a link between student members of the AWS and the older generations, answering student questions and providing advice and resources to any who reach out."

Lurie's volunteer work with the Section is motivated by her desire to be a positive example to other young women, especially her little sister.

"Being a female, especially a young one, in this trade can be difficult and maybe even a little toxic. I want young women to see they have the potential to be successful in a predominantly male trade," she said. "At school, I was the only girl in my shop for the class of 2018, and to this day I am the only woman in the machine shop at my place of employment. I want women to see that if I can do it and achieve my goals, they can as well."

Lurie's work with the Section was recognized when she was given the District Director Award in 2020. She is grateful to the Section's members for the support, knowledge, and opportunities they've offered her. Through her Section work, she aims to do the same for other young people interested in careers in welding.

"They [Section members] are an amazing group of men who have put their faith in me to be a valuable part of the executive committee, and I try my best every day to be a young voice that can change and improve the way we do things," she said. "I feel as if I will be a stepping stone for other young men and woman in this organization. The youth of this world are the future, and we are actively bringing change in not only the world but the industry."

Her future plans are to become a journeyman licensed pipefitter as well as a welding instructor. According to Lurie, it is a running joke within her Section that she will one day replace her high school welding instructor, Douglas A. Desrochers, when he retires. She credits Desrochers for her welding career and hopes to become an influential teacher like him.

"He had taken me under his wing to teach me everything he possibly could, and still does to this day. He has welcomed me into his family and is the reason I am where I am today. Without his guidance and support, I do not see my life being the way it is. I've got big shoes to fill in the teaching portion of this trade, and I have faith that through his unwavering support and dedication I will be able to fill the shoes he will leave behind," she affirmed. "Mr. Desrochers, if you are reading this, thank you for taking a chance on me. I will never be able to thank you enough."

District 1

Douglas A. Desrochers, director
(508) 763-8011
dadaws@comcast.net

District 2

Harland Thompson, director
(631) 546-2903
harland.w.thompson@ul.com

District 3

Sean Moran, director
(717) 885-5039
sean.moran@phillyshipyard.com

District 4

Mr. Lynn Showalter, director
(757) 848-8029
lynneshowalter@gmail.com

District 5

Howard Record, director
(352) 816-0835
howard@rtdtools.com

ATLANTA
November 5

Location: BTD Mfg., Dawsonville, Ga.
Presenters: Janet Jackson, human resources recruiter, and James Vogt, director of operations, BTD Mfg.
Summary: BTD hosted the Section's November meeting at its facility. Vogt spoke about the company's history and how it became a custom manufacturing facility for world-class brands such as Caterpillar, Kabota, and John Deere. The company has five locations and its services include metal fabrication, forming, welding and tool die work, prototyping, laser cutting, robotic welding, stamping, EDM, and powder coating. Attendees, which included members and students from area technical collges, were given a tour of the facility.

District 6

Ronald Stahura, director
(716) 207-7869
rstahura@esab.com

District 7

Roger E. Hilty, director
(740) 317-9073
rhilty@comcast.net

District 8

James Thompson, director
(256) 347-6481
jim.thompson@wallacestate.edu

District 9

Michael Skiles, director
(337) 501-0304
michaelskiles@cox.net

District 10

Tom Kostreba, director
(814) 881-0632
kostreba@hotmail.com

District 11

Phillip Temple, director
(734) 546-4298
nwcllc_ptemple@att.net

District 12

Dale Lange, director
(715) 732-3645
dale.lange@nwtc.edu

ATLANTA — *A robotic prototype welding on a postioner.*

ATLANTA — *Attendees of the Section's November meeting posed for a group photo.*

District 13

Ronald Ashelford, director
(815) 218-8766
r.ashelford@rockvalleycollege.edu

CHICAGO
December 16
Location: Mama Luigi's Restaurant, Bridgeview, Ill.
Summary: The Section held a dinner meeting for board members to discuss old and new business and to schedule 2021 gatherings.

District 14

Tony Brosio, director
(765) 215-7506
tbrosio@yahoo.com

District 15

Michael Hanson, director
(763) 221-5951
mikhan318@comcast.com

CHICAGO — *December meeting attendees included (front row, from left) Anghelina Iftimie, Pete Host, Costica Iftimie, and Craig Tichelar. In the second row (from left) are Jim Greer, John Hesseltine, Elisabeth Darnell, and Marty Vondra. In the back row (from left) are Section Chair Dave Viar and Jeff Stanczak.*

COLORADO — *Seen are participants of the Section's November meeting.*

District 16

Karl Fogleman, director
(402) 677-2490
fogleman3@cox.net

District 17

J Jones, director
(832) 506-5986
drtourch@yahoo.com

District 18

Thomas Holt, director
(409) 721-5777
tholt@techcorr.com

District 19

Shawn McDaniel, director
(509) 793-5182
shawnm@bigbend.edu

District 20

Denis Clark, director
(208) 357-6626
denis.clark.51@gmail.com

COLORADO
November 10
Location: Denver, Colo.
Presenter: Jesse Grantham, P.E., Level III, VT, MT, PT, UT; AWS CWI, CWE, and CRI, Welding and Joining Management Group
Summary: Grantham led a discussion on the various aspects of nondestructive examination and its place in the quality management system for welding professionals.

December 10
Location: Denver, Colo.
Presenters: Marj Oliver, Emitt Technologies; and Bob Teuscher, AWS past president
Summary: Oliver spoke to meeting attendees about the organizational structure of the American Institute of Steel Construction (AISC) and the process of becoming AISC certified. Teuscher spoke about the organizational structure of AWS and how the Sections interact with National.

District 21

Sam Lindsey, director
(858) 740-1917
slindsey@sandiego.gov

ARIZONA

December 8

Location: Western Maricopa Education Center (West-MEC), Buckeye, Ariz.

Summary: MEC students were awarded welding helmets by the Section.

SAN FERNANDO VALLEY

December 21

Summary: The Section announced it has established four $1250 scholarships through the AWS Foundation to be given out annually to area students. The establishment of scholarships for the advancement of welding programs is important to the area's aerospace region. The Section has also reached out to members to see if their companies are interested in establishing endowment scholarships.

District 22

Robert Purvis, director
(916) 599-5561
purviswelds@gmail.com

COLORADO — *Section Chair Marj Oliver opened the November meeting with Section news and notes for upcoming activities.*

COLORADO — *Marj Oliver (left) and Bob Teuscher were the presenters at the Section's December meeting.*

COLORADO — *Section members gathered for a group photo at the December meeting.*

ARIZONA — *The Section gave away two welding helmets to MEC students.*

GUIDE TO AWS SERVICES

American Welding Society®
8669 NW 36 St., #130
Miami, FL 33166-6672
(800/305) 443-9353
Phone extensions are in parentheses.

AWS PRESIDENT
Robert W. Roth..*rroth@romanmfg.com*
President and CEO, RoMan Manufacturing Inc.

SENIOR LEADERSHIP TEAM
Executive Director/Chief Executive Officer
Gary Konarska II.. *gkonarska@aws.org* . . . . .(207)

Chief Financial Officer/
Chief Administrative Officer
Gesana Villegas.. *gvillegas@aws.org* . . . . . .(252)

Senior Vice Presidents
Cassie Burrell.. *cburrell@aws.org* . . . . . .(253)
Marketing & Membership Development

John Gayler.. *gayler@aws.org* . . . . . .(472)
Welding & Technology

EXECUTIVE OFFICE
Associate Director
Chelsea Steel.. *csteel@aws.org* . . . . . .(294)

Program Administrator, National Awards
Malisa Mercado.. *mmercado@aws.org* . . . . . .(293)

HUMAN RESOURCES
Director
Alex Diaz.. *adiaz@aws.org* . . . . . .(209)

GOVERNMENT LIAISON SERVICES
Hugh Webster.. *hwebster@wc-b.com*
Webster, Chamberlain & Bean, Washington, D.C. (202) 785-9500; Fax: (202) 835-0243
Monitors federal issues of importance to the industry.

CERTIFICATION SERVICES
Dept. information . . . . . .(273)

Managing Director
Denny Smith.. *dsmith@aws.org* . . . . . .(263)

ACCREDITATION
Senior Manager
Emil Pagoaga.. *epagoaga@aws.org* . . . . . .(448)

CONFERENCES & EVENTS
Dept. information . . . . . .(213)

CUSTOMER SERVICE & SUPPORT
Customer Service..*customerservice@aws.org* (280)

SALES

Director, Global Sales
Michael Rovins.. *mrovins@aws.org* . . . . . .(350)

Senior Sales Executive, Corporate
Sandra Jorgensen.. *sjorgensen@aws.org* . . . .(254)

CONVENTION AND EXPOSITIONS
Director, Expositions
Matthew Rubin.. *mrubin@aws.org* . . . . . .(239)

Senior Sales Executive, Expositions
Sarah Dickson.. *sdickson@aws.org* . . . . . .(297)

EDUCATION & TRAINING
Director
Alicia Garcia.. *agarcia@aws.org* . . . . . .(229)

INFORMATION SYSTEMS
Managing Director
John Perry.. *jperry@aws.org* . . . . . .(247)

ITSA — INTERNATIONAL THERMAL SPRAY ASSOCIATION
Program Manager
Alfred Nieves.. *anieves@aws.org* . . . . . .(467)

RWMA — RESISTANCE WELDING MANUFACTURING ALLIANCE and WEMCO — ASSOCIATION OF WELDING MANUFACTURERS

Program Manager
Adrian Bustillo.. *abustillo@aws.org* . . . . . .(295)

MEMBER SERVICES
Dept. information . . . . . .(480)

Director, Membership
Nici Banks.. *nbanks@aws.org* . . . . . .(270)
Serves as a liaison between members and AWS headquarters.

Senior Manager, Sections and Student Chapters
Darrill Gaschler.. *dgaschler@aws.org* . . . . . .(260)

PUBLISHING & EDITORIAL
Dept. information . . . . . .(275)

Welding Journal
Publisher/Editor
Annette Alonso.. *aalonso@aws.org* . . . . . .(299)

Managing Editor
Kristin Campbell.. *kcampbell@aws.org* . . . . .(257)

Society News Editor
Katie Pacheco.. *kpacheco@aws.org* . . . . . .(275)

Section News Editor
Cindy Weihl.. *cweihl@aws.org* . . . . . .(256)

***Inspection Trends* Editor**
Carlos Guzman.. *cguzman@aws.org* . . . . . .(348)

STANDARDS DEVELOPMENT
Dept. information . . . . . .(340)

Director — Standards Development
Peter Portela.. *pportela@aws.org* . . . . . .(311)
Technical Committee Activities, Additive Manufacturing, Structural Subcommittee on Titanium

Director — International Activities
Andrew Davis.. *adavis@aws.org* . . . . . .(466)
International Standards Activities, American Council of the International Institute of Welding

Program Managers

Stephen Hedrick.. *steveh@aws.org* . . . . . .(305)
Metric Practice, Safety and Health, Joining of Plastics and Composites, Personnel and Facilities Qualification, Mechanical Testing of Welds, Welding in Sanitary Applications

Stephen Borrero.. *sborrero@aws.org* . . . . . .(334)
Definitions and Symbols, Structural Subcommittees on Bridge Welding, Reinforcing Steel and Stainless Steel, Joining of Metals and Alloys, Piping and Tubing

Rakesh Gupta.. *gupta@aws.org* . . . . . .(301)
Filler Metals and Allied Materials, International Filler Metals, UNS Numbers Assignment, Computational Weld Mechanics

Jennifer Molin.. *jmolin@aws.org* . . . . . .(304)
Structural Welding, Sheet Metal Welding

Mario Diaz.. *mdiaz@aws.org* . . . . . .(310)
Automotive, Resistance Welding, Resistance Welding Equipment, Welding and Brazing in Aerospace, Friction Welding

Kevin Bulger.. *kbulger@aws.org* . . . . . .(306)
Brazing and Soldering, Methods of Weld Inspection, High-Energy Beam Welding, Welding in Marine Construction, Welding of Machinery and Equipment

Jennifer Rosario.. *jrosario@aws.org* . . . . . .(308)
Oxyfuel Gas Welding and Cutting, Railroad Welding, Robotics Welding, Thermal Spraying, Welding Iron Castings, Welding Qualification

***Welding Handbook* Editor**
Kathy Sinnes.. *ksinnes@aws.org* . . . . . .(255)

AWS FOUNDATION INC.
aws.org/w/a/foundation
General Information
(800/305) 443-9353, ext. 212, *jdouglass@aws.org*

Chair, Board of Trustees
William A. Rice.. *brice@oki-bering.com*

Executive Director, Foundation
Monica Pfarr.. *mpfarr@aws.org* . . . . . .(461)

Associate Director, Foundation Services
John Douglass.. *jdouglass@aws.org* . . . . . .(212)

The AWS Foundation is a not-for-profit 501(c)(3) charitable organization established to provide support for the educational and scientific endeavors of the American Welding Society. Promote the Foundation's work with your financial support.

AWS American Welding Society

American Welding Society®
MEMBERSHIP

8669 NW 36 ST. #130 | Miami, FL 33166-6672
T: 800.443.9353 | F: 305.443.5647 | *aws.org*

Application for Membership

PRIMARY CONTACT INFORMATION (Please Print)

☐ Mr. ☐ Ms. ☐ Mrs. ☐ Dr.

Last Name: _____ First Name: _____ M.I: _____ Birthdate: _____

E-Mail: _____ Mobile Phone: ( ) _____ Secondary Phone: ( ) _____ ☐ Home ☐ Work

Company/School (if applicable): _____

Mailing Address: _____

City: _____ State/Province: _____ Zip/Postal Code: _____ Country: _____

☐ Check here if you would prefer to not receive email updates on AWS programs, Member benefits, savings opportunities and events.

Technical Interests (Circle All That Apply)

A Ferrous Metals
B Aluminum
C Nonferrous Metals Except Aluminum
D Advanced Materials/Intermetallics
E Ceramics
F High Energy Beam Processes
G Arc Welding
H Brazing and Soldering
I Resistance Welding
J Thermal Spray
K Cutting
L NDT
M Safety and Health
N Bending and Shearing
O Roll Forming
P Stamping and Punching
Q Aerospace
R Automotive
S Machinery
T Marine
U Piping and Tubing
V Pressure Vessels and Tanks
W Sheet Metal
X Structures
Y Other
Z Automation
1 Robotics
2 Computerization of Welding

STUDENT MEMBERSHIP ☐ New ☐ Renewal, Member #:

☐ 1 Year-Digital *Welding Journal* $15
☐ 1 Year-Print and Digital *Welding Journal* (US, Canada, and Mexico) $35
☐ 1 Year-Print and Digital *Welding Journal*..... $85 (outside of US, Canada, and Mexico)

$ _____

INDIVIDUAL MEMBERSHIP ☐ New ☐ Renewal, Member #:

Were you referred to AWS by an AWS Member? ☐ Yes ☐ No

Member's Name: _____ Member's # (if known) _____

DOMESTIC (INCLUDES US, CANADA, AND MEXICO)

New Member

☐ Initiation Fee $12
☐ 1 Year - Print and Digital *Welding Journal* $88
☐ 2 Year - Print and Digital *Welding Journal* $151

$ _____

Renewing Member

☐ 1 Year - Print and Digital *Welding Journal* $88
☐ 2 Year - Print and Digital *Welding Journal* $171

$ _____

INTERNATIONAL (OUTSIDE OF US, CANADA, OR MEXICO)

New Member

☐ Initiation Fee $12
☐ 1 Year - Digital *Welding Journal* $88
☐ 1 Year - Print and Digital *Welding Journal* $138
☐ 2 Year - Digital *Welding Journal* $151
☐ 2 Year - Print and Digital *Welding Journal* $251

$ _____

Renewing Member

☐ 1 Year - Digital *Welding Journal* $88
☐ 1 Year - Print and Digital *Welding Journal* $138
☐ 2 Year - Digital *Welding Journal* $171
☐ 2 Year - Print and Digital *Welding Journal* $271

$ _____

NEW MEMBER OPTIONAL BOOK SELECTION (Not available to renewals. Choose ONE option ONLY. Includes shipping & handling.) Visit *aws.org/memberships/page/new-member-book-offer* to view selections and write your choice here:

☐ Domestic $35
☐ International $85

$ _____

TOTAL $

Business (Circle ONE Letter Only)

A Contract Construction
B Chemicals & Allied Products
C Petroleum & Coal Industries
D Primary Metal Industries
E Fabricated Metal Products
F Machinery Except Electric (Incl. Gas Welding)
G Electrical Equipment, Supplies, Electrodes
H Transport Equip. – Air, Aerospace
I Transport Equip. — Automotive
J Transport Equip. — Boats, Ships
K Transport Equip. — Railroad
L Utilities
M Welding Distributors & Retail Trade
N Misc. Repair Services (Including Welding Shops)
O Educational Services (Univ., Libraries, Schools)
P Engineering & Architectural Services (Including Assns.)
Q Misc. Business Services (Including Commercial Labs)
R Government (Federal, State, Local)
S Other

Job Classification (Circle ONE Letter Only)

01 President, Owner, Partner, Officer
02 Manager, Director, Superintendent (Or Assistant)
03 Sales
04 Purchasing
05 Engineer — Welding
20 Engineer — Design
21 Engineer — Manufacturing
06 Engineer — Other
10 Architect Designer
12 Metallurgist
13 Research & Development
22 Quality Control
07 Inspector, Tester
08 Supervisor, Foreman
14 Technician
09 Welder, Welding or Cutting Operator
11 Consultant
15 Educator
17 Librarian
16 Student
18 Customer Service
19 Other

PAYMENT INFORMATION

Payment can be made (in U.S. dollars) by check or money order (international), payable to the American Welding Society.

☐ Check ☐ Money Order

☐ AMEX ☐ Diners Club ☐ MasterCard ☐ Visa ☐ Discover ☐ Other Application Date: _____

Name on Card: _____ CC#: _____ / _____ / _____ / _____

Expiration Date (mm/yy): _____ / _____ CVV: _____ Applicant Signature: _____

OFFICE USE ONLY Source Code: **WJ** Account #: _____ Check #: _____ Amount: _____

Date: _____ AWS Staff: _____

Mahr Chooses Northeast Regional Sales Manager and Quality Assurance Manager

Mahr Inc., Providence, R.I., a global manufacturer of precision measurement equipment, announced that Josh Howlett has joined the company as Northeast regional sales manager, and Celina Ortiz has been appointed manager of quality assurance. Howlett will focus on leading sales efforts in the Northeast region. He has extensive experience in the machinery industry and as a product sales manager. He has held sales management positions at Zeiss Industrial Metrology and HGH Infrared Systems. He also served as regional sales manager for Koma Precision.

Ortiz recently held the position of quality-assurance manager at Freeport-McMoRan in Norwich, Conn.

J. Howlett

C. Ortiz

Stäubli Welcomes CEO

Stäubli, a global provider of industrial and mechatronic solutions headquartered in Pfäffikon, Switzerland, has promoted Gerald Vogt to CEO. He was previously responsible for the global business of the robotics division as group division manager since 2016 and is already a member of the group management team. Vogt joined the company almost 20 years ago, moving from the development and production site in Faverges, France, to the United States for several years. As division manager, he expanded business for Stäubli Robotics North America. Afterward, he returned to Faverges as head of development before taking over the German business as head of Stäubli Robotics in Bayreuth.

NCCER Announces President and CEO

The National Center for Construction Education & Research (NCCER), Alachua, Fla., an international education foundation for the construction industry, has named Boyd Worsham as president and CEO. In 2018, Worsham, formally of The Haskell Co., was identified as the successor to

B. Worsham

lead NCCER into the future. In March of 2020, he was given full operational oversight of NCCER. The executive committee then made the recommendation to the board of trustees to promote him to president and CEO. The motion passed unanimously.

Lincoln Electric Promotes Senior Vice President, President International

P. Pletcher

The Lincoln Electric Co., Cleveland, Ohio, a manufacturer of welding and cutting products and equipment, has appointed Peter Pletcher to senior vice president, president international. He will be responsible for the company's business in Europe, Russia, and Turkey. He will also serve as a member of the company's management committee. Pletcher joined the company in 1995 and has held leadership positions in sales, applications engineering, marketing, product development, and operations. He recently led the company's business in Europe, and prior to that, he led its automation business.

AMETEK SMP Selects Manufacturing Manager

D. Nestor

AMETEK Specialty Metal Products (SMP), a producer of high-purity metal strips, specialty shaped wires, engineered shaped components, and thermal management materials, has hired Dylan Nestor as its manufacturing manager for strip. He will be based in Wallingford, Conn., and responsible for overseeing the company's primary, finishing, shipping, and receiving departments. Nestor brings with him experience in process engineering, continuous improvement, and operations leadership. In his previous role, he was responsible for the operations and maintenance of multiple departments, including rolling, annealing, and leveling.

Direct Wire Adds to Welding Team

Direct Wire, a manufacturer of industrial-grade copper wire and cable products, has added Daphne Ford as account executive and promoted Diana Forney to account representative within its welding division. The two roles will be instrumental in connecting with and assisting distribution and wholesale partners and cooperative purchasing groups. Ford joined the company after eight years with Republic Services. She will support cus-

— *continued on page 67*

NOMINATION DEADLINE FOR
AWS FELLOW OF THE SOCIETY

American Welding Society®

Friends and Colleagues:

The American Welding Society, in 1990, established the honor of Fellow to recognize members for distinguished contributions to the field of welding science and technology, and for promoting and sustaining the professional stature of the field. Election as a Fellow of the Society is based on outstanding accomplishments and the technical impact of the individual. Such accomplishments will have advanced the science, technology and application of welding, brazing, or soldering, as evidenced by:

- Sustained service and performance in the advancement of welding and joining science and technology
- Publication of papers, articles and books which enhance knowledge of welding and allied processes
- Innovative development of welding and allied technologies
- Society and Section contributions
- Professional recognitions

I want to encourage you to submit nomination packages for those individuals whom you feel have a history of accomplishments and contributions to our profession consistent with the standards set by the existing AWS Fellows. In particular, I would make a special request that, in considering members for nomination, you look to the most senior members of your Section or District. In many cases, the colleagues and peers of these individuals who are the most familiar with their contributions, and who would normally nominate the candidate, are no longer with us. I want to be sure that we make the extra effort required to ensure that those truly worthy are not overlooked because no obvious individual was available to start the nominating process.

For specifics on nomination requirements, please contact Chelsea Steel at csteel@aws.org at AWS headquarters in Miami, or simply follow the instructions on the Fellow nomination form located at *www.aws.org/fellow*. Please remember, we all benefit in the honoring of those who have made major contributions to our chosen profession and livelihood. The deadline for submission is August 1, 2021.
The Fellows Committee looks forward to receiving numerous Fellow nominations for 2022 consideration.

Sincerely,

Dr. Sudarsanam Babu
Chair, AWS Fellows Committee

IMPORTANT
Announcement

Do you know a leader with outstanding contributions to the advancement of welding science and technology?

Elect them now for the honor of Fellow of the Society.

August 1, 2021
Submission Deadline

PERSONNEL

— continued from page 65

tomers headquartered west of the Mississippi River and internationally in Canada and Mexico. Forney, who has spent the previous three years with Direct Wire, will be responsible for servicing customers located east of the Mississippi River.

CNDE Associate Scientist Named to ASNT RISE Program

Zhang Zhan, an associate scientist at Iowa State University's Center for Nondestructive Evaluation (CNDE), has been selected for the American Society for Nondestructive Testing's (ASNT's) inaugural class of the RISE leadership development program for nondestructive examination professionals.

Z. Zhan

The 15-month program includes nondestructive evaluation skill training, leadership preparation, mentoring, and networking with fellow ASNT members. Zhan manages the microCT and high-energy x-ray diffraction labs at the CNDE. He is also engaged in multiple research collaboration projects with industrial partners. Additionally, he has served as the chairman of the ASNT Iowa section since 2018 and is involved in multiple ASTM technical committees. WJ

NEWS OF THE INDUSTRY

— continued from page 11

and training thousands of skilled tradespeople, modernizing our facilities, and helping to bolster the supply base," said Kevin Graney, president of General Dynamics Electric Boat.

Alcoa Agrees to Sell Rolling Mill to Kaiser Aluminum

Alcoa Corp., Pittsburgh, Pa., has revealed an agreement to sell its rolling mill business, held by Alcoa Warrick LLC, to Kaiser Aluminum Corp. for a total consideration of approximately $670 million. This includes $587 million in cash and the assumption of $83 million in other postretirement employee benefit liabilities. The sale is expected to close by the end of the first quarter of 2021, pending regulatory approval and customary closing conditions.

The rolling mill is at Warrick Operations, an aluminum manufacturing site near Evansville, Ind. Alcoa will retain ownership of the site's 269,000 metric ton per year aluminum smelter and its electric generating units. Additionally, the company will enter into a ground lease agreement with Kaiser Aluminum for property it will continue to own at the Warrick site.

As part of the transaction, Alcoa will enter into a market-based metal supply agreement with Kaiser Aluminum at closing. It will continue to operate the smelter and the power plant, which together employ approximately 660 people.

National Apprenticeship Week Makes Waves

The sixth annual National Apprenticeship Week (NAW), held November 8–14, was deemed a success. Overall, there were 830 events and proclamations around the country; 659 events took place across 50 participating U.S. states, as well as the District of Columbia and one U.S. territory; and there were 171 proclamations made, including 91 industry, 41 local and county, 38 gubernatorial, and one presidential.

Growing and expanding apprenticeship is a top priority for the White House and the U.S. Department of Labor, which is why they are continuing to invest in programs and initiatives that will help grow and expand apprenticeship across the nation. Visit *apprenticeship.gov/NAW*.

Industry Notes

• **FANUC**, Rochester Hills, Mich., a supplier of computer numerical controls, robotics, and robomachines, was named a top workplace in Michigan by the *Detroit Free Press* for the ninth consecutive year. It ranks 15 out of 30 companies in the large employer category in Michigan. Additionally, the *Chicago Tribune* named FANUC's Hoffman Estate, Ill., regional office a top workplace in Illinois for the third year in a row.

"I'm so honored that even during these challenging and unprecedented times of a global pandemic we've been named a top workplace," said Mike Cicco, president and CEO, FANUC America.

• International technology group **ANDRITZ** has received an order from **Zouping Hongfa Aluminium Science Technology Co. Ltd.**, part of Weiqiao Aluminum Group, to supply one melting and holding furnace cell for its plant in Shandong Province, China. Start-up is scheduled for the first quarter of 2022. It's claimed the new furnace cell supplied by the company will incorporate the largest furnaces in China, with two 115-ton round-top melters and two 125-ton tilting holders. WJ

FOR SALE OR RENT

ADVERTISER INDEX

SUPPLEMENT TO THE *WELDING JOURNAL*, FEBRUARY 2021
Sponsored by the American Welding Society

Short-Pulse Resistance Spot Welding of Aluminum Alloy 6016-T4 — Part 1

The influence of welding time and current on weld quality was investigated

BY E. SCHULZ, M. WAGNER, H. SCHUBERT, W. ZHANG, B. BALASUBRAMANIAN, AND L. N. BREWER

ABSTRACT

Short-pulse welding parameters for resistance spot welding (RSW) of aluminum alloy AA6016-T4 using medium-frequency direct current (MFDC) systems were developed to reduce the heat input required for nugget formation. Optimization of current and time parameters is critical during RSW of aluminum alloys for reducing energy requirements and avoiding weld imperfections, such as solidification cracking and expulsion, while maintaining weld quality, particularly given the high electrical and thermal conductivities of the materials. The welding time and the applied current level of the current pulse were varied systematically for thin sheets (1 mm or 0.04 in.) of AA6016-T4. The quality of the welds was evaluated by pull-out testing, ultrasound testing, and metallography techniques. Simulations of the same welding processes were performed with the finite element-based SORPAS® software. The results showed short-pulse MFDC RSW can reduce the energy required for sound welds in this alloy without requiring an increase in welding current. The simulations and experiments also showed the welding process had distinct weld nugget nucleation and growth phases.

KEYWORDS

• Resistance Spot Welding (RSW) • Aluminum Alloys
• Welding Parameters • Numerical Simulation

Introduction

The use of aluminum materials in automotive body-in-white construction has become more widespread as manufacturers pursue vehicle lightweighting strategies to meet strict fuel-efficiency requirements. The body-in-white represents approximately 30% of the total vehicle weight, and hybrid construction concepts using a mix of steel and aluminum parts provide an opportunity for reducing vehicle weight (Ref. 1). Aluminum alloys from the 5000 and 6000 series are now widely used for body-in-white construction, and joining tasks exist over a range of sheet thicknesses and material combinations. For these joining tasks, suitable joining methods are needed.

Resistance spot welding (RSW) is an established joining technology for automotive body structures, but its application to aluminum alloys presents special challenges. The electrical and thermal conductivity of aluminum is much higher than of steel, which leads to much higher welding currents for successful joining. Aluminum alloy AA6016-T4 has a particularly high thermal conductivity of 190 W/mK (92.4 Btu/hftF), which requires especially high welding currents to enable a stable welding process. High welding currents, however, increase energy requirements and can lead to a number of disturbances in the welding process, such as large magnetic forces that cause the gun arms to deflect from each other, solidification cracking, expulsion, and rapid electrode wear (Refs. 2–4). Progress on RSW of aluminum alloys has been reported in recent welding literature with regards to the influence of electrode geometry (Ref. 5), surface pretreatments (Refs. 6–8), and, to some degree, parameterization on the process (Refs. 9, 10). Some information was also presented on the weld nugget nucleation and growth processes for alloy AA5182 (Ref. 11). However, until now, the literature has focused primarily on AA5182, and knowledge remains to be gained on AA6016-T4, which is highly sensitive to the RSW process in terms of process stability and electrode wear.

The influence of welding parameters on the heat input and generation of the weld nugget requires further investigation for RSW of AA6016-T4. In particular, the role of the current-pulse duration, or welding time, is of key concern. Recent research on capacitive discharge (CD) welding has shown that high current levels applied over very short time durations (e.g., on the order of 5 to 20 ms), can allow for the

https://doi.org/10.29391/2021.100.004

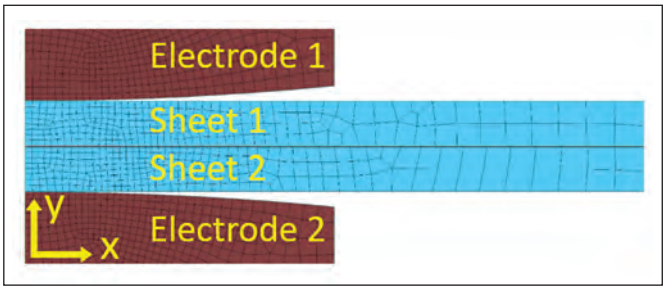

Fig. 1 — Numerical system for welding simulations with the SORPAS software.

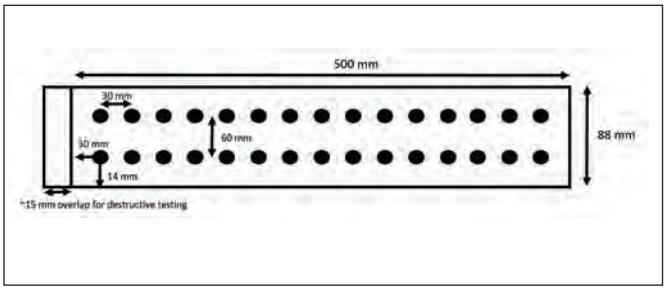

Fig. 2 — Experimental sample geometry and weld configuration.

Table 1 — Chemical Composition of AA6016-T4 by wt-%

Al	Si	Fe	Cu	Mn	Mg	Cr	Zn	Ti	V
96.4–98.8	≤ 1.50	≤ 0.50	≤ 0.25	≤ 0.40	≤ 1.00	≤ 0.15	≤ 0.30	≤ 0.25	≤ 0.15

successful welding of difficult alloys such as EN AW-7075, which suffers from solidification cracking under normal welding conditions (Ref. 12).

Short-pulse techniques in the context of RSW have also been applied to high-strength steel materials to reduce expulsion using medium-frequency direct current (MFDC) systems (Ref. 13) and to 5000 series aluminum alloys using CD systems to improve electrode wear characteristics (Ref. 10). In addition to these benefits, the use of short welding times with the CD systems reduces the heat input needed to make a successful weld and limits heat losses by conduction for high-conductivity materials. However, MFDC systems remain most attractive for automotive manufacturers given the cost and availability as well as the ability to control parameters in real time during the welding process. Given the prevalence of RSW in the automotive industry and the necessity for a long-term solution for joining 5000 and 6000 series aluminum alloys, the following question arises: Can short-pulse welding be performed using a MFDC technology that provides the benefits of low heat inputs?

This paper will systematically show that MFDC RSW for AA6016-T4 can benefit significantly from short-time current-pulse parameters with resultant high-quality welds at low welding currents. Both experimental and simulation results are used to show how the current-pulse duration and applied current level affect the nucleation and growth of the fusion zone.

Materials

The commercial aluminum alloy AA6016-T4, with nominal chemical composition and mechanical properties as listed in Tables 1 and 2, was the subject of this study. Material sheets in thicknesses from 1.0 to 2.0 mm (0.04 to 0.08 in.) in an as-received, pretreated condition were used. The pretreatment process was carried out according to the VDA 239-200, *Aluminum Sheet Material,* standard (Ref. 14). This included surface passivation to establish a reduced and consistent oxide layer thickness followed by application of forming oil in accordance with company standards.

Numerical Methods

The commercially available SORPAS® 2D Welding software package was used to simulate the RSW process. The software contains a module specific to the RSW process and databases of material, machine, electrode, and workpiece properties (Ref. 15). The solution algorithm contains mechanical, electrical, and thermal models within each time step as well as full coupling between the electrical and thermal models. A two-dimensional (2D), axisymmetric model of the welding process, including electrodes and sheets, was created in the SORPAS 2D Welding software. Due to the rotational symmetry around the vertical axis through the center of the electrodes and sheets, one half of the electrodes and sheets was represented in the model. Meshing of the system was completed using the automatic meshing feature with high-mesh density in the regions of large temperature gradients and mechanical deformation — Fig. 1.

The SORPAS software is based on the finite element method (FEM). It solved the governing differential equations below for electrical potential, transient heat transfer, and plastic deformation, respectively after discretization of the system using FEM formulations in two dimensions (Ref. 16).

$$\frac{\partial}{\partial x}\left(\sigma_x \frac{\partial \varphi}{\partial x}\right)+\frac{\partial}{\partial y}\left(\sigma_y \frac{\partial \varphi}{\partial y}\right)=0 \quad (1)$$

$$\frac{\partial}{\partial x}\left(k_x \frac{\partial T}{\partial x}\right)+\frac{\partial}{\partial y}\left(k_y \frac{\partial T}{\partial y}\right)+\dot{Q}=\rho C\frac{\partial T}{\partial t} \quad (2)$$

$$\pi=\int_V \overline{\sigma}\dot{\varepsilon}dV-\int_S FvdS, \quad \frac{\partial \pi}{\alpha v}=0 \quad (3)$$

For the electrical and thermal models, the material properties involved were σ, the electrical conductivity; k, the thermal conductivity; ρ, the mass density; and C, the heat capacity. $\dot{Q}$ was the internal heat energy source term. The time-dependent distributions of electrical potential, Φ, and

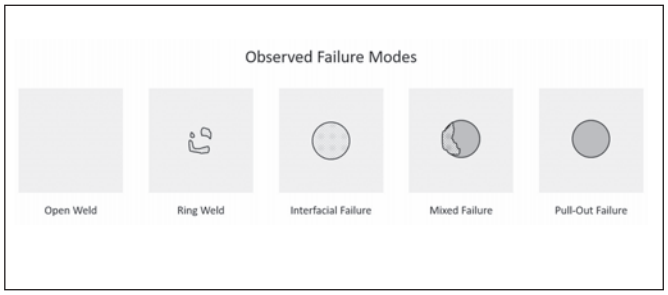

Fig. 3 — Failure modes in experimental pull-out tests.

Table 2 — Mechanical Properties of AA6016-T4

Yield Strength (MPa)	Ultimate Tensile Strength (MPa)	Elongation to Fracture
≤ 140	≤ 200	≤ 20%

temperature, T, were calculated at each time step. For the mechanical model, deformation and contact areas were calculated at each time step by the variation approach for plastic deformation (Equation 3). Electrical contact resistivity at the interfaces between electrodes/sheets and sheets/sheets was calculated according to Wannheim and Bay's friction theory for real contact areas (Ref. 16):

$$\rho_{contact} = 3\left(\frac{\sigma_{s\_soft}}{\sigma_n}\right)\left(\frac{\rho_1 + \rho_2}{2} + \rho_{contaminants}\right) \quad (4)$$

In the contact resistivity formulation, σ_{s_soft} represents the flow stress of the softer material in contact, σ_n is the normal pressure at the interface, and ρ_1 and ρ_2 are the temperature-dependent base material resistivity values of the two materials in contact. The $\rho_{contaminants}$ term accounts for the additional contact resistance introduced by the surface layer between the materials, such as from oxide layers, contamination, or pretreatment layers on the surface.

Detailed temperature-dependent material properties were available for a range of aluminum alloys in the software database, including for the alloy of interest. However, due to differences in manufacturers, pretreatment, age of the material, and other factors that affect the characteristics of the material surface, the contact resistivity functions had to be adjusted in the material model. Although base material properties do not show large variations within a given alloy designation, it was shown in Al Naimi et al. (Ref. 7) and Crinon et al. (Ref. 17) that there are large variations in resistances of the surface layers when roughness or characteristics of the oxide layer are changed via pretreatment processes. Therefore, it was necessary to calibrate the material model for the experimental material of interest to improve the accuracy of the simulation results.

Calibration of the model was performed by a linear scaling of surface resistivity values ($\rho_{contaminants}$) in the material model after comparison of the weld nugget diameter from the simulations to a small series of experimental pull-out tests. The tests were completed for the combination of two

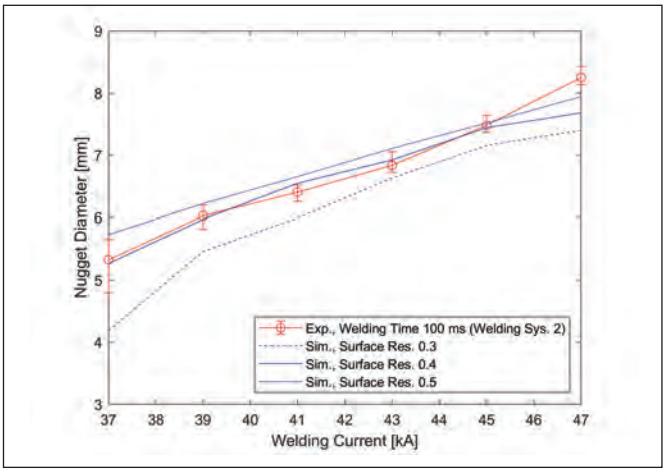

Fig. 4 — Simulation model calibration by variation of the surface resistivity factor using data from pull-out testing of welding system 2 (sheet thickness of 1.5 mm).

sheets of AA6016-T4 with a thickness of 1.5 mm (0.06 in.). A fixed welding time of 100 ms and a current range of 27 to 37 kA were used as welding parameters. The starting current value in the range was chosen as that which produced a weld nugget of approximately $4\sqrt{(t_{min})}$, where t_{min} is the minimum sheet thickness in the combination. This nugget diameter corresponds to the minimum weld size required. Five welding spots were made at each welding current value for increased precision. After establishing the necessary scaling value, additional tests were made to assess the model with further changes in welding conditions. Two additional sheet thicknesses, of 1 and 2 mm (0.04 and 0.08 in.), were considered as well as a variation of welding times. The results of the simulations and a discussion of the robustness of the model are presented in the following sections.

Experimental Procedures

Experimental tests were carried out using two MFDC machines with different power capabilities to evaluate the potentials for short-pulse welding. The first welding machine, referred to as welding system 1, included the MFDC inverter and control unit model PRC7000 from Bosch Rexroth as well as the Daimler-specified C-shaped welding gun construction from Düring Schweißtechnik GmbH. The Bosch Rexroth PSG 6180 welding transformers with a switching frequency of 1000 Hz as well as power ratings of 80 kVA at a 100% duty cycle and 178 kVA at a 20% duty cycle were connected in parallel for a maximum output current of approximately 50 kA.

The second welding machine, welding system 2, had a Nimak GmbH magnetic-drive system. The system included a control unit with Bosch Rexroth MFDC inverter components and a Nimak C-shaped gun geometry for short-pulse welding. The welding transformers used were the Nimak-type NMFT 1260 with a switching frequency of 1000 Hz as well as power ratings of 116 kVA at 100% duty cycle and 260 kVA at 20% duty cycle. Output currents up to 80 kA were possible but limited to 60 kA due to limitations on connector components. For the purposes of this study, the welding

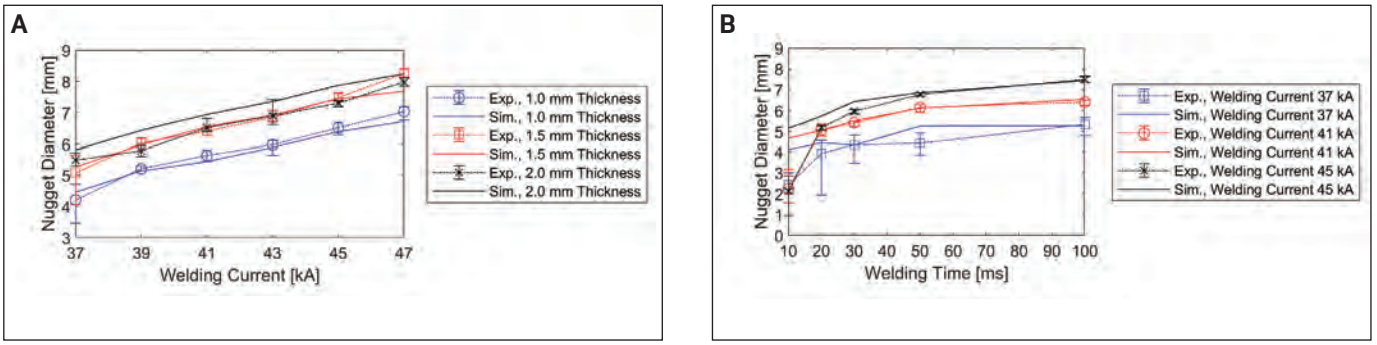

Fig. 5 — Validation of the simulation model: A — Variation of sheet thickness with a constant weld time of 100 ms; B — variation of welding time with a constant sheet thickness of 1.5 mm (0.06 in.).

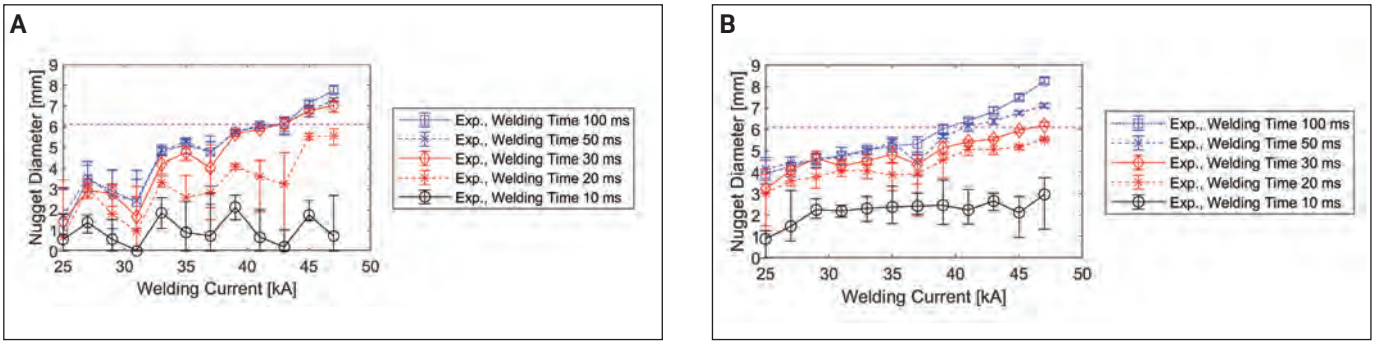

Fig. 6 — Experimental pull-out data for welding systems 1 (A) and 2 (B). The required nugget diameter of 6.1 mm (0.24 in.) is represented by a dotted line in the color magenta.

current was limited to a maximum of 47 kA. Both welding systems operated under closed loop, constant current, and constant force control. In all cases, Luvata copper-chromium-zinc electrodes with an A0-type geometry and an outer diameter of 20 mm were used, in accordance with the German standard DIN EN ISO 5821, *Resistance Welding — Spot Welding Electrode Caps* (Ref. 18).

For experimental tests, the aluminum material was cut into samples of 500 × 88 mm (19.4 × 3.5 in.). This geometry enabled 30 welding spots to be made on each sample. Spots were placed at equal distances, and minimum spacing values were upheld to prevent shunting effects from neighboring welds. The welding sample geometry is shown in Fig. 2. Electrodes were redressed by mechanical cutting every 15 spots to maintain consistent electrode surfaces.

Experimental weld nugget diameters were determined by pull-out testing on an internally designed machine. Fracture modes were classified according to Fig. 3 and recorded. Allowable current ranges for a given welding time were determined for each set of parameters based on pull-out data. These current ranges were defined by a starting current level for which all welds had a diameter greater than or equal to $5\sqrt{t_{min}}$ (required nugget diameter with the added factor of safety from the minimum diameter). The upper limit of the current range was defined as either the maximum allowable current (47 kA) or the lowest current level at which expulsion was observed. During tests, a Spatz Multi04 welding recorder was used to record the current and voltage signals

Table 3 — Prevalent Fracture Modes From Destructive Testing, Welding System 1 (Bosch PRC7000)

Welding Current (kA)	10 ms	20 ms	30 ms	50 ms	100 ms
25	Open weld 60%	Open weld 80%	Open weld 40%	Interfacial 60%	Open weld 60%
27	Ring 100%	Interfacial 100%	Interfacial 100%	Interfacial 60%	Interfacial 80%
29	Open weld 60%	Interfacial 60%	Interfacial 80%	Pull-out 40%	Interfacial 80%
31	Open weld 100%	Open weld 60%	Open weld 40%	Interfacial 60%	Interfacial 60%
33	Ring 100%	Interfacial 60%	Pull-out 100%	Pull-out 100%	Pull-out 80%
35	Open weld 60%	Pull-out 40%	Pull-out 80%	Pull-out 100%	Pull-out 100%
37	Open 60%	Pull-out 60%	Pull-out 60%	Pull-out 80%	Pull-out 100%
39	Interfacial 60%	Pull-out 100%	Pull-out 100%	Pull-out 100%	Pull-out 100%
41	Open 60%	Pull-out 60%	Pull-out 100%	Pull-out 100%	Pull-out 100%
43	Open 80%	Pull-out 60%	Pull-out 100%	Pull-out 100%	Pull-out 100%
45	Ring 100%	Pull-out 100%	Pull-out 100%	Pull-out 100%	Pull-out 100%
47	Open 60%	Pull-out 100%	Pull-out 100%	Pull-out 100%	Pull-out 100%

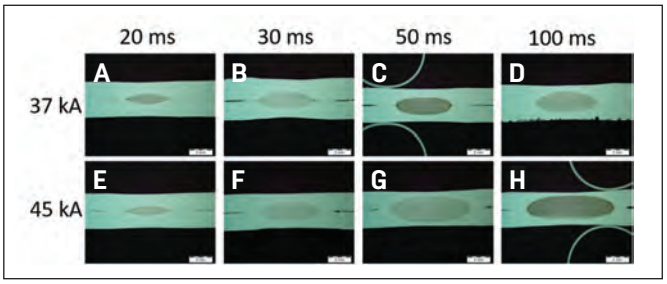

Fig. 7 — Optical microscopy images of samples from welding system 2 for two current levels: A–D — 37 kA; E–H — 45 kA. Images A and E show a welding time of 20 ms, images B and F show a welding time of 30 ms, images C and G show a welding time of 50 ms, and images D and H show a welding time of 100 ms.

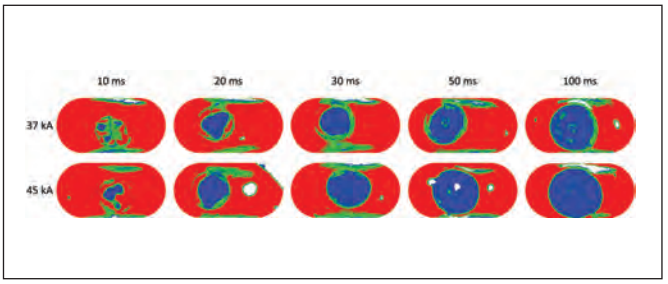

Fig. 8 — Ultrasonic results for the nugget development process and experimental samples from welding system 2 at the listed current and welding time conditions. The blue color represents the areas of fusion, green represents partial fusion or weak signal, and red represents areas of no fusion.

to be used for resistance and energy calculations.

Additional welded samples were inspected using nondestructive ultrasonic testing to measure nugget diameter and observe development and growth. The Mini Scanner ultrasonic device from AmsTech was used; it utilizes a scanning pulse-echo technology for high-resolution ultrasonic imaging of the weld area. Cross-sectioned samples were also prepared and polished according to standard metallography techniques and inspected by optical microscopy after etching in a 5% sodium hydroxide solution for 60 s. The Leitz DMRM microscope from Leica and the SZX12 microscope from Olympus were used.

Results

Welding Simulation Calibration and Evaluation

A scaling constant was obtained for surface resistivity values of AA6016-T4 in the SORPAS material database, with good agreement obtained between the simulated weld nugget diameter and the experimental results. The scaling factor found most suitable for the experimental material used in this study was 0.4, and it remained constant for all further simulations. Experimental results from both welding systems were used for the calibration process, and good agreement was obtained for both. A comparison between the simulation results using three different scaling factors and the experimental results from welding system 2 is shown in Fig. 4. Welding time was set to 100 ms and the current varied from 37 to 47 kA.

The robustness of the new material model was then evaluated by variation of two additional parameters: the material sheet thickness and the welding time. In the first set of tests, the welding time was left constant at 100 ms, and additional sheet thicknesses 1.0 and 2.0 mm (0.04 and 0.08 in.) were tested. As seen in Fig. 5A, a reasonable agreement between the simulations and experiments was maintained. However, a nearly constant difference in weld nugget diameter of approximately 0.5 mm (0.02 in.) was evident for the largest sheet thickness of 2.0 mm (0.08 in.). For the next set of tests, the original sheet thickness of 1.5 mm (0.06 in.) was used, and the welding time decreased from the original time of 100 to 10 ms. Figure 5B shows the comparison between simulated and experimental results. Good agreement in results was obtained for all welding times greater than or equal to 20 ms, regardless of current level. When the welding time was further reduced to 10 ms, discrepancy in results existed. This discrepancy can be explained by the difference in current profiles between the simulation, which utilized idealized current profiles with an infinite current rise speed, and the actual current profiles obtained during experiments. Due to the limited current rise speed of the welding machines, there was a large difference in total heat input between simulations and experiments at short welding times, which explains the difference in the final welding result.

Table 4 — Prevalent Fracture Modes from Destructive Testing, Welding System 2 (Nimak Magnetic Drive)

Welding Current (kA)	10 ms	20 ms	30 ms	50 ms	100 ms
25	Ring 80%	Interfacial 80%	Interfacial 80%	Interfacial 40%	Interfacial 40%
27	Ring 100%	Interfacial 100%	Interfacial 100%	Pull-out 60%	Pull-out 60%
29	Ring 100%	Interfacial 100%	Interfacial 100%	Interfacial 40%	Pull-out 100%
31	Ring 100%	Interfacial 100%	Interfacial 60%	Pull-out 100%	Pull-out 100%
33	Ring 100%	Interfacial 80%	Interfacial 100%	Pull-out 80%	Pull-out 100%
35	Ring 100%	Interfacial 60%	Pull-out 80%	Pull-out 100%	Pull-out 100%
37	Ring 100%	Interfacial 60%	Pull-out 80%	Pull-out 100%	Pull-out 100%
39	Ring 100%	Interfacial 100%	Pull-out 100%	Pull-out 100%	Pull-out 100%
41	Ring 100%	Pull-out 80%	Pull-out 100%	Pull-out 100%	Pull-out 100%
43	Ring 60%	Pull-out 80%	Pull-out 100%	Pull-out 100%	Pull-out 100%
45	Ring 100%	Pull-out 100%	Pull-out 100%	Pull-out 100%	Pull-out 100%
47	Ring 80%	Pull-out 100%	Pull-out 100%	Pull-out 100%	Pull-out 100%

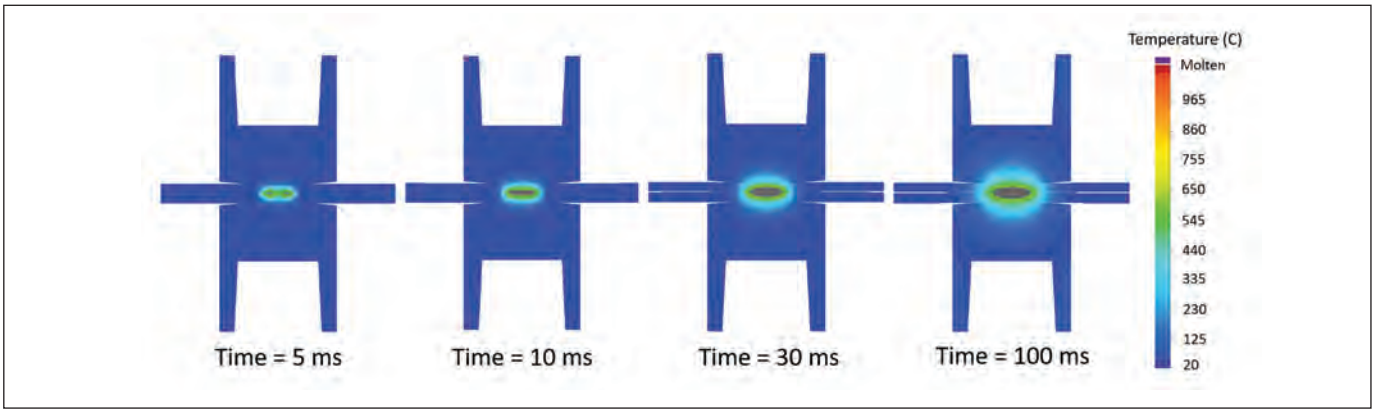

Fig. 9 — Nugget development process for a 100-ms, 41-kA welding pulse.

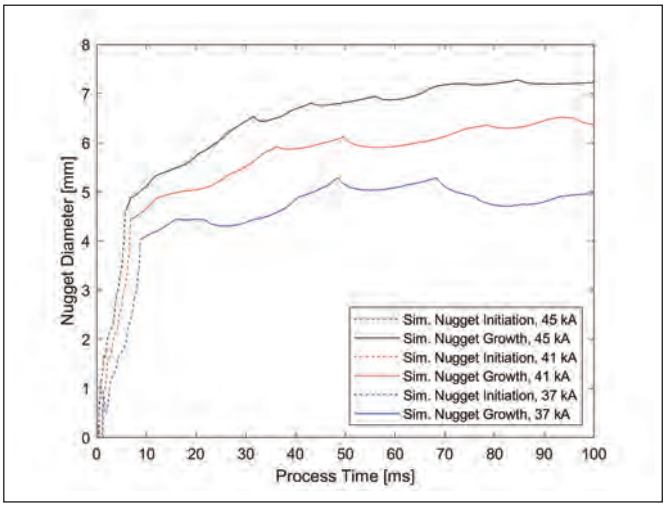

Fig. 10 — Dynamic weld nugget size from simulation data: shown for a 100-ms welding time and welding currents of 37, 41, and 45 kA.

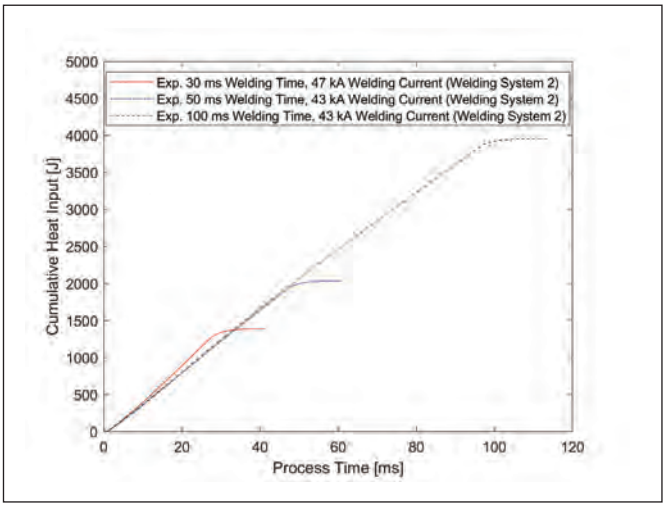

Fig. 11 — Total weld energy input measured experimentally for the welding times of 30, 50, and 100 ms, with current levels corresponding to the equally required final nugget diameter.

Weld Nugget Diameter and Failure Mode as a Function of RSW Parameters

The parameters tested in the previous section were used as the starting point for determining the minimum welding time necessary for the short-pulse welding of AA6016-T4 in 1.5-mm (0.06-in.) sheet thickness, and allowable current ranges as a function of welding time were determined for each of the two systems. Minimum required nugget diameter for this sheet thickness was calculated to be 4.9 mm (0.19 in.), while the required nugget diameter for the current range determination was 6.1 mm (0.24 in.). Using 100 ms as the starting value, the welding time was reduced to 50, 30, 20, and 10 ms. For each welding time, the current was varied from 27 to 47 kA, and pull-out testing was performed on the welded samples. As expected, an increase in either welding time or current resulted in a larger weld nugget diameter. However, while the increase in the nugget diameter with the increased current was generally linear, the increase in diameter with time was highly nonlinear. Figure 6A and B shows the results of pull-out testing for welding systems 1 and 2, respectively. The weld nugget diameter increased significantly between the welding times of 10 and 20 ms for both welding systems, showing that the growth rate during this stage of the process was high. Significant nugget growth continued up to 30 ms for welding system 1,

Table 5 — Weld Nugget Nucleation and Growth Rates from Simulation Data for 100-ms Welding Time and 37-, 41-, and 45-kA Welding Currents

Welding Current (kA)	Time, Nucleation Stage (ms)	Growth Rate, Nucleation Stage (mm/ms)	Correlation Coefficient, Nucleation Stage	Growth Rate, Growth Stage (mm/ms)	Correlation Coefficient, Growth Stage
37	9	0.374	0.96	0.008	0.39
41	7	0.568	0.97	0.018	0.87
45	6	0.746	0.95	0.022	0.82

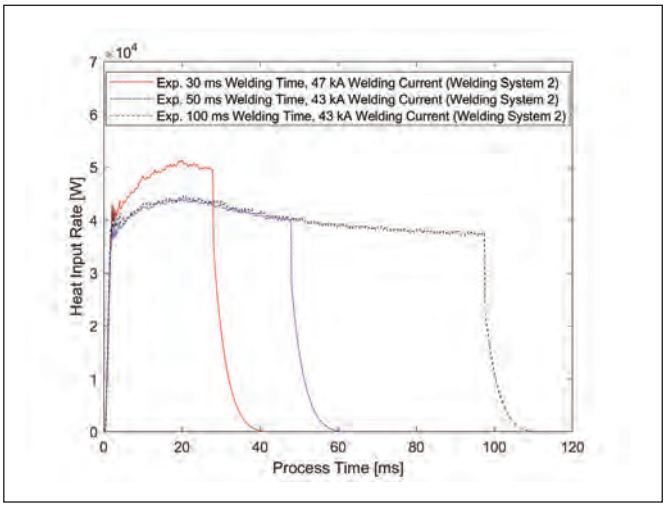

Fig. 12 — Heat energy input rate, measured experimentally for the welding times of 30, 50, and 100 ms. Current levels selected for equally required final nugget diameter.

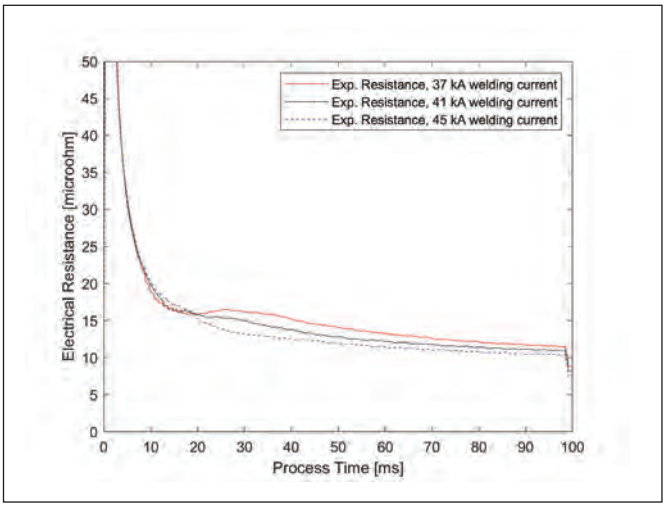

Fig. 13 — Total electrical resistance measured from electrode to electrode for welding system 1 at a 100-ms welding time and with welding currents of 37, 41, and 45 kA.

while the growth rate of the nugget decreased steadily after 20 ms for welding system 2. For both systems, the growth rate decreased significantly past a welding time of 30 ms.

For both welding systems, the acceptable current range was equal for the 50- and 100-ms welding time. No expulsions were detected during testing for any conditions; therefore, the current ranges extended to the maximum current of 47 kA. For welding system 1, the current range for both welding times was from 45 to 47 kA, and for welding system 2, it was from 43 to 47 kA. The 30-ms welding time had a current range of 45 to 47 kA for welding system 1 but no acceptable current range for welding system 2. At welding times lower than 30 ms, there was a high amount of scatter in the results, and no acceptable current range was obtained. The difference in results between the welding systems was a result of the different current control characteristics and current rise speeds, resulting in different heat inputs to the weld.

Tables 3 and 4 show the most prevalent fracture modes of the pull-out samples for all welding time and current conditions. At the 10-ms welding time, there were a high number of open welds and ring-shaped failures, showing that melting initiated at the periphery and that growth into a solid weld nugget was incomplete. With increased welding time, the fracture mode transitioned from ring-shaped to interfacial, and then to the desired pull-out failure. An increase in welding current also tended to change the fracture mode from interfacial to pull-out failure; however, the relationship was not as strong as with welding time. For all welding conditions where the required nugget diameter was achieved, 100% pull-out failure was observed.

Analysis of cross-sectioned weld samples gave additional insight into the influence of welding time and current on the nugget growth process. Samples welded with welding system 2 are seen in Fig. 7A–H, where the top row (Fig. 7A–D) shows the joints at a welding current of 37 kA and a welding time of 20, 30, 50, and 100 ms. The bottom row (Fig. 7E–H) shows the joints at the same welding times but at a 45-kA current level. No significant weld imperfections or irregularities were noted in the welds for any conditions.

Furthermore, the heat-affected zone revealed by etching of the samples was small, showing efficient heating of the material at the joining interface for the pulse shape used. At both current levels, the fusion zone diameter was similar for welding times of 50 and 100 ms, which was in agreement with pull-out test results. The fusion zone size was a function of welding current; however, the growth rate decreased with welding time independent on current level.

Samples were tested with nondestructive ultrasound testing to observe nugget development at shorter weld times. Ultrasonic testing has an advantage over cross-section imaging because nugget asymmetry is visible and there is no error from failing to section the sample in the middle of the nugget area. The sample results from welding system 2 are seen in Fig. 8. At a welding time of 10 ms, the formation of the weld nugget was incomplete and melting was seen at small, disconnected locations. Beginning at 20-ms weld time, a single nugget had formed, but it was not completely round in shape until 30 ms. Increasing the welding time past 30 ms resulted in additional nugget growth but at a much lower rate than in the initial stages of nugget nucleation and growth during the first 20 to 30 ms of welding. The difference in nugget size was not significant between the 50- and 100-ms welding time samples. Therefore, nugget growth was occurring at a slow rate during this time. Nugget diameter was increased as a function of current level for all welding times; however, the time of nugget nucleation and the overall characteristics of the nugget development process were again shown to be largely independent of the current level.

Weld Nugget Nucleation and Growth

Simulations were used for further analysis of the weld nugget development processes. While nodal temperature data and final nugget diameter were already available in the simulation software package, a new development was made to the software in cooperation with Swantec for this study to output the dynamic size of the molten zone during the welding process in both the nugget diameter and height di-

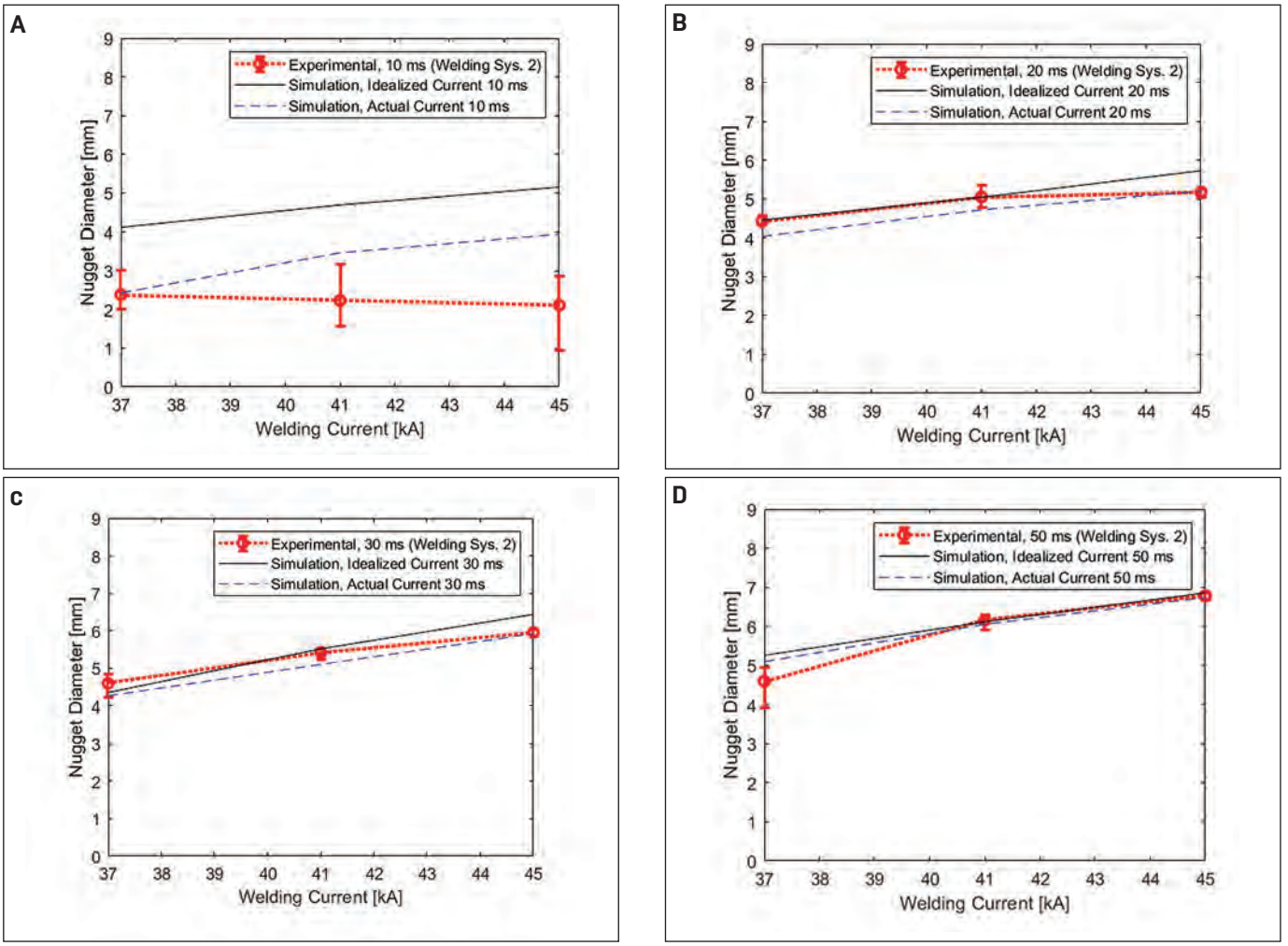

Fig. 14 — Simulations using idealized and actual current profiles: A — 10-ms welding time; B — 20-ms welding time; C — 30-ms welding time; D — 50-ms welding time.

rections. With this data, additional information was gained on the nugget development process that was not accessible by experimental testing. The nucleation and growth of the molten zone at different stages in the process are seen for the example of a 100-ms current pulse with 41 kA — Fig. 9.

Analysis of the dynamic nugget diameter data from simulations showed there are two distinct stages in the nugget development process. In the first stage, the weld nugget nucleated and grew rapidly to approximately 60–80% of its final size. In the simulations, this stage was completed within the first 10 ms and characterized by the large slope of the nugget diameter vs. time plots — Fig. 10. As compared to experiments, the nugget nucleation stage took place more quickly in the simulations. In evaluation of experimental samples using ultrasound and cross sections, nugget nucleation required 20 to 30 ms of current application. In this stage, the rapid growth of the nugget likely occurred due to the high contact resistances present. The second stage, called the nugget growth stage, was characterized by a much slower rate of growth of the weld nugget — Fig. 10. While the growth continued until the end of the current application time, the nugget size became almost constant within 70 to 80 ms. In this stage, the slower nugget growth likely took place by heat conduction from the nugget to the surrounding material. Figure 10 contains the dynamic nugget growth curves for the welding time of 100 ms and three current levels: 37, 41, and 45 kA. The presence of the distinct nugget nucleation and growth stages was independent of the current level, and the portion of the process spent in nugget nucleation vs. growth also did not differ greatly by the current level. The simulation data showed some wave-like change in the nugget size during the growth stage, an artifact likely caused by dynamic contact changes during welding.

From the dynamic nugget size data, it was possible to calculate nugget growth rates during the nucleation and growth stages as a function of welding current, the results of which are listed in Table 5. The growth rates in the nucleation stage were significantly greater than in the growth stage, and the time spent in the nucleation stage varied from 6 to 9 ms depending on current level. The higher heat input rate created by the increased current level led to a higher growth rate during the nucleation and growth stages. The nugget growth was highly linear during the nucleation stage, as evident by the high correlation coefficient between the data and linear approximation line. In the nugget growth stage, the growth rate decreased with time, and linear correlation was weaker than in

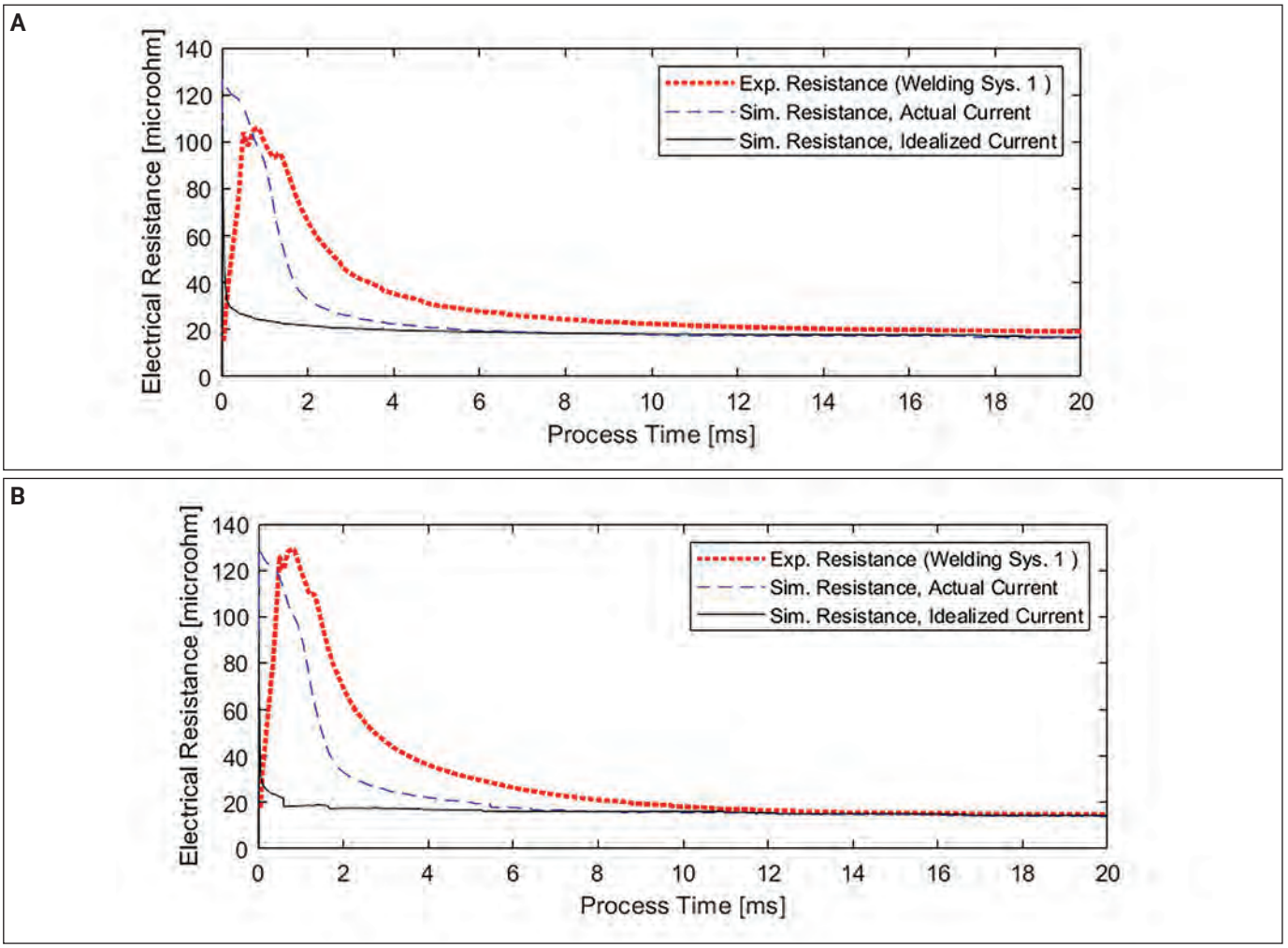

Fig. 15 — Comparison of experimental and simulated resistance profiles with the use of idealized and actual current input profiles. Data shown: A — 27 kA; B — 37 kA.

the nucleation stage. However, the process became more linear at higher current levels.

Discussion

The use of short welding pulses reduced the heat input required to generate a weld of a given size. The total heat input to the weld was calculated by measurement of current and voltage signals during welding and an integration of the product of these signals over time. In Fig. 11, the total energy input to the weld is shown for three different welding conditions, all of which produced a weld of a required nugget diameter. For the welding times of 100 and 50 ms, a current level of 43 kA was required. When welding time was further decreased to 30 ms, 47 kA was necessary. Although all three conditions produced the same size weld, shorter welding times required far lower heat inputs. The fact that no change in the current level was necessary when the welding time was decreased from 100 to 50 ms suggests that nugget growth is insignificant past 50 ms. This is supported by the experimental data presented in Figs. 6 and 8 as well as the simulation data in Fig. 10.

While the energy requirement can be even further decreased by a reduction of the welding time to 30 ms, the current level must then be increased by approximately 10% to partially compensate for the reduction in heat input and to increase the heat input rate. However, the increase in current also creates higher magnetic forces between the gun arms during welding, may cause more rapid electrode wear, and showed inconsistency in results for one of the welding systems tested. Therefore, a reduction of welding time past 50 ms would not be recommended. Nevertheless, reducing the welding time from 100 to 50 ms generated an energy saving of 48% per weld spot.

For a fixed pulse shape, the heat input rate was determined by the current level. In Fig. 12, the heat input rate is shown for the same parameter cases presented above. The result showed that the heat input rate to the weld was higher in the case of the 30-ms welding time, where the current level of 47 kA was used. Although the difference in heat input rates did not lead to a difference in weld size, it is evident that it does play a role in the weld nugget formation. For example, the higher heat input rate can compensate for a lower overall heat input to produce an equal weld size, as in the case of the 30-ms weld. Additionally, when materials have high thermal conductivity, such as AA6016-T4 and oth-

er 6000 series aluminum alloys, the heat input rate must be sufficiently high for a weld nugget to form. Heat produced at the joining interface is quickly conducted away and not utilized for the formation of a weld nugget when the heat input rate is too low. This is evident by the fact that at low current levels and extended welding times, no nugget formation occurred at all. In RSW of steel, long welding times are used for additional nugget growth; however, for high-conductivity aluminum materials, this practice would be unsuccessful. Instead, the current level must be sufficiently increased or another parameter solution must be found. This study focused on welding time and current, but the shape of the current pulse also affected the heat input rate. This is another important consideration for short-pulse welding and will be the subject of a follow-up study.

It can be observed that the heat input was not linear and the heat input rate varied with time. Heat input rates were initially very high but then began to decrease at approximately 20 ms. The calculation of heat input for resistance welding is represented by the Joule heating equation in which the heat input for any duration is given by the integral of the product of resistance and the square of the applied current, as seen in Equation 5.

$$Q = \int_{t_i}^{t_f} I^2 R \, dt \qquad (5)$$

For rectangular-shaped pulses, the applied current is nearly constant. Therefore, the heat input would vary linearly with time were it not for dynamic changes in resistance during welding. The decrease in the heat input rate is a result of the large decrease in resistance that occurs during the breakdown of contact resistances in the first milliseconds of welding. Examples of experimentally measured resistance curves for different current levels are seen in Fig. 13, where the breakdown of contact resistances during the first stages of current application are clearly visible.

The accuracy of welding simulations was influenced by the accuracy of the current profile used and the resulting resistance profiles. The agreement between simulation and experimental results decreased at welding times of less than 20 ms. This disagreement was logical because idealized current profiles were used as inputs to the simulations. While completely rectangular current pulses were programmed as inputs to the welding systems experimentally, they were impossible to achieve due to physical limitations of the current rise speed and control of the current signal during welding. Therefore, a comparison was done where the actual current profiles were recorded during welding and used as the inputs for simulations. The ability to use customized current-profile inputs was an existing capability of the SORPAS software. The result was an improvement in agreement with experimental results at short welding times. In Fig. 14A–D, and especially in Fig. 14A for a welding time of 10 ms, the improvement in agreement with experimental results is evident.

Nevertheless, some disagreement in results still remained for very short welding times (10 ms) and low current levels below 37 kA. By observing the difference in the resistance profiles from simulations and measured during experiments, as presented in Fig. 15, one can see that the reason for this was the difference in modeling of the nugget nucleation stage. The breakdown of contact resistances occurred much more quickly in the simulations than in experiments, resulting in a lower amount of heat generated at the start of the welding time. In the nugget growth stage, however, the resistance curves matched between simulations and experiments. Because the nugget nucleation stage represented a much larger fraction of the total process time for short welding times, it played a larger role and the modeling of this stage caused a disagreement in results. At lower welding currents, formation of a weld nugget was highly dependent on the heating occurring at the beginning of the process while contact resistances were high. When the contact resistances were broken down more quickly, as in the simulations, the remaining heat input was not sufficient to form a weld nugget; therefore, the simulation results reported small or zero nugget sizes. The difficulty in modeling the contact resistance breakdown and nugget nucleation helped to explain the discrepancies at short welding times and low welding currents.

The challenge of modeling the breakdown of contact resistances during aluminum RSW and in modeling contact resistance in general is a well-known and universal challenge in finite element analysis (FEA) simulations of the RSW process (Refs. 16, 19). The process is highly complex, especially for aluminum materials due to the presence of oxide layers on the surface of the material, which are broken down in the initial stages of welding. According to Song et al., the contact resistance is highly dynamic during the RSW process and is not only a function of temperature and pressure but also of the condition of the surface (Ref. 20). The surface layers of aluminum alloys are not only complex in their composition and corresponding mechanical and electrical properties but are also highly nonuniform. In the simulations performed, the contact properties were defined uniformly along the contact interfaces. Experience from experiments, as seen in the Fig. 8 ultrasound images at low welding times, shows that nugget nucleation does not always occur uniformly across the contact interface but rather at localized, isolated locations. Therefore, the surface layer and contact properties in reality are not uniform, and heating occurs locally at areas where electrical contact exists prior to the breakdown of the surface layer. The nonuniformity of the surface layer is likely the reason for unsuccessful modeling of the nugget nucleation stage, and this effect is more evident when the nugget nucleation stage plays a larger role in the process, such as at short welding times and at low current levels. This topic remains one of the most significant challenges for FEA modeling of the RSW process for aluminum materials, and future work is necessary to incorporate the nonuniform properties and behavior of the surface layer on a microscale to simulations to further improve numerical results.

Several beneficial impacts are to be gained by the short-pulse MFDC method. Using the short-pulse welding technique, it was possible to reduce the welding time to 50 ms without changing the acceptable current range for welding. The result was a reduction in energy requirement by approximately 48%, in addition to 50 ms of process time savings per weld. With the increasing importance of carbon emissions reduction and sustainability practices in manufac-

turing, the decrease in power and energy consumption for welding is an important and promising benefit provided by short-pulse MFDC. Furthermore, the process time savings enable more flexibility in process planning and efficient use of equipment. Additionally, as current levels were not increased by shortening the welding time, issues of gun arm deflections or electrode wear were not evident with the new parameter strategy. In a follow-up study, it will be shown that current levels may even be reduced for thin-sheet combinations of AA6016-T4 compared to standard practices by altering the pulse shape using short-pulse parameterization.

Conclusion

This paper investigated the use of short-current pulse durations (10–100 ms) as a function of applied current level (27–47 kA) on the RSW of AA6014-T4 using MFDC welding systems. The results have shown that short-pulse welding reduces the heat input necessary for sound welds. The rate of heat input increases with the welding current, thus more efficiently heating and melting the material to be joined. However, a minimum welding time of 50 ms is necessary for stability in the welding result. Both simulations and experiments suggest the weld nugget formation has distinct nucleation and growth stages in which the fusion zone nucleates on the periphery of the weld nugget and grows inward to the center. The applied current level influences the growth rate and final nugget size but not the nucleation time or shape of the growing weld nugget.

Acknowledgment

This study was supported by Daimler AG, Sindelfingen, Germany, and is published with their permission.

References

1. Hirsch, J. 2011. Aluminum in innovative light-weight car design. *Materials Transactions* 52(5): 818–824. DOI: 10.2320/matertrans.L-MZ201132

2. Manladan, S. M., Yusof, F., Ramesh, S., Fadzil, M., Luo, Z., and Ao, S. 2017. A review on resistance spot welding of aluminum alloys. *International Journal of Advanced Manufacturing Technology* 90: 605–634. DOI: 10.1007/s00170-016-9225-9

3. Gould, J. E. 2012. Joining aluminum sheet in the automotive industry — A 30 year history. *Welding Journal* 91(1): 23-s to 34-s.

4. Zhang, H., and Senkara, J. 2011. *Resistance Welding: Fundamentals and Applications*. CRC Press: Boca Raton, Fla.

5. Deng, L., Carlson, B. E., and Sigler, D. R. 2018. Effects of electrode surface topography on aluminum resistance spot welding. *Welding Journal* 97(4): 120-s to 132-s. DOI: 10.29391/2018.97.011

6. Han, L., Thornton, M., Boomer, D., and Shergold, M. 2010. Effect of aluminium sheet surface conditions on feasibility and quality of resistance spot welding. *Journal of Materials Processing Technology* 210(8): 1076–1082. DOI: 10.1016/j.jmatprotec.2010. 02.019

7. Al Naimi, I. K., Al Saadi, M. H., Daws, K. M., and Bay, N. 2015. Influence of surface pretreatment in resistance spot welding of aluminum AA1050. *Production & Manufacturing Research* 3(1): 185–200. DOI: 10.1080/21693277.2015.1030795

8. Li, Z., Hao, C., Zhang, J., and Zhang, H. 2007. Effects of sheet surface conditions on electrode life in resistance welding aluminum. *Welding Journal* 86(4): 81-s to 89-s.

9. Sigler, D. R., and Karagoulis, M. J. 2011. Weld schedule for resistance spot welding of aluminum alloy workpieces. U.S. Patent Application 2013/0048613.

10. Rusch, H. J., Geßler, R., and Jüttner, S. 2017. Widerstandspunktschweißen von aluminium mit mehrimpulsigem kondensatorentladungsstrom [Resistance spot welding of aluminum with multipulse capacitor discharge current]. *Schweißen und Schneiden* [*Welding and Cutting*] 69: 618–619.

11. Rashid, M., Medley, J. B., and Zhou, Y. 2011. Nugget formation and growth during resistance spot welding of aluminium alloy 5182. *Canadian Metallurgical Quarterly* 50: 61–71. DOI: 10.1179/000844311X552322

12. Riedel, F., and Heidrich, J. 2017. Potential of the capacitor discharge welding for difficult-to-weld similar and mixed materials. *Joining in Car Body Engineering Conference*. Bad Nauheim, Germany.

13. Hwang, I. S., Kang, M. J., and Kim, D. C. 2011. Expulsion reduction in resistance spot welding by controlling of welding current waveform. *Procedia Engineering*: 2775–2781. DOI: 10.1016/j.proeng.2011.04.461

14. Automobile Industry Association [Verband der Automobilindustrie]. 2013. VDA 239-200: *Aluminum Sheet Material*. Berlin, Germany.

15. Swantec Software and Engineering ApS. 2018. *SORPAS 2D Version 13 User Manual*.

16. Zhang, W. 2003. Design and implementation of software for resistance welding process simulations. *SAE International Journal of Materials and Manufacturing*. DOI: 10.4271/2003-01-0978

17. Crinon, E., and Evans, J. T. 1998. The effect of surface roughness, oxide film thickness and interfacial sliding on the electrical contact resistance of aluminium. *Materials Science and Engineering A* 242 (1–2): 121–128. DOI: 10.1016/S0921-5093(97)00508-X

18. German Institute for Standardization [Deutsches Institut für Normung]. 2010. DIN EN ISO 5821:2009: *Resistance Welding —Spot Welding Electrode Caps*.

19. De, A., Thaddeus, M. P., and Dorn, L. 2003. Numerical modelling of resistance spot welding of aluminium alloy. *ISIJ International* 43(2): 238–244. DOI: 10.2355/isijinternational.43.238

20. Song, Q., Zhang, W., and Bay, N. 2005. An experimental study determines the electrical contact resistance in resistance welding. *Welding Journal* 84(5): 73-s to 76-s.

ERIC SCHULZ (ewschulz@crimson.ua.edu), *MATTHIAS WAGNER, and HOLGER SCHUBERT are with Daimler AG, Sindelfingen, Germany. SCHULZ is also with The University of Alabama, Tuscaloosa, Ala. WENQI ZHANG is with Swantec, Kongens Lyngby, Denmark. BHARAT BALASUBRAMANIAN and LUKE N. BREWER are with the Center for Advanced Vehicle Technologies, The University of Alabama, Tuscaloosa, Ala.*

Shielding Gas and Inclusion Content Effects on Impact Toughness and Tensile Properties of 410NiMo Steel Welds

The effect of shielding gas on the mechanical and microstructural characteristics of ER410NiMo martensitic stainless steel weldments was investigated

BY B. TENNI, S. GODIN, D. THIBAULT, AND M. BROCHU

ABSTRACT

The effect of shielding gas on the mechanical and microstructural characteristics of ER410NiMo martensitic stainless steel weldments was investigated. Three weldments with various inclusion contents were manufactured using different shielding gas compositions and welding processes: gas metal arc welding (GMAW) with 100% argon (Ar), GMAW 85% Ar/15% carbon dioxide (CO_2), and flux cored arc welding (FCAW) 75% Ar/25% CO_2.

The inclusions in each weldment were characterized by means of scanning electron microscope observations and energy-dispersive spectroscopy analysis. The weldments underwent postweld heat treatment, after which the chemical composition and reformed austenite proportion were measured to account for microstructural effects. Hardness measurements, tensile tests, and impact toughness tests using the Charpy method were performed. The results showed that the Charpy V-notch (CVN) absorbed energy decreases with increasing inclusion content. The highest CVN absorbed energy, 195 J, was obtained for the GMAW 100% Ar weld, which had the lowest inclusion content. GMAW 85% Ar/15% CO_2, with four times more inclusions than the former, had a CVN absorbed energy of 63 J. The current manufacturing process, FCAW 75% Ar/25% CO_2, was found to have an inclusion content three times higher than the GMAW 100% Ar weld but a CVN absorbed energy of 66 J, which is close to the GMAW 85% Ar/15% CO_2 weld. The results showed that using GMAW 100% Ar as a replacement to FCAW 75% Ar/25 % CO_2 would lead to a three-fold improvement in terms of absorbed impact energy.

The effect of inclusions on tensile properties, which was not clearly identified as several factors, in addition to inclusion content, affects the weld strength and elongation. Overall, the yield and ultimate tensile strengths differed slightly: 724 and 918 MPa for GMAW 100% Ar, 746 and 927 MPa for GMAW 85% Ar/15% CO_2, and 711 and 864 MPa for FCAW 75% Ar/25% CO_2, respectively.

KEYWORDS

• Martensitic Stainless Steel • Inclusions • Welding
• Impact Toughness

Introduction

ER410NiMo is a low-carbon 13% Cr–4% Ni soft martensitic stainless steel. This filler metal is considered to be the best match to CA6NM base metal, which is the cast version of this steel.

For hydraulic turbine runners, which are the application of interest in this paper, several properties are important. These include good fatigue properties, corrosion resistance, cavitation erosion resistance, and weldability, as well as ease of casting. These requirements are satisfactorily met by soft martensitic stainless steels, which is the reason for their growing popularity in the hydropower industry.

Weldability and fatigue properties of weldments are especially important for hydraulic turbine runner manufacturers, because runners are assembled by welding, and for power plant owners because they often have to carry out on-site repairs of cavitation and fatigue damages through welding.

Welded regions, however, have particular features such as undesired residual stresses, welding discontinuities, and inclusions. Moreover, as demonstrated by Amrei et al. (Ref. 1), martensitic stainless steel weldments are characterized by a complex and heterogeneous microstructure due to the existence of coarse and fine-grain regions in the weld.

Currently, arc welding processes are used to assemble hydraulic turbine runners. The assembly process consists of welding the blades to the crown and belt. Current practices use the flux cored arc welding (FCAW) process with a shielding gas of 75% argon (Ar)/25% carbon dioxide (CO_2). To test the influence of oxides on mechanical properties, gas metal arc welding (GMAW) was used with two different shielding gas compositions and compared to current FCAW procedures. Procedures using shielding gases with more CO_2 trap more oxygen in the molten pool. This is due to the electric arc and the high temperatures involved during the welding operation, which lead to ionization of CO_2 decomposes into *C* and *O*, resulting in more oxygen in the weld pool. This oxygen is then free to form oxides through reactions with other alloying elements.

Teske and Martins (Ref. 2) conducted a study on the influence of shielding gas composition in GMAW using different mixtures with either CO_2 or O_2. When present, CO_2 and

https://doi.org/10.29391/2021.100.005

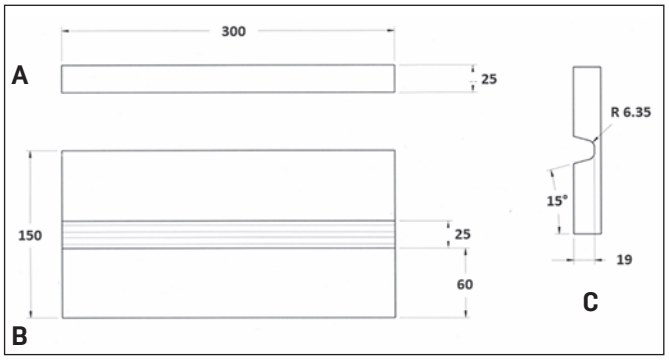

Fig. 1 — Dimensions, in millimeters, of the bare plates: A — Side view; B — view from the top of the weld; C — profile showing the U-notch.

Table 1 — Welding Conditions Used to Prepare the Weldments for Impact Toughness Testing

	GMAW 100% Ar	GMAW 85% Ar/ 15% CO_2	FCAW 75% Ar/ 25% CO_2
Voltage (V)	25	28.8	27.5
Current (A)	210	207.5	228
Torch speed (mm/s)	3.8	3.8	4.2
Heat input (J/mm)	1381	1572	1505
Number of weld beads	11	10	12

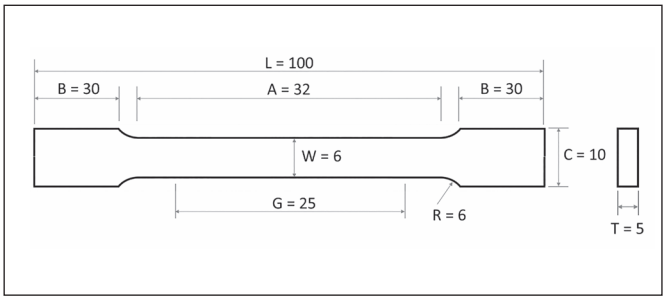

Fig. 2 — Tensile test specimen geometry (mm). Prior to testing, two points were punched 1 in. apart to establish the original length and calculate the elongation at fracture.

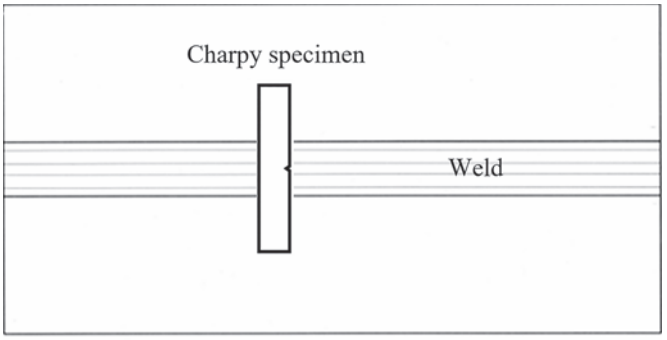

Fig. 3 — Schematic drawing showing the Charpy specimen orientation with respect to the weld.

O_2 cause the formation of oxide inclusions due to their oxidation potential; note that the oxidation potential is twice as high for O_2 than it is for CO_2. The welds with the highest occurrence of oxides showed the lowest impact toughness properties. Foroozmehr et al. (Ref. 3) examined the effect of inclusions on the impact toughness properties of two 13% Cr–4% Ni martensitic stainless steels, a cast version (CA6NM) and a wrought one (UNS S41500). The results showed that the higher content and the larger mean size of inclusions in CA6NM explained the lower impact toughness properties compared to UNS S41500. This was justified by microvoid formation from the inclusions.

Other metallurgical factors should also be accounted for when studying such steels. Though the microstructure is mostly martensitic, small amounts of delta ferrite and austenite are usually present and can affect mechanical properties. Delta ferrite, for example, is oftentimes considered detrimental to mechanical properties, especially in terms of fracture toughness and impact absorbed energy. Iwabuchi and Kobayashi (Ref. 4) attributed the deleterious effect of delta ferrite to the precipitation of carbides along delta-ferrite grain boundaries during heat treatment. To minimize the negative effect of delta ferrite, nickel, which is an austenite-stabilizing element, is added to chromium martensitic stainless steels to keep a martensitic microstructure, thus preventing carbides from precipitating. However, due to carbide precipitation along delta-ferrite grain boundaries, it is difficult to isolate the effect of delta ferrite from that of carbides as Wang et al. (Ref. 5) brought to attention.

By successfully isolating both effects, the authors concluded that delta-ferrite only influences the transition temperature region in terms of impact absorbed energy, and it does not have a significant effect on the upper- and lower-shelf energies. Aside from delta ferrite, another phase that can be present is retained austenite; usually only a very small fraction remains present after quenching. However, during tempering heat treatment, a greater amount of austenite can be reformed. Bilmes et al. (Ref. 6) studied tempering of martensitic stainless steel as well as the austenite resulting from such a treatment. It was found that the reformed amount can reach up to 30% in the form of finely precipitated at the prior austenite grain boundaries. This phase is believed to improve toughness and ductility of the studied steels. When tempering slightly above Ac_1, the reformed austenite is thermally stable and leads to optimal mechanical properties. Tempering at higher temperatures leads to the formation of unstable austenite, which transforms to fresh martensite upon cooling. However, under applied load, even thermally stable austenite can transform back to martensite, which makes austenite mechanically unstable. This mechanism is commonly known as the transformation-induced-plasticity (TRIP) effect and is responsible for the interesting mechanical properties resulting from reformed austenite. Thibault et al. (Ref. 7) studied this aspect, concluding that when the TRIP mechanism occurs, more energy is required for the fracture process due to the volumetric expansion accompanying the austenite to martensite transformation, which induces compressive stresses at the crack tip.

In addition to creating reformed austenite, tempering post-weld heat treatment relieves residual stresses in the weld and the heat-affected zone (HAZ) as well as softens the hard and brittle as-welded martensite as demonstrated in the work of Trudel et al. (Ref. 8) performed on welded CA6NM.

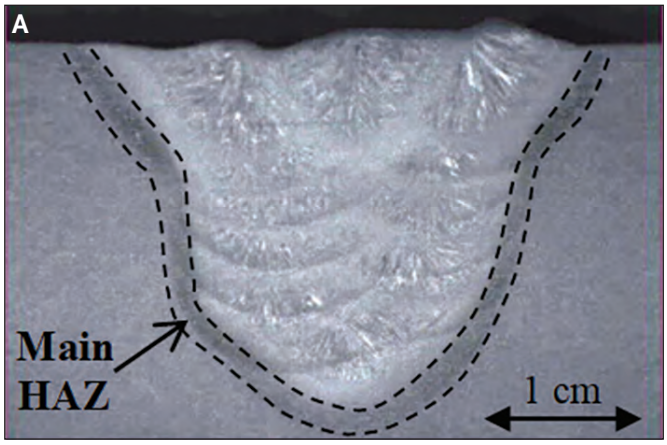

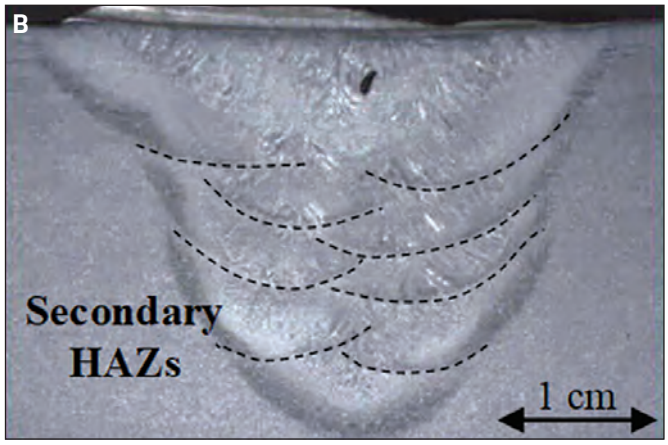

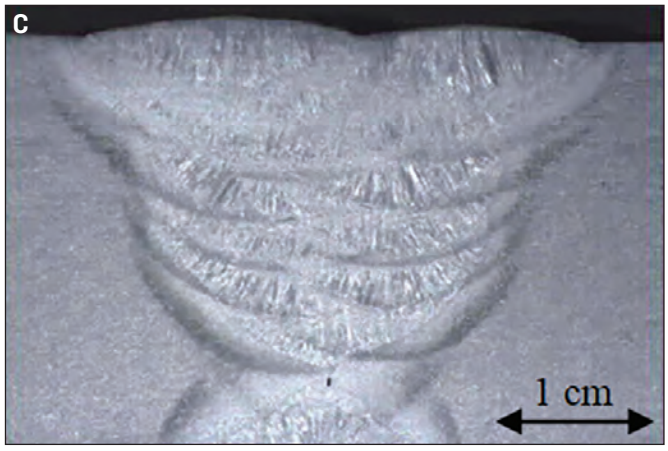

Fig. 4 — Macrographs of the postweld heat treated welds: A — GMAW 100% Ar; B — GMAW 85% Ar/15% CO_2; C — FCAW 75% Ar/25% CO_2.

Table 2 — Welding Conditions Used to Prepare the Weldments Destined for Tensile Testing

	GMAW 100% Ar	GMAW 85% Ar/15% CO_2	FCAW 75% Ar/ 25% CO_2
Voltage (V)	24.3	26.5	27.5
Current (A)	212	222	222
Torch speed (mm/s)	3.9	3.9	4.2
Heat input (J/mm)	1320	1508	1453

The aim of the research presented in this paper is to study the effect of shielding gas composition on the impact toughness and tensile properties of martensitic stainless steel weldments. The weldments made using different welding processes and shielding gas compositions produced varying inclusion contents.

Experimental Methodology

Materials

The welding procedure used FCAW with a shielding gas composition of 75% Ar/25% CO_2.

As discussed in the introduction, this relatively high content of CO_2 is believed to cause the formation of oxides, shown to negatively affect mechanical properties. Since GMAW requires less active gas in the shielding mixture, it was used to produce welds under different shielding gas compositions, which in turn resulted in different oxide contents. Hence, three welds were produced under the following atmospheres:

- FCAW 75% Ar/25% CO_2, the current process in use;
- GMAW 100% Ar, the process thought to generate the least oxide content and;
- GMAW 85% Ar/15% CO_2, an intermediate condition for research purposes.

Figure 1 gives the dimensions of the CA6NM plates that were used to produce the welds destined to machine the Charpy specimens. The U-notch preparation presented in Fig. 1C has been filled by multipass robotized welding with an AWS ER410NiMo filler metal wire of 1.6 mm in diameter.

Table 1 provides the welding conditions used in each procedure. An effort was made to keep the heat input energy constant in the three procedures because it directly affects the temperatures and, as a result, the weld microstructure. The objective was to vary the oxide content while keeping all other influencing factors constant.

Additional weldments were prepared by depositing weld metal on the entire surfaces of the plates. This is done to ensure the tensile test specimens are fully extracted from the weld metal. The same filler metal was used but the base metal was UNS-S41500, which is the wrought version of CA6NM used previously. Because UNS-S41500 and CA6NM have comparable chemical compositions, it was expected that the tensile properties of the second batch of welded plates were also characteristic of the first one. Table 2 gives the welding conditions used for this second batch.

Postweld Heat Treatment

After welding, the plates underwent a tempering postweld heat treatment at 600°C for a duration of 20 h. The furnace atmosphere was not controlled.

Austenite Measurements

After postweld heat treatment, the proportions of austenite were measured by x-ray diffraction from a Rietveld analysis (Ref. 9). The x-ray diffraction patterns were obtained with a Bruker D8 Advance diffractometer equipped

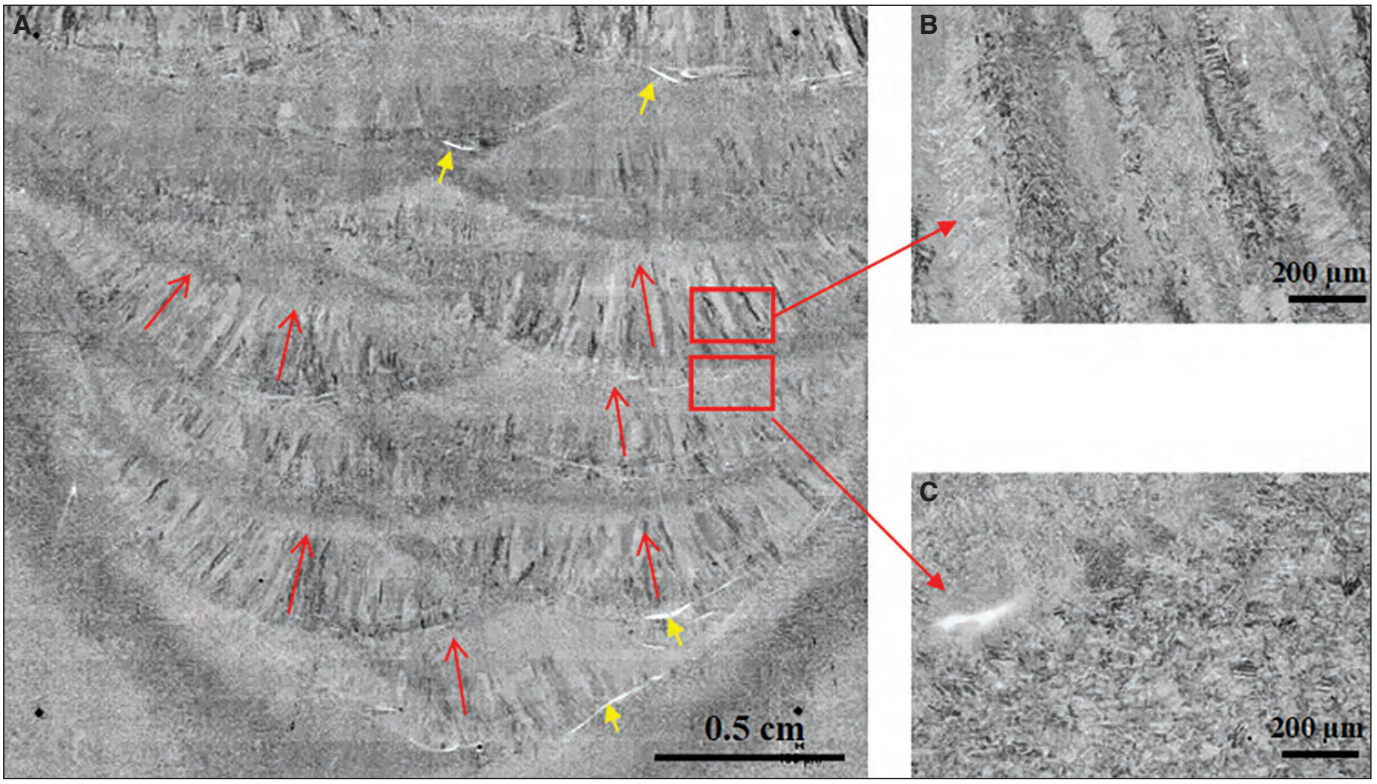

Fig. 5 — Weld microstructure observed in FCAW 75% Ar/25% CO_2 postweld heat treated: A — Macrograph of the weld; B — magnified view displaying a column-shaped martensite; C — magnified view displaying a HAZ with finer grains. The red arrows show the orientation of martensite columns, corresponding to the heat flow directed toward the top of the weld.

with a copper x-ray tube and a nickel filter. The measurements were done on thin slices cut transverse to the welds. Three samples per weld were prepared.

Chemical Composition Measurements

The chemical composition of both types of filler metals (solid wire and flux-cored wire), as well as the base metal and each of the fusion zones of the welds described above, were measured by inductively coupled plasma-emission atomic spectrometer in accordance with ASTM E1479 (Ref. 10) except for carbon, sulfur, oxygen, and nitrogen contents measured by combustion and inert gas fuel (ASTM E1019).

Hardness Measurements

To evaluate the hardness of the welds, and ensure the three welds were equivalent in terms of hardness, ten Vickers hardness measurements were made in each weld using a ZwickRoell ZHU 250 hardness tester in the transverse direction as well as in the as-welded and tempered conditions at 10 kgf in accordance with ASTM E92 (Ref. 12).

Quantification of Oxides

Metallographic cross sections cut transverse to the weld were prepared. Using a scanning electron microscope (SEM) Hitachi S-4700 equipped with an energy dispersive spectrometer (EDS), the oxides were observed, counted, and analyzed through EDS analysis. In total, 16 images at a 5000x magnification were used, yielding a total examined surface of seven 200 μm^2 for GMAW 85% Ar/15% CO_2 and FCAW 75% Ar/25% CO_2 welds. As for GMAW 100% Ar, extra images were taken to ensure at least 100 oxides were counted, yielding a total surface of 15 338 μm^2. For each observed oxide, the horizontal and vertical ferrets were measured, and the mean of both measurements was considered to produce size distribution spectra.

Tensile Testing

Three tensile tests per condition were realized in the weld metal in the transverse direction with respect to the deposited weld beads. A MTS Systems tensile tester model Exceed 40 using a 50-kN load cell was used. A MTS extensometer model 632.24-50 with a gauge length of 25 mm was used to monitor the elongation. The displacement rate was 2 mm/min, leading to a strain rate of about 0.06/min.

Figure 2 shows the geometry and dimensions of the test specimens, which correspond to an ASTM E8 (Ref. 13) subsize specimen.

Impact Toughness Properties

To perform impact toughness tests, five Charpy V-notch (CVN) bars of standard dimensions $10 \times 10 \times 55$ mm were machined from each weld. Impact tests were performed at 0°C, with a ZwickRoell RKP450 pendulum impact tester in accordance with ASTM E23 (Ref. 14). The specimens were

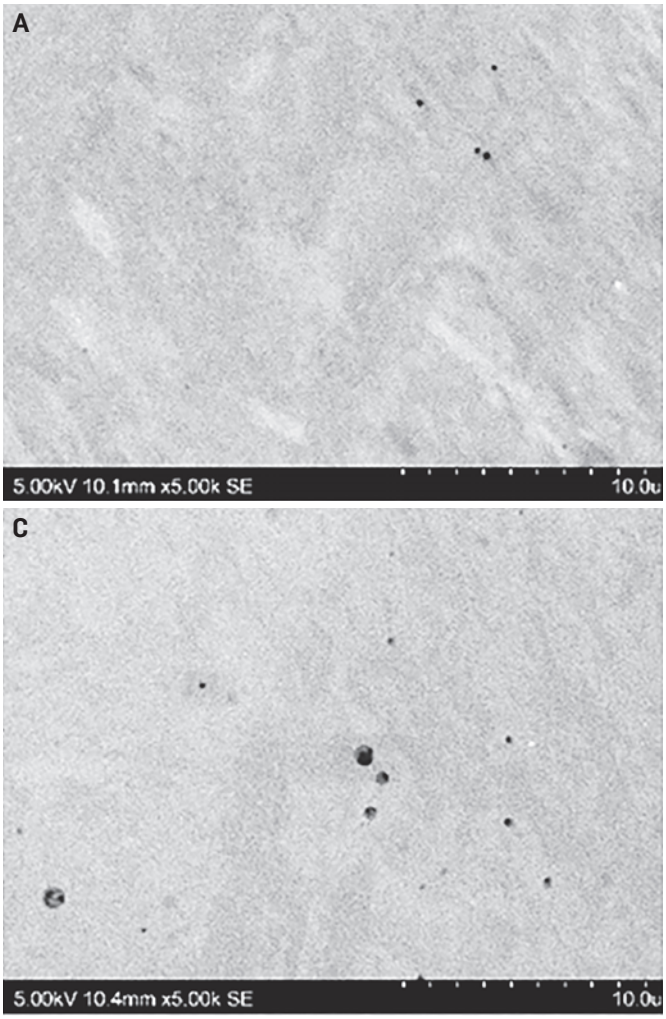

Fig. 6 — SEM images of as-polished cross sections transverse to the welds displaying oxides: A — GMAW 100% Ar; B — GMAW 85% Ar/15% CO_2; C — FCAW 75% Ar/25% CO_2.

machined in the transverse direction, in the center of the weld, as shown in Fig. 3.

Results and Discussion

Chemical Composition

Table 3 gives the measured chemical compositions of each weld and the specified chemical compositions for comparison. The measured chemical compositions are all compliant with the specifications, except for the manganese content in the 410NiMo solid wire and both GMAW welds. The higher-than-specified Mn content in the GMAW weldments is therefore most probably due to the high Mn content found in the corresponding filler metal, which might affect the austenite content because Mn is an austenite-promoting element. Also, GMAW 85% Ar/25% CO_2 has a slightly lower-than-specified Ni content, which might also affect the austenite content because nickel is an austenite-promoting element. Note that the carbon and oxygen contents are significantly higher in GMAW 85% Ar/15% CO_2 compared to the other welds.

Reformed Austenite Measurements

Table 4 provides the mean percentage of austenite and the standard deviation obtained from the measurements in each weld. These measurements include both residual and reformed austenite, but since residual austenite proportion is not expected to exceed 1% as measured by Godin (Ref. 17), the obtained proportions give a good indication on the amount of reformed austenite.

To compare the weldments in terms of the extent of their austenitic domain, hence their ability to create reformed austenite when tempered at 600°C, an estimation of their Ac_1 temperature was obtained using an empirical equation proposed by Gooch et al. (Ref. 18). The equation shows the effect of austenite-promoting elements (C, N, Ni, Mn) and ferrite-promoting elements (Si, Mo, Cr) on the Ac_1 temperature. Theoretically, if Ac_1 of a material reported in Table 4 is above 600°C, no austenite should reform during tempering. Below 600°C, the lower the Ac_1 of a given material is, the greater the proportion of austenite is expected to reform during tempering.

$$Ac_1(°C) = 850 - 1500(C + N) - 50\,Ni - 25\,Mn + 25\,Si + 25\,Mo + 20(Cr - 10) \quad (1)$$

The theoretical Ac_1 temperature was calculated using Equation 1 and the measured chemical composition given in Table 1. The results of these calculations are provided in Table 4.

Assuming the austenite reformed while tempering was stable at room temperature, its proportion should be maximum in the GMAW 85% Ar/15% CO_2 weld and inexistent in the FCAW 75% Ar/25% CO_2 weld. Nevertheless, the x-ray diffraction analysis showed more than 20% of austenite in all welds, with the highest amount in the FCAW 75% Ar/25% CO_2. This indicated Equation 1 cannot be used to estimate the austenite content of the studied welds.

The raw results that led to empirical Equation 1 have not been detailed in the work of Gooch et al. It was most probably based on homogeneous material chemistry and specific heating rates. Because of the potential differences between the experimental conditions, Equation 1 can hardly predict

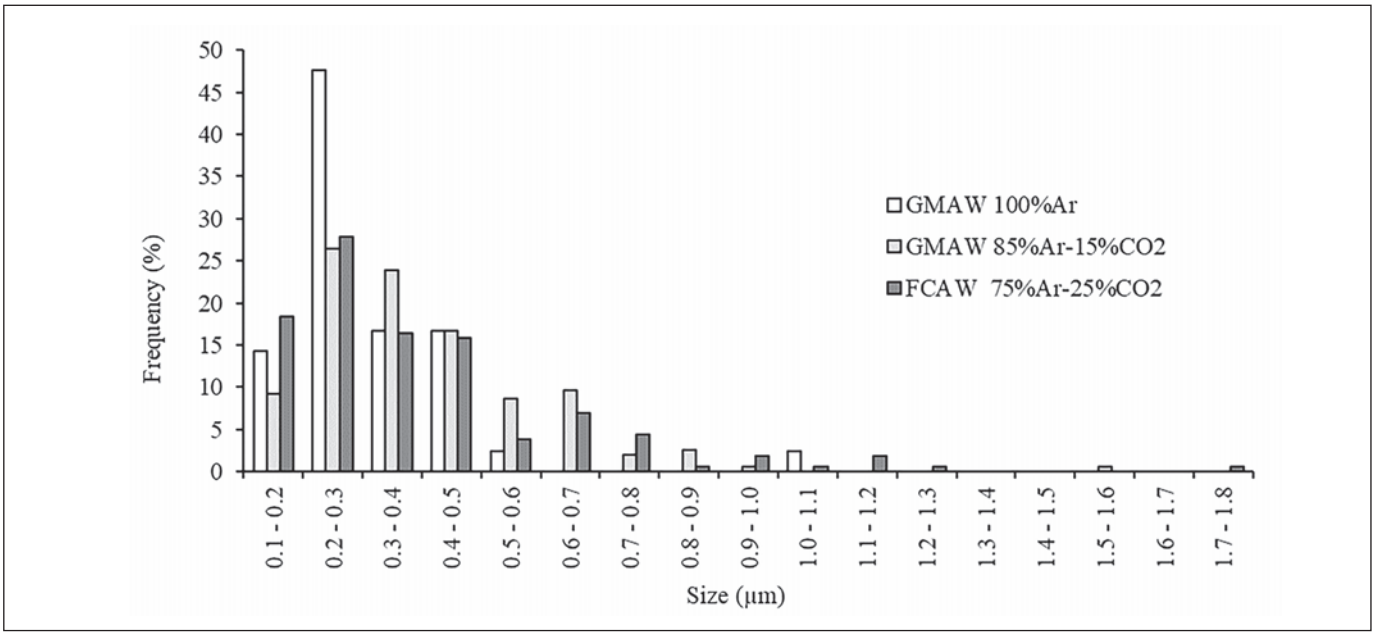

Fig. 7 — Size distribution of oxides.

the austenite content in the studied cases. The amount of austenite measured in the FCAW 75% Ar/25% CO_2 weld is close to the maximum amount reported by Bilmes et al. (Ref. 6), who specifically studied the formation and stability of reformed austenite 13Cr–NiMo martensitic steel weld metals.

Microstructure of the Welds

Figures 4 and 5A show macrographic views of the prepared metallographic cross sections of the the postweld heat treated welds, etched with Vilella's reagent. The main HAZ, as well as the secondary ones in between weld beads, is visible on the

Table 3 — Chemical Compositions of ER410NiMo and CA6NM as per Material Specifications and Measured Chemical Compositions of the Welds, Base Metal, and Filler Metals (wt-%)

		% C	% S	% O	% N	% P	% Si	% Mn	% Cr	% Ni	% Mo
Specified	Base metal CA6NM (Ref. 15)	0.06 max.	0.03 max.	N.S.[1]	N.S.	0.04 max.	1.0 max.	1.0 max.	11.5–14	3.5–4.5	0.4–1.0
	ER410NiMo (Ref. 16)	0.06 max.	0.03 max.	N.S.	N.S.	0.03 max.	0.5 max.	0.6 max.	11.0–12.5	4.0–5.0	0.4–0.7
Measured	Base metal CA6NM	0.033	0.0005	0.002	0.031	0.021	0.46	0.65	12.5	4.10	0.634
	410NiMo (solid wire for GMAW)	0.018	0.001	N.M.[2]	0.028	0.019	0.38	0.70	12.4	4.14	0.500
	410NiMo (flux-cored wire for FCAW)	0.021	0.011	N.M.	N.M.	0.008	0.37	0.36	12.5	4.39	0.560
	GMAW 100% Ar	0.024	0.002	0.013	0.036	0.027	0.41	0.77	12.3	4.04	0.546
	GMAW 85% Ar/ 15% CO_2	0.043	0.001	0.068	0.031	0.018	0.33	0.64	12.2	3.89	0.544
	FCAW 75% Ar/ 25% CO_2	0.026	0.007	0.070	0.01	0.018	0.38	0.44	12.0	4.30	0.605

[1] Not specified
[2] Not measured

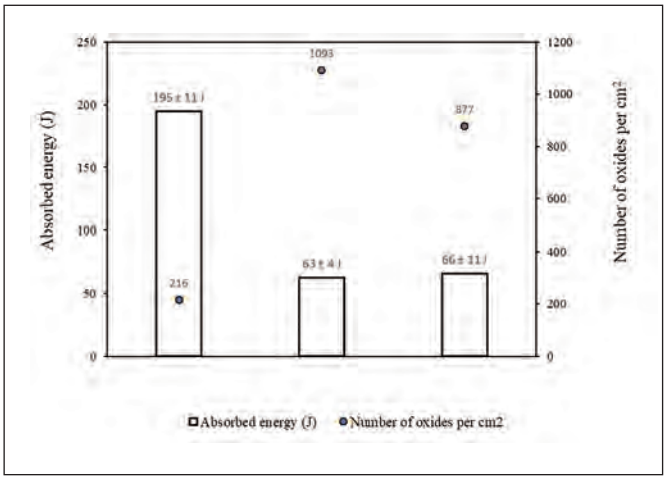

Fig. 8 — Charpy absorbed energy results and the oxide density in each weld.

macrographs due to its darker aspect. As observed, an effort was made to have similar weld pool and overall weld dimensions to create a comparable weld microstructure.

Figure 5B and C provides a magnified view of the FCAW 75% Ar/25% CO_2 postweld heat treated weld macrograph. Regions of columnar martensite, consisting of column-shaped packets, are shown in Fig. 5B separated by fine-grain regions as in Fig. 5C. A similar grain structure was observed by Amrei et al. (Ref. 19) in ER410NiMo filler metal deposited by FCAW using 75% Ar/25% CO_2. Note that martensite columns appear to be pointing to the top of the weld as depicted by the red arrows, which corresponds to the heat flow direction. Reformed austenite is not visible by optical microscopy because it is finely (60 to 200 nm wide) distributed between the martensite lath, as shown in other work performed on comparable material (Ref. 22).

Although it was not confirmed, the fine white stringers, observed in Fig. 5A and C indicated by the smaller yellow arrows, are most likely delta-ferrite stringers because they look similar to what was reported by Thibault et al. (Ref. 20) and Foroozmehr et al. (Ref. 3).

Table 4 — Mean Percentage of Austenite (% γ) with the Standard Deviation of the Measurements and Theoretical AC_1 Temperature

	% γ	AC_1 (°C)
GMAW 100% Ar	21 ± 1	609
GMAW 85% Ar/15% CO_2	25 ± 2	594
FCAW 75% Ar/25% CO_2	27 ± 1	634

Table 5 — Hardness and Standard Deviation of the Weldments Before and After Tempering Postweld Heat Treatment

	Mean HV10	
	As welded	Tempered
GMAW 100% Ar	356 ± 20	292 ± 5
GMAW 85% Ar/15% CO_2	368 ± 23	283 ± 8
FCAW 75% Ar/25% CO_2	327 ± 18	281 ± 8

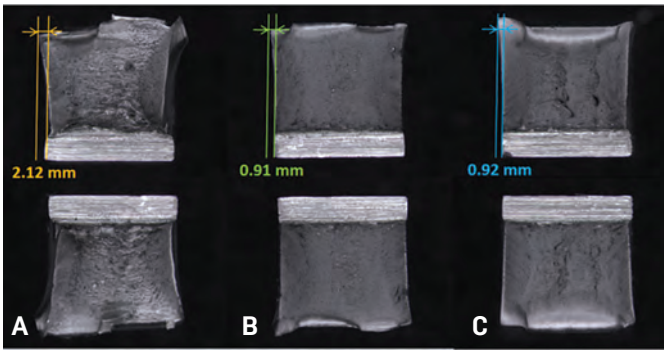

Fig. 9 — Fracture surfaces of Charpy V-notch specimens with the corresponding lateral expansions: A — GMAW 100% Ar; B — GMAW 85% Ar/15% CO_2; C — FCAW 75% Ar/25% CO_2.

Hardness

Table 5 gives the Vickers hardness measurements for each weld in both the as-welded and tempered conditions.

The obtained results show the softening effect of the tempering heat treatment. In each of the three welding conditions, the mean hardness decreased by 18%, 23%, and 14% after tempering. The standard deviation was reduced as well for all welds, suggesting a more uniform microstructure. Considering the standard deviations, the hardness intervals of the welds overlap, which means the welds can be considered comparable in terms of hardness.

Oxides Characterization

Figure 6 shows SEM images of as-polished cross sections cut transverse to the welds displaying oxides, which identification of was confirmed through detection of oxygen in EDS analyses.

Table 6 gives the quantification results, namely the number of oxides per 100 mm^2, the mean size of oxides, as well as the median size for each weld.

To verify if there are any significant differences between the welds in terms of inclusion size, an analysis of variance (ANOVA) test was used. This test is used to compare multiple statistical groups and determine whether they significantly differ. Setting the P value of the ANOVA test to 5%, we can't reject the hypothesis that all means are equal. This shows that it is not possible to consider with confidence the mean values of the oxides as different.

As expected, the GMAW 100% Ar had the lowest oxide content. However, the FCAW 75% Ar/25% CO_2 didn't have the highest oxide content, despite having the highest CO_2 concentrated shielding gas. This can be explained by the presence of

Table 6 — Oxides Median Size, Mean Size, and Density

	Median Size (μm)	Mean Size (μm)	Number of Oxides per cm^2
GMAW 100% Ar	0.39	0.49	216
GMAW 85% Ar/15% CO_2	0.36	0.40	1093
FCAW 75% Ar/25% CO_2	0.32	0.40	877

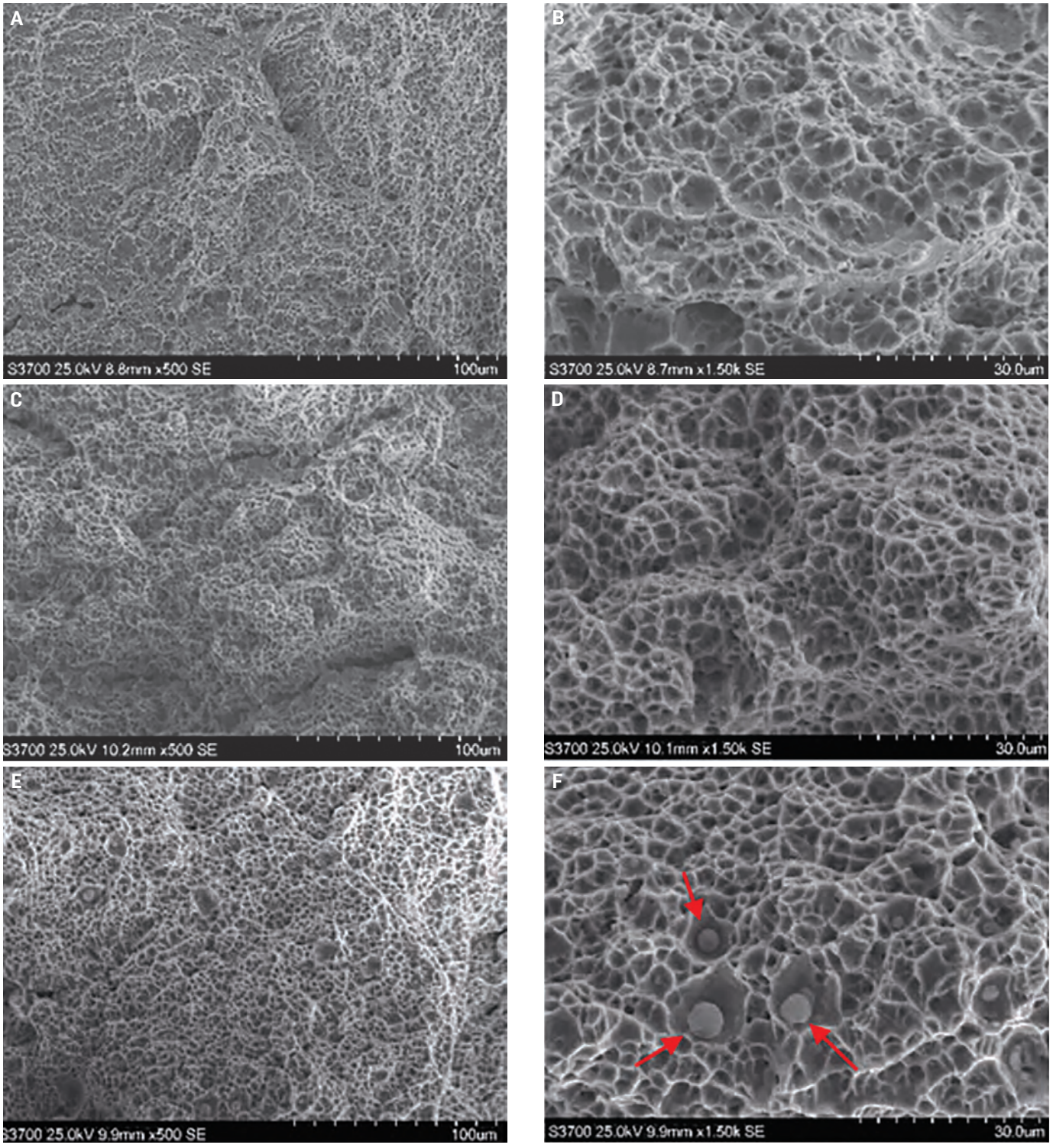

Fig. 10 — Dimpled fracture on Charpy fracture surfaces: 500x magnification: A, B — GMAW 100% Ar; C, D — GMAW 85% Ar/15% CO_2; E, F — FCAW 75% Ar/25% CO_2 at magnifications of 500x and 1500x, respectively.

Table 7 — Elements Present in the Oxides

	O	Si	Cr	Mn	Al	Mg	Ca	Ti	Zr
GMAW	x	x	x	x	x	x	x		
FCAW	x	x	x	x				x	x

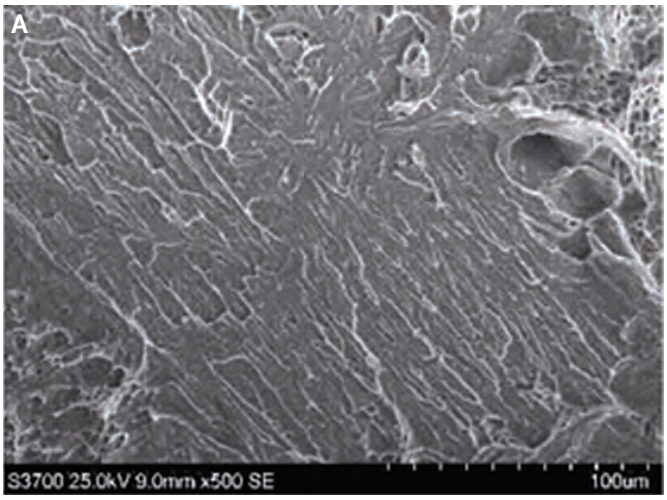

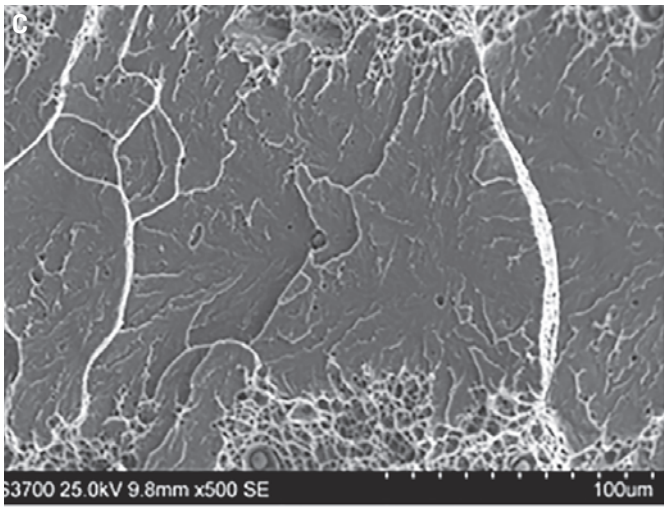

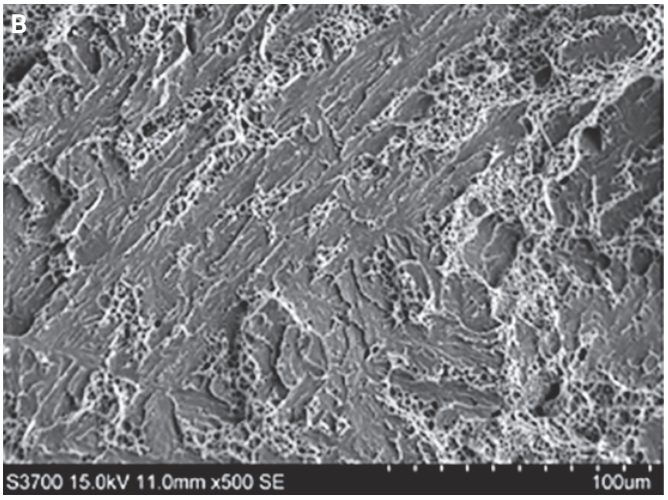

Fig. 11 — Examples of cleavage observed on fracture surfaces: A — GMAW 100% Ar; B — GMAW 85% Ar/15% CO_2; C — FCAW 75% Ar/25% CO_2.

the flux, which protects the weld pool from oxidation.

Figure 7 displays the size distribution of the measured oxides for each welding process. For all three welds, the class with the highest number of oxides is 0.2–0.3 µm.

The chemical composition of the oxides was determined using the EDS spectrometer coupled with the SEM. Though this method is standardless and semiquantitative, it gives a good idea about the chemical composition of the oxides. The analysis showed both GMAW welds to have oxides with similar compositions, but the FCAW weld had slightly different oxides. Table 7 gives the elements present in the weld oxides from both welding processes.

This difference between GMAW and FCAW might be caused by the elements present in the flux. Foroozmehr et al. (Ref. 3) reported that Si/Mn inclusions have a lower resistance against rupture and microvoid formation than Al inclusions (both types seem to be present in the GMAW welds) whereas Al inclusions weren't detected in FCAW.

Tensile Properties

Table 8 gives the means and standard deviations obtained from the tensile properties retrieved from the stress-strain curves following ASTM E8 (Ref. 13) recommendations.

Three material characteristics that could influence the weld's mechanical behavior are presented in Table 8: the inclusion content, the percentage of reformed austenite, and the carbon content. Indeed, the inclusion content was shown to be detrimental to the material ductility as reported by Foroozmehr et al. (Ref. 3), who compared the mechanical behavior and microstructure of CA6NM and UNS41500. Reformed austenite, on the other hand, is believed to increase the steel yield strength and ductility due to the TRIP mechanism. As for the carbon content, Krauss (Ref. 21) showed that the yield stress of low-carbon martensite has a square-root dependency with the solute carbon content. Despite having the largest inclusion content, GMAW 85% Ar /15% CO_2 shows the highest yield and tensile strengths without a significant drop of ductility when compared with the GMAW 100% Ar weld characterized by the lowest inclusion content. The higher carbon content within the GMAW 85% Ar/15% CO_2 weld, 0.043% vs. 0.024% and 0.026% for GMAW 100% Ar and FCAW 75% Ar/25% CO_2, could explain its higher strength. Moreover, the percentage of reformed austenite measured in this weldment was 25%, compared to 21% for GMAW 100% Ar, which could have compensated for a potential ductility loss caused by the presence of inclusions.

The FCAW 75% Ar/25% CO_2 weld also had a quite large inclusion content, but it is also characterized by the highest amount of austenite. In this case, as for GMAW 85% Ar/15% CO_2, it could explain that no significant decrease in ductility was observed.

Table 8 — Tensile Properties of the Welds

Weld	$\sigma_{y\ 0.2\%}$	σ_{UTS}	A (%)
GMAW 100% Ar	724 ± 7	918 ± 1	21 ± 1
GMAW 85% Ar/15% CO_2	746 ± 11	927 ± 4	19 ± 1
FCAW 75% Ar/25% CO_2	711 ± 32	864 ± 1	19 ± 5

Impact Toughness Properties

Figure 8 gives the CVN absorbed energy and the oxide density, while Fig. 9, the measured lateral expansions, illus-

trates the fracture surfaces. Given the results of Fig. 8, it seems that the inclusion content is the dominant influencing factor on CVN absorbed energy because the absorbed energy decreased with increasing inclusion content. GMAW 100% Ar with the lowest inclusion content had the highest absorbed energy, three times that of the other two conditions.

Measurements of the lateral expansion were realized on the fractured Charpy specimens and are illustrated in Fig. 9 with the fracture surfaces. As can be seen on the image, there is a good agreement between the absorbed energy and the measured lateral expansion: the higher the absorbed energy, the greater the deformation, hence, the lateral expansion.

The fracture surfaces were examined using a SEM to determine fracture mechanisms. SEM fractography revealed the fracture to be mostly ductile as evidenced by the dimpled rupture. Examples are displayed in Fig. 10.

All three welds exhibited some cleavage areas toward the center of the fracture surfaces. Examples are shown in Fig. 11. Although cleavage is usually suggestive of brittleness, it is not always the case. The center of the specimens represents the location of the highest hydrostatic stresses, which promotes cleavage fracture, even if the temperature is above the ductile-to-brittle transition temperature.

Based on the previous observations, the main fracture mechanism is microvoid formation and coalescence, as for most ductile materials. All oxides observed on the fracture surfaces are found sitting inside the dimples (as shown by red arrows in Fig. 10), suggesting the dimples nucleated at oxides.

Therefore, the effect of oxides on absorbed energy can be discussed as follows: In the case of a large inclusion content, void nucleation from oxide inclusions is the dominant mechanism, and the growth stage is instantaneous. However, when fewer oxides are present, fewer nucleation sites are available, making the growth stage dominant. This leads to higher deformation, and consequently, a more energy-consuming fracture.

The findings are consistent with the study of Foroozmehr et al. (Ref. 3), where the higher mechanical properties of the wrought steel were attributed to the lower inclusion content, lower mean size of inclusions, and type of inclusions; those in the wrought steel were found more resistant against rupture than the ones in the cast steel. As the size of the inclusions was found equivalent in the three studied welds, it was possible to isolate the effect of the inclusion density.

Conclusion

In light of the work described in this article, the following conclusions can be drawn:

1) A shielding gas with a higher concentration of CO_2 increases oxide content in the weld. If the current welding procedure using FCAW is to be replaced by GMAW under pure argon, oxide content could be decreased by a factor of three.

2) As far as impact toughness properties are concerned, replacing the FCAW 75% Ar/25% CO_2 process, which is the current manufacturing process, with the GMAW 100% Ar process would lead to a three-fold improvement.

3) CVN absorbed energy decreases as oxide content increases. A high inclusion content increases nucleation sites for microvoids, and coalescence then leads to rapid damage and rupture. On the other hand, a low inclusion content means less nucleation sites, which leads to more plastic deformation during the growth stage, resulting in higher absorbed energy.

In view of these three conclusions, for application where impact resistance is critical, it is recommended to weld 410NiMo with GMAW using a shielding gas composed of 100% argon because it limits the formation of inclusions that are detrimental to impact energy absorption. Though small variations were observed in tensile properties, it seemed that several factors were competing, namely the carbon, austenite, and inclusion content. Verification of the effect of each factor is saved for future work.

Acknowledgment

This work was supported by Institut de Recherche d'Hydro-Québec and Mathematics of Information Technology and Complex Systems (IT07240). Technologists René Dubois, Alexandre Lapointe, and Manon Provencher are gratefully acknowledged for their help.

References

1. Amrei, M. M., Verreman, Y., Bridier, F., Thibault, D., and Bocher, P. 2015. Microstructure characterization of single and multipass 13Cr4Ni steel welded joints. *Metal., Microstruct., and Anal.* 4(3): 207–218. DOI: 10.1007/s13632-015-0202-8

2. Teske, M., and Martins, F. 2010. The influence of the shielding gas composition on GMA welding of ASTM A 516 steel. *Weld. Int*. 24(3): 222–230. DOI: 10.1080/09507110902843875

3. Foroozmehr, F., Verreman, Y., Chen, J., Thibault, D., and Bocher, P. 2017. Effect of inclusions on fracture behavior of cast and wrought 13% Cr-4% Ni martensitic stainless steels. *Eng. Fract. Mech*. 175: 262–278. DOI: 10.1016/j.engfracmech.2017.02.002

4. Iwabuchi, Y., and Kobayashi, I. 2010. A study of toughness degradation in CA6NM stainless steel. *Mater. Sci. Forum* 654–656: 2515–2518. DOI: 10.4028/www.scientific.net/msf.654-656.2515

5. Wang, P., Lu, S. P., Xiao, N. M., Li, D. Z., and Li, Y. Y. 2010. Effect of delta ferrite on impact properties of low carbon 13Cr-4Ni martensitic stainless steel. *Mater. Sci. and Eng. A* 527(13–14): 3210–3216. DOI: 10.1016/j.msea.2010.01.085

6. Bilmes, P. D., Solari, M., and Lorente, C. L. 2001. Characteristics and effects of austenite resulting from tempering of 13Cr-NiMo martensitic steel weld metals. *Mater. Charact*. 46(4): 285–296. DOI: 10.1016/S1044-5803(00)00099-1

7. Thibault, D., Bocher, P., Thomas, M., Lanteigne, J., Hovington, P., and Robichaud, P. 2001. Reformed austenite transformation during fatigue crack propagation of 13%Cr-4%Ni stainless steel. *Mater. Sci. and Eng. A* 528(21): 6519–6526. DOI: 10.1016/j.msea.2011.04.089

8. Trudel, A., Sabourin, M., Lévesque, M., and Brochu, M. 2014. Fatigue crack growth in the heat affected zone of a hydraulic turbine runner weld. *Int. J. of Fat.* 66: 39–46. DOI: 10.1016/j.ijfatigue.2014.03.006

9. Young, R. A. 1993. *The Rietveld Method*. First Ed. Oxford University Press Inc. USA.

10. ASTM International. 2016. *ASTM E1479. Standard Practice for Describing and Specifying Inductively Coupled Plasma Atomic Emission Spectrometers*.

11. ASTM International. 2011. *ASTM E1019. Standard Test*

Methods for Determination of Carbon, Sulfur, Nitrogen, and Oxygen in Steel, Iron, Nickel, and Cobalt Alloys by Various Combustion and Fusion Techniques.

12. ASTM International. 2017. *ASTM E92. Standard Test Methods for Vickers Hardness and Knoop Hardness of Metallic Materials*.

13. ASTM International. 2016. *ASTM E8. Standard Test Methods for Tension Testing on Metallic Materials*.

14. ASTM International. 2016. *ASTM E23. Standard Test Methods for Notched Bar Impact Testing of Metallic Materials. ASTM International*.

15. ASTM International. 2015. *ASTM A743. Standard Specification for Castings, Iron-Chromium, Iron-Chromium-Nickel, Corrosion Resistant, for General Application*.

16. American Welding Society. 2012. *AWS A5.9, Specification for Bare Stainless Steel Welding Electrodes and Rods*. Eighth Ed. Miami, Fla.

17. Godin, S. Effet d'un enrichissement en nickel sur la stabilité mécanique de l'austénite de réversion lorsque soumise à de la fatigue oligocyclique. Master Thesis. 2014. École de Technologie Supérieure, Montréal.

18. Gooch, T. G., Woollin, P., and Haynes, A. G. 1999. *S99-22, Welding metallurgy of low carbon 13% chromium martensitic steels, supermartensitic stainless steel* 99. Belgian Welding Institute: 188–195.

19. Amrei, M. M., Monajati, H., Thibault, D., Verreman, Y., Germain, L., and Bocher, P. 2016. Microstructure characterization and hardness distribution of 13Cr4Ni multipass weld metal. *Mater. Charact*. 111: 128–136. DOI: 10.1016/j.matchar.2015.11.022

20. Thibault, D., Bocher, P., and Thomas, M. 2009. Residual stress and microstructure in welds of 13% Cr–4%Ni martensitic stainless steel. *J. of Mater. Process. Technol*. 209(4): 2195–2202. DOI: 10.1016/j.jmatprotec.2008.05.005

21. Krauss, G. 2015. *Steels: Processing, Structure, and Performance*. Second Ed. ASM International.

22. Godin, S., Hamel-Akré, J., Thibault, D., Serventi, A.-M., and Bocher, P. 2020. *Ni and Mn enrichment effects on reformed austenite: Thermodynamical and low cycle fatigue stability of 13%Cr–4%Ni and 13%Cr–6%Ni stainless steels*. Springer Nature, accepted for publication on February 4, 2020.

BOUCHRA TENNI and MYRIAM BROCHU (myriam.brochu@polymtl.ca) *are with École Polytechnique de Montréal, Montreal, Canada. STÉPHANE GODIN and DENIS THIBAULT are with Institut de Recherche d'Hydro-Québec, Quebec, Canada.*

The majority of the content in this article was published in the master's thesis Étude expérimentale de l'effet du contenu inclusionnaire sur les propriétés mécaniques de résilience et de fatigue-propagation au seuil de soudures en acier 410 NIMO, by Bouchra Tenni, École Polytechnique de Montréal.

Adaptive Intelligent Welding Manufacturing

An analysis of classical sensing, modeling, and control; modern machine learning; and human-robot collaborative approaches

BY Y. M. ZHANG, Q. Y. WANG, AND Y. K. LIU

ABSTRACT

Optimal design of the welding procedure gives the desired welding results under nominal welding conditions. During manufacturing, where the actual welding manufacturing conditions often deviate from the nominal ones used in the design, applying the designed procedure will produce welding results that are different from the desired ones. Adaption is needed to make corrections and adjust some of the welding parameters from those specified in the design. This is adaptive welding. While human welders can be adaptive to make corrections and adjustments, their performance is limited by their physical constraints and skill level. To be adaptive, automated and robotic welding systems require abilities in sensing the welding process, extracting the needed information from signals from the sensors, predicting the responses of the welding process to the adjustments on welding parameters, and optimizing the adjustments. This results in the application of classical sensing, modeling of process dynamics, and control system design. In many cases, the needed information for the weld quality and process variables of our concern is not easy to extract from the sensor's data. Studies are needed to propose the phenomena to sense and establish the scientific foundation to correlate them to the weld quality or process variables of our concern. Such studies can be labor intensive, and a more automated approach is needed. Analysis suggests that artificial intelligence and machine learning, especially deep learning, can help automate the learning such that the needed intelligence for robotic welding adaptation can be directly and automatically learned from experimental data after the physical phenomena being represented by the experimental data has been appropriately selected to make sure they are fundamentally correlated to that with which we are concerned. Some adaptation abilities may also be learned from skilled human welders. In addition, human-robot collaborative welding may incorporate adaptations from humans with the welding robots. This paper analyzes and identifies the challenges in adaptive robotic welding, reviews efforts devoted to solve these challenges, analyzes the principles and nature of the methods behind these efforts, and introduces modern approaches, including machine learning/deep learning, learning from humans, and human-robot collaboration, to solve these challenges.

KEYWORDS

• Arc Welding • Sensor • Robotic Welding • Sensing • Control

Introduction

In fusion welding (Ref. 1), the base materials (i.e., materials to be joined) are melted to allow them to mix together, with or without addition of a filler. The resultant welds are formed after the mixed melts are solidified. For solid-state welding such as friction stir welding (FSW) (Ref. 2), the temperature of the base materials is elevated to a level such that the base materials gain the flowability needed for being mixed/joined. Brazing/soldering (Ref. 2) is different as the base materials do not flow/move and are not directly mixed. Flowability of the base materials is thus a basic characteristic of welding, which distinguishes it from brazing/soldering.

The flowability needed for welding is typically gained by elevating the temperature of the base materials using an energy source. The energy source or the way to provide the energy is typically reflected in the name of the process. Arc/laser welding (Ref. 1) uses an arc/laser as the energy source while friction welding (Ref. 2) uses a mechanical energy. The interaction of the energy source with the base materials produces the heat to elevate their temperature, while in FSW the rotating tool is the carrier of the mechanical energy source that interacts with the base materials.

The requirements on the resultant welds are determined by their intended services. Applying energy into the base materials to produce welds meeting the requirements also produces side effects that adversely affect the ability of the resultant welded structure to meet the service requirements.

https://doi.org/10.29391/2021.100.006

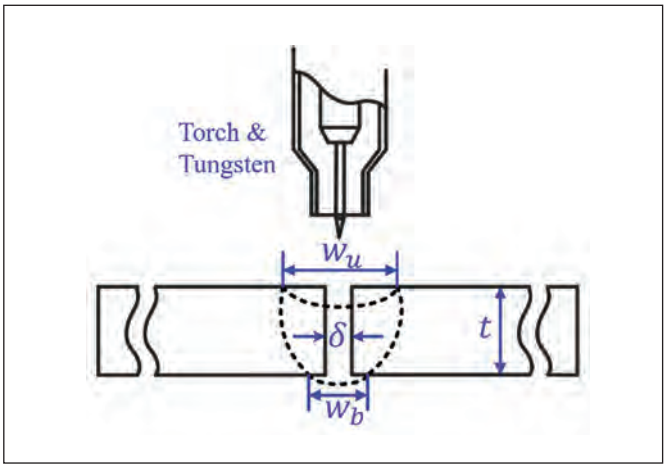

Fig. 1 — Application example to illustrate key issues in adaptive robotic welding.

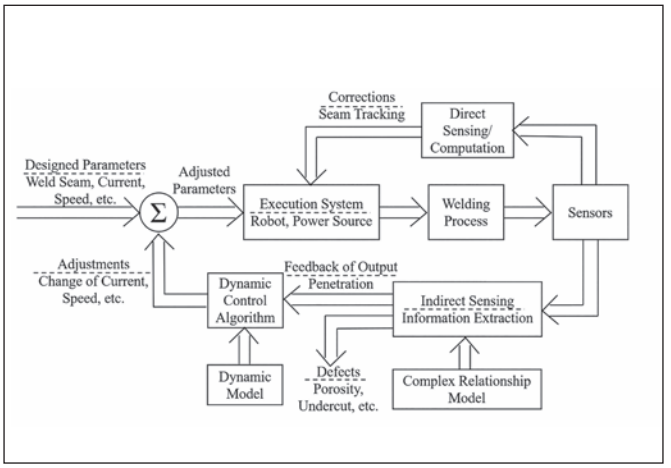

Fig. 2 — Adaptive intelligent robotic welding and its key elements.

Some of the adverse side effects are the distortion (Ref. 3) and degradation of the base materials in the heat-affected zone (HAZ) (Ref. 3). Such side effects impose restrictions on how the energy source is applied. An optimal design of the welding procedure (Ref. 4) gives the preferred way to apply the energy source to efficiently produce the desirable welds to meet the service requirements with acceptable side effects.

Implementation of an optimal design requires the ability to deliver the welding procedure as intended. This requires precise application of the energy source as intended. Unfortunately, all optimal designs are based on nominal welding conditions. While efforts need to be taken to minimize the deviation of the actual welding conditions from the nominal conditions on which the optimized design was based, such efforts may be too extensive, costly, or even impossible in many applications. Methods are thus often needed to minimize the deviations of the resultant welds from their nominal ones during the welding manufacturing process. This requires adaptations to make corrections and adjustments during the execution of the designed welding procedure (i.e., during welding manufacturing), resulting in adaptive intelligent welding manufacturing. Efforts addressing the issues and challenges in such adaptations are the focus of review and analysis in this paper.

The following section uses an example to analyze and present the issues and challenges for adaptive intelligent welding manufacturing. A diagram is presented to summarize the principle of an adaptive intelligent welding system and its key elements. The Visual Sensing of the Welding Process section reviews and analyzes the efforts to observe and understand the welding process. The efforts specifically devoted to the monitoring of the joint penetration, one of the most important and challenging targets of adaptive intelligent welding manufacturing, are reviewed and analyzed in the Monitoring of Joint Penetration section. The Modeling and Control section reviews the efforts in modeling of the welding process as a dynamic system and the decision-making that determines adjustments of welding parameters based on the dynamic model of the welding process. In the Machine/Deep Learning section, we first introduce the principles of machine learning and then review the use of machine learning in solving challenges related to adaptive intelligent welding that are difficult to solve using conventional ways. Finally, in the Learning from Human Welders and Human-Robot Collaborative Welding section, we introduce human-robot collaborative welding as an approach to use human adaptation for adaptive intelligent robotic welding and introduce related efforts.

Issues and Challenges

We use Fig. 1 as a relatively simple application example to illustrate and explain the issues and key elements related to adaptive intelligent robotic welding manufacturing. The joint design of the base materials, which are metals in this example, and the target weld to be produced per the optimal design are given by solid and dashed lines, respectively. The weld is made in a single pass using autogenous gas tungsten arc welding (GTAW) (Ref. 1) without a filler metal. (A second pass may be necessary to gain the needed convexity for the upper surface of the weld but is not of concern here for the illustration example, which is intended to be simple and straightforward.) During welding, the gas tungsten arc (GTA) is applied as the energy/heat source to melt the two members (left and right) of the base metals equally and symmetrically such that the solidified metal forms a weld as the dashed area that can be characterized by the two widths of the weld (w_u, w_b) for the major requirements on the fusion of the joint.

The design of the optimal welding procedure has specified 1) the nominal/desired position of the tungsten in relation to the joint and its travel speed along the weld axis, which is perpendicular to the cross section shown in Fig. 1, and 2) the current of the GTA. The welding procedure should have also specified the composition of the shielding gas, the diameter of the gas nozzle, the geometry of the tip of the tungsten, etc., but they are typically kept constant in the design values.

In this example, the most critical parameter in determining the weld is the heat input (Ref. 3), the energy imposed into the base metals per unit length along the weld axis whose cross section is characterized by the gap δ between the two

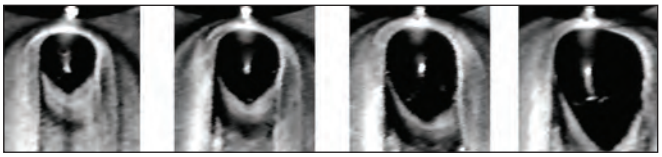

Fig. 3 — Images of the weld pool boundary using a synchronized pulsing illumination laser and camera. Images acquired during studies in Refs. 11–14.

base metals. It equals the power of the arc divided by the travel speed. The power is the product of the current supplied into the arc with the voltage of the arc. When the current and shielding gas are given, the arc voltage is determined by the position of the tungsten above the base metals or the arc length, which is loosely defined as the length of the arc established between the tungsten and the workpiece. In addition to the power, the heat source is also characterized by its distribution. For the same power at a given travel speed, the weld pool is broader and shallower if the distribution is broader. A shorter arc length tends to produce a less broad distribution of the arc energy/heat on the base metals.

Suppose the dashed area is quantified by the upper width and bottom width of the weld. This welding manufacturing process can thus be considered as a system whose outputs are the two widths, that is, $y(t) = (w_u(t), w_b(t))^T$, which is the output column vector where t is the time after the welding starts. Optimal design is to determine the welding parameters, current $i(t)$ and travel speed $v(t)$, and welding manufacturing conditions, such as the tungsten transverse position (should aim at the center of the gap), the gap δ, arc length l, etc., to produce the desired output $y^* = (w_u^*, w_b^*)^T$, which is a given vector constant. However, the nominal conditions in the design may not also be assured without excessive efforts as aforementioned. This implies that some of the welding manufacturing conditions such as the tungsten transverse position, arc length l, and gap δ may not be exactly the same as the nominal ones.

One of the major deviations of the welding manufacturing conditions from the nominal ones is the deviation of the tungsten transverse position in relation to the joint/gap. This deviation is referred to as weld seam error. It is critical because an error in the weld seam will result in a wrong position of heat source application. The resultant weld will not be symmetrical as needed. In the worst case, only one of the base metals is melted while another is not. The two members of the base metals are not joined together. This kind of critical deviation must be corrected. That is, seam tracking ability must be provided as a key adaptation during welding manufacturing. On the other hand, an inaccuracy in the arc length, how high the tungsten tip is above the base metals, affects the distribution of the heat source. The output produced will be affected but the weld may still be symmetrical, and the two members of the base metals can still be joined. The correction for the arc length is thus less critical and may be optional.

Because some of the deviations are not practically correctible, the welding parameters and conditions often cannot be the same as the nominal ones. Therefore, the resultant outputs would be different from the desired ones. To produce the desired outputs, some of the easily adjustable welding parameters, such as the welding current or the travel speed, may be adjusted to compensate for the effect of the uncorrected deviations on the outputs. These real-time adjusted welding parameters form the control variables of the system.

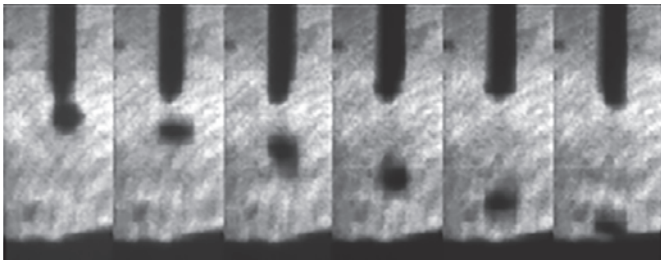

Fig. 4 — Monitoring of metal transfer in GMAW with a backlighting method. Images acquired during the studies for the droplet-oscillation-based active control of the metal transfer process (Refs. 21, 22).

However, how to decide the adjustments of the control variables is not straightforward. The complexity is caused by the dynamics of the system; an adjustment in the control variables would gradually reach its full effect on the outputs. The adjustments on the control variables must be made dynamically, and effective dynamic adjustments not only rely on the availability of the outputs (accurate real-time measurements of the outputs) but also on the understanding of the dynamics of the system (how the outputs dynamically respond to the control variables) and scientific decision-making (using the feedback of the outputs and dynamics to decide on the control variables such that the outputs reach the desired values in preferred ways). There are three elements in feedback control: 1) sensing of the feedback, 2) modeling of the system/process dynamics, and 3) control algorithm for decision-making.

Therefore, advanced welding involves at least optimal design of the welding procedure; deviation sensing of the welding manufacturing conditions from the nominal ones to make possible corrections to ensure the best possible execution of the optimal design; feedback control to correct the deviations of the actual produced outputs from the desired ones; process monitoring to find possible defects that are not specified as outputs and also affect the ability to meet the requirements, such as porosities, undercuts, etc.; and post processing and inspection of the resultant welds and welded structures. Optimal design and post processing and inspection are important but are not part of the real-time manufacturing activities. Therefore, they are excluded from the discussion of this paper, which focuses on adaptation of the manufacturing process to the environment (welding/manufacturing conditions) in intelligent ways.

The major deviation of welding conditions that is sensed and corrected is the weld seam error. Its correction is referred to as the seam tracking (Ref. 3). The upper width of the weld is typically obtained from a view of the liquid weld pool. This and the weld seam may be directly observed from the welding process and we may refer to such a sensing as direct sensing of the welding process. The bottom width of the weld reflects if the base metal has been fully melted in its entire thickness as desired and the degree of this complete joint penetration. If the bottom width is very small and the weld is not perfectly symmetrical as desired, one of

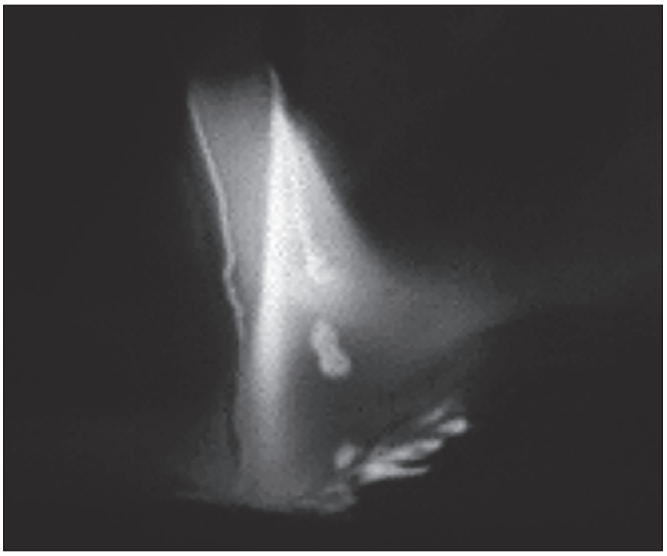

Fig. 5 — Monitoring of metal transfer in GMAW using a high-speed camera. Image acquired during studies for the double-electrode GMAW (Refs. 24, 25).

the base metals may have not been fully melted in its entire thickness. In this case, the metal mixing would not occur in the entire thickness of the base metals such that the two members of the base metals are not fully joined together. Therefore, the bottom width is an indicator of the complete joint penetration along the thickness of the base metals. In addition to the complete joint penetration, in certain applications we require the liquid metal does not reach to the opposite side of the base metals. The requirement is typically specified by how deeply the liquid metal reaches underneath the base metal. This type of application is referred to as incomplete joint penetration, and the degree of the incomplete joint penetration is specified by the depth of the penetration (i.e., how deeply the liquid pool has reached underneath the base metal surfaces). The problem for both cases is referred to as the joint penetration. Both of them occur underneath the base metals and are not directly observable. If the output is not directly measurable, we would have to find phenomena that are measurable/observable. This is indirect sensing, and its challenge lies in finding observables that have fundamental correlations with the unobservables (state of the joint penetration) and can be used to fully and accurately determine the unobservables of concern. Defects may be directly or not directly observable.

To summarize, we wish to first point out that we have identified weld seam tracking, joint penetration, and weld defects as major concerns and identified direct and indirect sensing as major types of problems. For direct sensing, the challenges arise primarily from the harsh environment of the welding process — arc radiation, high temperature, smoke, and spatters. For indirect sensing, the challenges lie in 1) if the correlation between the unobservable and observables is fundamental, that is, if the mapping is unique, under what conditions it is unique, etc.; and 2) how to find the mathematical model for the unique mapping such that the measurables are used to effectively determine the unobservables of our concern. All of these form the broad area of research called "real-time sensing of welding process," and the research focuses more on the indirect sensing, that is the extraction of the needed information (unobservable or not directly measured) from the measurables.

Then we wish to point out that the major concerns need to be adaptively controlled to compensate for the effect from the deviations of the manufacturing conditions. To be effective, we also need to model the dynamics of the system. For the welding process, these dynamics are often relatively complex. The welding process is intricate, involving many complex phenomena within the weld pool. The output produced is just part of the welding process with which we are concerned. The dynamics may thus be nonlinear. In addition, there are many parameters that affect the welding process and the output. The control variables are just those that can be easily and effectively adjusted to change the outputs. The uncorrected deviations in the manufacturing conditions also change the dynamic relationship between the control variables and the outputs. The dynamics thus may be uncertain depending on unmeasured manufacturing conditions. Modeling these dynamics mathematically thus may be relatively complex. For such a relatively complex dynamic process, the design of the feedback control algorithm may also not be easy. In addition to the sensing, this paper will survey efforts in modeling and control algorithm design for complex dynamic welding systems.

Finally, we wish to point out that all these research areas are related to intelligent adaptation using machines as shown in Fig. 2. Many adaptations being studied for use by machines may also be provided by human welders who seamlessly integrate abilities of sensing, information extraction, modeling, and decision-making. However, humans are not precise in execution. Human-robot collaboration can be used to combine the adaptation abilities of humans with the precise execution and physical strength of machines/robots to provide another way of intelligent adaptive welding manufacturing. It is another area of study surveyed in this paper.

Visual Sensing of the Welding Process

Despite the specific purposes that may vary from application to application, a general interest persistently exists to see what is happening during welding. We first wish to see what humans can see, and the visual of the welding process is thus often the first to consider. Human welders are capable of observing the welding process to extract the needed information to make appropriate adjustments so that they can adapt to the changes in the welding manufacturing conditions. Human welders can see where the weld seam is despite the arc radiation. Human welders can see the weld pool (boundary) and its variation. Human welders can also see the 3D weld pool surface. However, all these and other information human welders can see are not easily obtained using machines/sensors. Special requirements are needed for sensors to be capable of sensing what is occurring during welding, especially arc and laser welding.

Arc radiation is the first apparent obscurity for sensors to observe the scenes/objects during the arc welding process. The arc is too bright in comparison with other objects of interest, such as the weld pool boundary and the joint groove/weld seam. A smart method was proposed by Richardson and Gutow to install a camera to observe the weld pool area

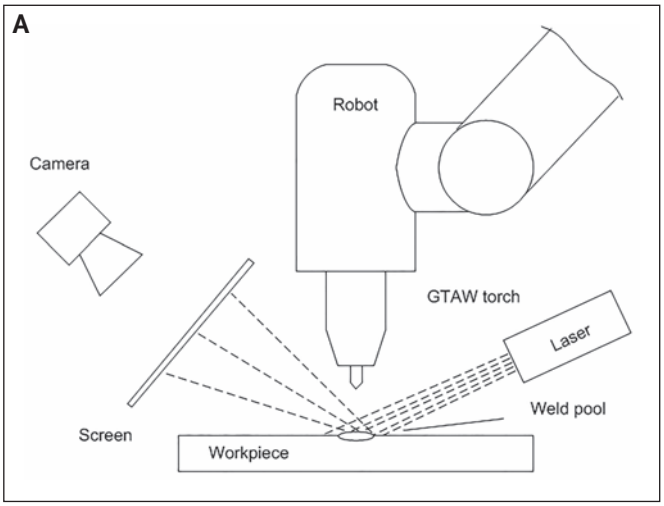

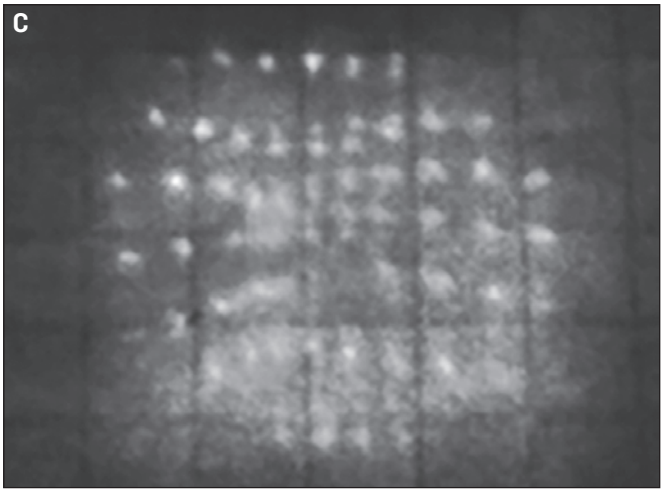

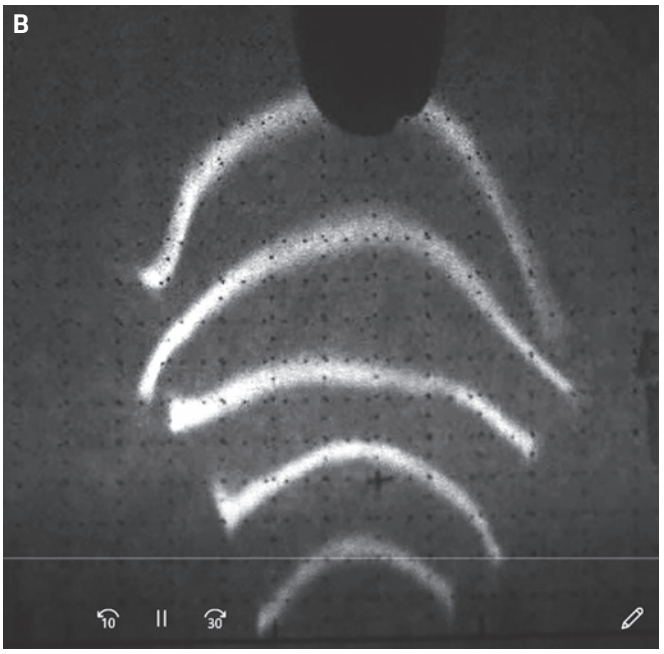

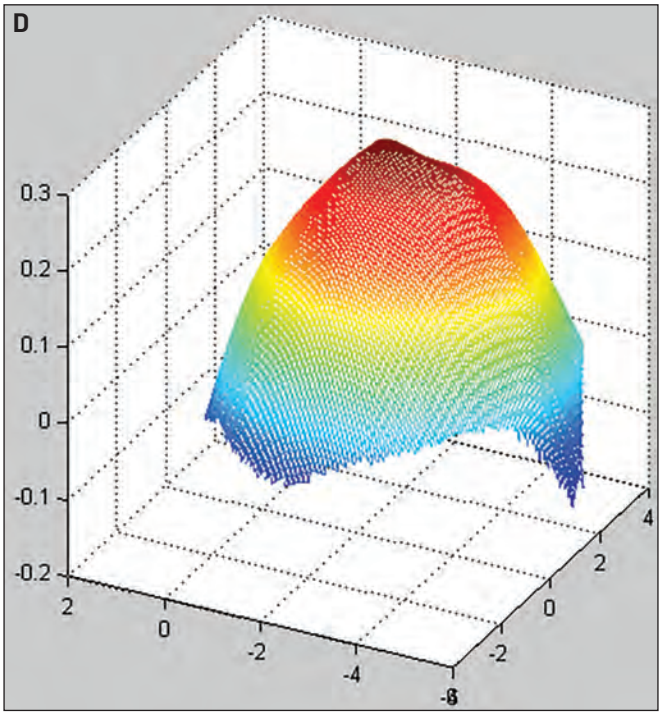

Fig. 6 — Measurement of the 3D weld pool surface from its specular reflections to projected laser patterns. Pool surface illustration, images, and results acquired during studies in Refs. 27–29. A — Principle; B — example image using laser stripes as the projected laser pattern; C — example image using a dot matrix as the projected laser pattern acquired during pool oscillation; D — example of calculated weld pool surface.

coaxially from above the tungsten (Ref. 5). This method is referred to as coaxial view of the weld pool, and the tungsten blocks the majority of the arc radiation from reaching the coaxial camera. Clear weld pool images were obtained. To observe from other directions, a direct solution is to use another light source that is even brighter than the arc radiation to illuminate the objects of our interest. This appears to be impossible, but using a laser, which is theoretically single color/wavelength, as the illumination source can make this possible. The energy of the arc radiation spreads in an extremely wide range (Refs. 6, 7), but the band pass optical filters with the full width-half max of less than 10 nm are standard commercial off-the-shelf products available for various wavelengths of lasers. And so the energy passing to the imaging sensor of a camera from the object as the reflection of the illumination laser can be much greater than that of the arc radiation. This results in the structured-light method by projecting the laser as a stripe across the joint approximately transversely ahead of the weld pool (Ref. 8), which is probably the most effective way to sense the joint groove/gap for seam tracking. To effectively reduce the effect from the arc radiation, the laser stripe is typically projected to the groove with a distance of a few millimeters from the front edge of the weld pool (Ref. 8). To further increase the illumination, the laser is focused, projected as a dot, and scanned across the groove/joint (Ref. 9).

The kind of machine vision methods that use an illumination light source are referred to as active vision (Ref. 10). While the above technologies take advantage of the wide-spreading characteristic of the arc energy spectral distribution, another method has been based on a different principle — using an illumination light that has much greater

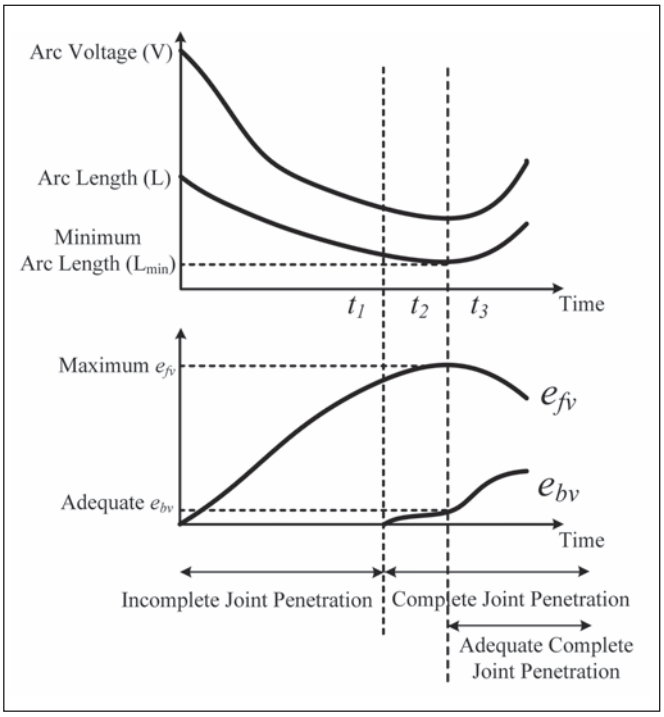

Fig. 7 — Arc voltage change during the establishment of the joint penetration. Illustration derived from the studies in Refs. 25 and 26.

power than that of the arc radiation, but just during its pulse (Ref. 11). This method uses a pulsed laser with a duration of nanoseconds. As a result, although the average power of the laser is 7 mW, the peak power during the pulse is 70 kW (Ref. 11), which is much greater than that of the arc radiation. To sense the reflections from this laser to the onjects, the shutter of the camera is synchronized with the pulse of the laser (Ref. 11). As a result, the arc radiation is completely removed from the image (Ref. 11). The image as shown in Fig. 3 can be obtained (Ref. 11). Using this technology, the weld pool boundary can be clearly observed, where the dark area is the weld pool, which specularly reflects the illumination laser so that the reflection is not collected in the imaging sensor of the camera; the bright area is due to the diffuse reflections of the laser from the solid metal, which is insensitive to the view angle. Using the technology, the boundary has been clearly monitored, processed, and modeled for process control (Refs. 11–15).

Another important scene in addition to the weld pool boundary is the evolution of the liquid droplet (Ref. 3) pending at and detached from the tip of the welding wire during gas metal arc welding (GMAW) (Ref. 3) and its variants (Ref. 1), including the double-electrode GMAW (Refs. 16, 17). This is referred to as the metal transfer process (Refs. 18, 19), which is critical in understanding the GMAW process. This is because the transfer mode — short-circuiting, globular, or spray transfer — plays a critical role in processing the base metals to produce the welds (Ref. 3). The challenge for monitoring the metal transfer process first lies in the radiation of the arc that roots at the droplet. One method to monitor it is to use a laser to project toward the imaging plane with the droplet/wire in between the laser and imaging plane (Ref. 20). As a result, the droplet blocks the laser, which travels straight. The arc radiation decays cubically such that its incident on the imaging plane is ignorable, but the laser intercepted by the imaging plane keeps its original intensity. A shadow of the droplet and wire is formed on the imaging plane due to the blockage of the laser by the droplet/wire. As a result, clear images of the droplet and wire, as given in Fig. 4, can be clearly acquired to understand the metal transfer process (Refs. 21, 22). This is an active vision method.

The metal transfer can also be monitored using a passive vision method where no illumination/auxiliary light source is used (Ref. 23). In a passive vision method, the camera directly aims at the scenes of interest where both the arc radiation and droplet are present. Using a high-speed camera, the integration time for forming an image frame can be reduced. The brightness associated with the arc radiation can be reduced. The arc radiation can become a suitable illumination source such that the droplet can be seen from the images. Using a neural filter, the arc radiation can be further reduced such that the frame rate needed can be moderate, rather than extremely high, to acquire clear metal transfer images, as examplified in Refs. 24 and 25.

In addition to the weld pool boundary and metal transfer, the 3D weld pool surface is another important scene of interest from which we may gain comprehensive understanding of the welding process. The challenge lies, in addition to

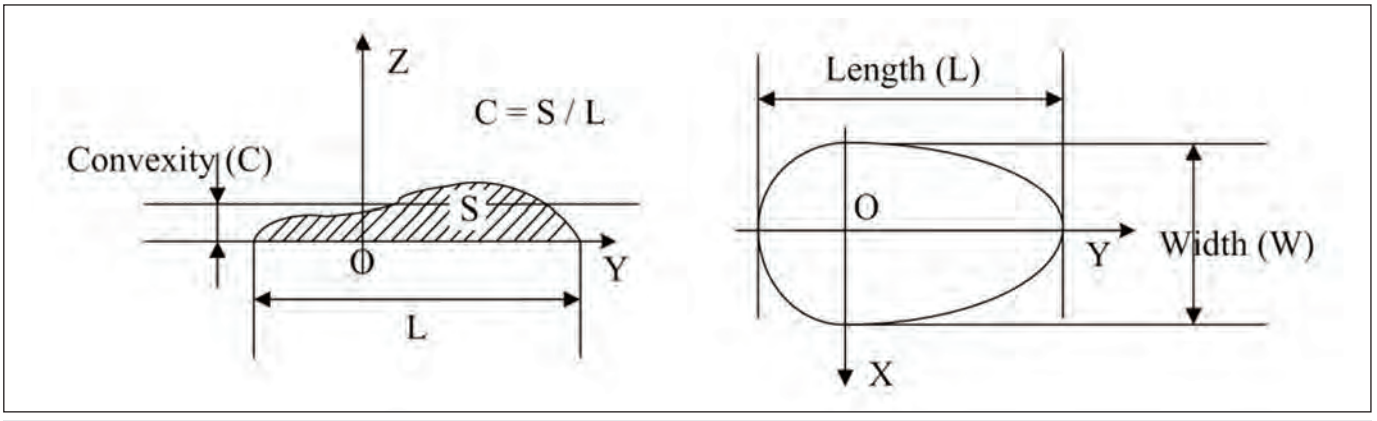

Fig. 8 — Characterization of the 3D weld pool surface in GTAW (Ref. 76).

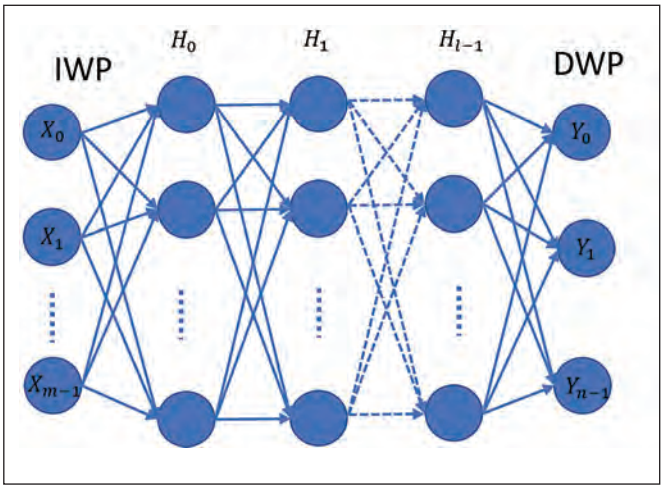

Fig. 9 — Schematic diagram for welding performance using fully connected ANNs with m *indirect welding parameters,* n *direct welding parameters, and* l *hidden layers.*

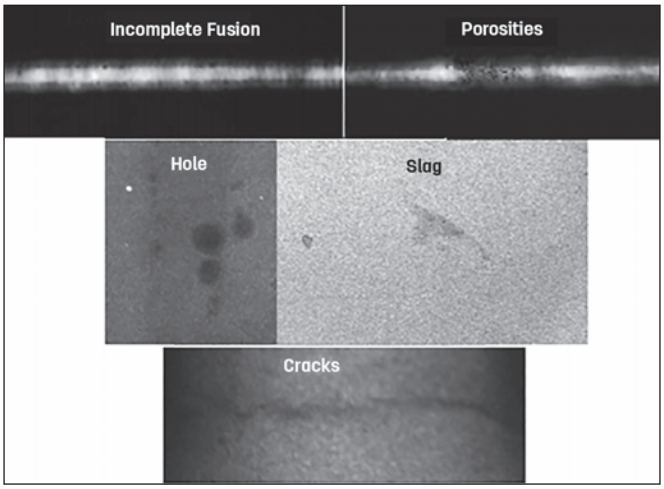

Fig. 10 — The radiographic images of common welding defects from public sources.

the arc radiation, in the specular nature (Ref. 26) of the surface of liquid metals, such as the weld pool, which disqualifies the structured-light machine vision method that has been used to measure the geometry of an ordinary object whose surface diffusely reflects unidirectionally for collection by a lens from any direction. For specular surfaces, a directional-incident-light-like laser can only be reflected to a given direction following the reflection law. If the lens/camera is not placed in the reflection path, the reflection is not captured/imaged.

To sense the geometry of the 3D surface, a laser pattern with an array of rays is projected onto the weld pool surface (Refs. 27, 28). Each incident ray is reflected to a particular direction depending on the direction of the incident ray and the slope of the local surface where the incident ray is reflected/hit. Reflections of the projected rays travel in different directions. When the slope of the surface does not change in an extremely large range, such as from the surface of a GTA weld pool, the directions of the reflections are still within a certain range such that a plane can be placed in their way to intercept the reflections. The intercepted reflections will illuminate the interception plane, and a camera can aim at the interception plane to acquire the image of the reflections. By placing the interception plane at a small distance (Ref. 27), for example 50 mm, the arc radiation significantly delays such that its images on the plane are much less bright than the unidirectional reflection of each incident unidirectional laser ray. Therefore, clear images of the reflection rays can be obtained as shown in Fig. 6. Using the reflection law and constraints due to the smoothness of the weld pool surface, the 3D weld pool surface has been real-time computed (Ref. 28).

The above method to measure the 3D weld pool surface is theoretically accurate, and the raw image can be very clear. It is also recognizable even if using a dot matrix (such that the intensity of the laser illumination reduces) and under an unfavorable imaging condition of pool oscillation as shown in Fig. 6C. However, it uses a laser pattern and an interception plane (Fig. 6A), reducing its compactness. A passive vision method has also been proposed to measure the 3D weld pool surface (Refs. 30–34). This method views the infrared radiation, which is determined by the temperature, from the scenes/objects on the weld pool from two directions using the stereo vision principle. This stereo vision method matches the two images, in two cameras, produced by infrared radiation from the same point. If the points matched in two images are sufficient and distribute over the weld pool, the weld pool surface can be fit/computed reasonably. However, the weld pool surface itself lacks features, and the matching is typically first found for feature points/scenes such as oxides/slags and then extends from these well-matched feature points to their featureless neighborhood (Ref. 34). The degree of matching reduces when moving away from the well-matched feature points (Ref. 34). In addition, the arc radiation is much stronger than the useful infrared radiation such that points matched in two images are reduced. Therefore, the effectiveness in measuring the 3D weld pool surface should be much less than the previously aforementioned method based on the specular nature of the surface, although the system becomes more compact. In Ref. 34, a biprism was used to reduce the number of cameras to one.

In addition to visuals, the welding process also has many other features that may be used to understand what is occurring during welding manufacturing. Among them are temperature distribution (Refs. 35–37), sound (Refs. 38, 39), arc light radiation (Refs. 40, 41), arc current waveform, arc length/voltage, etc. In particular, in GMAW, the needed current for the arc anode to complete the melting of the wire is reduced/increased as the wire extension (thus the resistance heat imposed on the wire) increases/reduces. Therefore, the wire can scan across the groove such that the wire extension is changed and the resultant current waveform can be monitored to determine the groove for seam tracking (Refs. 42, 43).

Monitoring of Joint Penetration

Monitoring of joint penetration is done to determine if the weld pool has complete joint penetration in the workpiece (base materials/metals) to distinguish incomplete from complete joint penetration, and to find the depth of

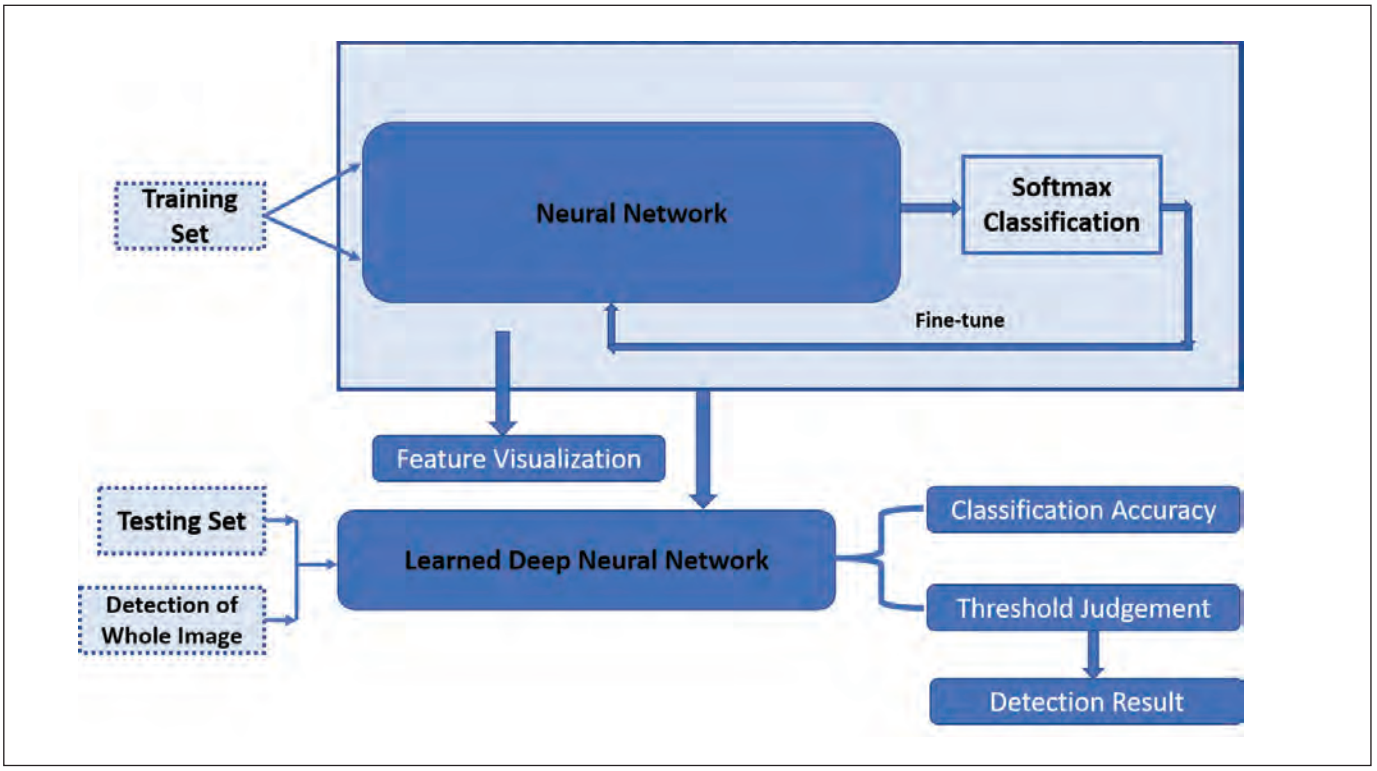

Fig. 11 — Principles of welding defect detection based on CNNs (Ref. 126).

the joint penetration in case of incomplete joint penetration or the bottom width of the weld pool in case of complete joint penetration. In critical applications, such as pipes and pressure vessels where high-pressure, high-temperature gases are transmitted or contained, the unmelted/unjoined interfaces of the two members of the workpiece would cause expulsion. The complete joint penetration must be ensured to meet the service requirements. Because the structures are enclosed after welding, the inspection of the joint penetration from inside becomes difficult. The complete joint penetration thus should be ensured during welding manufacturing. In addition, even if the entire thickness has been penetrated, the bottom width of the weld must be sufficient, in comparison with possible weld pool deviation from the weld seam, which may be caused by seam tracking error and arc blow (Ref. 1), to ensure the interfaces of the base metals are fully melted/joined. Because complete joint penetration is so critical, most of the efforts in this area have been focused on complete joint penetration. The challenge lies in 1) the joint penetration occuring underneath the workpiece and not being directly observable and 2) observables to be measured to determine the joint penetration must uniquely correlate with the joint penetration. To address these challenges, various sensing methods have been proposed.

Pool Oscillation

Deriving the state of the joint penetration from the oscillation of the weld pool is apparently an indirect sensing method where the observable (from pool oscillation) needs to have a unique correlation with the unobservable (state of the joint penetration) of concern.

Kotecki et al. was among the first to explore the scientific foundation for the correlation being sought (Ref. 44). When a stretched membrane, where the surface tension γ_0 consists of the stretching force, is brought to oscillation by an external force, which is then removed,

$$\gamma_0 = 3.41(a^2\rho / t_0^2)$$

where a is the radius and ρ is the mass per unit area of the membrane and t_0 is the period of the first harmonic of the oscillation. The oscillation consists of the several harmonics, but the amplitude rapidly reduces as the harmonic order increases. The first harmonic is thus the major component of the oscillation, referred to as the natural oscillation, and its frequency ($f_0 = 1/t_0$) is referred to as the natural frequency of the oscillation. When γ_0 is considered a constant, the mass of the membrane $m = \pi a^2\rho$ is apparently inversely proportional to the square of the natural frequency f_0.

The first subsequent follow-up efforts (Refs. 45, 46) in the pool oscillation method 1) assumed this relationship of inverse proportion between the oscillation frequency and the mass/radius/size may also be reasonable for a weld pool, although the weld pool is not a membrane, and 2) focused on experimental verifications of such an inverse proportion or tendency in various conditions. A famous effort was published in the *Welding Journal* by Richardson and brought the oscillation method wide attention from the welding research community (Ref. 45). In this study, a current pulse was applied to a stationary weld pool and removed to bring the weld pool to an oscillation. Since the arc pressure as an external force imposed on the weld pool is proportional to the square of the current, the removal of the current peak

changed the external force such that the pool oscillated. The waveform of the arc voltage was then measured as the change of the weld pool surface. The frequency from the analysis was correlated to the diameter of the weld pool in incomplete joint penetration. Another famous study was conducted by Hardt, who proposed a method to determine the back-side bead width by measuring the natural frequency of pool motion when driven by a time-varying arc plasma force (Ref. 46). One should note that, despite many assumptions that appear to be not accurate and scientific, including expending the membrane as a two-dimensional object without a thickness to a three-dimensional weld pool, the tendency between the mass and frequency still holds. However, the accuracy needed for a useful relationship for monitoring and control appears not assured.

The next milestone result that significantly changed the prospective of the pool oscillation method is the finding from Xiao and den Ouden that provides an effective way to distinguish among incomplete joint penetration and complete joint penetration (Ref. 47). They found the oscillation frequency of the pool abruptly reduces after the transition from incomplete to complete joint penetration, from approximately 200 to 50 Hz. This is due to the change in the condition of the bottom surface of the weld pool that was supported by the solid metal in incomplete joint penetration but changed to the surface tension in complete joint penetration. In incomplete joint penetration, the oscillation has never been natural because an external force other than the surface tension has never been removed. For a complete joint penetrated pool, only the "stretching" surface tension is present. The oscillation amplitude is greater, but the frequency is lower. Because of the large difference in the oscillation frequency, the threshold can be easily determined. Along this direction, Andersen and den Ouden developed a synchronous weld pool oscillation method for controlling the weld pool dimensions and state of penetration based on the fact that the weld pool resonates at natural frequencies that are related to its dimensions and state of penetration (Ref. 48).

The way to detect the pool oscillation including the use of signals has also progressed. In early studies, the arc voltage as a measurement of the arc length was analyzed to determine the oscillation (Refs. 45, 47). It was then found that the arc radiation is more sensitive to the arc length and can be used to better analyze the oscillation (Ref. 49). This is because the arc voltage is the sum of the anode, cathode, and column voltage. While the anode and cathode voltages are constant (Ref. 50) and only the arc column voltage reflects the oscillation, the column voltage only changes with the arc length in a very small range. On the other hand, the arc radiation is primarily due to the arc column whose length is what we need to sense and analyze.

While the previous methods tried to directly measure the oscillation, novel ideas have been proposed to measure the oscillation indirectly but extended from a one-dimensional signal (arc length, arc voltage, arc column) to two dimensional. The information becomes more comprehensive. Shi et al. proposed a novel method to monitor the oscillation by projecting a laser pattern onto the weld pool (Ref. 51). This is the method originally proposed to measure the 3D weld pool surface as illustrated earlier in Fig. 6. Instead of using the reflection law to compute the 3D surface, the movement of the reflection is used to analyze the oscillation of the mirror (sepcular weld pool surface, thus the weld pool) where the projected laser pattern is reflected. This gives amplified signals to analyze the oscillation more easily and accurately. Results showed that weld pool oscillation has the features of incomplete and complete joint penetration and generates two oscillation frequencies.

All previous methods, despite the use of different signals, must wait for a full period of oscillation to analyze the frequency to determine the joint penetration. The monitoring and control are delayed. In Ref. 29, Chen et al. proposed a method that does not actually measure the frequency of the weld pool oscillation. Through studying how the image of the laser dots reflected from the specular weld pool surface in pulsed GTAW change with the dynamic behaviors of a developing weld pool, it was found that the image of the reflected laser dots became less clear and dimmer as the joint penetration increased. Therefore, the brightness of the reflected laser dots can be used to detect the joint penetration instantaneously without waiting for the full period of oscillation.

Ultrasound

Ultrasound reflects at the interface/discontinuity of materials/material property. By appropriately delivering and collecting ultrasound, this principle may be used to detect the boundaries of the liquid and metal in the weld pool. In Ref. 52, an initial step toward realization of real-time weld pool cross section measurement using reflection ultrasound methods was evaluated. In Refs. 53 and 54, a similar concept was proposed where the joint penetration geometry was detected using a piezoelectric transducer, operating in the pulse-echo mode, to generate shear sound waves that traveled through the base metal to the weld region. The received echoes contained information that could be related to the side-wall joint penetration and thus to the quality of the weld. To overcome the contact requirement of the ultrasonic sensing method, various noncontact ultrasonic sensing methods have been developed, including laser ultrasonic sensing (Refs. 55–57), electromagnetic acoustic transducer (EMAT) ultrasonic sensing (Ref. 58), and laser-EMAT ultrasonic sensing (Ref 59). However, these sensing systems are very expensive and highly complicated, which are not preferable for welding applications.

Infrared

Infrared sensing is a type of noncontact thermal measurement technique, which has been widely used in various applications and provided important observations to understand abundant welding phenomena (Refs. 60, 61). Its use in the monitoring of joint penetration is based on its ability to accurately detect the weld pool boundary due to the work by Chin et al. This is possible because it does not directly measure the temperature, but it measures the intensity of the infrared radiation, which is determined by the temperature and emissivity. When leaving from the center of the weld pool toward the solid metal, the temperature reduces. If the emissivity is constant, the radiation sensed by the infrared camera would gradually reduce. However, at the boundary of the weld pool where

the solid and liquid metal has the same temperature nominally, the solid metal radiates more strongly because of the greater emissivity. Chin et al. proved that the radiation sensed by the infrared camera indeed has a small increase before it reduces again (Ref. 60). This causes a zero slope in the infrared profile such that the weld pool boundary can be detected without calibration and threshold. In addition to the weld pool boundary, infrared sensors have also been used to monitor weld process parameters including weld bead width, joint penetration depth, and torch position (Ref. 62). More recently, Alfaro and Franco discussed the use of infrared sensors as an indicator for defect detection during the GTAW process using a Kalman filter (Ref. 63). It was shown that infrared signal variations in direct current are related to joint penetration depth, while alternating current portions of the output can be correlated with surface irregularities. However, the correlations between the parameters of concern and the infrared measurements were mostly obtained empirically without a strong support of scientific foundation as the zero slope phenomenon based on which the boundary was detected.

Arc Sensing

Arc sensing has been used in arc stability control, seam tracking, and joint penetration control (Refs. 64–66). By using the arc itself as a sensor, there is no need for external sensors with their associated costs and concern for reliability in the harsh welding arc environment. A general impression is that the arc signal only contains limited, indirect, and mostly inaccurate information. However, a recent study made arc sensing a promising method to monitor and control the process to ensure complete joint penetration (Refs. 67, 68). This method measures the change of the arc voltage and switches the current from peak to the base when the arc voltage tends to increase. This is because when a peak current is applied to establish the joint penetration, the metal melted gradually increases. Due to the thermal expansion, the metal volume increases. Before the bottom of the workpiece is melted, the increased volume of metal can only increase the convexity of the weld pool such that the distance between the weld pool surface to the tungsten decreases. The arc voltage thus gradually decreases because the arc length decreases — Fig. 7. However, after the complete joint penetration is established such that the melted metal may move behind the bottom surface of the workpiece, the arc length will start to reduce more slowly and then increases after more metal moves behind the bottom surface as the volume increases due to thermal expansion. Therefore, an appropriate analysis of the arc voltage that measures the arc length can lead to a reliable detection of the establishment of complete joint penetration, as well as the degree of the complete joint penetration. Since there is no calibration and threshold, the physics foundation is solid, and there is no actual sensor attached, it may be a superior solution that also works in manual welding.

Vision

The weld pool surface provides important information for understanding welding processes and is the most direct source of information for human welders to obtain feedback. Observing the weld pool surface and measuring its parameters is thus vital to developing intelligent welding machines that can mimic a skilled human welder, who estimates the welding process by visually observing the weld pool and adjusting welding parameters accordingly.

Pioneering work on weld pool observation was conducted by Rokhlin and Guu using radiography (Refs. 69, 70). It was found that the radiation of the received x-ray increases with the depression depth. However, the principle behind this method is to measure the material thickness. For complete joint penetration where the backside pool surface deformation occurs, the pool surface shape will be difficult to extract. Mnich et al. developed a stereovision system for in-situ weld pool measurement, where two high-speed cameras were synchronized with a robotic welder to capture images during the time when the arc was off (Ref. 30). By using stereo image processing algorithms, the weld pool shape was rendered in 3D. Zhao et al. used the shape from the shading algorithm to reconstruct the surface from one single weld pool image (Ref. 71). Kovacevic and Zhang proposed a mechanism for observing the GTA weld pool surface shape using a short duration pulsed laser synchronized with a high-speed camera and a frosted glass (Refs. 12, 72). The proposed method can obtain specular reflections from the weld pool under the presence of the bright arc. However, the synchronization of the laser and high-speed shutter requires specific, costly, and sophisticated equipment.

While the laser-camera synchronization can be considered a “hard” way, a “soft” way may be to take advantage of the difference between the arc light and illumination laser. It is known that arc light intensity decreases rapidly with the distance, but the laser does not significantly lose its intensity as distance increases. Saeed and Song studied the structured light method in sensing the GTA weld pool surface (Refs. 73, 74). This approach makes use of a relatively simple idea to facilitate a practical solution to overcome the aforementioned two challenges (bright arc and specular surface): by exploiting the propagation difference between the laser and plasma, the laser rays mirrored from the weld pool surface can be clearly imaged in the presence of bright plasma, thus changing the specular surface from a difficulty to an advantage. More specifically, the reflected laser keeps straight travel without significant loss of intensity over distance, while the radiation of the arc energy decays rapidly over distance. However, the quality of the reflected images is highly sensitive with the shape of the weld pool. Zhang et al. modified the image processing algorithm accordingly, and the 3D weld pool surface can thus be reconstructed in real time (Ref. 75). The weld pool width, length, and convexity (Fig. 8) were further proven to be an acceptable set to effectively characterize the 3D weld pool surface geometry representing the joint penetration (Ref. 76).

Modeling and Control

As analyzed earlier, the welding process is dynamic and may also involve any complexity such as nonlinearity. Therefore, the determination on how to adjust the control variables to correct the deviation of the outputs from their desired values is relatively complex and requires an appropriate control algorithm. Availability of the feedback of the output/state is a necessary condition for the adjustments to be effective but is

not the sufficient condition. The control algorithm must also incorporate the dynamics of the process either during its design or during its on-line implementation. The model predictive control (Ref. 77) explicitly uses a dynamic model of the process being controlled to predict the future process output/state as a function of the adjustments of the control variables and minimize the difference between the prediction and the desired output/state to optimize the control variables. Other control methods, such as the pole placement, use the dynamic model in the design phase. The following is devoted to providing an overview of the control methods developed for welding processes. Depending on the sensing method used, the control systems can be categorized into pool oscillation-based control, radiography-based control, thermal-based control, and vision-based control. The modeling is part of the efforts in the establishment of these control systems and is not separately reviewed.

Hartman et al. developed a control system that regulated the total heat input to maintain constant fusion zone geometry by monitoring the arc light reflection from the oscillation of the molten metal surface (Ref. 78). Ju et al. proposed a new vibration method: the pulse shielding gas oscillating method (Ref. 79). A control system was constructed by controlling the welding current based on the natural vibration frequency measurements from an arc sensor. Yudodibroto et al. implemented the joint penetration control based on the weld pool oscillation sensing method during the GTAW process with cold filler wire addition (Ref. 80). Guu and Rokhlin utilized real-time radiography for controlling the joint penetration in solidified areas and depressions of the weld pool (Ref. 81). In Ref. 82, Yahia et al. implemented automatic control and inspection of welding defects with an edge detection method of radiographic images based on multilayer perceptron. Song and Hardt developed a closed-loop system to control the weld pool depth using a thermally based depth estimator from point temperatures measured on the backside of the workpiece (Ref. 83). In Ref. 84, a self-organizing fuzzy control method was proposed to obtain a uniform weld pool size in GMAW by regulating the surface temperature at a desired level. Banerjee et al. furthered their earlier finding that the slope of the infrared intensity became zero when the liquid-solid interface of the weld pool was crossed, which might be utilized to control the welding process (Ref. 85).

Compared to the above-mentioned control methods, a vision-based control method is considered more direct and prominent as an emulation of the estimation and decision-making process of the human welder. Extensive research has been conducted to explore the possibility to control the weld pool to some extent. Vorman and Brandt used a line scanner to detect the weld pool region and control the weld pool width (Ref. 86). Ohshima et al. proposed a pool width control in pulsed GMAW by observing the weld pool using a charged-couple device camera in low current intervals of the pulsed current (Ref. 87). Pietrzak and Packer developed a weld pool width control system that uses a miniature camera mounted in a modified coaxial viewing torch to view the weld pool (Ref. 88). Song and Hardt controlled the depth and width of the weld pool using top-side and back-side sensors (Ref. 89). Zhang and Kovacevic proposed adaptive predictive and neuro-fuzzy model-based control algorithms to control the front-side weld pool width and back-side bead width (Refs. 90, 91). Chen et al. proposed a self-learning fuzzy neural network controller to simultaneously control the weld pool length and width (Ref. 92). Zhao et al. developed a control system to control the back-side bead width and front-side reinforcement (Ref. 93). Tsai et al. proposed an automatic pulsed GTAW pipe welding system with fuzzy control technique to control the width of the pool (Ref. 94). Kong and Chen (Ref. 95) and Chen et al. (Ref. 96) controlled the penetration of Al alloy welding through passive vision of the weld seam and weld pool. Liu et al. controlled the weld penetration and 3D weld pool surface by utilizing the 3D weld pool sensing system and characterization of the weld pool surface (Refs. 97–99). In a separate effort, the welding process was controlled by either directly mimicking the human welder behavior (Refs. 100–103), or by fusing the human knowledge and machine intelligence (Refs. 104–107). Specifically, in Ref. 105, controlling human arm movement was realized for a virtualized welding system with a human in the control loop.

Most of the above efforts are considered empirical methods where the model is drawn from the data obtained from welding experiments. Researchers have also established numerical models to analyze the correlation between the weld pool and arc/heat source, as described in Refs. 108 and 109 for example. These models, in theory, could provide detailed information about the thermal dynamics of the arc and its interactions with the weld pool, which may help us understand the underlined complex correlation between the welding process inputs and the weld pool. However, these numerical models typically require extensive calculations to simulate the complex dynamics, which are not suitable for real-time weld pool monitoring and control applications.

From a modeling/control methodology perspective, the above efforts can also be categorized as linear modeling (Refs. 99, 104), nonlinear thermal modeling (Refs. 83, 108, 109), fuzzy modeling (Refs. 78, 84, 94), shallow neuro-network modeling (Refs. 82, 96), and neuro-fuzzy modeling (Refs. 91, 98, 100–102), etc. Although they could model and control the welding process with certain success, complex dynamics and highly nonlinear phenomena require more sophisticated models to accurately model such behaviors. In the following section, artifical intelligence and machine learning is introduced along with its application in welding process modeling and control.

Machine/Deep Learning — Standardizing the Learning of Complex Relationships Directly from Data

Referring back to Fig. 2 illustrating the adaptive intelligent robotic welding and its key elements, indirect sensing/information extraction and a dynamic control algorithm appear to be relatively less straightforward. They both involve decision-making from relatively complex information sources. For the dynamic control algorithm, its inputs and outputs are both well specified and the complexity is primarily from the dynamics; for the information extraction, the outputs of our concern, such as the state of the joint penetration or weld defects, are well specified, but the inputs are not. It is the job of researchers to 1) hypothesize that the data from selected sensors contains sufficient information to derive the outputs of concern, 2) study the subject/

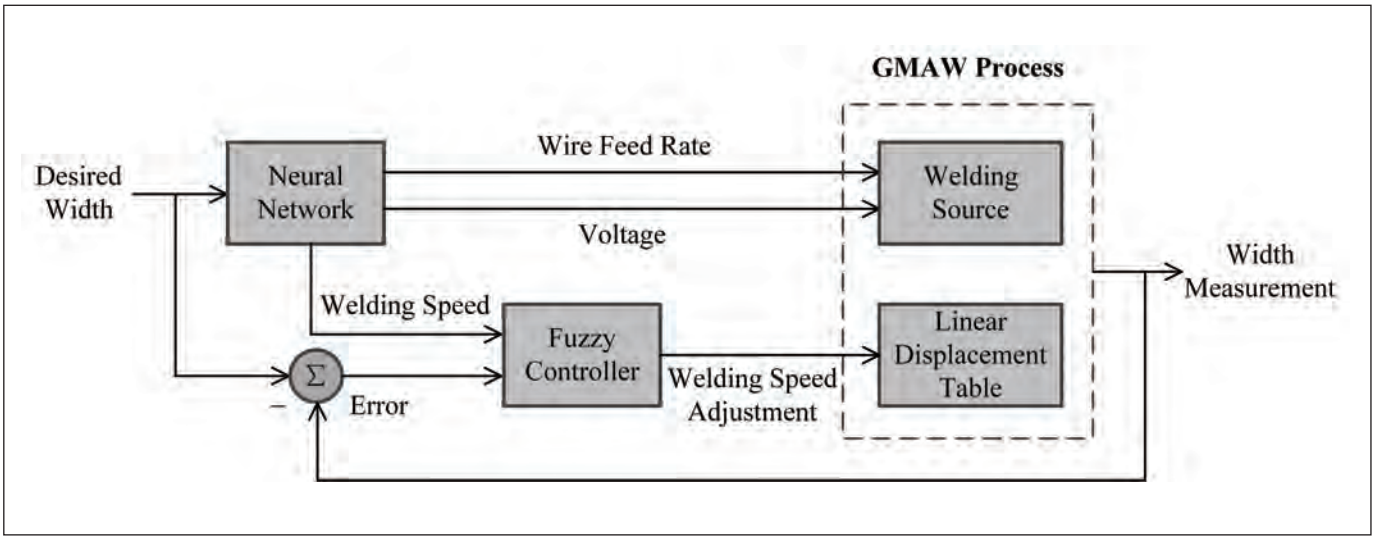

Fig. 12 — Principle of weld bead width control based on ANNs and fuzzy control (Ref. 131).

domain to determine what are the features (useful and efficient representation) of the sufficient but redundant information, 3) propose a model structure to correlate the features to the outputs, and 4) finally fit the model parameters and verify the model. This is the traditional way of information extraction.

It is apparent that this traditional way of information extraction is labor intensive and extremely time consuming, primarily due to step 2 because it is subject/domain specific and requires skilled researchers to perform. The subsequent steps 3 and 4 are also subject specific. This is a human process that is not automated. A possible way to improve the efficiency is to skip the features selection step and directly use the redundant data/information. A more complex, but less subject dependent, model may be used as a class of general model. For each class of general model, a general-fitting algorithm may be developed in advance. Therefore, once the data become available, extracting the needed information becomes an automated process. The efficiency is thus automated/revolutionized. This is the idea of machine learning, especially deep learning (Ref. 110), which uses a class of general model to directly extract the information/output from the data, which may be redundant. The expense is the need for a large amount of data for the less efficient general model and for extensive computation. The latter has been well addressed by increased/cheap computation power. Collecting/generating the needed large amount of data becomes the only major task for the researchers.

Machine Learning

In 1959, the concept of "machine learning" was first proposed by Arthur Samuel in his study about artificial players of the game of checkers: programming computers to learn from experience should eventually eliminate the need for much of this detailed programming effort (Ref. 111). Then, Tom M. Mitchell presented a more detailed definition widely accepted by academics: a computer program is said to learn from experience E with respect to some class of tasks T and performance measure P if its performance at tasks in T, as measured by P, improves with experience E (Ref. 112). The core idea of machine learning is to improve the performance of a task by learning from experience/data. In the last 20 years, with the availability of large-volume data and strong support from computing hardware, especially the highly effective matrix computing in graphics processing units, machine learning has developed rapidly and become a subdiscipline gradually. The architecture of machine learning models become more complex and their functions are more powerful and play an important role in computer vision, natural language processing, decision-making, etc. Compared with traditional methods, machine-learning-based methods have several advantages: 1) Diverse data processing ability: machine learning has the ability to handle multi-dimension and multi-variety data such as images, speech, text, point clouds, graphics etc. 2) Shorter development time: some artificial work in traditional methods can be done by machine learning methods themselves, such as feature selection and model structure optimization. This reduces development time and increases the development efficiency. 3) The ability to continuously improve: the performance can be continuously improved with available large and complex experience. Based on these principles, machine learning can be classified into supervised learning, unsupervised learning, and reinforcement learning.

Supervised Learning

Supervised learning distinguishes itself from unsupervised and reinforcement learning by its use of label data to specify the desired model output for its paired model input to tune the model parameters. It is preferred that the model input be raw, but redundant, information without preprocessing for the preferred automated process using a class of general model. The raw data can be preprocessed to reduce the redundancy, which reduces model complexity and data size but at the expense of reducing the level of automation. The set of paired data, label, and model input (with or without preprocessing) is split into training and testing data

sets. The training set is used to train the supervised learning models while the testing set is used for the evaluation and verification of the effectiveness of the trained model. Some common supervised learning models include decision tree, support vector machine (SVM), neural networks, and Bayesian networks. Simpler models may require more preprocessing for the data while relatively complex ones require less.

Artificial Neural Network (ANN)

In an ANN, a neuro is a nonlinear processing unit/cell whose output is a standardized nonlinear function, with a few free parameters that need to be trained, of its input. Neuros are arranged into layers. The input of a neuro is the weighted sum of the outputs from the neuros in its previous layers or of the inputs of the network for the input layer. The outputs from the neuros in the output layer are the network outputs. Training an ANN is to fit the weights in each weighted sum and the parameters in each neuro. The idea of ANN is to use the aforementioned class of standardized ways of network construction with standardized neuros. The standardization reduces efforts to construct the model structure and helps automate the model fitting.

Deep Learning

Because of the standardization, the ability to approximate a nonlinear relationship is less effective than a specific model structure. The effectiveness can be increased by increasing layers and neuros. Additional standardized processing functions can also be added, such as the convolution for images and regression for outputs from the last layer neuros. The requirement on the input of the network is reduced such that raw data with redundant information, such as images, can be directly used as network inputs to help automate the modeling process. An ANN is extended with a more complex network to learn more deeply. However, the training becomes more challenging and computation intensive in addition to the increase in the size of needed data. With the recent progress in training methods and algorithms (Ref. 110), such a complex, extended network can be trained using standard algorithms. Deep learning has thus recently gained many successful applications (Ref. 110), including those in welding as reviewed below.

Welding and Machine Learning

Welding is a chemicophysical process where complex mechanics-heat-metallurgy coupled reactions happen locally. Modeling welding processes based on basic physical rules (e.g., numerical simulation) can help us understand the intrinsic nature of welding itself. However, this computation process is very complex, and the computation volume is too large to be applied in practical manufacturing in real time. Machine-learning-based methods can decrease the computation time and have been applied successfully in welding process modeling. Deep learning is often needed because of the complexity of the welding process.

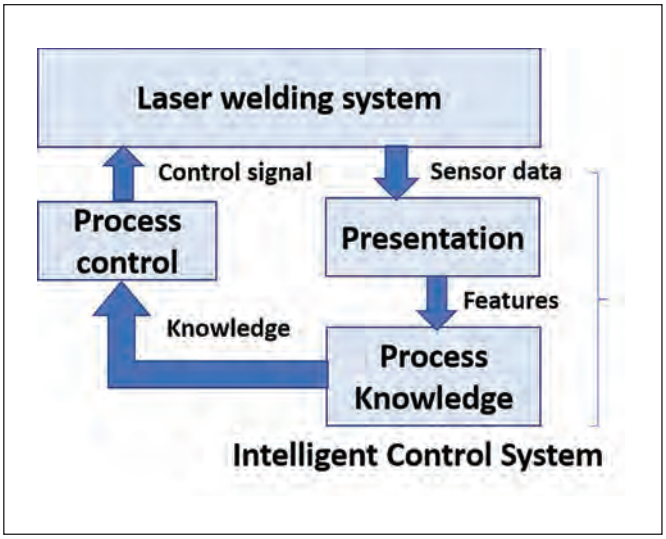

Fig. 13 — Principle of intelligent control of a laser welding system based on auto-encoder and reinforcement learning (Ref. 132).

Welding Performance Prediction

Predicting the performance of the welded workpiece can help to optimize the welding process and decrease the cost for welding parameters design. The model reported in Ref. 116 is a nonlinear multi-input multi-output mapping model for which machine learning is a feasible tool. This investigative work started in 1990 when Anderson et al. presented the framework and principles for weld performance prediction using ANNs (Ref. 113). The general model architecture of the fully connected ANNs for welding performance is shown in Fig. 9, mapping m indirect welding parameters (IWPs) to n direct welding parameters (DWPs) via l hidden layers. The IWPs are usually the welding parameters applied depending on the specific welding processes, and the DWPs are some characteristic properties of the welded workpieces, including the geometric profile and mechanical properties of the welded joints. By collecting the IWP-DWP data pairs, the ANNs are trained using backpropagation such that nonlinear regression models are built for predicting the welding performance. A lot of research work has been done using this framework for different IWPs and DWPs in different welding methods, which are summarized in Table 1.

Welding Defect Detection

Welding defect detection is another area where machine learning is widely used. Mirapeix et al. developed a real-time arc welding defect detection system using principle component analysis (PCA) and ANNs (Ref. 124). The plasma spectra of GTAW is collected and preprocessed using PCA such that the data dimension is reduced, and the reductant information is eliminated. Then principle information reserved is used to train an ANN, which has the nonlinear analysis ability to classify the welding defects. Compared with other information sources, a radiograph usually offers comprehen-

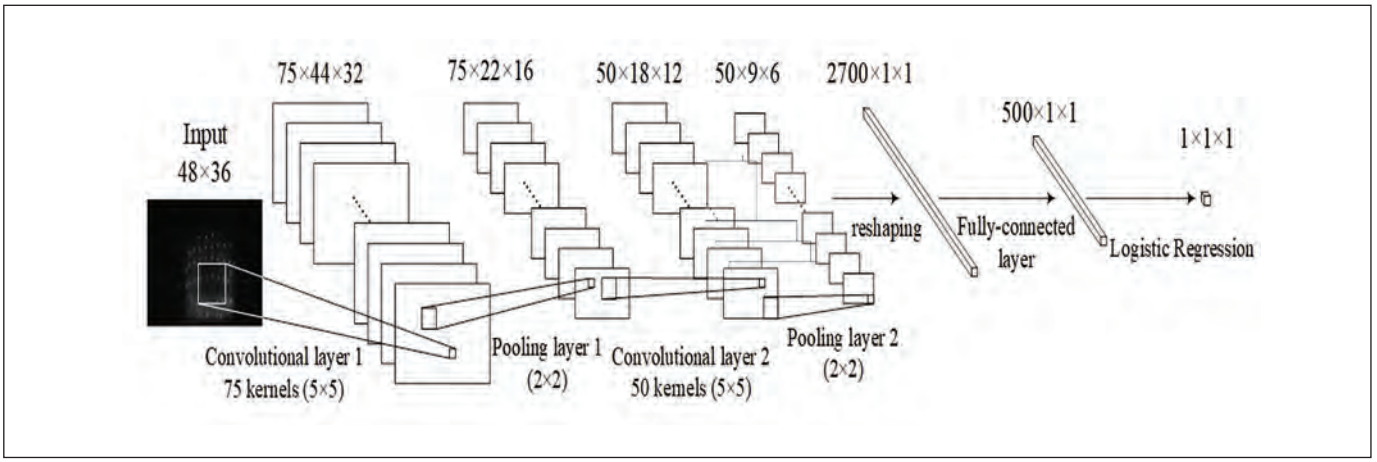

Fig. 14 — CNN architecture used to predict the weld penetration from a raw image of a reflection from an oscillation weld pool surface (Ref. 134).

sive and reliable information. However, extracting the useful information from the raw images is the foundation to accurately detect the welding defects. Valavanis et al. developed a multiclass welding defect detection system using radiographic images (Ref. 125). First, eight geometric features and 11 texture features are defined and extracted artificially. After analyzing the characterization (nonlinear and high dimensionality), three machine learning methods, including k nearest neighbor, SVM, and ANNs, are trained to classify six common welding defects, as shown in Fig. 10.

Defining and extracting features artificially depends on the experience of the developers and greatly determines the final accuracy. To address this problem, Hou et al. applied the convolutional neural networks (CNNs) to identify the existence of the welding defects where the features were extracted automatically, as shown in Fig. 11 (Ref. 126). This CNN-based method can learn the feature automatically, reduce the artificial work, and improve efficiency. In CNNs, the number of parameters to be trained is too large such that a lot of data needs to be collected to improve performance and decrease the risk of overfitting. This will greatly increase the cost in time and money to complete many welding experiments. Sassi et al. proposed a transferring learning-based method to solve this problem (Ref. 127). The parameters in CNNs are pretrained using the existing models with good performance in other tasks, and the transferring learning is done with small-volume weld appearance images. This method can decrease the requirement of dataset size without sacrificing performance much. To avoid the shortages due to a single information source, some multi-information sources, including visual information and plasma spectrum, are fused with or without preprocessing to train machine learning models, and the results show that multi-information sources can achieve better and more stable performance (Refs. 128–130).

Welding Process Control

To achieve high-quality weld joints in practical manufacturing, some machine learning-based control methods have been proposed. Cruz et al. proposed a weld bead width control algorithm based on ANNs and fuzzy control, as shown in Fig. 12 (Ref. 131). The trained ANN will present an optimal three-parameter set including wire feed rate, arc voltage, and welding speed, which are applied in GMAW based on the desired width. Then, a fuzzy controller is applied to control the weld bead width by adjusting welding speed. Reinforcement learning aims to learn a policy for agents interacting with the environment, which is proper for control policy development. Günther et al. developed an intelligent laser welding control system based on auto-encoder and reinforcement learning, as shown in Fig. 13 (Ref. 132). The unsupervised auto-encoder CNN is applied to extract the features from the images of the weld bead. Then, the actor-critic reinforcement learning is used to train a policy for welding quality control. Jin et al. combined the reinforcement learning and proportional-integral-derivative controller to control the width of the weld pool (Ref. 133).

Deep Learning of Joint Penetration Directly from Raw Images

In the section Monitoring of Joint Penetration, we reviewed an effort that projected a laser pattern onto an oscillating weld pool. Because of the changes in the 3D shape and in the oscillation amplitude and frequency with the joint penetration, the shape and oscillation of the weld pool surface as the reflection mirror changes with the joint penetration. Since the incident laser pattern is given, the reflection image is only determined by the reflection mirror, thus its shape and oscillation and consequently the joint penetration. This implies that the reflection contains sufficient information to determine the joint penetration However, the oscillation and images are so complex that human review to select/extract the right features accurately is impractical. Deep learning provides a perfect solution to solve this problem.

We used a CNN (Fig. 14) to directly map the reflection image (as exemplified by the image in Fig. 6C) as input to the output that is the area of hot metal on the bottom surface of the workpiece (Ref. 134). This area of the hot metal measures the state of the joint penetration and is obtained from the image taken from the bottom surface of the workpiece as shown

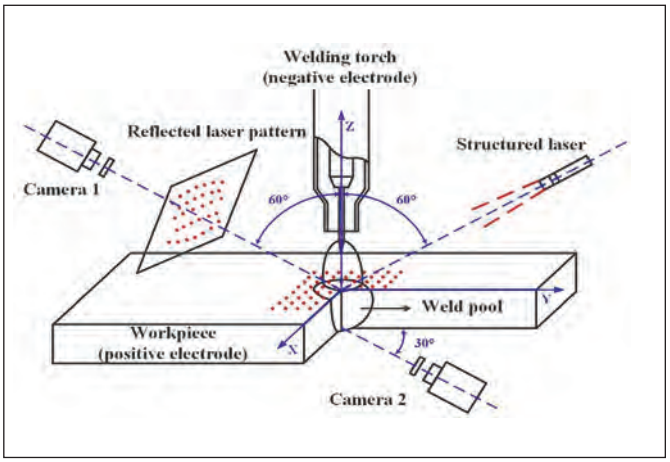

Fig. 15 — Monitoring of reflection image and back-side image (Ref. 134).

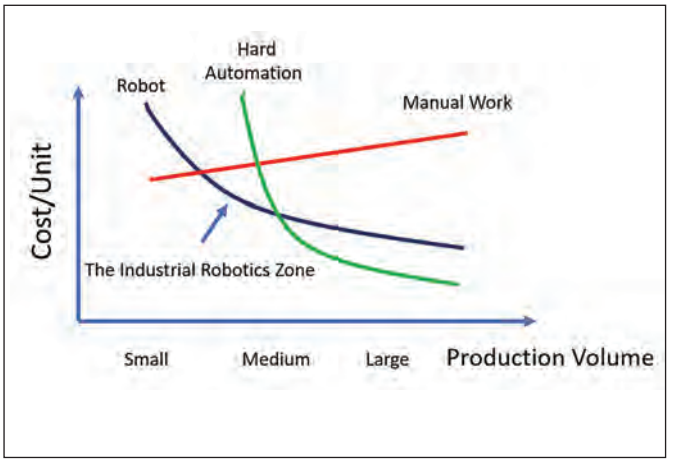

Fig. 16 — Cost performance for different welding performers (Ref. 135).

in Fig. 15. A reflection image is thus paired with a label. Figure 15 shows how the two cameras monitor the experimental process to obtain the reflection image and the back-side image for the label. Experiments have been conducted to collect 3540 image pairs in various welding conditions. Using data augmentation, we obtained 270,000 training examples, 45,000 validation examples, and 45,000 test examples. The trained CNN gave a final testing accuracy of 90.7% for classification of joint penetration in six different levels. We also used a voting mechanism for three neighboring images to increase the classification accuracy to 97.6%.

Learning from Human Welders and Human-Robot Collaborative Welding

A manufacturing operation may be completed by three kinds of performers: human, robot, and hard automation,

Table 1 — Research Work Summary for Welding Performance Prediction

Welding Method	IWPs	DWPs	Hidden Layers	Ref.
GTAW	Arc current, arc voltage, travel speed, wire speed	Bead width, penetration, reinforcement height	2	(113)
FSW	Welding speed, rotation speed	Quality evaluation threshold	2	(114)
Multipass GMAW	Pass number, weld speed, welding current, arc voltage	Bead height	1	(115)
Multipass GMAW	Pass number, weld speed, welding current, arc voltage	Bead width	1	(116)
Laser welding	Laser power, welding speed, defocus amount, gas flow, gas orientation	Penetration, weld width	1	(117)
Laser welding	Power, welding speed, standoff distance, clamp pressure	Lap-shear strength, weld-seam width	2	(118)
FSW	Tool rotation speed, welding speed, shoulder diameter, pin diameter	Tensile strength	1	(119)
FSW	Tool rotation speed, weld speed	Hardness of weld metal, hardness of HAZ, elongation, yield strength, tensile strength	1	(120)
Ultrasonic spot welding	Clamping force, vibration amplitude, vibration time	Tensile strength	2	(121)
Ultrasonic spot welding	Clamping force, vibration amplitude, vibration time	Tensile strength	2	(122)
GMAW	Plate thickness, frequency, wire feed rate, wire feed rate/travel speed ratio, peak current	Bead penetration depth, convexity index	1	(123)

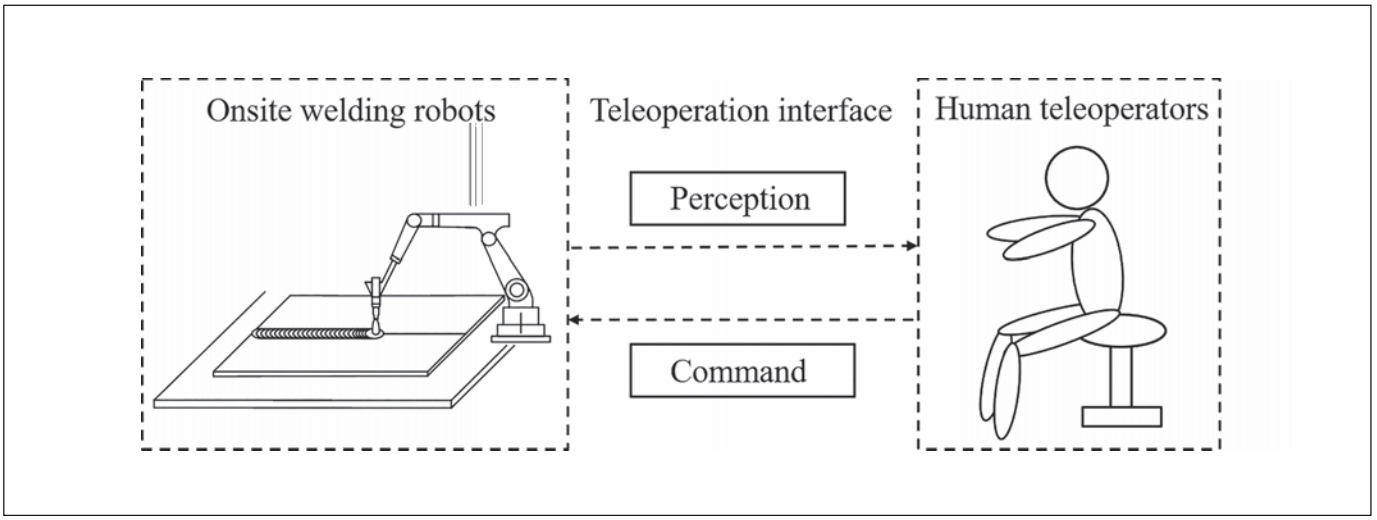

Fig. 17 — General framework of teleoperated welding robots.

where the flexibility is decreasing and the cost per unit is shown in Fig. 16 (Ref. 135). The robots are preferred in small/medium batch manufacturing, which is the mainstream market for current industry. Many welding methods, including resistance spot welding, arc welding, laser welding, and stud welding, have been robotized, and the welding robots account for more than 50% in the industrial robot market according to the International Federation of Robotics (Ref. 136). Currently, the working principle of the welding robot includes online teaching, offline programming, or a combination of them (Ref. 137). The welding robots execute the preprogrammed action with existing logic and have been successfully commercialized by some traditional robot manufacturers such as ABB, Fanuc, Kuka, and Yaskawa. Methods have been developed to increase the adaptability and flexibility of welding robots.

Learning from Human Welders

We have demonstrated the challenges in obtaining the needed knowledge to equip welding robots to improve their adaptations. This includes the information extraction and dynamic control algorithm in Fig. 2. However, all these can be performed by human welders relatively easily. This implies that humans have gained the skills through their years of practice for such adaptations. Therefore, we may learn from human welders how they respond to observed phenomena, such as changes in the weld pool surface, to adjust the welding parameters. This requires demonstrations of human welder operations, monitoring of the scene the welder observes to decide the adjustments, and monitoring of the operations of the welder. Most importantly, the sensors for monitoring the scene and welder operation must not be carried out by the human welder so that the welder can operate freely without interference. This requires a special welding and monitoring system. Such a system has been developed at the University of Kentucky to learn the human welder's response to the change in the 3D surface of the weld pool. The learned model has been integrated into a welding robot so that it can adapt to the welding process and ensure weld penetration (Refs. 138–140).

Teleoperated Welding Robots

In extreme working environments, robots are the preferred performer for welding tasks because they have higher physical limitations than humans. Due to the current development level of artificial intelligence, there are no fully intelligent welding robots that can perform well in an unstructured extreme environment. Teleoperated welding robots can combine high physical tolerance with the intelligence from humans. The general structure of a teleoperated welding robot is shown in Fig. 17. The welding robots and the human teleoperators are separated spatially and connected via the teleoperation interface. The information flows bidirectionally; that is, human teleoperation commands are transmitted to welding robots, and the welding scenes are sensed and shown to human operators. Some mainstream human-robot interaction interfaces, such as the spacemouse (Ref. 141), haptic controller (Ref. 142), gesture (Ref. 143), and virtual reality (VR) (Ref. 144), have been applied for humans to command the welding robots. Welding scene sensing, reconstruction, and display offer direct perception for human operators, which determines the decision made by human operators. The screen (Refs. 141, 142), VR (Ref. 144), and augmented reality (AR) (Refs. 100, 142) are applied for human operators perceiving the welding scene. From the view of the authors, VR and AR are two highest potential interfaces for welding teleoperation due to the following reasons: 1) The operation styles from VR and AR are the most natural and intuitive. The human operators can adjust the welding torches attached to welding robots like traditional human welders; and 2) the welding scene display styles generate an immersed 3D environment where the human operators can perceive the welding process as if they were onsite.

Human-Robot Collaborative Welding

Human-robot collaborative welding is a compromised welding style due to the limitation of current full-intelligent welding robots. In a human-robot collaborative welding system, the human and the robot are responsible for the duty they are good at. In such a system, the advantages of the humans and

robots can be combined. We have developed a human-robot collaborative welding system with a common welding method, weaving GTAW, conducted to verify its effectiveness (Ref. 145). In this system, the robot performs weaving welding with automatic seam tracking based on arc sensors. The human teleoperates the robot movement along the seam via a virtual welding environment generated by a commercial virtual reality system. The intelligent travel speed adjustment from humans could help to decrease the negative effect from environment disturbance. Both the intelligence from humans and movement accuracy from robots are combined so that the welded workpiece has better performance than that from either humans or robots separately.

Robot-Assisted Manual Welding

In some small-volume and unstructured welding tasks, manual welding is preferred over robots, considering the time and cost investment. However, the global shortage of human welders means skilled welders are not always available for small-volume welding. Some robot-assisted welding systems are developed for novice human welders to achieve high-quality welds. Erden et al. proposed a robot-assisted manual welding system by adding impedance such that the inevitable vibration during novice manual welding is greatly suppressed (Ref. 146). Wang et al. proposed a virtual reality robot-assisted welding system based on human intention recognition (Ref. 147). By modeling and recognizing human intention, the intended operation is extracted and applied to welding processes via robots, and the welding quality is improved.

Conclusion

Adaptive welding manufacturing is to make real-time corrections and adjust the welding parameters during welding to minimize the effects from not perfectly-controlled welding conditions. This can be considered a feedback control process that first requires sensors to obtain the actual welding conditions for corrections and the feedback of the concerned output from the welding manufacturing process. If the sensor signals are not direct measurements of the feedback, the information extraction sometimes may be complex. Such a complex problem may be solved by using deep learning and learning from human welders. To then make decisions on the adjustments of the welding parameters, we need an understanding of the dynamics of the welding process in response to the changes in the welding parameters/control variables. We also need appropriate ways to make decisions based on the dynamics and feedback. They are the dynamic modeling and control. Therefore, sensing, modeling, and control are the major elements in adaptive welding, and machine learning/deep learning, learning from human welders, and human-robot collaboration are modern ways to provide solutions to these elements.

References

1. American Welding Society. 2004. *Welding Handbook: Welding Processes*, Part 1, Vol. 2, 9th ed. O'Brien, A., ed. Miami, Fla.: American Welding Society.

2. American Welding Society. 2007. *Welding Handbook: Welding Processes*, Part 2, Vol. 3, 9th ed. O'Brien, A., ed. Miami, Fla.: American Welding Society.

3. American Welding Society. 2019. *Welding Handbook: Welding and Cutting Science and Technology*, Vol. 1, 10th ed. Sinnes, K., ed. Miami, Fla.: American Welding Society.

4. Liao, B., Shi, Y., Cui, Y., Cui, S., Jiang, Z., and Yi, Y. 2018. Mathematical model for prediction and optimization of weld bead geometry in all-position automatic welding of pipes. *Metals* 8(10): 756. DOI: 10.3390/met8100756

5. Richardson, R. W., Gutow, A., Anderson, R. A., and Farson, D. F. 1984. Coaxial arc weld pool viewing for process monitoring and control. *Welding Journal* 63(3): 43–50.

6. Węglowski, M. S. 2007. Investigation on the arc light spectrum in GTA welding. *Journal of Achievements of Materials and Manufacturing Engineering* 20(1–2): 519–22.

7. Li, P. J., and Zhang, Y. M. 2000. Analysis of an arc light mechanism and its application in sensing of the GTAW process. *Welding Journal* 79(9): 252-s to 260-s.

8. Kiddee, P., Fang, Z., and Tan, M. 2016. An automated weld seam tracking system for thick plate using cross mark structured light. *The International Journal of Advanced Manufacturing Technology* 87: 3589–3603. DOI: 10.1007/s00170-016-8729-7

9. Xu, P., Xu, G., Tang, X., and Yao, S. 2008. A visual seam tracking system for robotic arc welding. *The International Journal of Advanced Manufacturing Technology* 37: 70–75. DOI: 10.1007/s00170-007-0939-6

10. Xiong, J., and Zou, S. 2019. Active vision sensing and feedback control of back penetration for thin sheet aluminum alloy in pulsed MIG suspension welding. *Journal of Process Control* 77: 89–96. DOI: 10.1016/j.jprocont.2019.03.013

11. Kovacevic, R., Zhang, Y. M., and Ruan, S. 1995. Sensing and control of weld pool geometry for automated GTA welding. *Journal of Manufacturing Science and Engineering* 117(2): 210–222. DOI: 10.1115/1.2803297

12. Kovacevic, R., and Zhang, Y. M. 1997. Real-time image processing for monitoring of free weld pool surface. *Journal of Manufacturing Science and Engineering* 119(2): 161–169. DOI: 10.1115/1.2831091

13. Kovacevic, R., Zhang, Y. M., and Li, L. 1996. Monitoring of weld joint penetrations based on weld pool geometrical appearance. *Welding Journal* 75(10): 317-s to 329-s.

14. Zhang, Y. M., Kovacevic, R., and Li, L. 1996. Characterization and real-time measurement of geometrical appearance of the weld pool. *International Journal of Machine Tools and Manufacture* 36(7): 799–816. DOI: 10.1016/0890-6955(95)00083-6

15. Wu, C. S., Wang, L., Ren, W. J., and Zhang, X. Y. 2014. Plasma arc welding: Process, sensing, control and modeling. *Journal of Manufacturing Processes* 16(1): 74–85. DOI: 10.1016/j.jmapro.2013.06.004

16. Zhang, Y. M., Jiang, M., and Lu, W. 2004. Double electrodes improve GMAW heat input control. *Welding Journal* 83(11): 39–41.

17. Li, K. H., Chen, J. S., and Zhang, Y. 2007. Double-electrode GMAW process and control. *Welding Journal* 86(8): 231-s to 237-s.

18. Kim, Y., and Eagar, T. W. 1993. Metal transfer in pulsed current gas metal arc welding. *Welding Journal* 72(7): 279-s to 287-s.

19. Kim, Y., and Eagar, T. W. 1993. Analysis of metal transfer in gas metal arc welding. *Welding Journal* 72(6): 269-s to 275-s.

20. Allemand, C. D., Schoeder, R., Ries, D. E., and Eagar, T. W. 1985. Method of filming metal transfer in welding arcs. *Welding Journal* 64(1): 45–47.

21. Zhang, Y. M., and Li, P. J. 2001. Modified active control of metal transfer and pulsed GMAW of titanium. *Welding Journal* 80(2): 54-s to 61-s.

22. Zhang, Y. M., Liguo, E., and Kovacevic, R. 1998. Active met-

al transfer control by monitoring excited droplet oscillation. *Welding Journal* 77(9): 388-s to 395-s.

23. Teixeira, G. S., and Mazzaferro, J. A. E. 2019. GMA welding metal transfer mode study by high-speed imaging and electrical signal acquisition. *Journal of the Brazilian Society of Mechanical Sciences and Engineering* 41: 315. DOI: 10.1007/s40430-019-1814-8

24. Lu, Y., Chen, S., Shi, Y., Li, X., Chen, J., Kvidahl, L., et al. 2014. Double-electrode arc welding process: Principle, variants, control and developments. *Journal of Manufacturing Processes* 16(1): 93–108. DOI: 10.1016/j.jmapro.2013.08.003

25. Li, K., and Zhang, Y. M. 2007. Metal transfer in double-electrode gas metal arc welding. *Journal of Manufacturing Science and Engineering* 129(6): 991–999. DOI: 10.1115/1.2769729

26. Ready, J. F. 1976. Change of reflectivity of metallic surfaces during irradiation by CO2-TEA laser pulses. *IEEE Journal of Quantum Electronics* 12(2): 137–142. DOI: 10.1109/JQE.1976.1069106

27. Zhang, Y. M, Song, H. S., and Saeed, G. 2006. Observation of a dynamic specular weld pool surface. *Measurement Science and Technology* 17(6): L9–L12. DOI: 10.1088/0957-0233/17/6/L02

28. Zhang, W., Wang, X., and Zhang, Y. 2013. Analytical real-time measurement of a three-dimensional weld pool surface. *Measurement Science and Technology* 24(11): 115011. DOI: 10.1088/0957-0233/24/11/115011

29. Chen, J. S., Chen, J., Zhang, K., Feng, Z., and Zhang, Y. M. 2018. Dynamic reflection behaviors of weld pool surface in pulsed GTAW. *Welding Journal* 97(6): 191-s to 206-s. DOI: 10.29391/2018.97.017

30. Mnich, C., Al-Bayat, F., Debrunner, C., Steele, J., and Vincent, T. 2004. In situ weld pool measurement using stereovision. *Proceedings of 2004 Japan – USA Symposium on Flexible Automation,* 1–4. Denver, Colo.

31. Neill, A. M., and Steele, J. P. H. 2016. Modeling and simulation of three dimensional weld pool reconstruction by stereo vision. *2016 IEEE International Conference on Advanced Intelligent Mechatronics (AIM)*, 542–547. Banf, Alberta, Canada: IEEE. DOI: 10.1109/AIM.2016.7576824

32. Lee, D. H., and Kweon, I. 2000. A novel stereo camera system by a biprism. *IEEE Transactions on Robotics and Automation* 16(5): 528–541. DOI: 10.1109/70.880803

33. Yoo, C. D., and Lee, J. 2000. 3D measurement of weld pool using biprism stereo vision sensor. *http://joiningl.kaist.ac.kr/research/vision.html*

34. Liang, Z., Chang, H., Wang, Q., Wang, D., and Zhang, Y. M. 2019. 3D reconstruction of weld pool surface in pulsed GMAW by passive biprism stereo vision. *IEEE Robotics and Automation Letters* 4(3): 3091–3097. DOI: 10.1109/LRA.2019.2924844

35. Villar, M., Garnier, C., Chabert, F., Nassiet, V., Diez, J. C., Sotelo, A., et al. 2016. In-situ measurements of temperature distribution during transmission laser welding of poly(aryletherketone). *AIP Conf. Proc.* 1769(1). DOI: 10.1063/1.4963408

36. Alfaro, S. C. A., Vargas, J. A. R., De Carvalho, G. C., and De Souza, G. G. 2015. Characterization of "humping" in the GTA welding process using infrared images. *Journal of Materials Processing Technology* 223: 216–24. DOI: 10.1016/j.jmatprotec.2015.03.052

37. Cho, C.-H., Hsieh, Y.-C., and Chen, H.-Y. 2015. Welding pool measurement using thermal array sensor. *Proc. SPIE 9609, Infrared Sensors, Devices, and Applications V*: 960912. DOI: 10.1117/12.2187751

38. Zhang, Z., Wen, G., and Chen, S. 2018. Audible sound-based intelligent evaluation for aluminum alloy in robotic pulsed GTAW: Mechanism, feature selection, and defect detection. *IEEE Trans. Ind. Informatics* 14(7): 2973–2983. DOI: 10.1109/TII.2017.2775218

39. Lv, N., Xu, Y., Li, S., Yu, X., and Chen, S. 2017. Automated control of welding penetration based on audio sensing technology. *Journal of Materials Processing Technology* 250: 81–98. DOI: 10.1016/j.jmatprotec.2017.07.005

40. Li, P. J., and Zhang, Y. M. Robust sensing of arc length. 2001. *IEEE Trans. Instrum. Meas*. 50(3): 697–704. DOI: 10.1109/19.930442

41. Li, P. J., and Zhang, Y. M. 2001. Precision sensing of arc length in GTAW based on arc light spectrum. *Journal of Manufacturing Science and Engineering* 123(1): 62–65. DOI: 10.1115/1.1349719

42. Shi, Y. H., Yoo, W. S., and Na, S. J. 2006. Mathematical modelling of rotational arc sensor in GMAW and its applications to seam tracking and endpoint detection. *Sci. Tech. Weld. Join*. 11(6): 723–730. DOI: 10.1179/174329306x153196

43. Kim, C. H., and Na, S. J. 2001. A study of an arc sensor model for gas metal arc welding with rotating arc part 2: Simulation of an arc sensor in mechanically rotating gas metal arc welding. *Proc. Inst. Mech. Eng. Part B: J. Eng. Manuf.* 215(9): 1281–1288. DOI: 10.1243/0954405011519213

44. Kotecki, D. J., Cheever, D., and Howden, D. 1972. Mechanism of ripple formation during weld solidification. *Welding Journal* 51(8): 386-s to 391-s.

45. Renwick, R., and Richardson, R. W. 1983. Experimental investigation of GTA weld pool oscillations. *Welding Journal* 62(2): 29-s to 35-s.

46. Zacksenhouse, M., and Hardt, D. E. 1983. Weld pool impedance identification for size measurement and control. *J. Dyn. Syst. Meas. Control* 105(3): 179–184. DOI: 10.1115/1.3140652

47. Xiao, Y. H., and den Ouden, G. 1993. Weld pool oscillation during GTA welding of mild steel. *Welding Journal* 72(8): 428-s to 434-s.

48. Aendenroomer, A. J. R., and den Ouden, G. 1998. Weld pool oscillation as a tool for penetration sensing during pulsed GTA welding. *Welding Journal* 77(5): 181-s to 187-s.

49. Andersen, K., and Cook, G. E. 1997. Synchronous weld pool oscillation for monitoring and control. *IEEE Trans. Ind. Appl.* 33(2): 464–471. DOI: 10.1109/28.568011

50. Lancaster, J. F., ed. 1986. *The Physics of Welding*, 2nd ed. International Institute of Welding. DOI: 10.1016/C2013-0-03805-4

51. Shi, Y., Li, C., Du, L., Gu, Y., and Zhu, M. 2016. Frequency characteristics of weld pool oscillation in pulsed gas tungsten arc welding. *Journal of Manufacturing Processes* 24(1): 145–151. DOI: 10.1016/j.jmapro.2016.08.010

52. Hardt, D. E., and Katz, J. M. 1984. Ultrasonic measurement of weld penetration. *Welding Journal* 63(9): 273-s to 285-s.

53. Fenn, R. 1985. Ultrasonic monitoring and control during arc welding. *Welding Journal* 64(9): 18–24.

54. Carlson, N. M., and Johnson, J. A. 1988. Ultrasonic sensing of weld pool penetration. *Welding Journal* 67(11): 239-s to 246-s.

55. Aussel, J. D., Le Brun, A., and Baboux, J. C. 1988. Generating acoustic waves by laser: Theoretical and experimental study of the emission source. *Ultrasonics* 26(5): 245–255. DOI: 10.1016/0041-624X(88)90013-3

56. Graham, G. M., and Ume, I. C. 1997. Automated system for laser ultrasonic sensing of weld penetration. *Mechatronics* 7(8): 711–721. DOI: 10.1016/s0957-4158(97)00031-7

57. Mi, B., and Ume, C. 2006. Real-time weld penetration depth monitoring with laser ultrasonic sensing system. *Journal of Manufacturing Science and Engineering* 128(1): 280–286. DOI: 10.1115/1.2137747

58. Kita, A. 2005. Measurement of weld penetration depth using non-contact ultrasound method. PhD diss., Georgia Institute of Technology.

59. Dixon, S., Edwards, C., and Palmer, S. B. 1999. Laser-EMAT system for ultrasonic weld inspection. *Ultrasonics* 37(4): 273–281. DOI: 10.1016/S0041-624X(99)00002-5

60. Chen, W., and Chin, B. A. 1990. Monitoring joint penetration using infrared sensing techniques. *Welding Journal* 69(4): 181-s to 185-s.

61. Wikle, H. C., Kottilingam, S., Zee, R. H., and Chin, B. A. 2001. Infrared sensing techniques for penetration depth control of

the submerged arc welding process. *J. Mater. Process. Technol.* 113(1–3): 228–233. DOI: 10.1016/S0924-0136(01)00587-8

62. Nagarajan, S., Banerjee, P., Chen, W. H., and Chin, B. A. 1992. Control of the welding process using infrared sensors. *IEEE Trans. Robot. Autom.* 8(1): 86–93. DOI: 10.1109/70.127242

63. Alfaro, S. C. A., and Franco, F. D. 2010. Exploring infrared sensoring for real time welding defects monitoring in GTAW. *Sensors* 10(6): 5962–5974. DOI: 10.3390/s100605962

64. Corlett, B. J., Lucas, J., and Smith, J. S. 1991. Sensors for narrow-gap welding. *IEE Proc. A Sci. Meas. Technol.* 138(4): 213–222. DOI: 10.1049/ip-a-3.1991.0030

65. Bicknell, A., Smith, J. S., and Lucas, J. 1994. Arc voltage sensor for monitoring of penetration in TIG welds. *IEE Proc. Sci. Meas. Technol.* 141(6): 513–520. DOI: 10.1049/ip-smt:19941144

66. Bai, P., Wang, Z., Hu, S., Ma, S., and Liang, Y. 2017. Sensing of the weld penetration at the beginning of pulsed gas metal arc welding. *Journal of Manufacturing Processes* 28(1): 343–350. DOI: 10.1016/j.jmapro.2017.07.002

67. Li, X. R., Shao, Z., Zhang, Y. M., and Kvidahl, L. 2013. Monitoring and control of penetration in GTAW and pipe welding. *Welding Journal* 92(6): 190-s to 196-s.

68. Zhang, Y. M., Li, X., and Shao, Z. 2017. A method to monitor and control weld penetration in gas tungsten welding and full-position pipe welding. U.S. patent 9604301.

69. Rokhlin, S. I., and Guu, A. C. 1993. A study of arc force, pool depression, and weld penetration during gas tungsten arc welding. *Welding Journal* 72(8): 381-s to 390-s.

70. Rokhlin, S. I., and Guu, A. C. 1990. Computerized radiographic sensing and control of an arc welding process. *Welding Journal* 69(3): 83-s to 97-s.

71. Zhao, D. B., Yi, J. Q., Chen, S. B., Wu, L., and Chen, Q. 2003. Extraction of three-dimensional parameters for weld pool surface in pulsed GTAW with wire filler. *Journal of Manufacturing Science and Engineering* 125(3): 493–503. DOI: 10.1115/1.1556400

72. Kovacevic, R., and Zhang, Y. M. 1996. Sensing free surface of arc weld pool using specular reflection: Principle and analysis. *Proc. Inst. Mech. Eng. Part B: J. Eng. Manuf.* 210(6): 553–564. DOI: 10.1243/PIME_PROC_1996_210_154_02

73. Saeed, G., and Zhang, Y. M. 2007. Weld pool surface depth measurement using a calibrated camera and structured light. *Measurement Science and Technology* 18(8): 2570–2578. DOI: 10.1088/0957-0233/18/8/033

74. Song, H., and Zhang, Y. M. 2009. Error analysis of a three-dimensional GTA weld pool surface measurement system. *Welding Journal* 88(7): 141-s to 148-s.

75. Zhang, W., Liu, Y., and Zhang, Y. 2013. Real-time measurement of the weld pool surface in GTAW process. *2013 IEEE Instrum. Meas. Technol. Conf.,* 1640–1645. Minneapolis, Minn.: IEEE. DOI: 10.1109/I2MTC.2013.6555692

76. Zhang, W., Liu, Y. K., Wang, X., and Zhang, Y. M. 2012. Characterization of three-dimensional weld pool surface in gas tungsten arc welding. *Welding Journal* 91(7): 195-s to 203-s.

77. Borrelli, F., Bemporad, A., and Morari, M. 2017. *Predictive Control for Linear and Hybrid Systems*. Cambridge, England: Cambridge University Press. DOI: 10.1017/9781139061759

78. Hartman, D. A., DeLapp, D. R., Cook, G. E., and Barnett, R. J. 1999. Intelligent fusion control throughout varying thermal regions [arc welding]. *Conf. Rec. 1999 IEEE Ind. Appl. Conf. Thirty-Forth IAS Annu. Meet. (Cat. No.99CH36370)* 1: 635–644. Phoenix, Ariz.: IEEE. DOI: 10.1109/IAS.1999.800018

79. Ju, J., Suga, Y., and Ogawa, K. 2002. Penetration control by monitoring molten pool oscillation in TIG arc welding. *Int. J. Offshore Polar Eng.* 14(2): 145–149.

80. Yudodibroto, B. Y. B., Hermans, M. J. M., Hirata, Y., and den Ouden, G. 2004. Influence of filler wire addition on weld pool oscillation during gas tungsten arc welding. *Sci. Technol. Weld. Join.* 9(2): 163–168. DOI: 10.1179/136217104225012274

81. Guu, A. C., and Rokhlin, S. I. 1996. Arc weld process control using radiographic sensing. *NDT&E International* 29(3): 184. DOI: 10.1016/0963-8695(96)84884-5

82. Yahia, N. B., Belhadj, T., Brag, S., and Zghal, A. 2011. Automatic detection of welding defects using radiography with a neural approach. *Procedia Eng.* 10: 671–679. DOI: 10.1016/j.proeng.2011.04.112

83. Song, J.-B., and Hardt, D. E. 1993. Closed-loop control of weld pool depth using a thermally based depth estimator. *Welding Journal* 72(10): 471-s to 478-s.

84. Boo, K. S., and Cho, H. S. 1994. A self-organizing fuzzy control of weld pool size in GMA welding processes. *Control Eng. Pract.* 2(6): 1007–1018. DOI: 10.1016/0967-0661(94)91623-3

85. Banerjee, P., Govardhan, S., Wikle, H. C., Liu, J. Y., and Chin, B. A. 1995. Infrared sensing for on-line weld geometry monitoring and control. *Journal of Manufacturing Science and Engineering* 117(3): 323–330. DOI: 10.1115/1.2804337

86. Vorman, A. R., and Brandt, H. 1976. Feedback control of GTA welding using puddle width measurement. *Welding Journal* 55(9): 742–749.

87. Ohshima, K., Yamamoto, M., Tanii, T., and Yamane, S. 1992. Digital control of torch position and weld pool in MIG welding using image processing device. *IEEE Transactions on Industry Applications* 28(3): 607–612. DOI: 10.1109/28.137446

88. Pietrzak, K. A., and Packer, S. M. 1994. Vision-based weld pool width control. *Journal of Manufacturing Science and Engineering* 116(1): 86–92. DOI: 10.1115/1.2901813

89. Song, J. B., and Hardt, D. E. 1994. Dynamic modeling and adaptive control of the gas metal arc welding process. *J. Dyn. Syst. Meas. Control.* 116(3): 405–413. DOI: 10.1115/1.2899235

90. Kovacevic, R., and Zhang, Y. M. 1997. Neurofuzzy model-based weld fusion state estimation. *IEEE Control Syst.* 17(2): 30–42. DOI: 10.1109/37.581293

91. Zhang, Y. M., and Kovacevic, R. 1998. Neurofuzzy model-based predictive control of weld fusion zone geometry. *IEEE Trans. Fuzzy Syst.* 6(3): 389–401. DOI: 10.1109/91.705507

92. Chen, S. B., Zhao, D. B., Wu, L., and Lou, Y. J. 2000. Intelligent methodology for sensing, modeling and control of pulsed GTAW: Part I - Bead-on-plate welding. *Welding Journal* 79(6): 151-s to 163-s.

93. Zhao, D. B., Chen, S. B., and Wu, L. 2001. Intelligent control for the shape of the weld pool in pulsed GTAW with filler metal. *Welding Journal* 80(11): 253-s to 260-s.

94. Tsai, C. H., Hou, K. H., and Chuang, H. T. 2006. Fuzzy control of pulsed GTA welds by using real-time root bead image feedback. *Journal of Materials Processing Technology* 176(1–3): 158–67. DOI: 10.1016/j.jmatprotec.2006.02.027

95. Kong, M., and Chen, S. 2009. Al alloy weld pool control of welding robot with passive vision. *Sensor Review* 29(1): 28–37. DOI: 10.1108/02602280910926733

96. Chen, H., Lv, F., Lin, T., and Chen, S. 2009. Closed-loop control of robotic arc welding system with full-penetration monitoring. *J. Intell. Robot. Syst.* 56: 565–578. DOI: 10.1007/s10846-009-9329-7

97. Liu, Y. K., and Zhang, Y. M. 2014. Model-based predictive control of weld penetration in gas tungsten arc welding. *IEEE Trans. Control Syst. Technol.* 22(3): 955–966. DOI: 10.1109/TCST.2013.2266662

98. Liu, Y. K., Zhang, W. J., and Zhang, Y. M. 2015. Nonlinear modeling for 3D weld pool characteristic parameters in GTAW. *Welding Journal* 94(7): 231-s to 240-s.

99. Liu, Y. K., and Zhang, Y. M. 2013. Control of 3D weld pool surface. *Control Eng. Pract.* 21(11): 1469–1480. DOI: 10.1016/j.conengprac.2013.06.019

100. Liu, Y., and Zhang, Y. 2015. Iterative local ANFIS-based human welder intelligence modeling and control in pipe GTAW process: A data-driven approach. *IEEE/ASME Trans. Mechatronics*

20(3): 1079–1088. DOI: 10.1109/TMECH.2014.2363050

101. Liu, Y. K., and Zhang, Y. M. 2017. Supervised learning of human welder behaviors for intelligent robotic welding. *IEEE Trans. Autom. Sci. Eng.* 14(3): 1532–1541. DOI: 10.1109/TASE.2015.2453351

102. Liu, Y. K., Zhang, Y. M., and Kvidahl, L. 2014. Skilled human welder intelligence modeling and control: Part I — Modeling. *Welding Journal* 93(2): 46-s to 52-s.

103. Liu, Y. K., Zhang, Y. M., and Kvidahl, L. 2014. Skilled human welder intelligence modeling and control: Part II — Analysis and control applications. *Welding Journal* 93(5): 162-s to 170-s.

104. Liu, Y. K., and Zhang, Y. M. 2015. Controlling 3D weld pool surface by adjusting welding speed. *Welding Journal* 94(4): 125-s to 134-s.

105. Liu, Y. K., and Zhang, Y. M. 2014. Control of human arm movement in machine-human cooperative welding process. *Control Eng. Pract.* 32: 161–171. DOI: 10.1016/j.conengprac.2014.08.003

106. Liu, Y. K., and Zhang, Y. M. 2017. Fusing machine algorithm with welder intelligence for adaptive welding robots. *Journal of Manufacturing Processes* 27: 18–25. DOI: 10.1016/j.jmapro.2017.03.015

107. Liu, Y., and Zhang, Y. 2019. Human welder 3-D hand movement learning in virtualized GTAW: Theory and experiments. *Trans. Intell. Weld. Manuf.* 2(1): 3–25. DOI: 10.1007/978-981-10-8740-0_1

108. Traidia, A., and Roger, F. 2011. Numerical and experimental study of arc and weld pool behaviour for pulsed current GTA welding. *Int. J. Heat Mass Transf.* 54: 2163–2179. DOI: 10.1016/j.ijheatmasstransfer.2010.12.005

109. Mougenot, J., Gonzalez, J. J., Freton, P., and Masquère, M. 2013. Plasma-weld pool interaction in tungsten inert-gas configuration. *J. Phys. D: Appl. Phys.:* 46. DOI: 10.1088/0022-3727/46/13/135206

110. Lecun, Y., Bengio, Y., and Hinton, G. 2015. Deep learning. *Nature* 521: 436–444. DOI: 10.1038/nature14539

111. Samuel, A. L. 1959. Some studies in machine learning using the game of checkers. *IBM J. Res. Dev.* 3: 210–229. DOI: 10.1147/rd.33.0210

112. Mitchell, T. 1997. *Machine Learning*, 1st ed. McGraw Hill Higher Education.

113. Andersen, K., Cook, G. E., Karsai, G., and Ramaswamy, K. 1990. Artificial neural networks applied to arc welding process modeling and control. *IEEE Trans. Ind. Appl.* 26(5): 824–830. DOI: 10.1109/28.60056

114. Baraka, A., Panoutsos, G., and Cater, S. 2015. A real-time quality monitoring framework for steel friction stir welding using computational intelligence. *J. Manuf. Processes* 20(1): 137–148. DOI: 10.1016/j.jmapro.2015.09.001

115. Kim, I. S., Son, J. S., Park, C. E., Lee, C. W., and Prasad, Y. K. D. V. 2002. A study on prediction of bead height in robotic arc welding using a neural network. *J. Mater. Process. Technol.* 130–131: 229–234. DOI: 10.1016/S0924-0136(02)00803-8

116. Kim, I. S., Son, J. S., Lee, S. H., and Yarlagadda P. K. D. V. 2004. Optimal design of neural networks for control in robotic arc welding. *Robot. Comput. Integr. Manuf.* 20(1): 57–63. DOI: 10.1016/S0736-5845(03)00068-1

117. Yuguang, Z., Kai, X., and Dongyan, S. 2013. An improved artificial neural network for laser welding parameter selection and prediction. *Int. J. Adv. Manuf. Technol.* 68: 755–762. DOI: 10.1007/s00170-013-4796-1

118. Acherjee, B., Mondal, S., Tudu, B., and Misra, D. 2011. Application of artificial neural network for predicting weld quality in laser transmission welding of thermoplastics. *Appl. Soft Comput.* 11(2): 2548-2555. DOI: 10.1016/j.asoc.2010.10.005

119. Gupta, S. K., Pandey, K. N., and Kumar, R. 2018. Artificial intelligence-based modelling and multi-objective optimization of friction stir welding of dissimilar AA5083-O and AA6063-T6 aluminium alloys. *Proc. Inst. Mech. Eng., Part L: J. Mater. Des. Appl.* 232(4): 333–342. DOI: 10.1177/1464420715627293

120. Okuyucu, H., Kurt, A., and Arcaklioglu, E. 2007. Artificial neural network application to the friction stir welding of aluminum plates. *Mater. Des.* 28(1): 78–84. DOI: 10.1016/j.matdes.2005.06.003

121. Zhao, D., Ren, D., Zhao, K., Pan, S., and Guo, X. 2017. Effect of welding parameters on tensile strength of ultrasonic spot welded joints of aluminum to steel – By experimentation and artificial neural network. *J. Manuf. Processes* 30: 63–74. DOI: 10.1016/j.jmapro.2017.08.009

122. Zhao, D., Zhao, K., Ren, D., and Guo, X. 2017. Ultrasonic welding of magnesium–titanium dissimilar metals: A study on influences of welding parameters on mechanical property by experimentation and artificial neural network. *Journal of Manufacturing Science and Engineering* 139(3): 031019. DOI: 10.1115/1.4035539

123. Manikya Kanti, K., and Srinivasa Rao, P. 2008. Prediction of bead geometry in pulsed GMA welding using back propagation neural network. *J. Mater. Process. Technol.* 200(1–3): 300–305. DOI: 10.1016/j.jmatprotec.2007.09.034

124. Mirapeix, J., García-Allende, P. B., Cobo, A., Conde, O. M., and López-Higuera, J. M. 2007. Real-time arc-welding defect detection and classification with principal component analysis and artificial neural networks. *NDT&E Int.* 40(4): 315–323. DOI: 10.1016/j.ndteint.2006.12.001

125. Valavanis, I., and Kosmopoulos, D. 2010. Multiclass defect detection and classification in weld radiographic images using geometric and texture features. *Expert Syst. Appl.* 37(12): 7606–7614. DOI: 10.1016/j.eswa.2010.04.082

126. Hou, W., Wei, Y., Guo, J., Jin., Y., and Zhu, C. 2018. Automatic detection of welding defects using deep neural network. *J. Phys.: Conf. Ser.* 933: 012006. DOI: 10.1088/1742-6596/933/1/012006

127. Sassi, P., Tripicchio, P., and Avizzano, C. A. 2019. A smart monitoring system for automatic welding defect detection. *IEEE Trans. Ind. Electron* 66(12): 9641–9650. DOI: 10.1109/TIE.2019.2896165

128. You, D., Gao, X., and Katayama, S. 2014. Multisensor fusion system for monitoring high-power disk laser welding using support vector machine. *IEEE Trans. Ind. Informatics* 10(2): 1285–1295. DOI: 10.1109/TII.2014.2309482

129. You, D., Gao, X., and Katayama, S. 2015. WPD-PCA-based laser welding process monitoring and defects diagnosis by using FNN and SVM. *IEEE Trans. Ind. Electron.* 62(1): 628–636. DOI: 10.1109/TIE.2014.2319216

130. Zhang, Y., You, D., Gao, X., Zhang, N., and Gao, P. P. 2019. Welding defects detection based on deep learning with multiple optical sensors during disk laser welding of thick plates. *J. Manuf. Syst.* 51: 87–94. DOI: 10.1016/j.jmsy.2019.02.004

131. Cruz, J. G., Torres, E. M., and Absi Alfaro, S. C. 2015. A methodology for modeling and control of weld bead width in the GMAW process. *J. Brazilian. Soc. Mech. Sci. Eng.* 37: 1529–1541. DOI: 10.1007/s40430-014-0299-8

132. Günther, J., Pilarski, P. M., Helfrich, G., Shen, H., and Diepold, K. 2016. Intelligent laser welding through representation, prediction, and control learning: An architecture with deep neural networks and reinforcement learning. *Mechatronics* 34: 1–11. DOI: 10.1016/j.mechatronics.2015.09.004

133. Jin, Z., Li, H., and Gao, H. 2019. An intelligent weld control strategy based on reinforcement learning approach. *Int. J. Adv. Manuf. Technol.* 100: 2163–2175. DOI: 10.1007/s00170-018-2864-2

134. Li, C., Wang, Q. Y., Jiao, W. H., Johnson, M., and Zhang, Y. M. 2020. Deep learning-based detection of penetration from weld pool reflection images. *Welding Journal* 99(9): 239-s to 245-s. DOI: 10.29391/2020.99.022

135. Pires, J. N., Loureiro, A., Godinho, T., Ferreira, P., Fernando, B., and Morgado, J. 2003. Welding robots. *IEEE Robot. Autom.*

Mag. 10(2): 45–55. DOI: 10.1109/MRA.2003.1213616

136. Sprovieri, J. 2016. New technology for robotic welding. *assemblymag.com/articles/93555-new-technology-for-robotic-welding*

137. Pan, Z., Polden, J., Larkin, N., Van Duin, S., and Norrish, J. 2012. Recent progress on programming methods for industrial robots. *Robot. Comput. Integr. Manuf.* 28(2): 87–94. DOI: 10.1016/j.rcim.2011.08.004

138. Zhang, W., and Zhang, Y. M. 2012. Modeling of human welder response to 3D weld pool surface: Part I — Principles. *Welding Journal* 91(11): 310-s to 318-s.

139. Zhang, W., and Zhang, Y. 2012. Modeling of human welder response to 3D weld pool surface: Part II — Results and analysis. *Welding Journal* 91(11): 329-s to 337-s.

140. Liu, Y., Zhang, W., and Zhang, Y. 2015. Dynamic neuro-fuzzy-based human intelligence modeling and control in GTAW. *IEEE Trans. Autom. Sci. Eng.* 12(1): 324–335. DOI: 10.1109/TASE.2013.2279157

141. Zhang, L., Gao, H., Zhang, G., and Wu, L. 2006. Agent-based modelling and control of tele-robotic welding system. *Proc. Inst. Mech. Eng. Part B: J. Eng. Manuf.* 220(12): 2087–2094. DOI: 10.1243/09544054JEM544

142. Ni, D., Yew, A. W. W., Ong, S. K., and Nee, A. Y. C. 2017. Haptic and visual augmented reality interface for programming welding robots. *Adv. Manuf.* 5: 191–198. DOI: 10.1007/s40436-017-0184-7

143. Liu, Y., and Zhang, Y. 2015. Toward welding robot with human knowledge: A remotely-controlled approach. IEEE Trans. *Autom. Sci. Eng.* 12: 769–774. DOI: 10.1109/TASE.2014.2359006

144. Wang, Q., Jiao, W., Yu, R., Johnson, M. T., and Zhang, Y. 2019. Modeling of human welders' operations in virtual reality human-robot interaction. *IEEE Robot. Autom. Lett.* 4: 2958–2964. DOI: 10.1109/LRA.2019.2921928

145. Wang, Q., Cheng, Y., Jiao, W., Johnson, M. T., and Zhang, Y. M. 2019. Virtual reality human-robot collaborative welding: A case study of weaving gas tungsten arc welding. *J. Manuf. Processes*. 48: 210–217. DOI: 10.1016/j.jmapro.2019.10.016

146. Erden, M. S., and Billard, A. 2016. Robotic assistance by impedance compensation for hand movements while manual welding. *IEEE Trans. Cybern.* 46(11): 2459–2472. DOI: 10.1109/TCYB.2015.2478656

147. Wang, Q., Jiao, W., Yu, R., Johnson, M. T., and Zhang, Y. M. 2020. Virtual reality robot-assisted welding based on human intention recognition. *IEEE Trans. Autom. Sci. Eng.* 17(2): 799–808. DOI: 10.1109/TASE.2019.2945607

YUMING ZHANG (yuming.zhang@uky.edu) *and QIYUE WANG are with the Institute for Sustainable Manufacturing and Department of Electrical and Computer Engineering, University of Kentucky, Lexington, Ky. YUKANG LIU is with Cognex Corp., Natick, Mass.*

American Welding Society®

aws.org

BRING BRAND AWARENESS TO YOUR COMPANY

By placing your product video on the AWS website.

Contact AWS for more information

Sandra Jorgensen at 305-443-9353 ext: 254

Lea Owen at 305-443-9353 ext: 220

Arcos Delivers Solutions to Stainless Steel Alloy Welding Challenges.

Arcos Industries, LLC offers over 100 stainless steel electrode products to handle the countless array of demanding welding applications that challenge you daily. Our reputation for exceptional quality and outstanding service ensures that you can depend on Arcos to provide you with the finest in bare wire, covered and tubular stainless steel alloy welding electrodes.

Discover for yourself how Arcos **stainless steel alloy electrodes** can help you solve your critical welding problems. Call us today at **800-233-8460** or visit our website at **www.arcos.us**.

Arcos

Committed To Being Here. Committed To You.

We understand the meaning of essential. Businesses and industries count on you, just like you count on us. In these challenging times, we've continued to do what we do best: build a better world by developing welding products and solutions to keep you moving forward. Our commitment is to being here.

Our commitment is to you.

LINCOLN ELECTRIC